REGULATION OF AXON GUIDANCE RECEPTOR EXPRESSION AND ACTIVITY

DURING NEURONAL MORPHOGENESIS

Celine Santiago

A DISSERTATION

in

Cell and Molecular Biology

Presented to the Faculties of the University of Pennsylvania

in

Partial Fulfillment of the Requirements for the

Degree of Doctor of Philosophy

2016

Supervisor of Dissertation

_____

Greg J. Bashaw, Professor of Neuroscience

Graduate Group Chairperson

_____

Daniel Kessler, Associate Professor of Cell and Developmental Biology

Dissertation Committee:

Stephen DiNardo, Professor of Cell and Developmental Biology

Wenqin Luo, Assistant Professor of Neuroscience

Jonathan Raper, Professor of Neuroscience

Meera Sundaram, Associate Professor of Genetics

ACKNOWLEDGMENTS

I would like to thank the members of the Bashaw lab for their mentorship, support, and friendship throughout the years. In particular, I thank Greg for having created a stimulating research environment where curiosity and critical thinking are always encouraged. Our many conversations over the years helped me communicate more clearly and think more deeply about science, and were a major part of my growth and of the joy of working in the lab. I am also very grateful for all his encouragement, which gave me the confidence to get past disappointments, and to push myself to try new things, and for his relentless advocacy and support for me as I prepare to move on to the next stage of my career.

I thank Alexandra and Mike for having been such great mentors and friends. I am a better scientist for having worked by their side, and they continue to inspire me to be more ambitious and thoughtful. A special thank you to Alexandra for her wisdom and thoughtful words every time I needed advice. Thanks to Melissa for having shared all the milestones of graduate school with me, from the early days of our rotation to proof-reading each other's papers. I thank Tim and Elise for a productive collaboration on the Robo2 pro-crossing project, and all the other members of the Bashaw lab for having made it such a fun place to work.

I would also like to thank the members of my thesis committee for their advice and mentorship, both about experiments and about my career. I am also grateful for the guidance of mentors from before grad school: Daniel Wagner, for a wonderful

undergraduate research experience that led me down this path; and Robert Dennison and Deborah Crawford, for sharing their passion and curiosity about the natural world with their students.

Last but not least I would like to thank all of my other friends and family, especially Julie, for having been by my side through all the adventures of the past six years, and Michael, for his unwavering support and sense of humor. I thank my brother and my sister in law for their friendship and advice, especially during interviews in the past year. Finally, I thank my parents, to whom I dedicate this thesis. They did everything they could to help me and my brother find our paths, and their perseverance and courage in difficult moments throughout their own lives showed me how important it is to always keep trying.

ABSTRACT

REGULATION OF AXON GUIDANCE RECEPTOR EXPRESSION AND ACTIVITY DURING NEURONAL MORPHOGENESIS

Celine Santiago

Greg J. Bashaw

Receptors expressed on the surface of neurons during development direct cell migration, axon guidance, dendrite morphogenesis, and synapse formation by responding to cues in the neuron's environment. The expression levels and the activity of cell surface receptors must be tightly controlled for a neuron to acquire its unique identity. Transcriptional mechanisms are essential in this process, and many studies have identified requirements for specific transcription factors during the different steps of neural circuit assembly. However, the downstream effectors by which most of these factors control morphology and connectivity remain unknown. In Chapter 1, I highlight recent work that elucidated functional relationships between transcription factors and the cellular effectors through which they regulate neural morphogenesis and synaptogenesis in multiple model systems. In Chapters 2 and 3, I present data demonstrating that the homeodomain transcription factors Hb9 and Islet control motor axon guidance in *Drosophila* embryos through distinct effectors: Hb9 regulates the (Roundabout) 2 receptor in a subset of motor neurons, while Islet acts in the same cells to regulate the Frazzled/DCC receptor. Genetic rescue experiments indicate that these relationships are functionally important for the guidance of motor axons to their muscle targets. In

addition, Islet regulates motor neuron dendrite targeting in the central nervous system

(CNS) through Frazzled, demonstrating how an individual transcription factor can control

multiple aspects of neuronal connectivity through the same effector. In Chapter 4, I

characterize a non-canonical function for the Robo2 receptor during midline crossing,

and present data suggesting that this activity requires Robo2 to be expressed in midline

cells, providing an example of how mechanisms that regulate guidance receptor gene

expression are key to regulating receptor function and nervous system formation. In

Chapter 5, I explore the implications of these findings, and propose future directions of

research to build upon them.

TABLE OF CONTENTS

LIST OF ILLUSTRATIONS

PREFACE

All experiments in Chapters 2 and 3 were performed by the author, with the exception of

the genome-wide DAM ID data in Figure 3.2. Experiments in Chapter 4 that were

performed by Tim Evans or Elise Arbeille are indicated in the figure legends.

CHAPTER 1

INTRODUCTION: TRANSCRIPTION FACTORS AND EFFECTORS THAT REGULATE AXON GUIDANCE, DENDRITE MORPHOLOGY, AND SYNAPTOGENESIS IN THE DEVELOPING NERVOUS SYSTEM

Introduction

The formation of a functional nervous system requires that the cells that compose it find the appropriate synaptic partners. The position of a neuron and the shape of its axonal and dendritic extensions are therefore fundamental aspects of its identity. Genetic analyses have confirmed that the initial pattern of neural connections in the embryo is intrinsically specified, and a wealth of studies has identified requirements for specific transcription factors in regulating cell migration, axon guidance, dendritic branching, and synaptic partner selection (Chédotal and Rijli, 2009; Dalla Torre di Sanguinetto et al., 2008; Jan and Jan, 2010; Polleux et al., 2007). In parallel, the identification of many guidance receptors and their downstream signaling partners over the last two decades has allowed for a molecular understanding of how neuronal connections are formed (Huberman et al., 2010; Kolodkin and Tessier-Lavigne, 2011; O'Donnell et al., 2009). However, one central challenge that remains is to characterize the relationships between transcriptional regulators and the cell surface proteins or cytoskeletal modifiers that mediate their effects on neural morphogenesis and connectivity.

Correlative data identifying targets of transcription factors have accumulated in multiple neurodevelopmental contexts. However, until recently, few studies validated the observed changes in gene expression with experiments to demonstrate the functional relevance of these relationships. Here, we highlight research that places transcription

1

factors upstream of identified cellular effectors in the contexts of axon guidance in the motor system and during midline crossing, as well as during the acquisition of dendritic morphology in sensory neurons, and synaptogenesis in motor neurons.

Transcription factors and effectors regulating motor axon guidance

Studies of the embryonic motor systems of invertebrates and vertebrates paved the way for understanding the transcriptional control of axon pathfinding. In mouse, chick, zebrafish, *C.elegans*, and *Drosophila*, correlations between the transcription factors expressed in motor neurons and the target areas of their axons were documented over a dozen years ago (Appel et al., 1995; Thor and Thomas, 2002; Tsuchida et al., 1994). Subsequent studies demonstrated that these correlations are functionally significant, as many of these factors are required for the trajectory of motor axons and can redirect axons to abnormal territories when ectopically expressed (reviewed in Thor and Thomas, 2002). Below, we discuss recent work that has identified downstream effectors of transcription factors during motor axon guidance in vertebrates and in *Drosophila*.

LIM homeodomain transcription factors and their effectors in vertebrate motor axon guidance

In mice and chick embryos, a transcriptional cascade regulates motor neuron development (reviewed in Catela et al., 2015). Motor neuron progenitors, which express the basic helix loop helix (bHLH) transcription factor Olig2 (oligodendrocyte transcription factor 2) and the homeodomain transcription factor Nkx6.1 (NK6 homeobox

1), are generated in the ventral spinal cord in response to Sonic hedgehog (Shh) secreted from the notochord and floor plate. The homeodomain transcription factors Hb9 (Mnx1), Islet 1 (Isl1), Nkx6.1, and Lhx3 (LIM homeobox protein 3) are initially expressed in all post-mitotic motor neurons whose axons exit the spinal cord ventrally, and are required for early events in their development, but their expression patterns subsequently become more restricted. Along the rostro-caudal axis, motor columns are specified by homeobox (Hox) transcription factors, whose expression domains are established by gradients of retinoic acid (RA) and fibroblast growth factor (FGF), and reinforced by cross-repressive interactions. Limb-specific domains of Hox gene expression further differentiate limb motor neuron pools from each other, allowing them to acquire distinct cell body positions and innervate specific muscles. Once motor axons reach their targets, retrograde signals induce the expression of ETS (E26 transformation specific) transcription factors, which control the final stages of axonal and dendritic arborization and partner matching.

Two examples of transcription factor effectors that act in spinal motor neurons, the Eph receptor tyrosine kinases EphA4 and EphB1, were identified in elegant studies of mouse and chick embryonic lateral motor column (LMC) neurons (Fig. 1.1). LMC axons fasciculate together as they exit the spinal cord and separate into a dorsal branch and a ventral branch at the base of the limb. Dorsal-ventral pathway selection is controlled by the LIM homeodomain transcription factor Lhx1 (Lim1) and Isl1. Lhx1 and Isl1 are expressed in a mutually exclusive pattern, with Lhx1 restricted to the dorsally-projecting LMC-lateral (LMC-l) neurons, and Isl1 to the ventrally-projecting LMC-medial (LMC-m) neurons (Kania et al., 2000). Although they can repress each other when over-expressed, there is no indication that Lhx1 and Isl1 establish the expression domains of

3

one another (Kania and Jessell, 2003; Kania et al., 2000; Luria et al., 2008). Recent studies indicate that Lhx1 and Isl1 regulate LMC guidance through Eph receptors, which are conserved regulators of axon guidance (reviewed in Klein, 2012) that have been shown through *in vitro* experiments to mediate repulsion in motor axons in response to ephrin ligands (Kao and Kania, 2011). In LMC-l neurons, EphA4 is expressed in an Lhx1-dependent manner, whereas EphB1 is expressed in LMC-m neurons in an Isl1-dependent manner (Kania and Jessell, 2003; Luria et al., 2008). In the limb mesenchyme, ephrin-A ligands are enriched ventrally, whereas ephrin-Bs are enriched dorsally (Kania and Jessell, 2003; Luria et al., 2008). Over-expression of Lhx1 induces *EphA4* expression in LMC neurons and redirects them dorsally, phenocopying EphA4 over-expression, whereas loss of Lhx1 causes LMC-l axons to misproject ventrally, phenocopying *EphA4* mutants (Eberhart et al., 2002; Helmbacher et al., 2000; Kania and Jessell, 2003). Similarly, over-expression of Isl1 induces *EphB1* expression and redirects LMC axons ventrally, while loss of *Isl1* or EphB function causes LMC-m axons to misproject dorsally (Kania and Jessell, 2003; Luria et al., 2008). Importantly, the *Isl1* loss of function phenotype can be rescued by EphB1 over-expression, providing strong evidence that EphB1 acts downstream of Islet1 (Luria et al., 2008).

The ephrin-A and ephrin-B expression patterns in the limb are established by another LIM homeodomain protein, Lmx1b (LIM homeobox transcription factor 1-beta), which is restricted to the dorsal limb mesenchyme, where it induces *ephrin-B2* expression and represses the expression of ephrin-A ligands (Kania and Jessell, 2003; Luria et al., 2008). Lmx1b also regulates the expression of the guidance molecule Netrin in the dorsal limb, and is essential for the correct pathfinding of LMC neurons (Kania et al., 2000;

Krawchuk and Kania, 2008). Interestingly, a recent study found that LMC-m axons express the repulsive Netrin receptor Unc5c and misproject dorsally in the absence of either Netrin or Unc5c (Poliak et al., 2015). Thus, a LIM homeodomain factor in target tissues regulates the expression of molecules that influence the trajectory of motor axons, which also carry out the instructions of a LIM homeodomain code, raising the possibility that these relationships coordinately evolved to ensure the fidelity of axon targeting.

Other cell surface receptors that regulate the guidance of subsets of LMC neurons include Ret, GFRalpha1 (glial cell line derived neurotrophic factor family receptor alpha 1), and neuropilin-2 (Bonanomi et al., 2012; Huber et al., 2005; Kramer et al., 2006). It remains to be determined whether Lhx1 and Isl1 control the expression of these receptors, of Unc5c, or of ephrins, which act in motor neurons to control guidance through reverse signaling and cis-inhibition (Bonanomi et al., 2012; Dudanova et al., 2012; Kao and Kania, 2011). Moreover, Lhx1 and Islet1 are required for the medio-lateral positioning of LMC cell bodies, and although EphA4 regulates the rostro-caudal position of a subset of LMC neurons, Eph receptors do not appear to contribute significantly to mediolateral settling position, suggesting that LIM transcription factors regulate these two aspects of neuronal morphology through distinct downstream programs (Coonan et al., 2003; Palmesino et al., 2010). Indeed, a recent study found a requirement for Lhx1 in specifying the mediolateral position of LMC-l cell bodies through upregulation of the Reelin signaling protein Dab1 (disable-1) (Palmesino et al., 2010). As it is not known whether Lhx1 and Islet1 directly bind to their target genes, elucidating the mechanisms through which these transcription factors regulate their effectors remains a major challenge for the future. Another important question that

5

remains unresolved is how subsets of neurons within the major motor nerves are differentiated from each other. A recent study on forelimb-innervating motor neurons begins to dissect this problem, and demonstrates that subset-specific patterns of Hox genes establish the fates and trajectories of different motor neuron pools in part by regulating the expression levels of Ret and GFRalpha3 (Catela et al., 2016). Ret/GDNF signaling is required for the target-dependent expression of the ETS factor Etv4/Pea3, which is important for axon branching within target muscles, as well as for soma positioning and dendrite targeting in the spinal cord (Catela et al., 2016; Livet et al., 2002; Vrieseling and Arber, 2006). The downstream effectors by which Pea3 regulates axonal branching and dendrite patterning remain unknown. In addition, how specific codes of Hox and LIM homeodomain proteins work together to result in specific transcriptional programs, and to what extent these co-expressed factors act through distinct or overlapping effectors, presents an important problem for future work.

Transcriptional regulation of motor axon guidance in spinal accessory motor neurons

The downstream effectors of transcription factors in other subsets of vertebrate motor neurons are beginning to be identified. Spinal accessory motor neurons (SACMNs) are dorsally-exiting neurons found at cervical levels of the spinal cord that innervate neck and back muscles (Dillon et al., 2005). SACMNs are derived from an *Nkx2.9+* progenitor domain and retain *Nkx2.9* expression post-mitotically. In the absence of *Nkx2.9*, SACMN axons fail to exit the spinal cord (Dillon et al., 2005; Pabst et al., 2003). A recent study found that Nkx2.9 likely regulates spinal cord exit through the Slit receptor Roundabout

(Robo) 2 (Bravo-Ambrosio et al., 2012). Robo receptors have been well studied in the context of midline crossing, where Robo1 and Robo2 signal repulsion in response to floorplate-derived Slit (Dickson and Zou, 2010; Long et al., 2004). More recently, Robo1 and Robo2 were shown to regulate motor axon pathfinding and fasciculation in ventrally-exiting spinal motor neurons (Jaworski and Tessier-Lavigne, 2012). *Robo2* mutants and *Slit1, Slit2* double mutants display SACMN exit defects that resemble those of *Nkx2.9* mutants, and *Robo2* levels are decreased in the absence of *Nkx2.9* (Bravo-Ambrosio et al., 2012). Slit is enriched at the site of SACMN exit, and Slit treatment causes outgrowth of SACMN axons in vitro, suggesting that Robo2-Slit interactions may facilitate exit by promoting growth through the Slit-expressing zone. This model would be further confirmed by determining if the *Nkx2.9* mutant phenotype is rescued upon Robo2 over-expression in SACMNs, and how Slit-Robo2 signaling promotes outgrowth in these axons.

Transcriptional regulation of motor axon guidance in Drosophila

Many of the same principles involved in motor neuron development and axon guidance in vertebrates are observed in *Drosophila*, although there are some interesting differences. Motor neurons that innervate the body wall muscles required for larval crawling arise from multiple embryonic neuroblast lineages that express distinct combinations of transcription factors and are found at stereotyped positions within a segment (Landgraf et al., 1997). There are no known early-acting factors that act in progenitors to specify a general motor neuron fate, although the zinc finger homeodomain factor *zfh1* is expressed in all motor neurons and regulates axon guidance

(Layden et al., 2006). There are 36 motor neurons in each hemisegment, forming six major nerves that target different muscle regions. Unlike in vertebrates, the position of motor neuron cell bodies in the *Drosophila* nerve cord does not necessarily correlate with the targeting of their axons in the periphery, as neurons that innervate adjacent muscles can often be found far apart within a segment (Landgraf et al., 2003; Mauss et al., 2009). Instead, recent studies have shown that both the larval and the adult *Drosophila* neuromuscular systems use a myotopic map in which the position of motor neuron dendrites, rather than their somas, correlates with the position of their target muscles (Brierley et al., 2009; Mauss et al., 2009). This may be a well conserved feature of motor systems across phyla, as the dendritic patterning of at least four motor neuron pools in the spinal cord correlates with muscle target identity in mouse, but whether this is broadly true across motor neuron classes in vertebrates remains to be determined (Vrieseling and Arber, 2006).

In the *Drosophila* neuromuscular system, as in vertebrates, the transcription factor profile of motor neurons correlates with the projection pattern of their axons. Motor neurons that innervate the dorsal-most muscles of the body wall fasciculate along the intersegmental nerve (ISN) and express the homeodomain transcription factor Even-skipped (Eve) and the GATA family transcription factor Grain (Fig. 1.2). Motor neurons that co-express the transcription factors Hb9 (exex), Nkx6 (Hgtx), Islet (Tailup), Lim3, Oli (Olig family) and Drifter form the ISNb nerve, which innervates a group of ventral muscles (Fig 1.2). Each of these genes is required for motor axon guidance in a subset-specific manner (reviewed in Landgraf and Thor, 2006).

Eve and Grain are restricted to motor neurons that innervate dorsal muscles, and are required for their correct trajectory (Fujioka et al., 2003; Garces and Thor, 2006; Landgraf et al., 1999). Two recent studies found that Eve and Grain act in part through the Netrin receptor Unc-5 (Labrador et al., 2005; Zarin et al., 2012). In the absence of *eve* or *grain*, *unc-5* expression is reduced in the dorsally-projecting ISN pioneer neurons RP2 and aCC. Loss of *unc-5* results in stalling of the ISN nerve, similar to the defects observed in *eve* or *grain* mutants. Moreover, Unc-5 over-expression partially rescues the CNS exit defects in *eve* mosaic mutants, as well as ISN stalling in *grain* mutants, providing strong evidence that Unc5 acts downstream of both Eve and Grain.

A recent genome-wide study of mRNA isolated from FACs-sorted dorsally-projecting motor neurons (d-MNs) identified additional downstream effectors of Eve (Zarin et al., 2014). Candidate targets include four cell surface receptors of the immunoglobulin superfamily (IgSF): *unc-5*, *beat1a (beaten-path 1a), fasciclin 2* (*fas2*) and *neuroglian* (*nrg*), all of which are positively regulated by Eve. The authors of this study present a model in which Eve specifies the trajectory of d-MNs through the combinatorial regulation of guidance receptors and adhesion molecules. Although *unc-5*, *beat1a*, *nrg*, or *fas2* single mutants only weakly phenocopy *eve* mutants, simultaneous removal of these genes produces an additive phenotype that more closely resembles the loss of *eve*. Moreover, restoring the expression of the four targets in an *eve* mutant significantly rescues the CNS exit and dorsal targeting defects, once again in an additive manner. Finally, ectopic expression of *eve* in a subset of interneurons induces the expression of *unc-5*, *beat1a, nrg,* and *fas2*, and causes their axons to leave the CNS and assume a motor axon-like trajectory. Co-misexpression of these target genes reproduces

this effect. Altogether, these results strongly argue that Unc-5, Beat1a, Nrg, and Fas2 act

downstream of Eve to regulate motor axon guidance.

Zfh1 and Grain are co-expressed with Eve in dorsally-projecting motor neurons,

and Zarin et al. found that they also contribute to the expression of *unc-5*, *beat1a*, and

fas2 (Zarin et al., 2014). Moreover, ectopic expression of Zfh1 can induce *unc-5*, *beat1a*,

and *fas2* in interneurons and redirect their axons peripherally, and co-expression of Zfh1

and Eve results in an additive effect. Similarly, co-expression of Grain and Eve produces

stronger *unc-5* induction than mis-expression of either alone. Although previous studies

identified a requirement for Eve in promoting *grain* and *zfh1* expression (Zarin et al.,

2012), over-expression of Eve can induce the expression of its targets without inducing

zfh1 or *grain*. In addition, *eve; grain* double mutants have a greater decrease in *unc5*

expression than either single mutant (Garces and Thor, 2006; Zarin et al., 2012). Thus, a

coherent narrative emerges in which Eve, Grain, and Zfh1 function in parallel to promote

the expression of a shared set of downstream effectors (Fig. 1.2). Additional effectors of

Eve likely ensure that dorsal motor axons reach their target muscles, as the strongest

phenotype produced by triple *unc-5*, *beat1a*, and *nrg* mutants does not recapitulate the

effect of loss of *eve*. Nevertheless, by demonstrating a functional connection between

upstream regulatory factors and target genes, this study provides insight into how

transcriptional regulators exert their activities through a battery of effectors (Zarin et al.,

2014).

One major challenge will be to identify the cis-acting elements to which these

transcription factors bind, to allow for a mechanistic understanding of how combinations

of transcription factors impinge on common targets. For example, if multiple factors bind

to the same site, this might suggest that they form higher-order complexes that affect

their target specificities, as was recently shown for Islet1/Lhx3 and Islet1/Phox2a (paired-

like homeobox 2a) in cultured cells (Mazzoni et al., 2013; Thaler et al., 2002). In

Drosophila d-MNs, Grain might activate *unc5* directly, as the *unc5* promoter contains

consensus GATA sequences, but the relevance of these motifs to the expression pattern

of *unc5* has not been tested (Zarin et al., 2012). In contrast, Eve likely acts as a repressor,

because its conserved repressor domain is required for rescue of motor axon guidance

(Fujioka et al., 2003). Eve may regulate guidance through Hb9, as *hb9* is de-repressed in

eve mosaic mutants, and rescue experiments suggest a correlation between the extent of

motor axon guidance rescue and the extent of *hb9* de-repression (Fujioka et al., 2003).

Moreover, *grain* was identified as a down-regulated target of Hb9 and Nkx6 in a recent

microarray analysis, and a DAM-ID (DNA adenine methyltransferase identification)

analysis of the binding sites for Hb9 revealed that it is enriched near the *unc5* and *fas2*

loci (Lacin et al., 2014; Wolfram et al., 2014). Thus, one can propose a model in which

Eve represses *hb9* in RP2 and aCC, to allow for the expression of d-MN genes. In the

absence of *eve*, *hb9* is de-repressed in these cells, which might in turn lead to repression

of *grain, unc5*, and *fas2*, but future experiments will be necessary to confirm this.

A different combination of transcription factors regulates the trajectory of a subset

of ventrally-projecting motor neurons (v-MNs). The RP motor neurons 1, 3, 4, and 5

form the ISNb nerve and innervate several ventral muscles (Fig. 1.2). They co-express

the homeodomain transcription factors Hb9, Nkx6, Lim3, and Islet. Unlike their

vertebrate orthologs, these factors are not required for early aspects of motor neuron

development or survival; instead, they play subset-specific roles during late stages of

motor neuron differentiation, including axon guidance (Broihier and Skeath, 2002; Broihier et al., 2004; Thor and Thomas, 1997; Thor et al., 1999). Interestingly, although Islet1, Nkx6.1, and Lhx3 are initially broadly expressed in motor neurons in the mouse and chick spinal cord, their expression patterns subsequently become more restricted, and they act at later stages of development to regulate axon guidance and target selection in a subset-specific way, suggesting that this late role in motor neuron differentiation and axon guidance may reflect an ancient and well-conserved function for these genes (De Marco Garcia and Jessell, 2008; Luria et al., 2008; Shirasaki et al., 2006).

Until recently, it was not known how these transcription factors regulate axon guidance. In the following chapters, I present data showing that *Drosophila* Hb9 and Nkx6 act in parallel to promote the expression of the Roundabout family receptor Robo2, whereas Islet regulates a distinct downstream effector, the Netrin receptor Frazzled/DCC (Santiago et al., 2014 and Santiago and Bashaw, in preparation). *Hb9* and *islet* are sufficient to ectopically induce their respective target genes when over-expressed, and genetic rescue experiments demonstrate that these regulatory relationships are important for the guidance of ventrally-projecting motor axons to their target muscles. Interestingly, Hb9 regulates the medio-lateral position of a different subset of axons within the CNS through *robo2* and the closely related gene *robo3* (Santiago et al., 2014). Islet, in turn, coordinates dendrite targeting of motor neurons in the neuropile through *frazzled*. Together, these data suggest that the relationships we have identified during motor axon guidance are reused in multiple contexts during nervous system development, including during axon and dendritic guidance at the midline.

Transcription factors and effectors regulating midline crossing

In bilaterian animals, commissural axons cross the midline to innervate targets on the opposite side of the body, allowing for the left-right coordination of sensory input and behavior (reviewed in Dickson and Zou, 2010). In the vertebrate spinal cord, the secreted ligands Netrin and Shh promote the extension of axons toward the floor plate by signaling through the DCC and Boc [bi-regional cell-adhesion molecule-related/downregulated by oncogenes (Cdon) binding protein] receptors, respectively. Midline-derived Slits, Semaphorins, and Ephrins engage their respective receptors to ensure that commissural axons do not stall or recross the midline. These repulsive cues are also detected by ipsilateral axons, which never cross the midline. The complement of guidance receptors expressed by growth cones as they approach the midline thus determines whether they will acquire a commissural or ipsilateral trajectory. In particular, recent studies in the spinal cord and in retinal ganglion cells (RGCs) of mice embryos have revealed the importance of the transcriptional regulation of Robo and Eph receptors in this process (Fig. 1.3).

Transcriptional control of midline crossing through the regulation of Robo3 expression

In mice, Robo1 and Robo2 prevent the inappropriate crossing of axons by signaling repulsion in response to Slit secreted from the floor plate (Long et al., 2004). *Robo1* and *Robo2* mRNA are detected in both commissural and ipsilateral neurons in the spinal cord, suggesting that their transcriptional regulation is not instructive in this system. The divergent Robo family member Robo3 (previously Rig-1) promotes midline crossing by antagonizing Robo1 and Robo2 by an unknown mechanism (Sabatier et al.,

13

2004). In *Robo3* mutants, commissural axons are prematurely responsive to Slit and fail

to cross the midline. The *Robo3* phenotype in the spinal cord is partially rescued by loss

of *Robo1* and *Robo2*, suggesting that Robo3 acts in part by inhibiting repulsive Robo

signaling (Jaworski et al., 2010; Sabatier et al., 2004). Analyses of the expression pattern

of *Robo3* in the spinal cord reveal that it is restricted to commissural neurons, and that its

mis-expression causes ipsilateral axons to ectopically cross the midline, demonstrating

that one key feature of commissural identity involves turning on *Robo3* (Chen et al.,

2008; Escalante et al., 2013; Inamata and Shirasaki, 2014).

In the dI1c interneurons, a subset of contralateral interneurons in the dorsal spinal

cord, the LIM homeodomain transcription factors Lhx2 and Lhx9 are required for

midline crossing and *Robo3* expression (Wilson et al., 2008) (Fig. 1.3). The dI1

interneurons receive proprioceptive information from sensory neurons and relay it to the

brain. After neurogenesis, they segregate into dI1c neurons, which settle at a medial

position and are commissural, and dI1i neurons, which are found more laterally and are

ipsilateral. In *Lhx2/Lhx9* double mutants, dI1c axons fail to cross the midline, and *Robo3*

mRNA and protein levels are reduced (Wilson et al., 2008). Other dI1 transcription

factors are expressed at normal levels, as are *DCC* and *Robo1*, and the initial ventral

trajectory of dI1c axons is unaffected, indicating that Lhx2 and Lhx9 do not regulate all

aspects of dI1c differentiation. The severity of the dI1c midline crossing phenotype in the

Lhx2/Lhx9 double mutants resembles that of *Robo3* mutants, suggesting that *Robo3* is a

downstream effector of *Lhx2* and *Lhx9*. Moreover, Lhx2 binds in vitro to a *Robo3*

genomic fragment containing two LIM homeodomain binding sites, and chromatin

immunoprecipitation (ChIP) experiments found that Lhx2 binds to the *Robo3* promoter in

14

spinal cord extracts (Marcos-Mondéjar et al., 2012). Together, these data strongly argue

that Lhx2 and Lhx9 promote midline crossing by directly activating the expression of

Robo3 in dI1c neurons. Of note, midline crossing and *Robo3* expression are not affected

in other classes of commissural neurons, implying that multiple programs activate *Robo3*

in a subset-specific manner. Furthermore, although both dI1c and dI1i neurons initially

express Lhx2 and Lhx9, Lhx2 is subsequently down-regulated in dI1i neurons. In the

absence of the Bar-class homeobox gene Barhl2, dI1i neurons ectopically express Lhx2

and Robo3 and aberrantly cross the midline, suggesting that down-regulation of Lhx2 is

critical for maintaining an ipsilateral trajectory in these cells (Ding et al., 2011).

Zic2 regulates an ipsilateral trajectory through Eph receptors

Recent studies have demonstrated an instructive role for the zinc homeodomain

transcription factor Zic2 in promoting ipsilateral guidance through the regulation of Eph

receptors. In the brain and spinal cord, EphA4 regulates midline crossing by signaling

repulsion in response to midline-localized ephrins (Dottori et al., 1998; Kullander et al.,

2001). *EphA4* mutant mice have a hopping gait caused by ectopic midline crossing of a

subset of ventral interneurons that contribute to the central pattern generator (Kullander et

al., 2003). EphA4 is also required in a group of dorsal interneurons to prevent crossing at

the dorsal midline (Escalante et al., 2013; Paixão et al., 2013). Zic2 is required for *EphA4*

expression and ipsilateral guidance in dILB neurons, which are distinct from dI1i neurons

and do not express Barhl2, Lhx2, or Lhx9 (Escalante 2013) (Fig. 1.3). ChIP experiments

demonstrate that Zic2 binds to the *EphA4* promoter in spinal cord extracts. In addition,

Zic2 can induce *EphA4* and repress *Robo3* and *Lhx2* when ectopically expressed,

suggesting it may regulate midline crossing through multiple effectors, although an endogenous requirement for *Zic2* in repressing *Robo3* and *Lhx2* was not demonstrated. Finally, EphA4 is expressed in many neurons in the brain and spinal cord that do not express Zic2, suggesting that distinct transcription factors act in a subtype-specific manner to activate *EphA4*, reminiscent of the manner by which *Robo3* is regulated.

Zic2 also regulates midline guidance at the optic chiasm by promoting the expression of EphB1 in retinal ganglion cells, demonstrating how the regulatory relationship between Zic2 and Eph receptors is reused in multiple contexts (García-Frigola et al., 2008; Herrera et al., 2003; Lee et al., 2008b). In mice, most retinal ganglion cell (RGC) axons project across the midline to innervate targets on the opposite side of the brain, and a small subset of ipsilateral projections allows for binocular vision (Herrera et al., 2003). EphB1 is exclusively expressed in ipsilateral RGCs and regulates their trajectory by signaling repulsion in response to midline-localized ephrin-B2 (Williams et al., 2003). Zic2 is also restricted to ipsilateral RGCs, where it is required for *EphB1* expression and for ipsilateral guidance (Fig. 1.3). Over-expression of Zic2 causes an increase in *EphB1* mRNA and a decrease in midline crossing, and this phenotype is partially suppressed in an *EphB1* mutant. Interestingly, in a subset of contralateral RGCs, Islet2 is required to promote midline crossing and to repress *Zic2* and *EphB1* expression (Pak et al., 2004) (Fig. 1.3). Although direct binding data for these transcription factors to their targets has yet to be demonstrated, a model emerges in which a transcriptional repressor specifies the trajectory of one class of retinal axons by restricting the expression of another transcription factor, which itself impinges on an axon guidance receptor,

similar to what occurs with Barhl2 and Lhx2 in spinal interneurons (Ding et al., 2011), and with Eve and Hb9 in *Drosophila* motor neurons (Fujioka et al., 2003).

The factors that regulate *Robo3* and *EphA4* expression in other subsets of spinal cord neurons remain to be identified. In addition, the mechanism by which Robo3 promotes midline crossing is unclear, although genetic evidence suggests that Robo3 is required to down-regulate Robo1/2-mediated repulsive signaling, as discussed above. Mammalian Robo3 does not bind Slit with high affinity, suggesting that it is not likely to act by titrating Slit away from Robo1 and Robo2 (Zelina et al., 2014). Interestingly, a recent study found that Robo3 forms a complex with DCC and potentiates DCC's response to Netrin during the migration of pontine nucleus neurons in the mouse brain (Zelina et al., 2014). Whether this mechanism is also used by spinal commissural neurons during midline crossing remains to be determined. The expression pattern of *Robo3*, together with analyses of the transcription factor mutants described above, strongly suggest that Robo3 acts cell autonomously in commissural neurons to promote midline crossing. In Chapter 4, I describe a new mechanism by which *Drosophila* Robo2 promotes midline crossing through non cell-autonomous inhibition of Robo1. It is curious that Robo receptors in both insect and vertebrate lineages evolved the ability to down-regulate Robo-mediated repulsion. This appears to be an example of convergent evolution, as *Robo* genes diversified independently through genome duplication events specific to each lineage (Evans and Bashaw, 2012; Zelina et al., 2014). It will be highly informative to obtain a more detailed understanding of the mechanisms by which *Drosophila* Robo2 and vertebrate Robo3 regulate repulsive Robo signaling, and to

determine how the mechanisms that control their expression patterns contributed to the diversification of their functions.

Transcription factors and effectors regulating dendritic morphology in sensory neurons

The position, size and shape of a neuron's dendritic arbor are critical aspects of its identity, as they determine its sites of synaptic input. Indeed, genetic manipulations that disrupt dendrite morphology or position can result in defects in connectivity and function (Kostadinov and Sanes, 2015; Sun et al., 2013; Vrieseling and Arber, 2006). A large body of evidence suggests that multiple aspects of dendrite morphology are intrinsically programmed by cell autonomous factors (reviewed in Lefebvre et al., 2015; Puram and Bonni, 2013), and while many transcription factors have been shown to act in a cell-type specific manner to regulate dendrite development across the nervous system, the downstream programs by which these factors act in the CNS remain poorly characterized (Enriquez et al., 2015; Komiyama and Luo, 2007; Komiyama et al., 2003; Vrieseling and Arber, 2006). Sensory neuron dendrites of invertebrates have served as a powerful model for understanding how intrinsic and extrinsic factors regulate the formation of dendritic arbors (Jan and Jan, 2010; Lefebvre et al., 2015). Below, we discuss recent studies in *Drosophila* and *C. elegans* sensory neurons that identify functional effectors of transcription factors that control dendrite morphology.

Transcriptional regulation of morphology in Drosophila dendritic arborization neurons

The dendritic arborization (da) sensory neurons of *Drosophila* larvae form a largely two-dimension array between the body wall muscles and the epidermis (Corty et al., 2009; Jan and Jan, 2010). There are four classes of da neurons, which can be distinguished by their transcription factor profile, dendritic morphology, and sensory function (Fig. 1.5). Class I neurons are proprioceptive and have the simplest dendritic arbors (Grueber et al., 2002; Hughes and Thomas, 2007). They can be identified by the expression of the BTB/zinc finger transcription factor Abrupt (Ab), which is both required and sufficient to promote their simple morphology (Li et al., 2004; Sugimura et al., 2004). Class II neurons respond to gentle touch and form larger and more complex arbors than class I neurons (Grueber et al., 2002; Tsubouchi et al., 2012). They express low levels of the homeodomain transcription factor Cut, which is required for their growth (Grueber et al., 2003a). Class III neurons respond to gentle touch and form more complex arbors than class I or II neurons (Grueber et al., 2002; Grueber et al., 2003b; Tsubouchi et al., 2012; Yan et al., 2013). They can be identified by the presence of actin-rich filopodial spikes along their dendrites, and by the highest levels of Cut expression. Cut is required for the formation of these filopodia, and for dendritic growth and branching (Grueber et al., 2003a). Class IV neurons are polymodal nociceptive detectors that are activated by harsh mechanical stimuli and high temperatures (Hwang et al., 2007). They form extensive, space-filling dendritic arbors that display self-avoidance and that do not overlap with dendrites from neighboring class IV neurons (Grueber et al., 2002). Class IV neurons express intermediate levels of Cut, which is required for their normal growth and branching (Grueber et al., 2003a). Expression of the COE

(Collier/Olf-1/EBF) transcription factor Knot in da neurons is restricted to the class IV

neurons, where it is required for the formation of their complex dendritic arbors

(Crozatier and Vincent, 2008; Hattori et al., 2007; Jinushi-Nakao et al., 2007). Below, I

discuss several recent studies that have identified putative downstream effectors of these

transcription factors in regulating da neuron morphology (Fig. 1.4).

In class IV da neurons, the microtubule severing protein Spastin may act

downstream of Knot by creating new sites for microtubule growth (Jinushi-Nakao et al.,

2007). *Spastin* heterozygotes display class IV da neuron defects that resemble those of

knot mutants, including reduced dendritic arbors and decreased branching. Furthermore,

spastin is upregulated when Knot is over-expressed, and knocking down *spastin*

suppresses the ectopic branching phenotype caused by Knot mis-expression. However,

this model awaits evidence that endogenous *spastin* levels are down-regulated in da

neurons in the absence of Knot.

The actin-bundling protein Singed/Fascin is required for class III da neuron

morphology, and a recent study suggests its activity may be Cut-dependent (Nagel et al.,

2012). Fascin is present in the cell bodies of all da neurons, but is not found within the

dendrites of class I, II, or IV neurons, whereas it is enriched in the filopodial spikes of

class III neurons, and is required for their formation. Cut over-expression produces

ectopic Fascin-positive filopodia. To determine if Fascin is a downstream effector of Cut,

the authors over-expressed Cut in *fascin* mutants, and observed reduced ectopic filopodia.

As Fascin is expressed in all da neurons, it is unlikely that Cut regulates its expression in

a class-specific manner; instead, high levels of Cut might promote Fascin activity

indirectly, by inducing the expression of programs that control Fascin sub-cellular localization in class III neurons.

The guanine nucleotide exchange factor (GEF) Trio may also act downstream of Cut, as it is upregulated by Cut over-expression and its absence produces a similar phenotype to that seen in the absence of Cut (Iyer et al., 2012). Moreover, *trio* knockdown suppresses the ectopic branching phenotype generated by Cut mis-expression, and Trio over-expression partially rescues branching defects caused by loss of Cut. However, Cut is not endogenously required for Trio expression in da neurons, suggesting that additional factors act redundantly with Cut to regulate *trio*. Similarly, Cut can induce expression of the cell surface receptor Turtle, and reducing Turtle levels suppresses the effect of Cut over-expression, but Cut is not required for *turtle* expression (Sulkowski et al., 2011). Thus, the main transcriptional targets of Cut that mediate its effects on dendritic morphology remain to be identified.

Uemura and colleagues recently undertook an unbiased approach to identify novel targets of Ab and Knot (Hattori et al., 2013). They performed genome-wide DAM-ID analyses for Ab and Knot binding sites, as well as gene expression analyses in larvae over-expressing Ab or Knot in da neurons. They cross-referenced these data to identify genes that were bound by either factor, and that responded to changes in Ab or Knot levels. Candidate targets were then validated by examination of their loss of function phenotypes.

One shared upregulated target of Ab and Knot that emerged from this analysis was the BTB/POZ transcription factor Lola, and a subsequent study by van Meyel and colleagues demonstrated that Lola controls dendritic morphogenesis through the actin

nucleating protein Spire (Ferreira et al., 2014). Lola is expressed in all classes of da neurons, where it is required for dendritic branching and growth. In its absence, Cut and Knot levels are decreased in class IV neurons, suggesting a positive feedback loop between Lola and Knot. In addition, Lola is required in class I and IV neurons to inhibit the formation of actin-rich protrusions near the cell body. Loss of *lola* results in increased levels of the actin regulator Spire, suggesting that *spire* misregulation may contribute to the *lola* phenotype. Indeed, heterozygosity for *spire* suppresses the ectopic protrusions in *lola* mutant neurons, and partially rescues dendritic growth. Moreover, *lola* knock-down in class IV neurons results in a head-turning defect that is characteristic of defective nociception. Strikingly, heterozygosity for *spire* also rescues these behavioral defects. Together, these data suggest that Lola regulates dendrite morphogenesis by down-regulating *spire*.

Another target of Ab and Knot identified by Uemura and colleagues that plays a role in regulating dendritic morphology is the cell surface receptor Teneurin-m (ten-m), which mediates synaptic partner selection in the adult olfactory system and larval neuromuscular system (Hattori et al., 2013; Hong et al., 2012; Mosca et al., 2012). Both Ab and Knot can upregulate *ten-m*, although Ab has a greater effect. Accordingly, Ten-m is expressed in both class I and IV da neurons, with higher levels in class I neurons. *ab* mutants have decreased Ten-m expression, and *ten-m* loss of function disrupts the directionality of the class I dendritic branches, reproducing one aspect of the *ab* mutant phenotype. Importantly, the knockdown of *ten-m* in class IV neurons also results in defects in the position of their dendrites, demonstrating an endogenous requirement for low levels of Ten-m in these cells. In addition to its expression in da neurons, Ten-m is

22

present in the epidermis in a non-uniform manner, and epidermal-specific *ten-m* knockdown or over-expression can change the directionality of dendritic projections, suggesting that homophilic Ten-m interactions between neurons and epidermal cells influence dendritic patterning. Following on this, Uemura and colleagues present a model in which Abrupt ensures that high levels of Ten-m are present in class I da neurons to signal repulsion and direct dendrites posteriorly, whereas Knot promotes low levels of Ten-m in class IV neurons to confer normal dendritic morphology (Hattori et al., 2013). Additional genetic experiments, such as a rescue of the *ab* or *knot* phenotypes, would further strengthen the model, and identifying the factors that regulate epidermal Ten-m expression would shed light on how its expression is coordinately regulated across tissues.

Transcriptional regulation of dendritic morphology in the C. elegans PVD neuron

Recent studies of the *C. elegans* PVD polymodal sensory neuron have emphasized the importance of neural-epidermal interactions during sensory dendrite morphogenesis, and shed light on how transcription factors establish cell-type specific morphologies. PVD neurons are required for the worm's avoidance response to harsh touch, cold and hyperosmolarity (Chatzigeorgiou et al., 2010; Way and Chalfie, 1989). During larval development, the two PVD neurons form highly branched dendritic arbors which grow to envelop the animal on each side of the body (Fig. 1.4). These arbors exhibit many of the typical features of sensory neurons, including self-avoidance among sister branches and tiling with the functionally related FLP neuron in the head (Smith et al., 2010).

23

MEC-3 is a LIM homeodomain factor required for the specification of both PVD neurons and light touch neurons (Way and Chalfie, 1989; Zhang et al., 2002). In *mec-3* mutants, the PVD cell body position and axon are normal, but PVD dendrites display dramatic growth defects and fail to initiate secondary branches (Smith et al., 2010; Tsalik et al., 2003). These defects are rescued by PVD-specific expression of MEC-3 (Smith et al., 2013). A recent study identified *hpo-3/claudin* as a downstream effector of MEC-3 in regulating PVD morphology (Smith et al., 2013). Miller and colleagues compared the mRNA profiles of PVD neurons from wild type animals with those from *mec-3* mutants, and identified many putative MEC-3 targets, including *hpo-30/claudin*. *hpo-30* is required cell autonomously for the formation of dendritic branches in PVD neurons; in its absence, secondary branches initiate but are not stabilized. The similarity of the loss of function phenotypes of *hpo-30* and *mec-3*, as well as the observation that *mec-3* is required for expression of an *hpo-30::GFP* reporter in PVD neurons, make HPO-30 a likely downstream effector of MEC-3. However, HPO-30 over-expression in *mec-3* mutants does not rescue their branching defects, suggesting that additional targets of MEC-3 are required for normal PVD morphology (Fig. 1.4).

MEC-3 is also expressed in light touch neurons, which have very simple dendrites (Way and Chalfie, 1989). How does MEC-3 regulate dendritic morphology in a cell-type specific manner? Smith et al. (2013) demonstrate that in the AVM light touch neuron, the bHLH transcription factor AHR-1 down-regulates MEC-3 targets that promote a PVD morphology, while simultaneously promoting expression of *mec-3* itself (Smith et al., 2013). In *ahr-1* mutants, the AVM neuron is transformed into a PVD-like neuron both morphologically and functionally; the morphological change is *mec-3*-dependent.

24

Therefore, the authors hypothesize that AHR-1 is required to repress MEC-3 targets that promote a PVD morphology. Indeed, *hpo-30/claudin* is not expressed in light touch neurons in wild type animals, but is ectopically expressed in the AVM neuron in *ahr-1* mutants. Moreover, in *ahr-1; hpo-30* double mutants, the ectopic dendritic branches in the AVM neuron are fully suppressed, further demonstrating HPO-30's role as a key regulator of dendritic morphology.

Another essential regulator of PVD morphology is DMA-1, a transmembrane receptor expressed in PVD neurons. In its absence, dendritic arbors are greatly reduced (Liu and Shen, 2012). Two recent studies demonstrated that DMA-1 forms a complex in trans with the MNR-1 and L1CAM/SAX-7 receptors expressed in the skin, and that this complex promotes dendritic growth (Dong et al., 2013; Salzberg et al., 2013). The *dma-1* phenotype is strikingly similar to the *mec-3* and *hpo-30* phenotypes. Although *dma-1* was not identified as a MEC-3-dependent gene by Smith et al. 2013, it will be interesting to determine if HPO-30 converges on the same pathway as DMA-1, MNR-1, and SAX-7 to regulate interactions between sensory neurons and epidermal cells that promote dendritic growth and branching.

Transcriptional effectors that instruct synaptogenesis in *C. elegans* motor neurons

Axonal targeting and dendrite morphogenesis are essential for neural connectivity, as the position of a neuron's axons and dendrites will restrict its choice of available synaptic partners. However, the neurites of neurons often extensively overlap in space without forming synapses, and it is therefore clear that additional cues drive partner selection and synaptogenesis. Many such pre- and post-synaptic molecules have been

identified, and have been shown to exhibit cell-type specific patterns and to act before the onset of neural activity, reflecting an intrinsic genetic program (reviewed in Shen and Scheiffele, 2010). However, how the expression of these cues is regulated remains largely unclear. Below, I briefly review recent studies in *C. elegans* motor neurons that shed light on the transcriptional mechanisms that regulate synapse formation during development.

The DD and VD motor neurons are GABAergic motor neurons in the ventral nerve cord that receive input from cholinergic motor neurons. DD neurons undergo extensive synaptic remodeling between larval stages and adulthood: at the L1 stage, they receive input from dorsal motor neurons and innervate ventral muscles. By adulthood, this is reversed, such that mature DD neurons receive input from ventral motor neurons, and innervate dorsal muscles (Fig. 1.5). VD neurons develop after the L1 molt, and receive input from dorsal motor neurons, and innervate ventral muscles (Fig. 1.5). A pair of recent studies identified a transcription factor network that regulates synapse positioning in the DD and VD neurons, and demonstrated that these factors act at least in part through the regulation of the secreted immunoglobulin (Ig)-domain protein OIG-1 (He et al., 2015; Howell et al., 2015).

OIG-1 is a short, single Ig domain-containing protein that is highly expressed in VD neurons throughout adulthood, and in DD motor neurons before L1. In contrast, OIG-1 is not expressed in mature DD neurons. Loss of function experiments indicate that OIG-1 organizes the synaptic inputs and outputs of DD and VD motor neurons. In *oig-1* mutants, L1 DD neurons lose their dorsal cholinergic inputs. Pre-synaptic markers are ectopically localized dorsally, while post-synaptic markers are ectopically localized

ventrally. Similarly, in *oig-1* mutants, VD neurons receive fewer dorsal inputs, and form

fewer ventral synapses and ectopic dorsal synapses. What factors regulate the expression

of *oig-1* in these neurons to direct synapse assembly? The Pitx-type homeodomain

transcription factor UNC-30 is expressed in DD and VD neurons at all stages, and was

previously shown to control GABAergic neurotransmitter identity (Eastman et al., 1999).

unc-30 mutants lose *oig-1* expression in both DD and VD neurons, and phenocopy the

synaptic defects of *oig-1* mutants. However, UNC-30 is expressed in mature DD neurons,

which do not express *oig-1*. What, then, distinguishes young DD neurons from mature

ones? LIN-14, a transcription factor expressed throughout the body during embryonic and

early larval stages, is required for *oig-1* expression in L1 DD neurons, and prolonged

expression of *lin-14* results in prolonged expression of *oig-1* in mature DD neurons

(Howell et al., 2015). In addition, the Iroquois homeodomain family transcription factor

IRX-1 is expressed in mature DD neurons, where it is required for *oig-1* repression. In

VD neurons, the COUP-TF factor Unc-55 represses IRX-1, allowing for *oig-1*

expression. To summarize, in L1 DD neurons, high levels of OIG-1, driven by UNC-30

and LIN-14, promote the formation of dorsal cholinergic inputs and ventral GABAergic

outputs (Fig. 1.5). As DD neurons mature, they lose *oig-1* expression, both due to the loss

of LIN-14 expression and the repressive activity of IRX-1; thus, synaptic remodeling

occurs. In VD neurons, UNC-55 represses IRX-1, allowing for high levels of OIG-1,

which drives VD neurons to receive cholinergic input on the dorsal side of the body, and

to innervate ventral muscles (Fig. 1.5).

How OIG-1 coordinates pre- and post-synaptic assembly remains unknown. OIG-

1 is a secreted molecule, but interestingly, both studies found that it acts cell

autonomously, though they differed in their reports on its protein localization (He et al., 2015; Howell et al., 2015). Though the mechanism by which OIG-1 acts remains to be elucidated, these studies clearly demonstrate a novel role for this protein during synapse assembly in a subset of motor neurons, and show that multiple transcription factors operate together to ensure that this synaptic organizer is expressed in the right cells at the right time.

Another recent study from Hobert and colleagues found that a transcription factor required for the expression of genes that confer neurotransmitter identity is also required for the structural assembly of synapses (Kratsios et al., 2015). The COE-type transcription factor UNC-3 is expressed in a subset of cholinergic motor neurons, where it is required for the acquisition of a cholinergic identity, as well as for axonal morphology (Kratsios et al., 2012; Prasad et al., 1998). It was recently found that in the head SAB motor neurons, UNC-3 also regulates synapse assembly, in part through *madd-4* (Kratsios et al., 2015) (Fig. 1.5). MADD-4/Punctin is a secreted protein of the Adam-TS family (extracellular proteins related to Adam metalloproteases that lack catalytic activity), which was previously shown to act in cholinergic motor neurons to regulate the clustering of acetylcholine receptors in their post-synaptic target muscles (Maro et al., 2015; Pinan-Lucarré et al., 2014; Tu et al., 2015). UNC-3 is required for *madd-4* expression in a subset of motor neurons, including the SAB head motor neurons and the DA and DB motor neurons in the ventral nerve cord, and likely acts by directly binding to COE sites within the *madd-4* promoter, as demonstrated by *in vivo* experiments using GFP reporters fused to enhancer fragments (Kratsios et al., 2015). In *unc-3* mutants, post-synaptic acetylcholine receptors are mis-localized in the muscle cell targets of SAB

neurons, phenocopying the defects seen in *madd-4* mutants. In addition, pre-synaptic

components fail to localize correctly in motor neurons, a phenotype that is not observed

in *madd-4* mutants, suggesting that UNC-3 acts through distinct downstream effectors to

coordinate pre- and post-synaptic assembly. Moreover, several other SAB markers,

including ion channels and neurotransmitter receptors, fail to be expressed in *unc-3*

mutants. Importantly, *unc-3* is not required for the expression of genes that are broadly

expressed in the nervous system, confirming previous reports that it selectively regulates

cell-type specific gene programs (Kratsios et al., 2012). In addition, synaptic clustering

and *unc-3* expression are normal in animals in which SAB neurons are silenced,

demonstrating that this molecular program acts independently of neural activity (Kratsios

et al., 2015).

Whether other transcription factors previously found to specify neurotransmitter

identity also act in a cell-type specific manner to regulate synapse formation remains an

open question. Interestingly, the co-regulation of genes related to morphology and neural

function has been reported in several other instances, including some involving the

transcription factors discussed in previous sections: Zic2 regulates the expression of the

serotonin transporter *SerT* in the retina (García-Frigola and Herrera, 2010); Isl1 promotes

cholinergic identity in motor neurons and in a subset of forebrain neurons (Cho et al.,

2014); and in *Drosophila* sensory neurons, Knot is required for the expression of the

class IV da neuron gene *pickpocket*, which encodes a subunit of a Degenerin/epithelial

sodium channel family protein that is required for the response to nociceptive touch

(Crozatier and Vincent, 2008; Hattori et al., 2007; Zhong and Hwang, 2010). It will be

informative to determine if other transcription factors that have been characterized

primarily for their roles during neuronal morphogenesis have broader functions in determining multiple aspects of neural identity and function.

Conclusion

As we begin to build a detailed map of regulatory relationships during neural circuit formation in diverse model systems, common themes emerge, and suggest key questions for future research. It is interesting that repressive interactions between transcription factors, which were shown many years ago to be an essential mechanism by which cell fates are patterned in the spinal cord (Muhr et al., 2001), continue to be important for later events in neuronal morphogenesis and synaptic differentiation. In many cases, how combinations of transcription factors result in specific cell surface receptor profiles remains unclear, however. In the following chapters, I show that Hb9 and Nkx6 act in parallel to regulate axon guidance through the Robo2 receptor in a subset of neurons, and that Islet acts in the same cells to regulate the Frazzled receptor, thus demonstrating how a transcription factor code is read to produce a particular complement of guidance receptors that work together to direct axon pathfinding.

Mounting evidence suggests that the co-regulation of multiple features of neural morphology by individual transcription factors may be a broadly used developmental strategy, but whether regulatory relationships between transcription factors and cellular effectors are redeployed during the different steps of neural circuit assembly remains an open question. In Chapter 3, I demonstrate that Islet coordinately regulates the targeting of motor axons in the periphery and of motor neuron dendrites in the CNS through *fra*,

providing an example of how a single transcription factor can specify both the inputs and outputs of a neuron through an effector gene involved in both processes.

Finally, it is important to note that the regulation of cell surface receptor expression continues long after transcription. Mechanisms that control mRNA stability, processing, and translation have all been shown to contribute to achieving precise spatio-temporal patterns of guidance receptor expression, as have post-translational mechanisms that regulate surface levels through trafficking or endocytosis (Allen and Chilton, 2009; Bai and Pfaff, 2011; Hörnberg and Holt, 2013; O'Donnell et al., 2009; Yap and Winckler, 2012). Moreover, once a receptor is present at the surface of a neuron, its activity can be silenced by antagonistic factors. In Chapter 4, I present a mechanism in which *Drosophila* Robo2 acts in a non-cell autonomous manner to down-regulate the activity of Robo1, demonstrating how regulatory mechanisms continue post-transcriptionally, and how the precise expression pattern of a guidance receptor can allow it to exert multiple distinct activities during nervous system development.

Figure 1.1. Downstream effectors of transcription factors during vertebrate motor axon guidance.
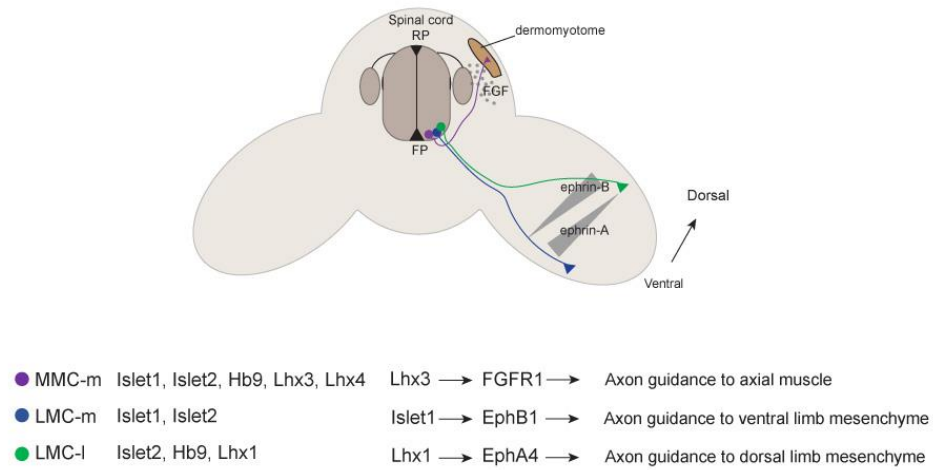
Figure 1.1. Downstream effectors of transcription factors during vertebrate motor axon guidance.

Cross-section of a mouse spinal cord at limb levels. In MMC-m neurons (purple), Lhx3 promotes the expression of the FGF receptor FGFR1 and guides axons to the dermomyotome (dm), which expresses FGF ligands and is attractive to motor axons. In LMC-m neurons (blue), Islet1 directs motor axons into the ventral limb mesenchyme through upregulation of EphB1. In LMC-l neurons (green), Lhx1 promotes EphA4 expression and the selection of a dorsal trajectory into the limb. EphB1 and EphA4 signal repulsion in response to ephrin-B and ephrin-A ligands present in the limb mesenchyme, respectively. Abbreviations: RP, roof plate. FP, floor plate. FGF, fibroblast growth factor. MMC-m, medial class of medial motor column. LMC-m, medial class of lateral motor column. LMC-l, lateral class of lateral motor column.

Figure 1.2. Downstream effectors of transcription factors during *Drosophila* motor axon guidance.
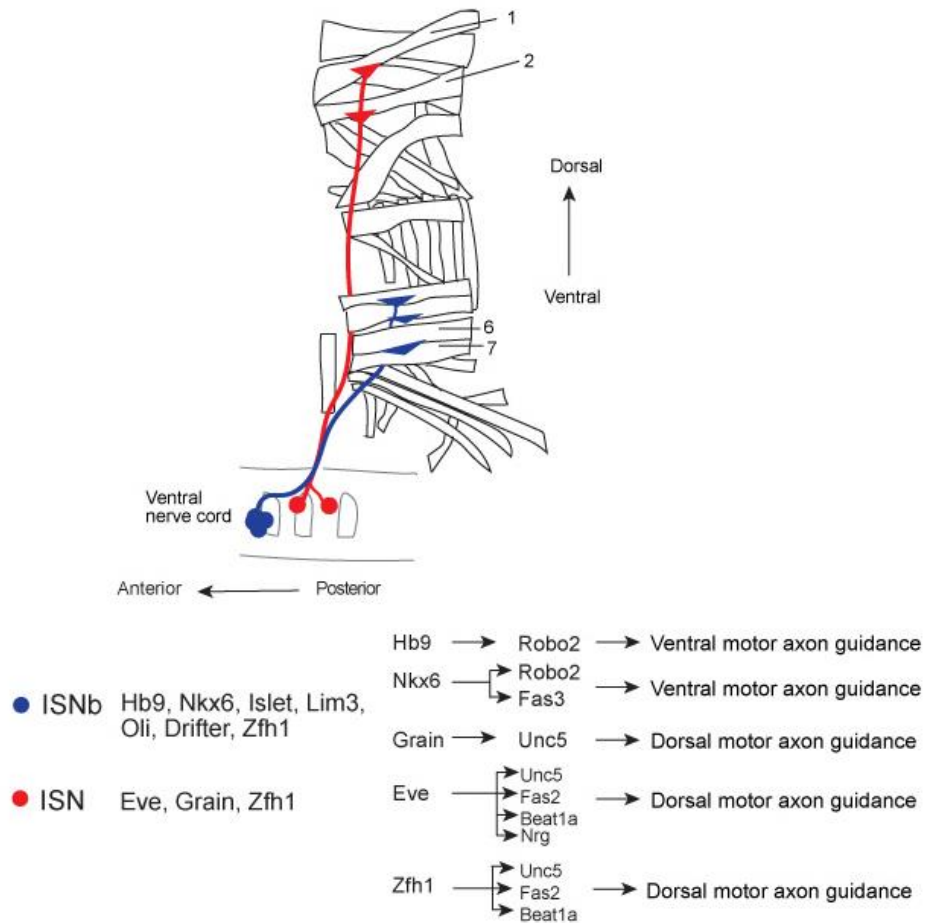
Figure 1.2. Downstream effectors of transcription factors during *Drosophila* motor axon guidance. A single hemisegment in a filleted late stage 17 *Drosophila* embryo. Not all motor nerves are shown. In ISNb motor neurons (blue), Hb9 and Nkx6 promote the expression of Robo2 and Fas3 and direct axons to the ventral muscles 6 and 7. In dorsally-projecting ISN motor neurons (red), Eve, Grain, and Zfh1 regulate guidance by promoting the expression of Unc5, Fas2, Beat1a, and Nrg receptors. Abbreviations: ISNb, Intersegmental nerve b. ISN, intersegmental nerve.

Figure 1.3. Downstream effectors of transcription factors during midline crossing in the mouse spinal cord and visual system.
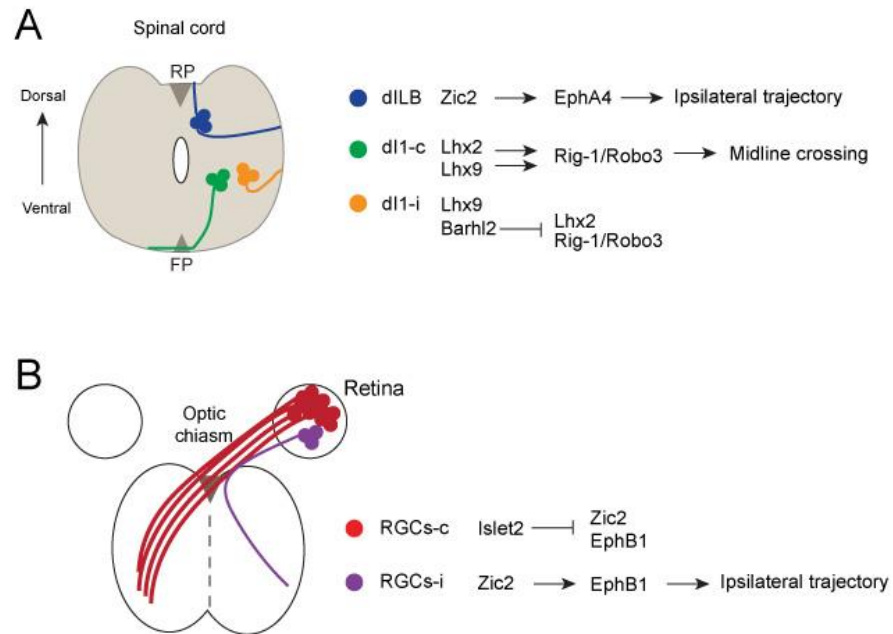
Figure 1.3. Downstream effectors of transcription factors during midline crossing in the mouse spinal cord and visual system.

A: Cross-section of a mouse spinal cord at E16. In dILB interneurons (blue), Zic2 promotes the selection of an ipsilateral trajectory through the upregulation of EphA4. In dI1-c interneurons (green), Lhx2 and Lhx9 are required for Robo3 expression and midline crossing. In dI1-i interneurons (orange), Barhl2 is required for the repression of Lhx2 and Robo3, and for maintenance of an ipsilateral trajectory. Abbreviations: RP, roof plate. FP, floor plate.

B: Schematic of the mouse visual system at E15.5. In a subset of contralateral retinal ganglion cells (RGCs-c, red), Islet2 is required to repress Zic2 and EphB1 expression, and to promote midline crossing. In ipsilateral RGCs (RGCs-I, purple), Zic2 is required for EphB1 expression and an ipsilateral trajectory.

Figure 1.4. Transcriptional regulation of dendritic morphology in *Drosophila* dendritic arborization neurons and the *C.elegans* PVD neuron.
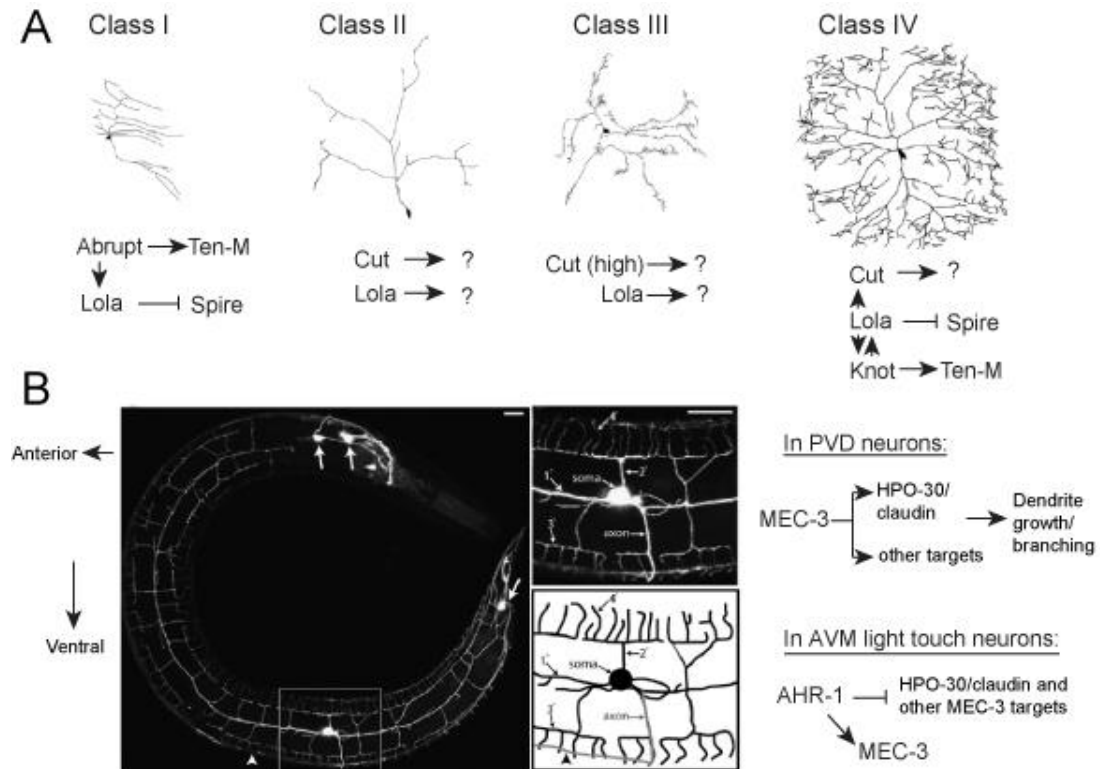
Figure 1.4. Transcriptional regulation of dendritic morphology in *Drosophila* dendritic arborization neurons and the *C. elegans* PVD neuron.

A: Camera lucida drawings of the four classes of dendritic arborization (da) neurons. Adapted with permission from (Grueber et al., 2003a). In class I da neurons, Abrupt (Ab) regulates morphology in part through up-regulation of the cell surface receptor Teneurin-m (Ten-m) and the transcription factor Lola. Lola promotes class I neuron morphology by repressing the expression of the actin regulator Spire. In class II and III neurons, Lola and Cut act via unknown effectors to regulate dendritic morphology. Knot/Collier is restricted to class IV neurons, where it regulates dendritic morphology in part through Ten-m. Lola and Cut are also required in class IV neurons for dendritic growth, and Lola promotes class IV neuron morphology by repressing *spire*.

B: The LIM homeodomain factor MEC-3 regulates the dendritic morphology of the *C.elegans* PVD sensory neuron. Left: Adult worm expressing a *PVD::GFP* reporter. Images adapted with permission from (Smith et al., 2010). The PVD neuron forms an elaborate dendritic network that wraps around the body; the insets show a higher magnification view of the PVD cell body, its axon, and its dendritic branches. The arrows indicate other neurons that express *PVD::GFP*. The arrowhead denotes the ventral nerve cord. Scale bar is 15 μm. Right: In PVD neurons, MEC-3 drives the expression of HPO-30/claudin and other genes that promote dendritic growth and branching. In the AVM light touch neuron, AHR-1 promotes MEC-3 expression and represses the expression of MEC-3 targets that regulate branching, including HPO-30/claudin.

Figure 1.5. Transcriptional regulation of synaptogenesis in *C. elegans* motor neurons.
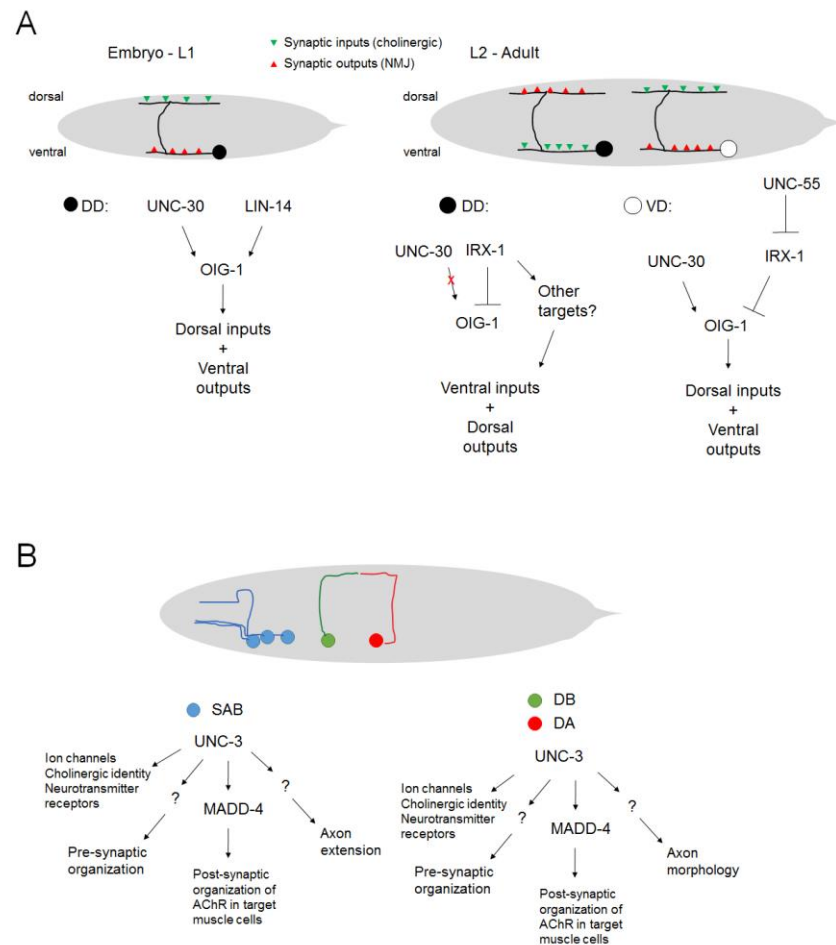
Figure 1.5. Transcriptional regulation of synaptogenesis in *C.elegans* motor neurons.

A: Schematic of DD and VD synaptic inputs and outputs at different developmental stages. Up to the L1 larval stage, DD neurons receive cholinergic inputs from dorsal motor neurons, and form GABAergic synapses onto ventral muscles. UNC-30 and LIN-14 are both required for OIG-1 expression in DD neurons, and OIG-1 is required for normal synapse organization. VD neurons are not present. At the L2 stage and later, DD neurons no longer express OIG-1, due to the absence of LIN-14, and due to repression of OIG-1 by IRX-1. Their synapses remodel such that they now receive input from cholinergic neurons on the ventral side of the body, and form outputs onto dorsal muscles. In VD neurons, both UNC-30 and UNC-55 are required for OIG-1 expression. OIG-1 drives VD neurons to form pre-synaptic structures on the ventral side, and to receive cholinergic input from dorsal neurons. Abbreviations: NMJ, neuromuscular junction.

B: Schematic of a subset of cholinergic motor neurons in *C. elegans*. In the SAB head motor neurons, as well as the DA and DB neurons in the ventral nerve cord, UNC-3 regulates morphology, synapse development, and functional genes, through diverse downstream targets. MADD-4, a direct target of UNC-3, mediates UNC-3's function directing the assembly of post-synaptic structures in the targets of these motor neurons. Abbreviations: AChR, acetylcholine receptor.

Acknowledgments

CHAPTER 2

THE HOMEODOMAIN TRANSCRIPTION FACTOR HB9 CONTROLS AXON GUIDANCE IN DROSOPHILA THROUGH THE REGULATION OF ROBO RECEPTORS

Transcription factors establish neural diversity and wiring specificity; however, how they orchestrate changes in cell morphology remains poorly understood. The *Drosophila* Roundabout (Robo) receptors regulate connectivity in the central nervous system, but how their precise expression domains are established is unknown. Here we show that the homeodomain transcription factor Hb9 acts upstream of Robo2 and Robo3 to regulate axon guidance in the *Drosophila* embryo. In ventrally-projecting motor neurons, *hb9* is required for *robo2* expression, and restoring Robo2 activity in *hb9* mutants rescues motor axon defects. Hb9 requires its conserved repressor domain and functions in parallel with Nkx6 to regulate *robo2*. Moreover, *hb9* can regulate the medio-lateral position of axons through *robo2* and *robo3*, and restoring *robo3* expression in *hb9* mutants rescues the lateral position defects of a subset of neurons. Together, these data identify Robo2 and Robo3 as key effectors of Hb9 in regulating nervous system development.

Introduction

Combinations of transcription factors specify the tremendous diversity of cell types in the nervous system (Dasen, 2009; Hobert, 2011; Shirasaki and Pfaff, 2002). Many studies have identified requirements for transcription factors in regulating different events in circuit formation as neurons migrate, form dendritic and axonal extensions, and

43

select their final synaptic targets (reviewed in Polleux et al., 2007; Zarin et al., 2013). In most cases the downstream effectors through which transcription factors control changes in neuronal morphology and connectivity remain unknown, although several functional relationships have been demonstrated (Jinushi-Nakao et al., 2007; Labrador et al., 2005; Luria et al., 2008; Marcos-Mondéjar et al., 2012; Nóbrega-Pereira et al., 2008; van den Berghe et al., 2013; Wilson et al., 2008).

Conserved homeodomain transcription factors regulate motor neuron development across phyla. Studies in vertebrates and invertebrates have shown that motor neurons that project to common target areas often express common sets of transcription factors, which act instructively to direct motor axon guidance (Kania and Jessell, 2003; Kania et al., 2000; Landgraf et al., 1999; Thor and Thomas, 1997). In mouse and chick embryos, Nkx6.1/Nkx6.2 and MNR2/Hb9 are required for the specification of spinal cord motor neurons, and for axon pathfinding and muscle targeting in specific motor nerves (Arber et al., 1999; De Marco Garcia and Jessell, 2008; Sander et al., 2000; Thaler et al., 1999; Vallstedt et al., 2001). In *Drosophila*, Nkx6 and Hb9 are expressed in embryonic motor neurons that project to ventral or lateral body wall muscles, and although they are not individually required for specification, they are essential for the pathfinding of ventrally-projecting motor axons (Broihier and Skeath, 2002; Broihier et al., 2004; Odden et al., 2002). Axons that project to dorsal muscles express the homeodomain transcription factor Even-skipped (Eve), which regulates guidance in part through the Netrin receptor Unc5 (Fujioka et al., 2003; Labrador et al., 2005; Landgraf et al., 1999). *Eve* exhibits cross-repressive interactions with *hb9* and *nkx6*, which function in parallel to repress *eve* and promote *islet* and *lim3* expression (Broihier and Skeath, 2002; Broihier et al., 2004).

44

Hb9 and Nkx6 act as repressors to regulate transcription factors in the spinal cord (Lee et al., 2008a; Muhr et al., 2001; William et al., 2003); however, guidance receptors that act downstream of Hb9 and Nkx6 have not been characterized. Interestingly, in both flies and vertebrates, Hb9 and Nkx6 are also expressed in a subset of interneurons, and knockdown experiments in *Drosophila* have suggested a role for *hb9* in regulating midline crossing (Broihier et al., 2004; Odden et al., 2002; Sander et al., 2000; Vallstedt et al., 2001; Wilson et al., 2005).

Robo receptors regulate midline crossing and lateral position within the developing central nervous systems of invertebrates and vertebrates (Jaworski et al., 2010; Kastenhuber et al., 2009; Kidd et al., 1998; Long et al., 2004; Rajagopalan et al., 2000a, 2000b; Sabatier et al., 2004; Simpson et al., 2000a, 2000b). Two recent studies in mice have also identified a role for Robos in regulating motor axon guidance in specific motor neuron populations (Bravo-Ambrosio et al., 2012; Jaworski and Tessier-Lavigne, 2012). The three *Drosophila* Robo receptors have diversified in their expression patterns and functions. Robo, hereafter referred to as Robo1, is broadly expressed in the ventral nerve cord and prevents inappropriate midline crossing by signaling repulsion in response to midline-derived Slit (Kidd et al., 1998a; Kidd et al., 1999). Robo2 is initially expressed in many ipsilateral pioneers, and also contributes to Slit-mediated repulsion (Rajagopalan et al., 2000a; Simpson et al., 2000a). Subsequently, *robo2* expression is more restricted, and it is required to specify the medio-lateral position of axons (Rajagopalan et al., 2000b; Simpson et al., 2000b). Robo3 is expressed in a subset of CNS neurons, and also regulates lateral position (Rajagopalan et al., 2000b; Simpson et al., 2000b).

Characterization of the expression domains of the *Drosophila* Robos revealed an intriguing pattern, in which Robo1 is expressed on axons throughout the width of the CNS, Robo3 is found on axons in intermediate and lateral zones, and Robo2 is enriched on the most lateral axons (Rajagopalan et al., 2000b; Simpson et al., 2000b). These patterns are transcriptional in origin, as replacing any *robo* gene with the coding sequence of another Robo receptor results in a protein distribution that matches the endogenous expression of the replaced gene (Spitzweck et al., 2010) (C.S., T. Evans and G.J.B., unpublished). A phenotypic analysis of these gene-swap alleles revealed the importance of transcriptional regulation for the diversification of *robo* gene function (Spitzweck et al., 2010). *Robo2* and *robo3*'s roles in regulating lateral position are largely dependent on their expression patterns, although unique structures within the Robo2 receptor are also important for its function in lateral position (Evans and Bashaw, 2010b; Spitzweck et al., 2010). In the peripheral nervous system, the *atonal* transcription factor regulates *robo3* in chordotonal sensory neurons, directing the position of their axon terminals (Zlatic et al., 2003). In the CNS, the transcription factors *lola* and *midline* contribute to the induction of *robo1* (Crowner et al., 2002; Liu et al., 2009). However, how the expression patterns of *robo2* and *robo3* are established to direct axons to specific medial-lateral zones within the CNS remains unknown.

This study identifies a functional relationship between Hb9 and the Robo2 and Robo3 receptors in multiple contexts. We show that Hb9 acts through Robo2 to regulate motor axon guidance, and can direct the medio-lateral position of axons in the nerve cord through *robo2* and *robo3*. Furthermore, *hb9* interacts genetically with *nkx6* and requires its conserved repressor domain to regulate *robo2*. Together, these data establish a link

between transcriptional regulators and cell surface guidance receptors, providing an example of how upstream factors act through specific guidance receptors to direct circuit formation.

Results

Robo2 is required in neurons for motor axon pathfinding

Hb9 regulates motor axon pathfinding across species, but its downstream effectors remain unknown. In *Drosophila*, *hb9* is required for the formation of the ISNb nerve, which innervates a group of ventral muscles (Broihier and Skeath, 2002). In our hands, approximately 20% of hemisegments in *hb9* mutant embryos lack innervation at the muscle 6/7 cleft, while these defects are rarely observed in wild type animals or *hb9* heterozygotes (Figure 2.1). To identify potential targets of *hb9*, we examined the expression patterns of axon guidance genes by *in situ* hybridization. We found that during the stages when motor axons navigate the muscle field, *robo2* mRNA is enriched in ventrally-projecting motor neurons (Figure 2.1).

To determine whether *robo2* regulates motor axon guidance, we examined *robo2* mutant embryos for innervation defects. In *robo2* mutants, the axon that normally innervates the muscle 6/7 cleft is either absent or stalled at the main ISNb trunk in 20% of hemisegments (Figure 2.1). This phenotype is similar to that of *hb9* mutants, and is observed using multiple *robo2* alleles (Figure 2.1 and data not shown). *Robo2* heterozygotes and *robo2/+; hb9/+* double heterozygotes do not have significant defects (Figure 2.1 and data not shown). *Robo2* mutants have no defects in axons forming the ISN, SNa, SNc, TN, or ISNd nerves. Importantly, restoring one copy of an 83.9 kb BAC

transgene that contains the *robo2* locus and its flanking genomic sequence fully rescues the 6/7 innervation defects of *robo2* mutants (Figure 2.1).

Robo2 is expressed in ventral muscles and in motor neurons (Figure 2.1 and data not shown). To determine if *robo2* acts in neurons to regulate motor axon pathfinding, we expressed a *UAS-Robo2RNAi* transgene using *ftzng-Gal4*, which drives expression in many motor neurons and their precursors (Thor et al., 1999). Expressing *UAS-Robo2RNAi* with *ftzng-Gal4* in an otherwise wild type background produces no effect, but causes significant 6/7 innervation defects when expressed in *robo2* heterozygotes (Figure 2.1). Conversely, expressing *UAS-Robo2 RNAi* in *robo2* heterozygotes using the pan-muscle driver *24bgal4* has no effect (Figure 2.1). Together, these data suggest that *robo2* is required neuronally to regulate ISNb pathfinding.

Hb9 is required for robo2 expression in the RP motor neurons

To test if *hb9* regulates *robo2* in ventrally-projecting motor neurons, we examined *robo2*'s expression pattern in *hb9* mutants. In Stage 16 wild type or *hb9* heterozygote embryos, *robo2* mRNA is readily detected in the RP motor neurons (Figure 2.1). In particular, *robo2* transcript is enriched in RP3, the neuron that innervates the muscle 6/7 cleft (Figure 2.1). In *hb9* mutants, *robo2* mRNA is significantly decreased in the RP motor neurons (Figure 2.1). An average of 83% of RP3 neurons in $hb9^{kk30}$/+ embryos, but only 49% of RP3 neurons in $hb9^{kk30}$/$hb9^{ij154e}$ mutants express detectable *robo2* at Stage 16 ($p<0.001$, Student's t-test) (Figure 2.1). This difference is observed as early as Stage 14, when *robo2* mRNA begins to accumulate in RP3, and is detected using multiple *hb9* alleles (Figures 2.1, 2.3 and data not shown). Interestingly, *hb9* mutants

display no change in the expression of *robo1,* which is broadly expressed in many motor

neurons including the RPs (data not shown). To quantify the fluorescent *robo2* mRNA

signal in RP3 neurons, we measured pixel intensity and normalized the mRNA signal to

the myc signal from *islet-tau-myc*. The average relative fluorescence intensity of *robo2*

mRNA in *hb9* heterozygotes is more than twice the average value measured in *hb9*

mutants (p<0.01, Student's t-test) (Figure 2.1). We conclude that *hb9* is an essential

regulator of *robo2* in the RP motor neurons.

Robo2's activity in motor axon guidance depends on unique features of its cytodomain

Robo2 has multiple activities in the embryonic CNS, some of which cannot be

substituted for by the other Robo receptors (Evans and Bashaw, 2010b; Spitzweck et al.,

2010). To determine if Robo2's activity in motor axon guidance is a unique property of

Robo2, we examined knock-in alleles in which the coding sequences of Robo1, Robo2,

or Robo3 are knocked into the *robo2* locus, hereafter referred to as *robo2^X*, where X

represents the inserted coding sequence (Spitzweck et al., 2010). Embryos homozygous

for the *robo2^{robo2}* allele have no significant defects in motor axon pathfinding, whereas

embryos homozygous for either *robo2^{robo1}* or *robo2^{robo3}* have as many RP3 innervation

defects as *robo2* mutants (Figure 2.2). To define the protein domains required for

Robo2's activity in motor axon guidance, we examined knock-in alleles encoding either

of two chimeric receptors: Robo2-1 (Robo2's ectodomain and Robo1's cytodomain) or

Robo1-2 (Robo1's ectodomain and Robo2's cytodomain) (Spitzweck et al., 2010) (Figure

2.2). We found that *robo2$^{robo2-1}$* embryos have as strong a motor axon phenotype as *robo2*

mutants, while *robo2$^{robo1-2}$* embryos are phenotypically normal (Figure 2.2). Together,

these results suggest that neither Robo1 nor Robo3 can substitute for Robo2 in motor axon guidance, and that this Robo2-specific activity maps to its cytodomain.

Restoring Robo2 activity in hb9 mutants rescues motor axon guidance defects

To determine if Robo2 acts as an effector of Hb9 during motor axon guidance, we tested whether over-expressing *robo2* in *hb9* mutants rescues their muscle 6/7 innervation defects. However, over-expressing a *UAS-Robo2* transgene using *hb9-Gal4* in otherwise wild type embryos produces severe motor axon defects, affecting RP3 innervation in more than 50% of hemisegments (data not shown). We therefore sought to identify a variant of the Robo2 receptor that retains its endogenous activity in ISNb pathfinding, but does not generate defects when over-expressed. As our results with the knock-in alleles indicate a requirement for Robo2's cytodomain in motor axon guidance (Figure 2.2), we tested whether over-expression of a chimeric receptor that contains the ectodomain of Robo1 and the cytodomain of Robo2 (Robo1-2) results in motor axon guidance defects. We found that over-expression of *UAS-Robo1-2* with *hb9-Gal4* does not result in 6/7 innervation defects, whereas expressing the reciprocal chimera (Robo2-1) produces significant errors in motor axon pathfinding (data not shown).

We could now test if expressing a receptor that is functional in *robo2*'s endogenous context (Robo1-2) rescues motor axon guidance in *hb9* mutants. We used the *hb9-Gal4* enhancer trap to perform this experiment (Broihier and Skeath, 2002), as we have found that when placed over a null *hb9* allele, this allelic combination results in nearly undetectable levels of *hb9* protein, and has as strong a motor axon phenotype as the null itself (Figure 2.2 and data not shown). Over-expressing *UAS-Robo1-2* in *hb9*

50

mutants using *hb9-Gal4* significantly rescues RP3 innervation defects (22% to 13%, p=0.03, Student's t-test) (Figure 2.2). A similar result is observed using the *lim3b-Gal4* driver (Certel and Thor, 2004) and a different *hb9* allelic combination (18% to 10%, p =0.04, Student's t-test) (Figure 2.2). The incomplete rescue may be a consequence of the timing or expression levels caused by Gal4-driven expression. Alternatively, *robo2* may be one of multiple downstream targets of *hb9*, and restoring Robo2 activity might not be sufficient to fully rescue *hb9* mutants. Nevertheless, together with the loss of function phenotypes and the requirement for *hb9* in promoting *robo2* expression, these results strongly suggest that Robo2 acts as a downstream effector of Hb9 during motor axon guidance.

Hb9 requires its conserved repressor domain and functions in parallel with Nkx6 to regulate robo2

       Vertebrate Hb9 acts as a repressor to regulate gene expression when over-expressed in the spinal cord, but the requirement for Hb9's repressor activity for axon guidance has not been studied (Lee et al., 2008a; William et al., 2003). Two conserved putative repressor domains are found in *Drosophila* Hb9: an Engrailed homology (Eh) domain similar to sequences that interact with the Groucho co-repressor (Broihier and Skeath, 2002; Smith and Jaynes, 1996), and a domain similar to sequences that interact with the C-terminal binding protein (CtBP) co-repressor (William et al., 2003). To test the contribution of these domains to Hb9 function, we generated Hb9 transgenes in which either or both domains were deleted, and compared their ability to rescue *hb9* mutants relative to full length Hb9 (Figure 2.3). All transgenes are inserted in the same genomic

location and are expressed at similar levels (data not shown). We found that whereas a

full-length Hb9 transgene (Hb9 FL) fully rescues both muscle 6/7 innervation defects and

robo2 expression in *hb9* mutants, the Eh domain deletion (Hb9ΔEh) does not rescue

motor axon pathfinding, and only weakly rescues *robo2* expression (Figure 2.3).

Conversely, the CtBP-binding domain deletion (Hb9ΔCtBP) fully rescues both guidance

and *robo2* expression (Figure 2.3). The double deletion (Hb9ΔEhΔCtBP) is not

significantly different from Hb9ΔEh in either assay (Figure 2.3). These results suggest

that Hb9 indirectly activates *robo2*, perhaps by repressing a direct regulator of *robo2,*

likely through a Groucho-dependent mechanism.

The embryonic expression patterns of *hb9* and the homeodomain transcription

factor *nkx6* largely overlap, and genetic analyses suggest that Hb9 and Nkx6 act in

parallel to regulate motor axon guidance and multiple transcription factors (Broihier et

al., 2004). We hypothesized that *robo2* might be a shared downstream target of *hb9* and

nkx6. Indeed, *nkx6* mutants have a significant decrease in *robo2* expression in the RP

motor neurons (81% *robo2+* RP3 neurons in *nkx6* heterozygotes versus 51.4% *robo2+*

RP3 neurons in *nkx6* mutants, p<0.001, Student's t-test) (Figure 2.4). To determine if *hb9*

and *nkx6* function in parallel to regulate *robo2,* we examined *robo2* expression in *hb9,*

nkx6 double mutants and observed a decrease relative to either single mutant (data not

shown). However, we were not able to quantify *robo2* expression in the double mutants,

as many cells are not labeled by *hb9-Gal4* or *islet-tau-myc*. Therefore, we looked for an

alternative background to address whether *nkx6* regulates *robo2* in parallel with *hb9*.

Removing one copy of *nkx6* in *hb9* mutants strongly enhances the motor axon phenotype

(from 21.6% of hemisegments with 6/7 innervation defects in *hb9/hb9* embryos to 45% in

hb9, nkx6/hb9,+ embryos, p<0.001, Student's t-test) without producing the changes in markers observed in *hb9, nkx6* double mutants (Figure 2.4). In this background *robo2* expression is significantly decreased relative to *hb9* mutants (from 41% *robo2+* RP3 neurons in *hb9/hb9* embryos to 19% in *hb9, nkx6/hb9,+* embryos, p<0.001, Student's t-test) suggesting that *nkx6* promotes *robo2* expression independently of *hb9* (Figure 2.4). *Nkx6* single mutants have a severe ISNb phenotype in which most ventrally-projecting motor axons fail to exit the nerve cord (Broihier et al., 2004)*,* implying that Nkx6 regulates downstream targets other than *robo2.* Nevertheless, our data argue that Hb9 and Nkx6 are essential regulators of *robo2* in the RP motor neurons and that they act in parallel to regulate ISNb guidance and achieve normal levels of *robo2* expression*,* thus demonstrating how a combination of transcription factors regulates axon guidance by impinging on a common downstream target.

Hb9 regulates lateral position in a subset of neurons

     Robo2 regulates midline crossing and lateral position within the embryonic CNS (Rajagopalan et al., 2000a; Rajagopalan et al., 2000b; Simpson et al., 2000a; Simpson et al., 2000b). As *hb9* is expressed in many neurons other than the RP motor neurons, we asked if it acts through *robo2* to regulate axon guidance in other contexts. The enhancer trap *hb9-Gal4* is expressed in all neurons that endogenously express *hb9* (Broihier and Skeath, 2002)*,* labeling three parallel axon tracts on either side of the midline (Figure 2.5). These align with, but are distinct from, Fasciclin II (FasII)-expressing axons, which form three bundles at specific medio-lateral positions (Figure 2.5). *Hb9* mutants do not have defects in the organization of FasII+ axons (Figure 2.5 and data not shown).

However, in *hb9* mutants, the two outer *hb9-Gal4+* bundles are often disrupted and the inner pathway appears thicker (Figure 2.5). The lateral-most *hb9-Gal4+* pathway is missing or discontinuous in approximately 30% of hemisegments, and the intermediate pathway is missing in close to 50% of hemisegments (Figure 2.5). These defects are fully rescued by expression of a *UAS-Hb9* transgene (Figure 2.5). No changes in the number or position of *hb9-Gal4+* neurons are observed (data not shown). To determine if *nxk6* also regulates the trajectory of *hb9-Gal4+* axons, we examined the organization of these pathways in embryos with reduced *nkx6* activity. *Nkx6* mutants have no defects in the lateral position of *hb9-Gal4+* axons (data not shown). However, *hb9* mutants heterozygous for *nkx6* have a significantly stronger disruption of the outer-most *hb9-Gal4+* pathway relative to *hb9* mutants (25% of hemisegments with lateral pathway defects in *hb9/hb9* embryos compared to 67% in *hb9, nkx6/hb9*, $p<0.001$), suggesting that *nkx6* also regulates lateral position, although its requirement is only revealed in the absence of *hb9*.

Robo2 and *robo3* are essential regulators of lateral position in the developing CNS (Evans and Bashaw, 2010b; Rajagopalan et al., 2000b; Simpson et al., 2000b; Spitzweck et al., 2010). Their expression patterns mirror their requirements: Robo2 is expressed on axons that select a lateral trajectory, and is required for the formation of lateral pathways, while Robo3 is expressed in both lateral and intermediate zones and is required for the formation of intermediate pathways (Rajagopalan et al., 2000b; Simpson et al., 2000b). Gene-swap experiments underscored the importance of the transcriptional regulation of *robo2* and *robo3* for their function in lateral position (Spitzweck et al., 2010), but upstream regulators within the CNS remain unknown. To determine if *hb9*

54

regulates medio-lateral position through *robo2* or *robo3*, we first asked whether *robo2* or *robo3* regulate the position of axons labeled by *hb9-Gal4*. In *robo2* mutants, the outer *hb9-Gal4+* pathway is missing in approximately 30% of hemisegments (Figure 2.5). The intermediate pathway is mildly affected, while the medial pathway appears intact (Figure 2.5). In *robo3* mutants, the intermediate *hb9-Gal4+* pathway is absent or strongly shifted in close to 50% of hemisegments, the outer pathway is not disrupted, and the medial pathway is intact (Figure 2.5). *Robo2, robo3* double mutants have a stronger phenotype in which the outer two *hb9-Gal4+* pathways are disrupted in a majority of hemisegments (Figure 2.5). However, the dramatic decrease in the width of the nerve cord in *robo2, robo3* double mutants made it difficult to quantify the presence of lateral pathways. We conclude that loss of *robo2* and *robo3* reproduces the lateral position defects observed in *hb9* mutants.

Hb9 can regulate lateral position by inducing robo2

To test whether *hb9* regulates lateral position through *robo2* or *robo3,* we searched for *hb9*-expressing neurons that also express *robo2* or *robo3* and project to intermediate or lateral zones. Several *hb9+* cells co-express *robo2*, including a cluster of neurons found immediately anterior and slightly dorsal to dMP2 (Figure 2.6). We scored *robo2* expression in these cells and observed a decrease in the percentage expressing *robo2* mRNA in *hb9* mutants compared to heterozygotes (52% to 24%, p<0.0001, Student's t-test, Figure 2.6). However, we were not able to achieve the resolution necessary to determine whether these neurons contribute to lateral pathways. It is likely that most of these cells are interneurons, as few motor neuron cell bodies reside in this

area of the nerve cord (Landgraf et al., 1997). Together with the similarity in the lateral position defects of *hb9* and *robo2* mutants, as well as the observation that Robo2 is an effector of *hb9* in motor neurons, these data suggest that *hb9* may endogenously regulate the medio-lateral position of a subset of interneurons via its effect on *robo2*.

 To study the consequences of manipulating *hb9* levels on lateral position in a defined group of neurons, we used the *apterous-Gal4* driver, which labels ipsilateral interneurons that normally do not express *hb9*, and express little to no *robo2* and *robo3* (Figure 2.8 and data not shown). In wild type embryos, the apterous (ap) axons form a fascicle that projects along the medial FasII bundle on either side of the midline (Figure 2.7). Over-expressing Robo2 or Robo3 in the ap neurons causes their axons to shift laterally away from the midline (Evans and Bashaw, 2010b; Rajagopalan et al., 2000b; Simpson et al., 2000b). We found that over-expressing Hb9 produces a very similar phenotype, in which ap axons are shifted in more than 75% of hemisegments, now aligning with the intermediate or lateral FasII tracts (Figure 2.7). To determine if this phenotype is due to the induction of *robo2* or *robo3*, we examined the effect of *hb9* over-expression on *robo2* and *robo3* mRNA levels. Over-expression of Hb9 in ap neurons does not result in *robo3* induction (data not shown). In contrast, we observed significant upregulation of *robo2* (Figure 2.7). In control embryos, *robo2* mRNA is detected in less than 20% of ventral ap cells, whereas more than 60% of ventral ap neurons express *robo2* when Hb9 is present ($p<0.001$, Student's t-test) (Figure 2.7). Interestingly, we do not observe *robo2* induction in the dorsal ap neurons (data not shown) which express a different transcription factor profile than their ventral counterparts (Allan et al., 2005; Baumgardt et al., 2007).

56

To determine if the lateral shift phenotype caused by Hb9 over-expression in ap neurons is due to the induction of *robo2,* we over-expressed Hb9 in *robo2* mutants. Strikingly, removing both copies of *robo2* results in a full suppression of Hb9's gain of function phenotype, and ap axons appear wild type (Figure 2.7). Together, these data indicate that ectopic expression of Hb9 is sufficient to induce *robo2*, and that Hb9-driven changes in *robo2* expression can dramatically affect the medio-lateral position of axons.

Hb9 endogenously regulates lateral position through robo3

The requirement for *hb9* in regulating the position of intermediate *hb9-Gal4+* axons suggests it may also regulate *robo3*, which is expressed in neurons that project to intermediate regions of the nerve cord and is essential for the formation of intermediate pathways (Rajagopalan et al., 2000b; Simpson et al., 2000b). The peptidergic midline neuron MP1 expresses both *hb9* and *robo3* and is one of the pioneers for the intermediate FasII pathway (Broihier and Skeath, 2002; Hidalgo and Brand, 1997; Simpson et al., 2000a). We used the *C544-Gal4* driver (Wheeler et al., 2006) to identify MP1 neurons and score *robo3* expression and the position of the MP1 axon. The mosaic expression of *C544-Gal4* allowed us to score the axonal trajectory of individual cells. Whereas almost all MP1 neurons express high levels of *robo3* mRNA and project along the intermediate FasII bundle in *hb9* heterozygous embryos, in *hb9* mutants 56 % of MP1 neurons do not express *robo3* and 47% of MP1 axons project along the medial FasII tract (Figure 2.8). A strong correlation between *robo3* expression and the position of a cell's axon is detected in both *hb9* heterozygotes and mutants, suggesting that the loss of *robo3* is responsible for the medial shift phenotype (p<0.0001, Fisher's exact test) (Figure 2.8). MP1 neurons

57

also express *nkx6*; however, we detected no significant change in *robo3* expression or in the MP1 axonal projection in *nkx6* mutants (data not shown).

To determine if restoring Robo3 rescues the lateral position of MP1 axons in *hb9* mutants, we used *C544-Gal4* to over-express a *UAS-HARobo3* transgene. *Robo*3 over-expression produces no effect on the lateral position of MP1 axons in *hb9* heterozygous embryos (data not shown), but results in a robust rescue of the lateral position defects of *hb9* mutants (50.4% of MP1 axons shifted medially in *hb9* mutants versus 19% in *hb9* mutants over-expressing Robo3, p<0.0001, Fisher's exact test) (Figure 2.8). We conclude that in at least one defined group of neurons, *hb9* acts through *robo3* to direct the selection of an intermediate pathway.

Interestingly, all of the Hb9 deletion variants fully rescue the lateral position defects of the intermediate *hb9-Gal4+* axons in *hb9* mutants (data not shown). Moreover, they all rescue *robo3* expression in MP1 neurons, and while variants lacking the Eh domain are slightly weaker than Hb9 FL in this assay, these differences are not statistically significant (data not shown). While we cannot rule out that Hb9 acts as a repressor to regulate *robo3*, the observation that its Engrailed homology domain is not strictly required for *robo3* regulation suggests the intriguing possibility that Hb9 may regulate *robo2* and *robo3* via distinct mechanisms.

Discussion

We have demonstrated a functional relationship between Hb9 and the Robo2 and Robo3 receptors in multiple contexts in the *Drosophila* embryo. In the RP motor neurons, *hb9* is required for *robo2* expression, and genetic rescue experiments indicate that *robo2*

58

acts downstream of *hb9*. Hb9 requires its conserved repressor domain and acts in parallel with Nkx6 to regulate *robo2* and motor axon guidance. Moreover, *hb9* contributes to the endogenous expression patterns of *robo2* and *robo3* and the lateral position of a subset of axons in the CNS, and can redirect axons laterally when over-expressed via upregulation of *robo2*. Finally, restoring Robo3 rescues the medial shift of MP1 axons in *hb9* mutants, indicating that *hb9* endogenously acts through *robo3* to regulate medio-lateral position in a defined subset of neurons.

Robo2 is a downstream effector of Hb9 during motor axon guidance

   Hb9 and *nkx6* are required for the expression of *robo2* in motor neurons, and rescue experiments suggest that the loss of *robo2* contributes to the phenotype of *hb9* mutants. However, *nkx6* mutants and *hb9* mutants heterozygous for *nkx6* have a stronger ISNb phenotype than *robo2* mutants, implying the existence of additional downstream targets. One candidate is the cell adhesion molecule Fasciclin III, which is normally expressed in the RP motor neurons, and appears reduced in *nkx6* mutant embryos (Broihier et al., 2004). Identifying the constellation of effectors that function downstream of Hb9 and Nkx6 will be key to understanding how transcription factors expressed in specific neurons work together to drive the expression of the cell surface receptors that regulate axon guidance and target selection.

   We have identified a new activity for *Drosophila* Robo2 in regulating motor axon guidance. While Robo1 can replace Robo2's repulsive activity at the midline (Spitzweck et al., 2010), Robo2's function in motor axon guidance is not shared by either Robo1 or Robo3. Moreover, Robo2's anti-repulsive activity at the midline and its ability to shift

59

axons laterally when over-expressed both map to Robo2's ectodomain, whereas we have found that Robo2's activity in motor axon guidance maps to its cytodomain (Evans and Bashaw, 2010b; Spitzweck et al., 2010). The signaling outputs of Robo2's cytodomain remain unknown, as it lacks the conserved motifs within Robo1 that engage downstream signaling partners (Bashaw et al., 2000; Fan et al., 2003; Yang and Bashaw, 2006). How does Robo2 function during motor axon guidance? In mice, Robo receptors are expressed in spinal motor neurons and prevent the defasciculation of a subset of motor axons (Jaworski and Tessier-Lavigne, 2012). Does *Drosophila* Robo2 regulate motor axon fasciculation? The levels of adhesion between ISNb axons and other nerves must be precisely controlled during the different stages of motor axon growth and target selection, and several regulators of adhesion are required for ISNb guidance (Fambrough and Goodman, 1996; Huang et al., 2007; Winberg et al., 1998). Furthermore, whereas Slit can be detected on ventral muscles, it is not visibly enriched in a pattern that suggests directionality in guiding motor axons (Kramer et al., 2001), making it difficult to envision how Robo2-mediated repulsive or attractive signaling might contribute to ISNb pathfinding. Future work will determine how Robo2's cytodomain mediates motor axon guidance, whether this activity is Slit-dependent, and whether Robo2 signals attraction, repulsion, or modulates adhesion in *Drosophila* motor axons.

Hb9 regulates lateral position through robo2 and robo3

Elegant gene swap experiments revealed the importance of transcriptional regulation in establishing the different expression patterns and functions of the *Drosophila* Robo receptors (Spitzweck et al., 2010). By analyzing a previously

uncharacterized subset of axon pathways, we have uncovered a requirement for *hb9* in regulating lateral position in the CNS. While *hb9* can act instructively to direct lateral position when over-expressed, its endogenous expression in a subset of medially-projecting neurons suggests that its ability to shift axons laterally is cell type-dependent. A complex picture emerges in which multiple factors act in different groups of neurons to regulate *robo2* and *robo3*. In a subset neurons, including MP1, *hb9* is endogenously required for lateral position through the upregulation of *robo3*, and likely acts in a different subset to regulate lateral position through *robo2*. In neurons that do not express *hb9*, such as those that form the outer FasII tracts, the expression patterns of *robo2* and *robo3* rely on additional upstream factors. What might be the significance of a regulatory network in which multiple sets of transcription factors direct lateral position in different groups of neurons? One possibility is that *hb9*-expressing neurons may share specific functional properties, such as the expression of particular neurotransmitters or ion channels. Alternatively, *hb9* may regulate other aspects of connectivity. Robo receptors have been shown to mediate dendritic targeting in the *Drosophila* CNS, raising the exciting possibility that *hb9* regulates both axonal and dendritic guidance through its effects on axon guidance receptor expression (Brierley et al., 2009; Furrer et al., 2003; Mauss et al., 2009).

How does Hb9 regulate robo2 and robo3?

What is the mechanism by which Hb9 regulates the expression of *robo2, robo3,* and its other downstream effectors? We have found that Hb9 requires its conserved Engrailed homology domain and acts in parallel with Nkx6 to regulate *robo2* and motor

axon guidance. It has previously been shown that *hb9* and *nkx6* function in parallel to regulate several transcription factors (Broihier and Skeath, 2002; Broihier et al., 2004). *Hb9, nkx6* double mutants show decreased expression of *islet* and *lim3*, and upregulation of *eve* and the *Nkx2* ortholog *vnd* (Broihier et al., 2004). Are Hb9 and Nkx6 regulating *robo2* or *robo3* through any of their previously identified targets? *Hb9* and *nkx6* single mutants show no change in *islet*, *lim3*, or *vnd* expression (Broihier and Skeath, 2002; Broihier et al., 2004), arguing that *hb9* and *nkx6* do not act solely through these factors to regulate *robo2* or *robo3*. *Eve* expression is unaffected in *nkx6* mutants (Broihier et al., 2004), and while it is ectopically expressed in two neurons per hemisegment in *hb9* mutants (Broihier and Skeath, 2002), these do not correspond to RP3 or MP1, the identifiable cells in which we can detect changes in *robo2* and *robo3* (data not shown). Therefore, our data do not support the hypothesis that Hb9 and Nkx6 regulate *robo2* or *robo3* primarily through their previously identified targets *islet, lim3, vnd* or *eve*. Gain of function experiments in vertebrates suggest that Hb9 and Nkx6 act as repressors to regulate gene expression in the spinal cord (Lee et al., 2008a; Muhr et al., 2001; William et al., 2003). Our finding that Hb9's Engrailed homology domain is required for motor axon pathfinding and *robo2* regulation suggests that Hb9 acts as a repressor in this context as well, most likely through a previously unidentified intermediate target. On the other hand, the Eh domain is not required for Hb9's ability to regulate *robo3* or lateral position in *hb9-Gal4+* neurons that project to intermediate zones of the CNS. The finding that Hb9ΔEh retains significant activity in rescuing lateral position and *robo3* expression indicates that Hb9 may regulate *robo2* and *robo3* via distinct mechanisms, perhaps involving different transcriptional co-factors or intermediate targets. In support of this

hypothesis, *hb9* over-expression in the apterous neurons can induce *robo2*, but not *robo3*. These data raise the intriguing possibility that Hb9's ability to regulate *robo2* and *robo3* via different mechanisms contributed to the diversification of their expression patterns in the CNS.

Determining how Hb9 and Nkx6 regulate their effectors will be key to achieving a complete understanding of how these conserved transcription factors control changes in cell morphology and axon pathfinding during development. Of note, *Hb9* mutant mice exhibit defects in a subset of motor nerves, including the phrenic and intercostal nerves, which are also affected in *Robo* mutants (Arber et al., 1999; Jaworski and Tessier-Lavigne, 2012; Thaler et al., 1999). It will be of great interest to determine if despite the vast divergence in the evolution of nervous system development between invertebrates and vertebrates, Hb9 or Nkx6 have retained a role for regulating Robo receptors across species.

Experimental Procedures

Genetics

The following alleles were used: *robo2^{x123}* (Simpson et al., 2000a); *robo2^{x33}* (Simpson et al., 2000a); *hb9^{kk30}*, *hb9^{ad121}*, *hb9^{JJ154e}*, *hb9^{gal4}* (Broihier et al., 2002); *nkx6^{D25}* (Broihier et al., 2004); *ap^{Gal4}* (O'Keefe et al., 1998); *robo3^{1}* (Rajagopalan et al., 2000b); *robo3^{3}* (Pappu et al., 2011); *Df(2L)ED108* (Ryder et al., 2007); *robo2^{robo2}*, *robo2^{robo1}*, *robo2^{robo3}*, *robo2$^{robo2-1}$*, *robo2$^{robo1-2}$* (Spitzweck et al., 2010); *robo2^{F}* (gift from L. Zipursky). *Robo2^{F}* is a loss of function allele generated by EMS mutagenesis on the *robo3^{3}* chromosome. The following transgenes were used: *UAS-Robo2RNAi* (Vienna *Drosophila* Research

63

Center); *C544-Gal4* (Wheeler et al., 2006); *UAS-Hb9* (Broihier et al., 2002); *isletH-tau-myc* (Thor et al., 1997); *lim3A-tau-myc* (Thor et al., 1999); *lim3b-gal4* (Certel et al., 2004); *[UAS-HARobo1-2].T39, [UAS-HARobo2-1].T6, [UAS-HARobo2].T1, [UAS-HARobo3].T15* (Evans et al., 2010); *[UAS-HARobo2]86FB, [UAS-HARobo1]86FB* (Evans et al., 2012); *UAS-Tau-Myc-GFP*, *ftz-ngGal4*, *24b-Gal4*, *RN2-Gal4* (Bloomington Stock Center); *[UAS-Hb9 FL]51C, [UAS-Hb9 ΔEh]51C, [UAS-Hb9 ΔCtBP]51C, [UAS-Hb9 ΔEhΔCtBP]51C, [22K18-robo2BAC]51C*. All crosses were performed at 25°C. Embryos were genotyped using a combination of marked balancer chromosomes or the presence of tagged transgenes.

Molecular Biology

Hb9 constructs with an N-terminal Myc tag were cloned into a pUAST vector containing 10xUAS and an attB site for ΦC31-mediated targeted insertion. Hb9ΔEh (lacking amino acids 219-229) and Hb9ΔCtbp (lacking amino acids 336-340) were generated by serial overlap extension PCR. Transgenes were inserted at cytological site 51C by Best Gene (Chino Hills, CA, USA). The *22K18-robo2* BAC was obtained from BACPAC Resources (Children's Hospital, Oakland) and inserted at 51C by Rainbow Transgenics (Carmarillo, CA, USA).

Fluorescent in situ hybridization and quantification

Fluorescent mRNA *in situ* hybridization was performed as described (Labrador et al., 2005). Fluorescence quantification was performed using ImageJ as described (Yang et al., 2009). Briefly, max projections were obtained for embryos from the same collection.

A region of interest (ROI) was generated around the RP cell bodies, using the *islet-tau-myc* staining as a reference. Total fluorescence intensity above a set threshold was obtained for each channel by multiplying the area of the ROI by the average fluorescence intensity within the ROI above the threshold. Relative fluorescence intensity of *robo2* mRNA was calculated as absolute *robo2* mRNA fluorescence intensity divided by absolute myc fluorescence intensity.

Immunostaining and imaging

Embryo fixation and staining were performed as described (Kidd et al., 1998a). The following antibodies were used: mouse MAb 1D4/Fasciclin II [Developmental Studies Hybridoma Bank (DSHB); 1:100], mouse anti-ßgal (DSHB; 1:150), mouse anti-HA (Covance #MMS-101P; 1:250), rabbit anti-GFP (Invitrogen #A11122; 1:500), rabbit anti-c-Myc (Sigma #C3956; 1:500), chick anti- ßgal (Abcam #9361; 1:1000), guinea pig anti-Hb9 (gift from J. Skeath; 1:1000), Cy3 goat anti-mouse (Jackson #115-165-003; 1:1000), Alexa-488 goat anti-rabbit (Molecular Probes #A11008; 1:500), Cy3 goat anti-chick (Abcam #97145; 1:500), Alexa-647 goat anti-Guinea Pig (Molecular Probes #A-21450; 1:500). Images were acquired with Volocity using a spinning disk confocal (Perkin Elmer) using a Nikon 40x objective with a Hamamatsu C10600-10B CCD camera and Yokogawa CSU-10 scanner head. Images were processed using ImageJ.

Phenotypic quantification

Phenotypes were scored on Volocity imaging software. For scoring *robo2* and *robo3* expression, if the cell body of a neuron could be detected by the *in situ* signal, that neuron

was scored as positive. RP3 neurons were identified by using *islet-tau-myc* and their position; ventral apterous neurons were identified by using *ap-Gal4* and their position; MP1 neurons were identified by using *C544-Gal4* and FasII. For motor axon phenotypes, hemisegments in A2-A6 of late stage 17 embryos in which a FasII+ axon could not be detected between the ventral muscles 6 and 7 were scored as lacking the innervation. For *hb9-Gal4+* axon phenotypes, the presence of the medial, intermediate, or lateral *hb9-Gal4+* axon bundles was scored for hemisegments in A1-8 in Stage 17 embryos. If a bundle was visibly shifted to another lateral zone, it was scored as absent. For ap axon phenotypes, if a hemisegment in A1-8 of stage 17 embryos contained an ap axon that projected along the intermediate or lateral FasII tracts, it was scored as shifted. For MP1 axon phenotypes, the lateral position of MP1 axons was scored relative to the FasII pathways. A1-A7 were scored in Stage 16 embryos.

Figure 2.1. *Robo2* and *hb9* mutants have similar motor axon guidance defects, and *hb9* is required for *robo2* expression in the RP motor neurons.
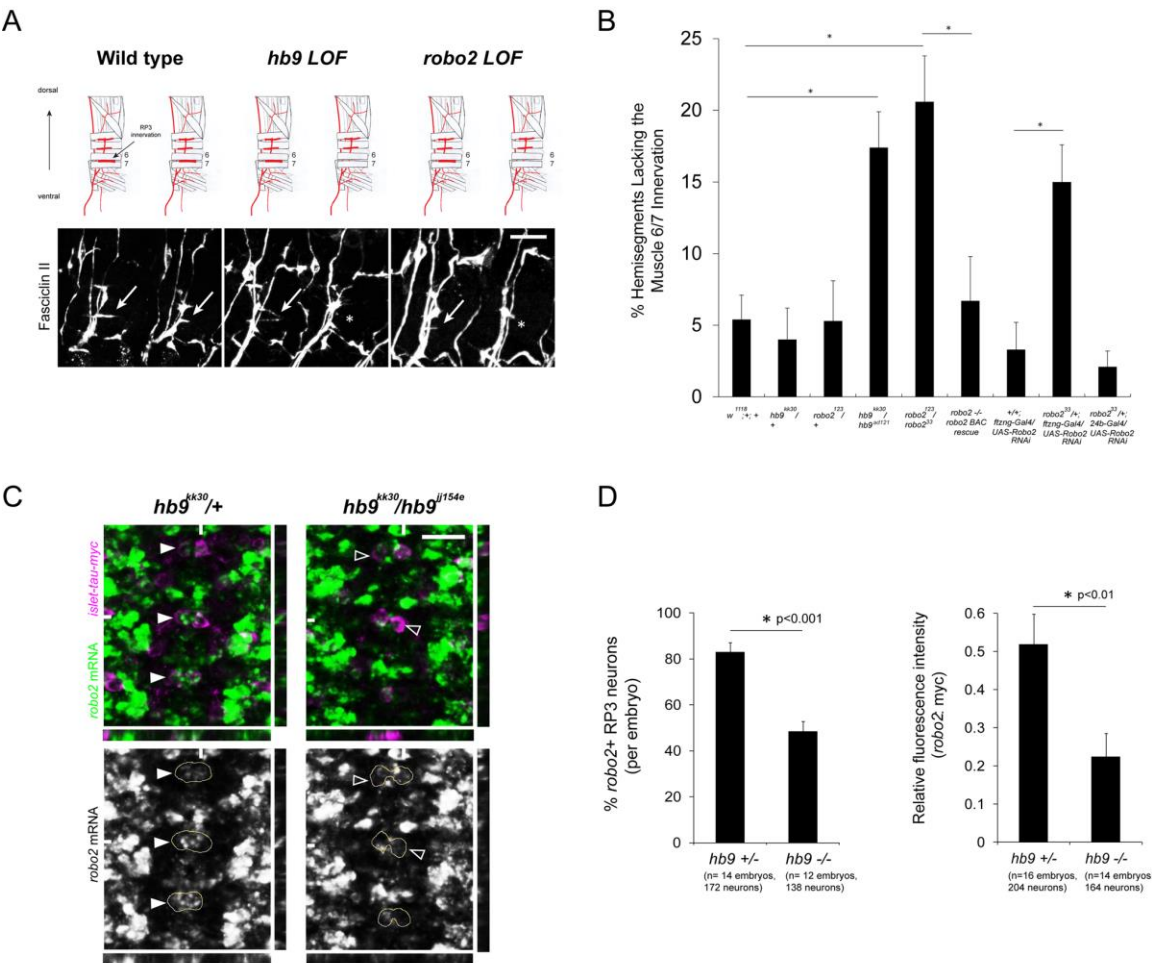
Figure 2.1. *Robo2* **and** *hb9* **mutants have similar motor axon guidance defects, and** *hb9* **is required for** *robo2* **expression in the RP motor neurons.**

A: Stage 17 embryos stained for Fasciclin II (FasII). Anterior is left. Arrows point to the muscle 6/7 innervation, which is often absent in *hb9* or *robo2* mutants (asterisks). **B**: The percentage of hemisegments lacking the 6/7 innervation is shown; asterisks indicate a significant difference (Student's t-test, $p<0.01$). Error bars = s.e.m. **C**: Fluorescent *in situ* for *robo2* mRNA in Stage 16 embryos. Anterior is up. The RP3 motor neurons are labeled by the *islet-tau-myc* transgene, and circled in the single-channel images. Most RP3 neurons express *robo2* in *hb9* heterozygotes (filled arrowheads), whereas many RP3 neurons do not express *robo2* in *hb9* mutants (empty arrowheads). YZ and XZ cross-sections are shown; hash marks indicate the planes of the sections. **D**, Left: RP3 neurons were scored as positive or negative for *robo2*. *Hb9* mutants have significantly fewer *robo2+* RP3 neurons than heterozygous siblings (Student's t-test, $p<0.001$). Error bars = s.e.m. **D**, Right: The mean gray value of the *robo2* mRNA signal in RP3 neurons was normalized to the mean gray value of the myc signal. The average relative fluorescence intensity of *robo2* mRNA is significantly lower in *hb9* mutants than in *hb9* heterozygotes (Student's t-test, $p<0.01$). Error bars = s.e.m. Numbers of embryos and neurons analyzed are shown in parentheses. Scale bars represent 10 μm. *Robo2 -/- robo2 BAC rescue* denotes *robo2^{123}, 22K18robo2BAC/ robo2^{33}*. *Hb9 +/-* denotes *hb9^{kk30}, isl-taumyc/TM3*. *Hb9 -/-* denotes *hb9^{kk30}, isl-taumyc/hb9^{jj154e}*.

Figure 2.2. Restoring Robo2 activity in *hb9* mutants rescues motor axon guidance defects.
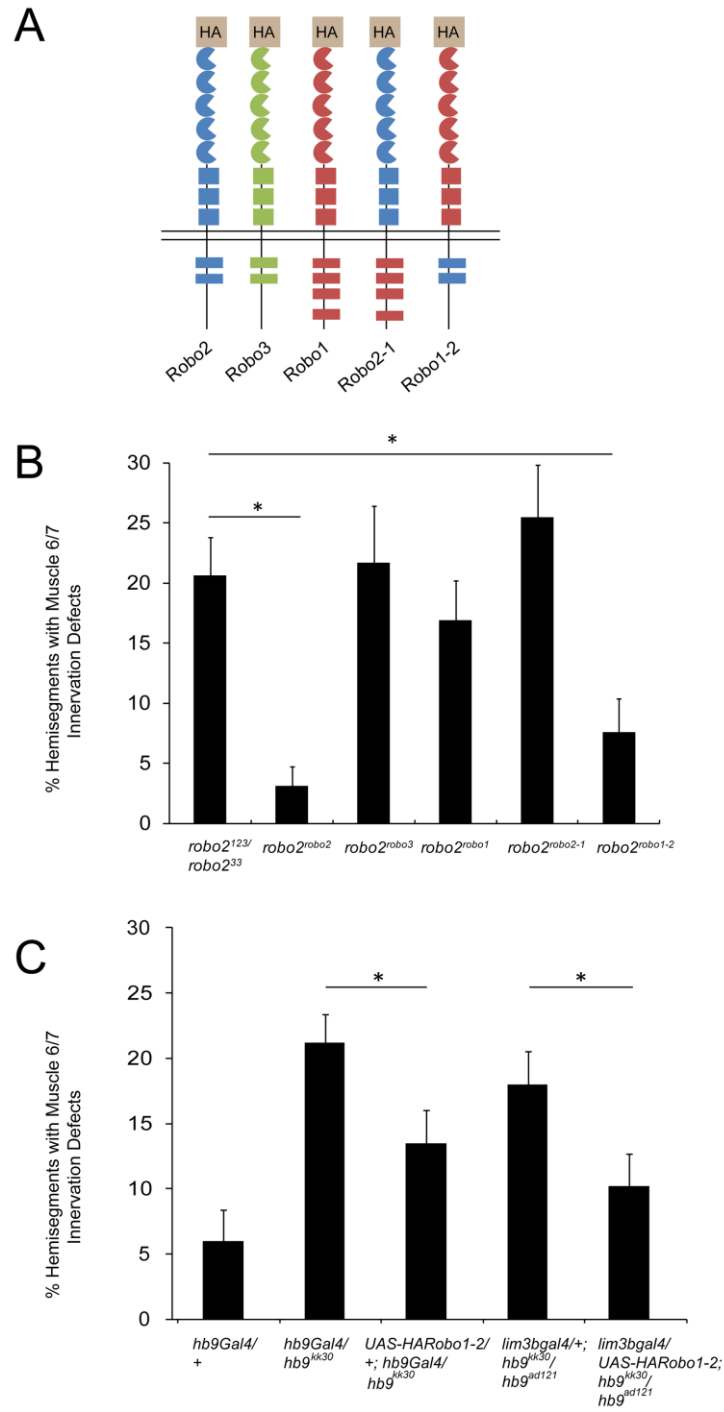
Figure 2.2. Restoring Robo2 activity in *hb9* mutants rescues motor axon guidance defects.

A: Schematic of the Robo receptors analyzed for their ability to replace endogenous Robo2. **B**: Embryos homozygous for knock-in alleles in which the coding sequences of Robo2, Robo3, Robo1, Robo2-1, or Robo1-2 are inserted in the *robo2* locus were analyzed for motor axon guidance defects. Only Robo2 and Robo1-2 can restore muscle 6/7 innervation. Asterisks indicate a significant difference (Student's t-test, $p<0.01$). Error bars = s.e.m. B: *Hb9* mutant embryos over-expressing *UAS-HARobo1-2* have fewer defects than mutants lacking the transgene (Student's t-test, $p<0.05$). All *hb9* mutants were scored blind to genotype. Error bars = s.e.m.

Figure 2.3. Hb9's Eh domain is required for its activity in motor axon guidance and for *robo2* regulation.
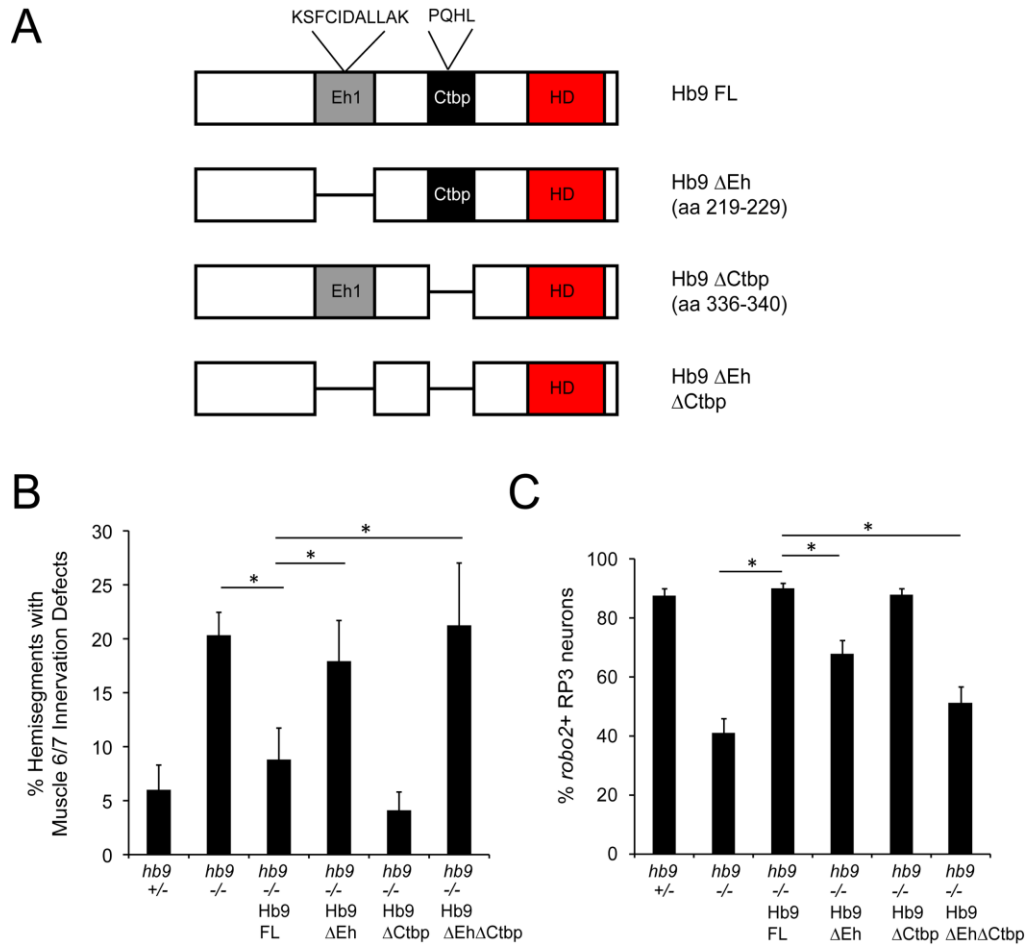
Figure 2.3. Hb9's Eh domain is required for its activity in motor axon guidance and for *robo2* regulation.

A: Schematic of the Hb9 variants analyzed for their ability to rescue *hb9* mutants. **B**: Muscle 6/7 innervation was quantified in late Stage 17 embryos; asterisks indicate a significant difference (Student's t-test, $p<0.01$). Hb9 transgenes lacking the Eh domain failed to rescue motor axon guidance defects in *hb9* mutants. **C**: The percentage of *robo2+* RP3 neurons per embryo is shown; asterisks indicate a significant difference (Student's t-test, $p<0.01$). Hb9's Eh domain is required for rescue of *robo2* expression. Error bars = s.e.m. *Hb9 +/-* denotes *hb9^{gal4}/TM3*. *Hb9 -/-* denotes *hb9^{gal4}/hb9^{kk30}*. *Hb9 -/-* Hb9 (variant) denotes *UAS-Hb9 (variant)/+; hb9^{gal4}/hb9^{kk30}*.

Figure 2.4. Hb9 and Nkx6 function in parallel to regulate motor axon guidance and
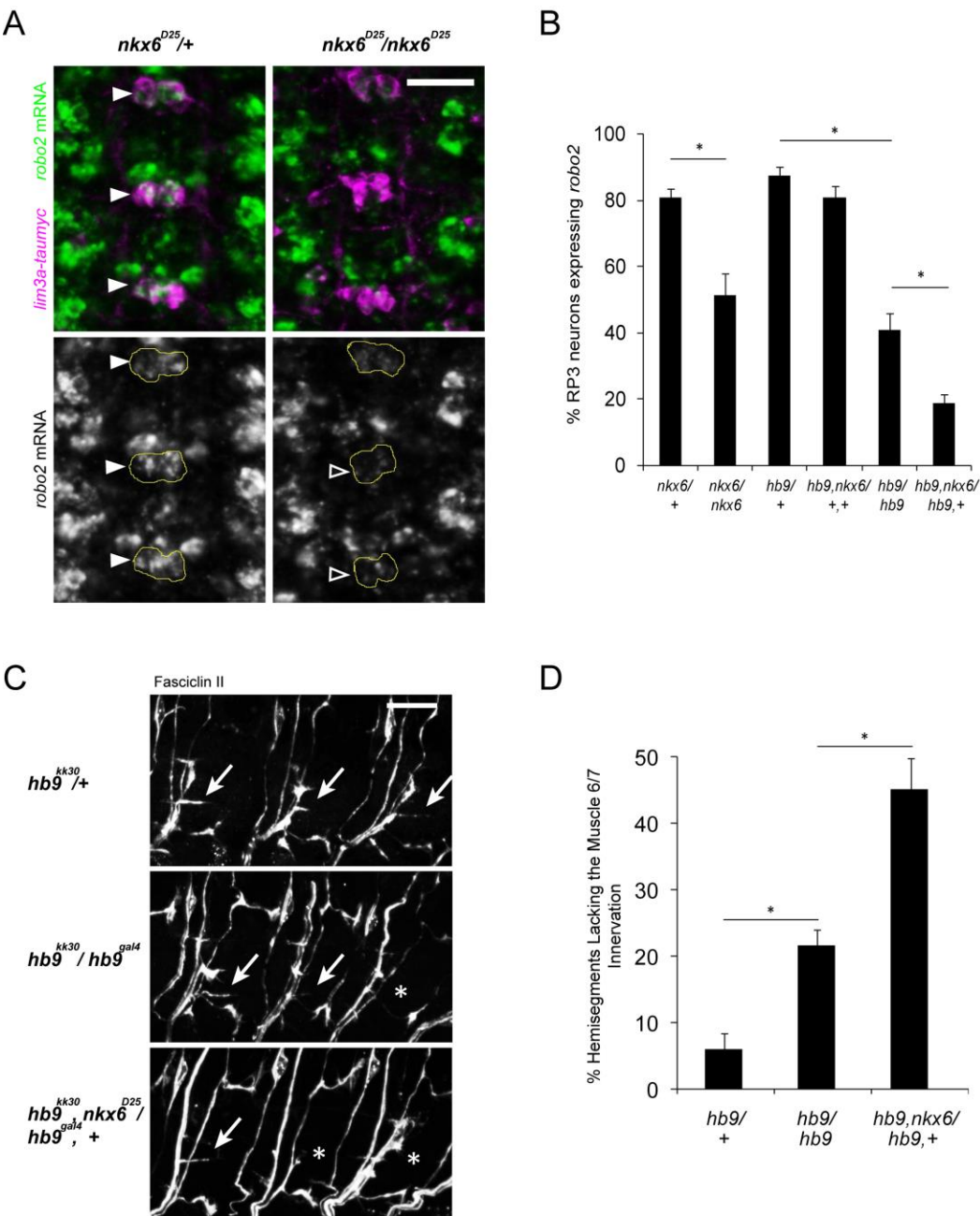
robo2.

Figure 2.4. Hb9 and Nkx6 function in parallel to regulate motor axon guidance and
***robo2*.**

A: Fluorescent *in situ* for *robo2* mRNA (green) in Stage 16 embryos. Anterior is up. The
RP motor neurons are labeled by the *lim3a-taumyc* transgene (magenta). Filled
arrowheads point to *robo2+* RP3 neurons; empty arrowheads indicate *robo2-* neurons. **B**:
Nkx6 mutants have fewer *robo2+* RP3 neurons than *nkx6* heterozygotes (p<0.001,
Student's t-test). Removing one copy of *nkx6* enhances the loss of *robo2* in *hb9* mutants
(p<0.001, Student's t-test). Error bars = s.e.m. **C**: Stage 17 embryos stained for FasII.
Anterior is left. The arrows point to the muscle 6/7 innervation, while asterisks indicate
its absence. **D**: The percentage of hemisegments lacking the 6/7 innervation was
quantified; asterisks indicate a significant difference (p<0.001, Student's t-test). Loss of
nkx6 dominantly enhances the 6/7 innervation defects of *hb9* mutants. Error bars = s.e.m.
Scale bars represent 10 μm. *Nxk6/+* denotes *nkx6^{D25}/TM6B. Nkx6/nkx6* denotes
nkx6^{D25}/nkx6^{D25}. Hb9/+ denotes *hb9^{kk30}/TM3. Hb9, nxk6/+,+* denotes *hb9^{gal4},
nkx6^{D25}/TM3. Hb9/hb9* denotes *hb9^{gal4}/hb9^{kk30}. Hb9, nkx6/hb9,+* denotes *hb9^{gal4}, nkx6^{D25}/
hb9^{kk30}*.

Figure 2.5. The lateral position of *hb9-Gal4*-expressing axons is disrupted in the absence of *hb9*, *robo2*, or *robo3*.
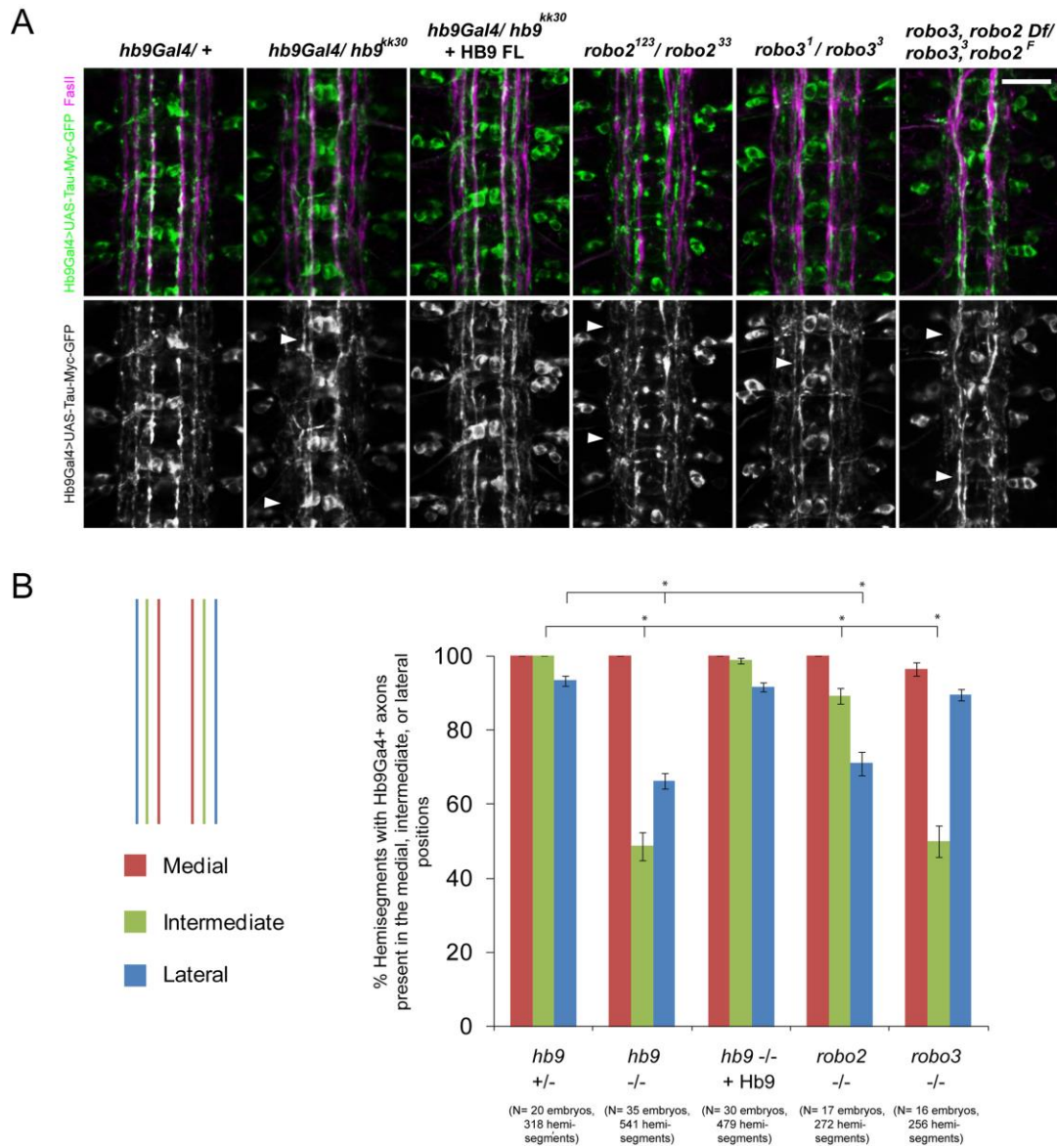
Figure 2.5. The lateral position of *hb9-Gal4*-expressing axons is disrupted in the absence of *hb9*, *robo2*, or *robo3*. A: Stage 17 embryos, anterior is up. FasII staining is shown in magenta. *Hb9-Gal4> UAS-TauMycGFP* (green) labels axons that form three bundles on each side of the midline in *hb9* heterozygotes. In *hb9* mutants, the outer *hb9-Gal4+* pathways are disrupted or shifted medially (arrowheads). *Robo2* and *robo3* mutants partially phenocopy these defects (arrowheads). **B**: The percentage of hemisegments containing *hb9-Gal4+* axons in the medial, intermediate, or lateral positions is shown. Asterisks indicate a significant difference (Student's t-test, $p<0.001$). Error bars = s.e.m. Numbers of embryos and hemisegments scored are shown in parentheses. Scale bars represent 10 μm. *Hb9 +/-* denotes *hb9^{gal4}/TM6B*. *Hb9 -/-* denotes *hb9^{gal4}/hb9^{kk30}*. *Hb9 -/- + HB9* denotes *UAS-Hb9/+; hb9^{gal4}/hb9^{kk30}*. *Robo2 -/-* denotes *robo2^{123}/ robo2^{33}; hb9^{gal4}/+*. *Robo3 -/-* denotes *robo3^{1} / robo3^{3}; hb9^{gal4}/+*. *Robo3, robo2 Df/ robo3^{3}, robo2^{F}* denotes *Df(2L)ED108/ robo2^{F}, robo3^{3}; hb9^{gal4}/+*.

Figure 2.6. *Hb9* is required for *robo2* expression in a subset of neurons.
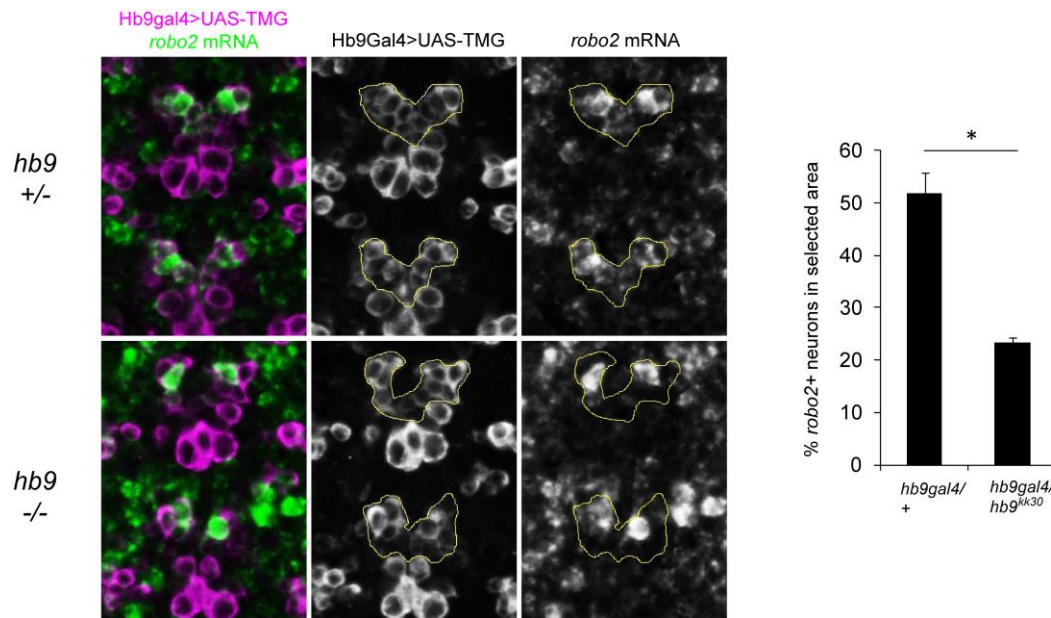
Figure 2.6. *Hb9* is required for *robo2* expression in a subset of neurons.

A: Fluorescent *in situ* hybridization for *robo2* mRNA (green) in Stage 15 embryos; anterior is up. *Hb9-Gal4>UAS-TauMycGFP* (magenta) labels a V-shaped cluster of neurons, outlined in yellow in the single-channel images. In *hb9* heterozygotes, most of these cells are positive for *robo2* mRNA, whereas there are fewer *robo2+* neurons in this cluster in *hb9* mutants. **B**: The percentage of *robo2+/hb9-Gal4+* neurons in the region of interest was quantified for *hb9* heterozygous and mutant embryos. *Hb9* mutants have a significant decrease compared to heterozygous siblings (p<0.0001, Student's t-test). Error bars = s.e.m.

Figure 2.7. *Hb9* **gain of function in ap neurons induces** *robo2* **expression and a**

*robo2***-dependent lateral shift.**
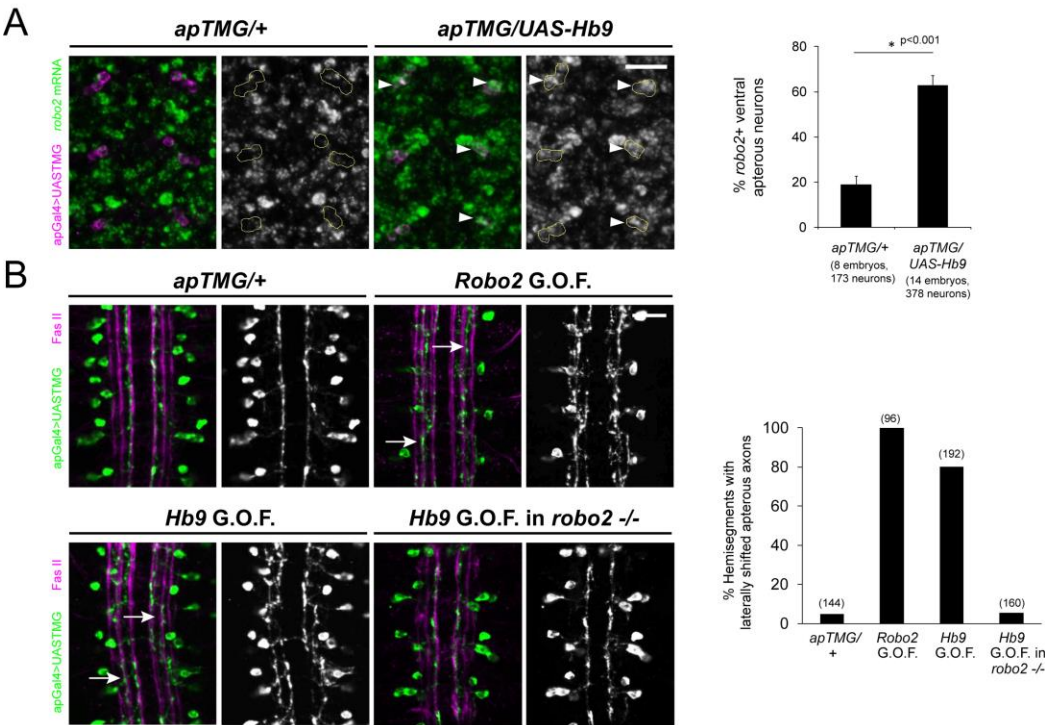
Figure 2.7. *Hb9* **gain of function in ap neurons induces** *robo2* **expression and a**
*robo2***-dependent lateral shift.**

A, Left: Fluorescent *in situ* for *robo2* mRNA (green) in Stage 15 embryos. Anterior is up.

The ventral ap neurons are labeled in magenta and circled in the single channel images.

Wild-type embryos express little *robo2* in the ap neurons, whereas many ventral ap

neurons express *robo2* when Hb9 is present (arrowheads). **A**, Right: The percentage of

ventral ap neurons expressing *robo2* is shown. *Hb9* gain of function results in a

significant increase compared to controls (p<0.001, Student's t-test). Error bars = s.e.m.

B, Left: Stage 17 embryos stained for FasII (magenta) and GFP (green), which labels the

ap axons. Over-expression of *robo2* or *hb9* in ap neurons shifts their axons laterally

(arrows). *Hb9* over-expression in *robo2* mutants does not induce a lateral shift phenotype.

B, Right: The percentage of hemisegments in which ap axons project along the

intermediate or lateral FasII tracts is shown. Numbers of hemisegments scored are

indicated in parentheses. Scale bars represent 10 μm. *apTMG/+* denotes *apGal4,UAS-*

TauMycGFP/CyO. *Robo2* G.O.F. denotes *UAS-HARobo2.T1/apGal4, UAS-TauMycGFP*.

Hb9 G.O.F denotes *UAS-Hb9/apGal4,UAS-TauMycGFP*. *Hb9* G.O.F. in *robo2 -/-*

denotes *robo2^{123},UAS-Hb9/robo2^{33}, apGal4*; *UAS-TauMycGFP/+*.

Figure 2.8. Robo3 acts downstream of Hb9 to direct the lateral position of MP1 axons.
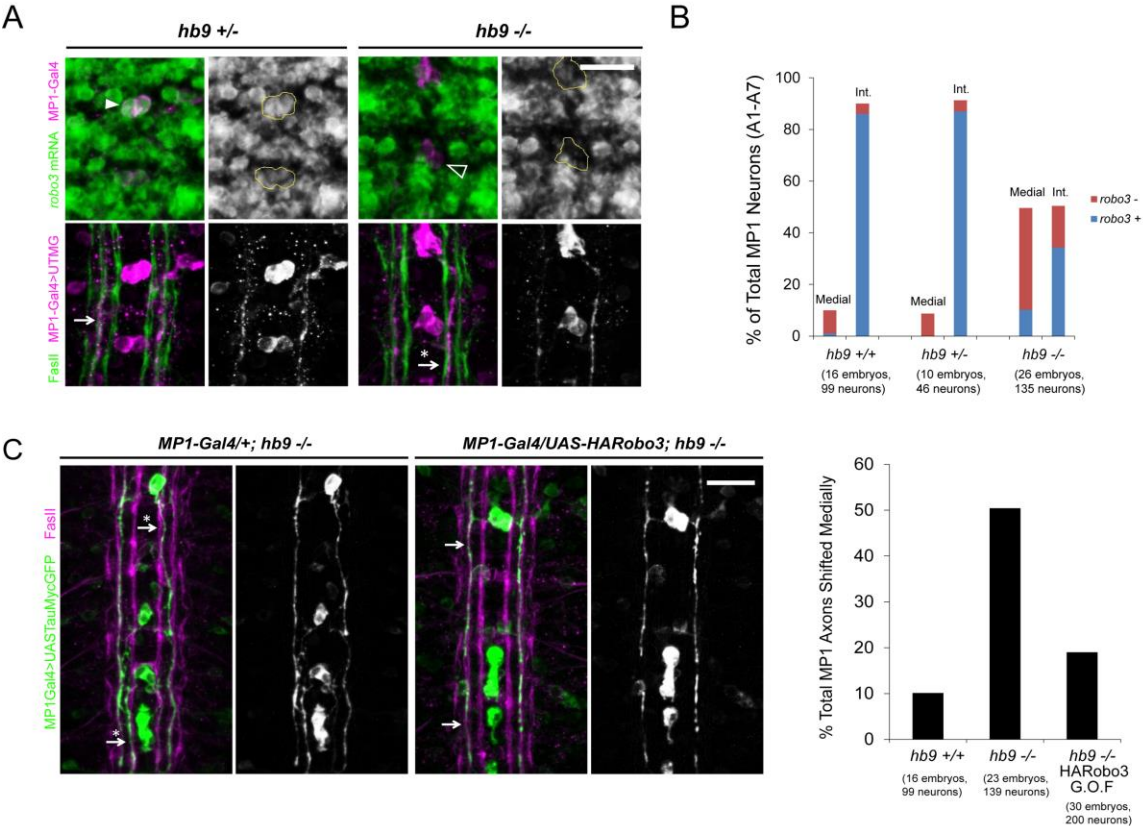
Figure 2.8. Robo3 acts downstream of Hb9 to direct the lateral position of MP1 axons.

A, Top: Fluorescent *in situ* for *robo3* mRNA (green) in Stage 16 embryos. Anterior is up. MP1 neurons are labeled by *C544-Gal4* in magenta and circled in the single-channel images. Many MP1 neurons do not express *robo3* in *hb9* mutants (empty arrowhead). **A**, Bottom: MP1 axons project along the intermediate FasII bundle in *hb9* heterozygotes (arrow), but are often shifted to the medial pathway in *hb9* mutants (arrow with an asterisk). **B**: MP1 neurons were scored as *robo3+* or *robo3-* and as projecting along the medial or intermediate (Int.) FasII tract. A significant correlation was detected between *robo3* expression and lateral position in both *hb9 +/- and hb9-/-* embryos (Fisher's exact test, p<0.001). **C**: Over-expressing *robo3* rescues the medial shift phenotype of MP1 axons in *hb9* mutants (p<0.001, Fisher's Exact Test). Arrows point to MP1 axons in the correct position; arrows with asterisks point to medially shifted axons. All mutants were scored blind to genotype. Scale bars represent 10 μm. *Hb9 +/+* denotes *C544-Gal4/+; UAS-TauMycGFP/+*. *Hb9 +/-* denotes *C544-Gal4/+; hb9^{ad121}, UAS-TauMycGFP/TM3*. *Hb9 -/-* denotes *C544-Gal4/+; hb9^{ad121}, UAS-TauMycGFP/hb9^{kk30}*. *Hb9 -/-* HARobo3 G.O.F. denotes *C544-Gal4/UAS-HARobo3.T15; hb9^{ad121}, UAS-TauMycGFP/hb9^{kk30}*.

Acknowledgments

I would like to thank members of the Bashaw lab for helpful comments on the

manuscript, in particular Alexandra Neuhaus-Follini. I thank Tim Evans for generating

the Robo chimeric transgenes, and Barry Dickson for providing the knock-in alleles.

This chapter was published in the following article:

Santiago, C., Labrador, J.-P. and Bashaw, G. J. (2014). The homeodomain transcription factor Hb9 controls axon guidance in Drosophila through the regulation of Robo receptors. *Cell Rep.* **7**, 153–65.

CHAPTER 3

THE LIM HOMEODOMAIN FACTOR ISLET COORDINATELY REGULATES AXON GUIDANCE AND DENDRITE TARGETING IN DROSOPHILA THROUGH THE FRAZZLED/DCC RECEPTOR

In *Drosophila*, motor axon targeting in the periphery correlates with the position of motor neuron dendrites in the CNS, but intrinsic programs that direct the formation of this myotopic map are unknown. Here we show that the LIM homeodomain factor Islet controls targeting of axons and dendrites in ventrally projecting motor neurons through regulation of the Frazzled (Fra)/DCC receptor. Islet is required for *fra* expression in RP3 neurons, and *islet* and *fra* mutants have similar axon guidance defects. Single-cell labeling indicates that *islet* and *fra* are required for RP3 dendrite targeting, and that *fra* expression in different subsets of motor neurons correlates with dendrite position. Finally, over-expression of Fra rescues muscle targeting and the position of RP3 dendrites in *islet* mutants. These results indicate that Fra acts downstream of Islet in the periphery and in the CNS, demonstrating how a regulatory relationship is reused in multiple cellular compartments to coordinate neural circuit wiring.

Introduction

The vast diversity of neuronal cell types is one of the nervous system's most remarkable features, and understanding how this diversity is achieved remains a major challenge. Many studies have shown that combinations of transcription factors act in a cell type specific manner to specify a neuron's morphological and functional properties (reviewed in Corty et al., 2009; Hobert, 2015; Polleux et al., 2007). The regulation of

axon and dendrite targeting is key to determining a neuron's initial pattern of connectivity, and is controlled through the combined action of guidance receptors, adhesion molecules, and cytoskeletal regulators (Lefebvre et al., 2015; O'Donnell et al., 2009). While recent studies have begun to delineate relationships between cellular effectors and the transcription factors that control their expression, it remains unclear to what extent individual transcription factors regulate multiple aspects of morphogenesis (reviewed in Santiago and Bashaw, 2014). In particular, several factors have been shown to control both axon and dendrite development, but whether they do so through shared or distinct targets is unknown. In mice, the target-induced ETS factor Pea3 (Etv4) is required for axonal branching in a subset of limb-innervating neurons, and for the position and connectivity of motor neuron dendrites in the spinal cord (Livet et al., 2002; Vrieseling and Arber, 2006). In *Drosophila*, the POU factor Acj6 is required in olfactory projection neurons both for axonal branching in the lateral horn and for dendrite targeting in the antennal lobe (Komiyama et al., 2003). However, in these and other examples, the downstream programs that mediate the effects of these transcription factors on axon and dendrite targeting remain unidentified (Baek et al., 2013; Enriquez et al., 2015).

In the *Drosophila* larval and adult nervous systems, motor neuron dendrites form within stereotyped medio-lateral regions in the CNS that correlate with cell identity and with the position of motor axons in the periphery (Brierley et al., 2009; Mauss et al., 2009). Slit-Robo and Netrin-Frazzled signaling are key regulators of dendrite targeting, and manipulating the levels of Robo or Fra by either loss or gain of function experiments causes shifts in dendrite position, suggesting that these receptors act in a cell autonomous manner (Brierley et al., 2009; Mauss et al., 2009).

Dendritogenesis initiates simultaneously in medial and lateral regions of the CNS, and time-lapse experiments do not reveal a major contribution from pruning or space-filling mechanisms. In adult motor neurons, birth order correlates with dendrite position, suggesting the involvement of a temporal code of transcription factors (Brierley et al., 2009). There is no indication that birth order plays a role in dendrite targeting in the embryo (Mauss et al., 2009); instead, the correlation between the dorsal-ventral position of axons and the medio-lateral position of dendrites suggests the intriguing hypothesis that the same factors that specify axon guidance may also regulate dendrite position. Taken together, these data suggest that subset-specific transcription factors are likely to regulate dendrite targeting through their effects on *fra*, *robo*, or genes in those pathways in *Drosophila* motor neurons. However, this model remains uncorroborated.

The well-conserved transcription factors Even-skipped (Eve), Hb9/exex, Islet/tailup, and Lim3 are expressed in restricted subsets of embryonic motor neurons, and have been extensively studied in the context of axon guidance, but whether the same transcriptional regulators specify dendrite development is not known (Broihier and Skeath, 2002; Fujioka et al., 2003; Labrador et al., 2005; Landgraf et al., 1999; Thor and Thomas, 1997; Thor et al., 1999; Zarin et al., 2014). We have previously shown that Hb9 acts through the Roundabout (Robo) receptor Robo2 to regulate axon guidance in RP3 neurons, a subset of ventrally-projecting motor neurons (Santiago et al., 2014). Here, we describe a parallel pathway by which Islet regulates *fra* expression in the same neurons, and demonstrate through genetic rescue experiments that this pathway is important for muscle target selection. We also characterize a novel requirement for *isl* in regulating the medio-lateral position of RP3 dendrites, and show that the dendrite targeting defects in *isl*

mutants can be rescued by cell-type specific over-expression of Fra. These results

provide an example of how a single transcription factor specifies neural map formation

by coordinately regulating the guidance of axons to their peripheral targets, and of

dendrites to their final positions in the central nervous system, through a single

downstream effector.

Results

Islet is required for fra expression in RP motor neurons

The RP3 motor neurons innervate the NetrinB-expressing muscles 6 and 7 and are

enriched for *fra* mRNA during the late stages of embryonic development, and it was

previously reported that in the absence of *fra* or Netrins there are significant defects in

the innervation of muscles 6 and 7 (Kolodziej et al., 1996; Labrador et al., 2005; Mitchell

et al., 1996). This phenotype is also detected in the absence of *hb9/exex* or *islet/tailup*,

two transcription factors expressed in RP3 as well as in other ventrally-projecting motor

neurons, suggesting that *hb9* or *islet* may be upstream regulators of *fra* (Broihier and

Skeath, 2002; Thor and Thomas, 1997). Interestingly, Hb9, Islet, and the LIM

homeodomain factor Lim3 were all recently shown to bind directly to the *fra* locus *in*

vivo, as determined by a genome-wide DNA adenine methyltransferase identification

(DAM-ID) analysis performed in *Drosophila* embryos (Wolfram et al., 2014) (Figure

3.2). However, DAM-ID results do not provide information about the functional

significance of the detected binding events, or the cell types in which they occur. To

determine if Hb9, Islet, or Lim3 regulate the expression of *fra* in embryonic motor

neurons, we performed *in situ* hybridization experiments and analyzed *fra* mRNA

expression with single-cell resolution in embryos mutant for these factors (Figure 3.1 and Figure 3.4). We found that only *islet (isl)* is required for *fra* expression in the RP3 motor neurons at stage 15, when RP motor axons have reached the ventral muscle field but have not yet selected their final targets. 80% of RP3 neurons in abdominal segments A2-7 in *isl/+* embryos are positive for *fra* transcript versus 38% in *isl* mutant embryos (p<0.001, Figure 1D, see Methods for quantification procedure). We also observed a significant difference in the average *fra* mRNA levels in RP3 neurons between mutants and heterozygotes when quantifying pixel intensity from the fra *in situ*, whereas we detect no difference in the signal of the *isl-H-tau-myc* transgene used to label the RPs (p<0.01, Figure 3.1B). We detect no change in the number or position of RP3 neurons in *isl* mutants, consistent with previous data demonstrating that Islet is not required for the generation or survival of *Drosophila* motor neurons (Thor and Thomas, 1997). Importantly, we did not find a requirement for either *hb9* or *lim3* in regulating *fra* mRNA expression in any of the RP motor neurons, demonstrating that the regulatory relationship between *islet* and *fra* is highly specific, and could not have been predicted simply by similarities in loss of function phenotypes, or by transcription factor binding data (Figure 3.4).

We previously found that Hb9 is required for *robo2* expression in RP3 (Santiago et al., 2014). Interestingly, just as *hb9* is not required for *fra* expression in the RP neurons, *islet* is not required for *robo2* expression (Figure S2). A previous study reported that *isl; hb9* double mutants have a stronger ISNb phenotype than either single mutant, but muscle 6/7 innervation defects were not quantified (Broihier et al., 2002). To further

investigate this, we scored motor axon guidance defects in *isl; hb9* double mutants and found that the double mutants display significantly more muscle 6/7 innervation defects than either single mutant (38% of hemisegments with 6/7 innervation defects in *isl; hb9* double mutants compared to 20% in *isl* mutants and 17% in *hb9* mutants, p<0.01 in both cases, Figure 3.2). Similarly, embryos mutant for both *robo2* and *fra* have a stronger motor axon phenotype than either *robo2* or *fra* single mutants (44% in *robo2^{ex123}*, *fra3/robo2^{ex135}*, *fra4* mutants versus 20% in *fra^3/fra^4* mutants and 21% in *robo2^{ex123}/robo2^{ex33}* mutants; p<0.001 in both cases, Figure 3.4. Note that as *robo2, fra* double mutants have severe defects in midline crossing, motor axon phenotypes should be interpreted with caution; see Evans et al., 2015). These results suggest that Hb9 and Islet act in parallel to regulate distinct downstream programs in RP3 neurons, demonstrating how combinations of transcription factors are read by the cell to result in specific cell surface receptor profiles and axon trajectories.

Restoring frazzled expression in islet mutants rescues ventral muscle innervation

To determine to what extent *isl* and *fra* act in the same genetic pathway during RP3 guidance, we first examined embryos mutant for both genes. In *isl* null mutants, 20% of hemisegments lack muscle 6/7 innervation, whereas *fra^3* null mutants have a stronger phenotype (34% of hemisegments, Figure 3.3B). Embryos mutant for both *isl* and *fra* do not have significantly more muscle 6/7 innervation defects than *fra* single mutants (40% Figure 3.3B), consistent with *isl* and *fra* acting in the same pathway to regulate this process. If *fra* acts downstream of Islet during motor axon targeting, we

reasoned that restoring Fra levels in *isl* mutant neurons might rescue muscle 6/7 innervation. Indeed, we found that pan-neural over-expression of Fra in *isl* mutants partially but significantly rescues the defects in muscle 6/7 innervation (Figure 3.3D). The difference between genotypes was most striking when we counted hemisegments in which a growth cone stalls at the 6/7 cleft, as well as those in which it fails to reach it (all embryos were scored blind to genotype; see Methods). In *isl* mutants, a growth cone fails to reach the 6/7 cleft or stalls near it in 27% of hemisegments, compared to 15% of hemisegments in sibling mutants over-expressing Frazzled (p=0.003, Figure 3.3D). We also analyzed the data by comparing the number of embryos with stalled or missing 6/7 innervations. We observed that in *isl* mutants, 0% of embryos have no 6/7 innervation defects in A2-A6, 44% have 1 defect, and 56% have 2 or more defects (n=16 embryos). In contrast, in *isl* mutants over-expressing Frazzled, 29% of embryos have 0 innervation defects, 29% have 1 defect, and 41% have 2 or more defects (n= 24 embryos, p=0.03 by Fisher's exact when comparing the number of embryos with no defects). The incomplete rescue could be due to differences in the timing or levels of *GAL4/UAS* mediated expression of Fra compared to its endogenous regulation, or could indicate that Islet regulates additional downstream effectors important for motor axon pathfinding. Nevertheless, these data strongly suggest that Fra is an essential downstream effector of Islet during the guidance of the RP3 axon to its target muscles, and that Hb9 and Islet coordinately regulate this process through distinct effectors.

Over-expression of Islet in ipsilateral neurons induces fra expression and fra-dependent

midline crossing

To further investigate the functional relationship between *isl* and *fra*, we asked

whether ectopic expression of *isl* is sufficient to induce *fra* expression. For these

experiments we used the apterous (ap) neurons, a subset of interneurons that normally

form a single fascicle on either side of the midline and that are labeled by the enhancer

trap *ap-Gal4*. The ap neurons express low levels of *fra* (see below), do not express *isl*

(Thor et al., 1997 and data not shown), and do not cross the midline. Fra over-expression

has been shown to cause ectopic midline crossing of ap axons (Neuhaus-Follini and

Bashaw, 2015a; O 'Donnell and Bashaw, 2013).

We found that over-expression of Islet with *ap-Gal4* produces high levels of

midline crossing, phenocopying the effect of Fra over-expression (Figure 3.5). In stage

17 control embryos, ap axons cross the midline in 12% of segments, whereas in embryos

over-expressing *UAS-Islet* with *ap-Gal4*, ap axons cross the midline in 60% of segments

(Figure 3.5). This phenotype is dose-dependent, as embryos over-expressing Islet from

two copies of an *UAS-Islet* insertion display significantly more ectopic midline crossing

than embryos with one insert (84%, n=19 embryos, p<0.001).

To determine if *isl* over-expression results in *fra* induction, we analyzed the

expression of *fra* mRNA in ap neurons (Figure 3.5). We found that in stage 15 wild-type

embryos, a low percentage of ap neurons express *fra* (25% of ventral ap clusters were

scored as *fra+*). In contrast, in embryos over-expressing *isl* from two *UAS-Islet* inserts,

37% of the ventral ap clusters were scored as *fra+* (p<0.01 when compared to controls).

The frequency at which we detect increased *fra* expression in embryos over-expressing Islet relative to controls is lower than expected based on the ectopic crossing phenotype. *Fra* might be transiently induced in ap neurons and therefore difficult to detect by *in situ*. Alternatively, the midline crossing phenotype may be partly due to Islet's effects on other genes. To determine whether the ectopic crossing phenotype depends on *fra* induction, we over-expressed Islet in embryos homozygous for a null allele of *fra*. Strikingly, over-expression of Islet in *fra* mutants results in a complete suppression of the midline crossing phenotype (15% of segments with ap midline crossing in *fra³/fra³* embryos over-expressing *UAS-Islet*, p<0.0001 compared to 1x GOF in controls, Figure 3.5). While we cannot rule out that Islet is affecting the expression of other genes in the Fra pathway to cause midline crossing, these results demonstrate that ectopically expressing Islet in a subset of interneurons causes a detectable increase in *fra* expression, and a *fra*-dependent phenotype, and suggest that the functional relationship between *islet* and *fra* may be reused in multiple contexts.

Islet is not essential for early fra expression or for RP axon midline crossing

        fra mutants have defects in RP axon midline crossing, as shown by retrograde labeling of single motor neurons (Furrer et al., 2003). In addition, Netrin/Fra signaling controls the medio-lateral position of dendrites in several groups of motor neurons, though the targeting of RP3 dendrites in *Netrin* or *fra* mutants was not reported in this study (Mauss et al., 2009). Therefore, we asked if *isl* regulates midline crossing or the position of RP3 dendrites through *fra*. To score both phenotypes, we used a genetic strategy to label single motor neurons by the mosaic expression of a membrane-tagged

GFP transgene under the control of *lim3b-GAL4*, which labels the RP motor neurons, sensory neurons, and several other motor and interneurons (Certel and Thor, 2004). We identified RP3 neurons in control embryos by the stereotyped position of the RP3 cell body, and by the targeting of its axon to muscles 6 and 7. Due to the axon targeting defects observed in *isl* and *fra* mutants, we relied upon cell body position to identify RP3 neurons in mutant embryos (see Methods). By this approach, we detect significant defects in RP3 axon midline crossing in *fra* mutants, as previously reported (17/22 axons fail to cross the midline in *fra/fra* embryos, versus 0/13 axons in *fra/+* embryos). To our surprise, however, we observed no defects in RP axon midline crossing in *isl* mutants (33/33 RP3 axons cross the midline in *isl/isl* embryos).

      Isl and *fra* expression both initiate earlier than stage 13, the time at which RP axons cross the midline (Broadie et al. 1993, Thor et al. 1997, data not shown). Therefore, we examined whether *isl* is required for *fra* expression during the early stages of commissural axon guidance. Interestingly, we found that *isl* is not required for *fra* expression at stage 13 in any of the ventrally-projecting RPs (Figure 3.6). In contrast, in stage 15 *isl* mutant embryos from the same collection, we observed a decrease in *fra* expression in RP1 and RP3 (Figures 3.1 and 3.11). The temporal pattern of *fra* expression in RP motor neurons is dynamic, such that a larger proportion of RP1 and RP3 neurons express *fra* mRNA during the late stages of embryogenesis than during the stages of midline crossing (Figures 3.1, 3.6, and 3.11). We detect a requirement for *isl* in regulating *fra* in RP1 and RP3 as early as stage 14, when the RP motor axons have exited the CNS (58% of RP3 neurons are *fra+* in *isl/+* embryos; 42% of RP3 neurons are *fra+* in *isl/isl* embryos, p=0.01; 72% of RP1 neurons are *fra+* in *isl/+* embryos; 22% of RP1 neurons

are *fra+* in *isl/isl* embryos, p<0.001, Figure 3.6). Taken together, these results suggest

that *isl* is not essential for early *fra* expression or for midline crossing in RP neurons, but

is required for *fra* expression during the late stages of motor neuron differentiation in a

subset of RP neurons, including RP3. The stages at which we detect a requirement for *isl*

in regulating *fra* correspond to the stages when RP3 axons are exploring their ventral

muscle targets, consistent with the loss of function phenotypes we observe, and with a

model in which Islet instructs the final stages of RP3 axon targeting through Frazzled.

A difference in dendritic targeting between RP3 and RP5 neurons correlates with a

difference in fra expression

Another essential feature of *Drosophila* larval motor neurons that is established

during late stages of embryogenesis is the morphogenesis and targeting of their dendrites

in the ventral nerve cord. Motor neuron dendrites begin to form as extensions off the

primary neurite at stage 15 (Kim and Chiba, 2004), which corresponds to a time period

when we detect a requirement for *isl* in regulating *fra* (Figure 1). By early stage 17 (15

hours after egg laying, AEL), RP3 has assumed its stereotyped morphology, consisting of

a small ipsilateral projection extending from the soma, and a large dendritic arbor

forming off the contralateral primary neurite (Mauss et al., 2009). Putative sites of

synaptic contact have been detected on the contralateral arbor, identified by the overlap

between *UAS-bruchpilot* expression in pre-synaptic cholinergic neurons and the signal

from lipophilic dye fills of RP3 (Couton et al., 2015).

We used the FLP-out genetic labeling strategy to visualize individual late-stage RP motor neurons and analyze the development of their dendrites. We focused on the large contralateral arbor of the RP motor neurons, which spans the width of one side of the nerve cord in wild type embryos and forms branches that extend into several medio-lateral zones (Mauss et al., 2009) (Figure 3.7A-B). Analyses using *islet-tau-myc* and *lim3a-tau-myc* transgenes confirmed that the RP cell bodies retain their stereotyped positions in *isl* mutants, and that the relative dorsal-ventral positions of RPs 1/4, 3, and 5 are preserved, allowing us to identify specific classes of motor neurons (Landgraf et al., 1997) (Figure 1 and data not shown).

We found that almost all RP3 neurons in late stage *isl/+* embryos neurons form contralateral arbors that send projections into the zone between the medial FasII+ axon pathways and the intermediate FasII+ axons, hereafter referred to as the "intermediate zone", consistent with previously published images of RP3 neurons from wild type embryos (89%, n=18, Figure 3.7A-B, see also Mauss et al., 2009). Interestingly, the dendritic morphology of RP3 was distinct from that of a related neuron, RP5, which also expresses Islet and Lim3b-Gal4, and which can be unambiguously identified in both wild type and mutant embryos as its cell body is found in a more ventral plane than the other RP neurons (Landgraf et al., 1997 and data not shown). In wild type embryos, the RP5 axon targets muscles 12 and 13 (VL1 and VL2) as well as other ventral muscles (Landgraf et al., 1997, Mauss et al., 2009, and data not shown). Interestingly, most RP5 dendrites in *isl/+* embryos are found exclusively in the lateral zone of the neuropile, and do not target the intermediate zone (80%, n=20) (Figure 3.7A). Furthermore, the

difference we observe in the dendritic targeting of RP3 and RP5 neurons correlates with a difference in *fra* expression. While *fra* expression in RP3 and RP5 neurons in control embryos is comparable at stage 13 (Figure 3.6), by stage 15 significantly fewer RP5 than RP3 neurons express *fra* (Figure 3.7). Islet is not required for the low levels of *fra* expression in late-stage RP5 neurons, in contrast to its role in promoting high levels of *fra* in late-stage RP3 neurons (Figure 1 and Figure 3.7C). Furthermore, when we monitor endogenous Netrin expression in late-stage nerve cords using a Myc-tagged *NetB* knock-in allele (Brankatschk and Dickson, 2006), we detect enrichment of NetrinB protein in the area between the intermediate and medial FasII+ axon bundles, corresponding to the intermediate zone where we detect contralateral dendritic projections from RP3 neurons (Figure 3.7D), and suggesting that high levels of Fra in RP3 neurons may instruct the formation of dendritic extensions in this region.

Islet and fra regulate the targeting of RP3 motor neuron dendrites in the CNS

We next analyzed RP motor neuron dendrites in *isl/isl* embryos to determine whether Islet regulates dendritic position or morphogenesis through Fra or other effectors. We did not observe a significant difference in the morphology or medio-lateral position of RP5 dendrites in *isl/isl* embryos (data not shown). In striking contrast, many RP3 neurons in *isl/isl* embryos fail to target their contralateral dendrites to the intermediate zone (48%, n=33, p=0.01 compared to *isl/+* embryos, Fisher's exact test, Figure 3.8A-B). Instead, the medial-most dendrites in these RP3 neurons remain fasciculated with the intermediate FasII+ axon pathways, and do not send extensions

96

toward the midline, a phenotype that was rarely seen in control RP3 neurons (Figure

3.8A-B). To more quantitatively measure the lateral shift and to address the possibility

that defects in targeting were secondary to defects in outgrowth, we traced RP3 neurons

from *isl/+* and *isl /isl* embryos using the Imaris software and measured total contralateral

dendrite lengths and total number of contralateral dendrite tips (see Methods) (Figure

3.8C; see Figure 3.10 for additional examples of traces). We also measured the total

length of contralateral dendrites in the intermediate zone of the neuropile (Figure 3.8C-

D). There was no significant difference in the average total length or tip number of RP3

dendrites between *isl* mutants and heterozygotes, suggesting that targeting defects in *isl*

mutants are not caused by reduced outgrowth (Figure 3.8E-F). However, the ratio of the

length of dendrites in the intermediate zone over total dendrite length was significantly

reduced in *isl* mutants, confirming that *isl* mutant RP3 dendrites are shifted laterally

relative to controls, independent of any change in arbor size (p=0.014, Figure 3.8C-D).

We next analyzed the dendrites of RP3 neurons in *fra/+* and *fra/fra* embryos. As

with *isl* mutants, we relied upon cell body position to identify RP3 neurons, and excluded

neurons with ambiguous positions (see Methods). In *fra* mutant RP3 neurons whose

axons fail to cross the midline, a single large dendritic arbor forms off the ipsilateral

primary neurite, and we traced this arbor to measure its size and medio-lateral position.

We observed a significant lateral shift in the position of RP3 dendrites in *fra* mutants,

both by scoring for the presence of dendrites in the intermediate zone, and by quantitative

analysis of the dendrite extensions of traced neurons (Figure 3.9A-C). The lateral shift in

fra mutants was more pronounced than in *isl* mutants, consistent with our observation

that some RP3 neurons retain *fra* expression in the absence of *isl* (Figure 1). Of note, the lateral shift phenotype did not correlate with whether the RP3 axon had crossed the midline, as we detected it at similar frequencies in both contralateral and ipsilateral arbors (Figure 3.9A). Curiously, several RP3 contralateral dendritic arbors appeared reduced in size in *fra* mutants (Figure 3.9A, right-most panel), whereas this phenotype was not seen in control embryos. However, as in the case of *isl* mutants, there was no significant change in the total dendrite tip number or total dendrite length in *fra* mutants compared to heterozygous embryos, though the distribution of these data was broader in the mutants, and there was a trend toward a decrease (Figure 3.9D,F). These findings are consistent with previous reports that Netrin-Fra signaling does not play a major role in regulating the outgrowth of motor neuron dendrites in the nerve cord (Brierley et al., 2009; Mauss et al., 2009).

We next asked whether *isl* and *fra* regulate dendrite development in other classes of motor neurons. RP1 and RP4 also express *islet*, *fra*, and *lim3b-Gal4*. We detect a requirement for *isl* in regulating *fra* expression in RP1, but not in RP4, at stage 15 (Figure 3.11C). Interestingly, most RP1 neurons, like RP3 neurons, retain high levels of *fra* at this stage, whereas few RP4 neurons are *fra+* in late stage control embryos (Figure 3.11C). Previous descriptions of RP1 and RP4 indicate that they form contralateral dendritic arbors of distinct morphologies: RP1's is taller, and found more medially (Mauss et al., 2009). However, as the axons of RP1 and 4 target adjacent muscles external to muscles 6 and 13, and their cell bodies are both found close to the midline at a similar dorsal-ventral position, we could not unambiguously distinguish between them in

our single-cell labeling experiments. Nevertheless, when we scored RP1 and RP4 neurons together, we observed a significant lateral shift in the position of RP1 and 4 dendrites in *isl* mutants compared to their heterozygous siblings: 3/22 RP1 and 4 neurons were excluded from the intermediate zone in *isl/+* embryos (14%) compared to 16/22 in *isl/isl* embryos (73%) (p=0.0002, Fisher's exact test) (Figure 3.11A-B). Although additional work will be necessary to determine if the defects in lateral position we detect in RP1 and/or RP4 correlate with changes in *fra* expression, these data demonstrate that Islet regulates the medio-lateral position of dendrites in multiple motor neuron subsets. Together, these results indicate that *isl* is required for the high levels of *fra* in late stage RP1 and RP3 neurons, as well as for dendrite targeting in this class of motor neurons.

Axon and dendrite targeting defects are not correlated in individual RP3 neurons

Our single cell labeling method allows us to precisely describe the axon targeting defects in *isl* and *fra* mutants, and to determine whether they correlate with defects in dendrite position. Axon and dendrite targeting occur at approximately the same developmental stage, and to date there is no evidence that one process depends on the other (Kim and Chiba 2004; Landgraf et al., 2003). A strong correlation in our single-cell genetic analyses could indicate that the two processes could be linked. Importantly, previous studies using retrograde labeling of motor neurons in mutant embryos were not able to test this hypothesis, as they relied upon motor axons reaching the correct muscles in order to be visualized (Mauss et al., 2009).

99

To address this question, we scored axon and dendrite targeting of single labeled RP3 neurons in embryos with muscles fully preserved following dissection. All of the RP3 axons that we were able to score in *isl/+* embryos innervated the muscle 6/7 cleft (n=14) (Figure 3.8G). In contrast, 18/26 *isl/isl* RP3 axons innervated muscles 6/7, and 8 stalled at the 6/7 cleft or earlier along RP3's trajectory, or bypassed the choice point entirely (31% have defects, n=26) (Figure 3.8G). In *fra/fra* embryos, 10/21 RP3 neurons failed to innervate the muscle 6/7 cleft, and stalled at or bypassed the choice point (48% have defects, not shown). This phenotype is stronger than the frequency at which we detect a complete loss of muscle 6/7 innervation in *isl* or *fra* mutants by scoring with anti-FasII (Figure 2). To determine if this enhancement was due to the heat shock (H.S.) step that is required for the genetic labeling protocol, we scored muscle innervation using anti-FasII in *isl/isl* embryos heat shocked for either 5 minutes or 1 hour (see Methods), and found that the 1 hour heat shock mildly enhances muscle innervation defects in *isl* mutants (to 30.4%), whereas a 5 minute heat shock does not (24.7% of hemisegments have defects, not shown). Importantly, the two heat shock protocols did not result in any difference in the frequency of dendrite targeting defects in *isl* mutants (7/17 RP3 dendrites in *isl/isl* mutants are shifted laterally in embryos treated with 1 hour H.S, and 9/16 dendrites are shifted after 5 min H.S).

Surprisingly, we did not detect a correlation between axon and dendrite defects in *isl* mutant RP3 neurons (Figure 3.8G). While 5/26 mutant RP3 neurons displayed defects in both axons and dendrites, 12/26 neurons showed defects in one process but not the other (Figure 3.8G). A similar analysis in *fra* mutants revealed that 8/21 RP3 neurons

displayed defects in both muscle 6/7 innervation and dendrite position, whereas 7/21

displayed normal targeting in one process but not the other (data not shown). These data

suggest that axon and dendrite targeting can occur independently within an individual

RP3 neuron, and that the central targeting defects we observe in *isl* mutants are not likely

to be secondary to defects in muscle innervation.

Islet regulates dendrite development in RP3 neurons through fra

To directly test whether *isl* regulates RP3 dendrite position through its effect on

fra expression, we over-expressed a *UAS-HA-Frazzled* transgene using *lim3b-GAL4* in *isl*

mutants, and used the *hsFLP* technique to sparsely label RP motor neurons, as described

above (Figure 8). Strikingly, in *isl* mutant embryos over-expressing Fra, 0/21 RP3

contralateral dendritic arbors were excluded from the intermediate zone, compared to

8/22 (36%) in sibling mutants lacking the *UAS-Frazzled* transgene (p<0.01, Fisher's

exact test) (Figure 8B). To more quantitatively measure dendrite position, we obtained

traces of contralateral RP3 dendrites by using Imaris. We detected a robust rescue of the

lateral shift phenotype in *isl* mutants, as measured by the summed lengths of dendrites in

the intermediate zone over the total dendrite length (p<0.001, Student's t-test) (Figure

8C). Indeed, the ratio of dendrites in the intermediate zone in rescued mutants was higher

than in heterozygous controls (compare to Figure 5), perhaps reflecting a gain of function

effect caused by artificially high levels of Fra from transgenic over-expression.

Importantly, Fra over-expression did not affect total dendritic arbor lengths or tip

numbers (Figure 8D-E), consistent with our observation that Fra regulates the distribution

of dendrites rather than their growth, and strongly arguing that the rescue we observe is not caused by an increase in the total size of the dendritic arbor. While we cannot rule out that Islet regulates dendrite position in part through additional downstream effectors, our observation that cell-type specific over-expression of Fra in *isl* mutants rescues dendrite targeting provides compelling support for the model that *fra* acts downstream of *isl* to control RP3 dendrite morphogenesis. Together with our demonstration that *isl* directs motor axon targeting through the regulation of *fra*, we conclude that *isl* coordinately regulates the targeting of axons in the periphery and of dendrites in the CNS through a common downstream effector.

Discussion

Identifying the cellular effectors that act downstream of subset-specific transcription factors during the different steps of neural morphogenesis remains a major challenge, as does understanding how individual transcription factors coordinately establish multiple aspects of cell fate. In this study, we show that Islet is required for *frazzled/DCC* expression in a subset of *Drosophila* motor neurons, and that this is important for two key aspects of motor neuron identity. Loss of function and genetic rescue experiments indicate that *fra* acts downstream of *isl* in motor neurons both during axon guidance in the periphery and dendrite targeting in the central nervous system. These data describe a mechanism by which a single transcription factor establishes neural map formation by controlling multiple aspects of cell morphology through an identified downstream effector.

A role for a cell-type specific transcription factor in controlling myotopic map formation

From the onset of their development, *Drosophila* larval and adult motor neuron dendrites target stereotyped medio-lateral positions in the central nervous system (Brierley et al., 2009; Mauss et al., 2009). Slit-Robo, Netrin-Frazzled, and Sema-Plexin signaling have all been shown to control motoneuron dendrite targeting in *Drosophila*, and rescue experiments suggest that guidance receptors act cell autonomously in this process (Brierley et al., 2009; Mauss et al., 2009; Syed et al., 2016). In addition, the initial targeting of motoneuron dendrites in the embryo is largely unaffected by manipulations that affect the position or the activity of pre-synaptic axons or the presence of muscles, suggesting this process is likely to be under the control of intrinsic, cell autonomous factors (Landgraf et al., 2003; Mauss et al., 2009)

We address several key questions about how motor neuron dendrite targeting is specified in the embryonic nervous system. First, we show that *fra* expression in two classes of motor neurons (RP3 and RP5) correlates with the medio-lateral position of their dendrites. Second, we demonstrate that Islet, a LIM homeodomain transcription factor previously shown to regulate axon targeting in a subset-specific way, also regulates dendrite targeting. Third, we find that Islet regulates both of these processes through its effect on *fra* expression. Surprisingly, we did not detect a significant correlation between axon and dendrite phenotypes in *isl* mutants, perhaps because Islet regulates both processes in part through additional targets. The absence of a correlation suggests that the dendrite positioning defects are not secondary to defects in target selection, consistent with a previous study in which the general patterning of motor neuron dendrites was not disrupted in muscle-less embryos (Landgraf et al., 2003). However, additional

experiments that disrupt axon targeting and monitor the medio-lateral position of dendrites will be necessary to confirm that the two processes occur independently.

Future work will also be necessary to identify additional transcription factors that regulate dendrite development in motor neurons. In particular, the factors regulating Robo signaling during this process remain unknown. We previously identified a role for Hb9 in regulating *robo2* and *robo3* expression, but it is not known whether these receptors regulate motor neuron dendrite development (Santiago et al., 2014). We detect no change in *robo1* mRNA levels in RP3 neurons in either *hb9* or *isl* mutants (data not shown). Robo signaling could be regulated post-transcriptionally. The endosomal sorting protein Comm is required for midline crossing of motor neuron dendrites, and may also regulate their medio-lateral position (Furrer et al., 2003; Furrer et al., 2007). The temporal pattern of *comm* expression does not support a role in dendrite targeting, however, as *comm* is not expressed in RP motor neurons at late stages of embryogenesis (Keleman et al., 2002; data not shown).

The functional consequences of dendrite targeting defects remain to be explored. It is likely that shifting the position of motor neuron dendrites alters their connectivity, but testing this hypothesis will require identifying the pre-synaptic neurons that impinge on the RP neurons during locomotive behavior. Forcing a lateral shift of the dendrites of dorsally-projecting motor neurons does not abolish their connectivity with known pre-synaptic partners, but does change the number of contacts established (Couton et al., 2015). In mice, the ETS factor Pea3 is required for the dendritic patterning of a subset of limb-innervating motor neurons, and electrophysiological recordings reveal changes in connectivity in *Pea3* mutant spinal cords (Vrieseling and Arber, 2006). It will be of high

interest to investigate whether analogous defects are detected in *isl* or *fra* mutant

embryos.

Islet is an essential regulator of multiple features of RP3 identity

        Drosophila Islet was initially described as a subset-specific regulator of axon

guidance, as it is required in ventrally-projecting motor neurons for their axons to reach

the correct muscles, and can affect the guidance of dorsally-projecting axons when mis-

expressed (Landgraf et al., 1999; Thor and Thomas, 1997). More recently, Baines and

colleagues demonstrated that Islet also acts instructively to establish the

electrophysiological properties of RP motor neurons through repression of the potassium

ion channel Shaker (Wolfram et al., 2012). In addition, DAM-ID data shows Islet binding

near the acetylcholine receptor genes nAcRalpha-7E (CG2302), nAcRalpha-30D

(CG4128), and nAcRalpha-34E (CG32975), though it remains to be determined whether

Islet regulates their expression (Wolfram et al., 2014). Our data shows that in addition to

regulating the axonal trajectory and the physiological properties of the RP3 neuron, Islet

also establishes its dendritic position. Thus, Islet is essential for at least three late-arising

features of RP3 identity. Hobert and colleagues have defined terminal selectors as

transcription factors that coordinately regulate gene programs conferring multiple aspects

of a cell's identity, including its neurotransmitter phenotype, ion channel profile, and its

connectivity (Hobert, 2015). Unlike the early acting factors that act transiently to specify

cell fate, terminal selectors are expressed throughout the life of an animal, and are

required for the maintenance of neural identity. While there are several described

examples of transcription factors that act this way from studies in both invertebrates and

vertebrates, it remains unclear how widespread a phenomenon it is (Allan et al., 2005; Eade et al., 2012; Hobert and Flames, 2009; Kratsios et al., 2012; Kratsios et al., 2015; Lodato et al., 2014). Does Islet fit the criteria for a terminal selector? Islet is not required for all aspects of RP3 identity, as RP motor neurons retain expression of other motor neuron transcription factors in *isl* mutants, and their axons successfully exit the nerve cord (Thor et al., 1997, and data not shown). Future work will be necessary to determine whether Islet is required throughout larval life for the maintenance of RP3's physiological and morphological features. It will also be interesting to determine whether the other motor neuron transcription factors that have been primarily studied in the context of axon guidance are also involved in the establishment of other subset-specific properties, including dendrite targeting and morphogenesis.

Hb9 and Islet act in parallel to regulate axon guidance through distinct downstream effectors

Co-expressed transcription factors could act synergistically to regulate specific downstream programs, in parallel through completely distinct effectors, or by some combination of the two mechanisms. Indeed, examples of all of the above scenarios have been described. Both in vitro and in vivo studies demonstrate that in vertebrate spinal motor neurons, Isl1 forms a complex with Lhx3, and that the Isl1-Lhx3 complex binds to and regulates different genes than Lhx3 alone, or than a complex composed of Isl1 and Phox2b, a factor expressed in hindbrain motor neurons (Cho et al., 2014; Mazzoni et al., 2013; Thaler et al., 2002). In a subset of spinal commissural neurons, Lhx2 and Lhx9 act in parallel to promote midline crossing through upregulation of Rig-1, as *Lhx2; Lhx9*

double mutants display strong midline crossing defects and decreased Rig-1 expression, whereas *Lhx2* or *Lhx9* single mutants do not (Wilson et al., 2008). In *Drosophila* dorsally-projecting motor neurons, Eve, Zfh1 and Grain act in parallel to promote the expression of *unc5*, *beat1a*, and *fas2*, though Eve also regulates additional targets important for axon guidance that not shared by Zfh1 or Grain (Zarin et al., 2014). Here we show that Islet and Hb9 act in parallel through at least two distinct effectors, and propose that they regulate their targets by different mechanisms. Hb9 likely indirectly promotes *robo2* expression by repressing one or multiple intermediate targets, as its conserved Engrailed homology domain is required for its function in *Drosophila* motor axon guidance and for *robo2* regulation (Santiago et al., 2014). In vertebrate motor neurons, Isl1 forms a complex with Lhx3 to directly activate several of its known targets (Cho et al., 2014; Lee et al., 2016; Thaler et al., 2002). A recent genome-wide DAM-ID analysis found that Islet binds to multiple regions within and near the *fra* locus in *Drosophila* embryos, suggesting it may directly activate *fra* (Wolfram et al., 2014). Our finding that *lim3* is not required for *fra* expression in the RP motor neurons, together with evidence that Islet can alter the electrical properties of muscle cells independently of Lim3, suggest that *Drosophila* Islet does not need to form a complex with Lim3 for all of its functions (Wolfram et al., 2014). Future research will be necessary to detect Islet binding events in embryonic motor neurons, though these experiments are particularly challenging if binding occurs transiently or in a small number of cells (Agelopoulos et al., 2014). The generation of many large-scale datasets for transcription factor binding sites *in vitro* and *in vivo* presents the field with the task of reconciling these data with clearly defined genetic relationships during a specific biological process (Lacin et al., 2014; Lee

et al., 2008a; Mazzoni et al., 2013; Wolfram et al., 2014). Our study and others have initiated this effort, but it will be important to investigate other potential transcription factor-effector relationships, in order to achieve a better understanding of how transcriptional regulators control cell fate (Cho et al., 2014; Hattori et al., 2013; Lodato et al., 2014; Wolfram et al., 2012).

Experimental Procedures

Genetics

The following Drosophila mutant alleles were used: *tup^1, tup^{isl}* (Tao et al., 2007); *Df(2L)Exel 7072* (Boukhatmi et al., 2012)*; hb9^{kk30}, hb9^{ad121}*(Broihier et al., 2002); *lim3^{Bd7}, lim3^{Bd6}* (Thor et al., 1999), *fra^3, fra^4; robo2^{x33}, robo2^{x123}, robo2^{x135}* (Simpson et al., 2000a)*; ap^{Gal4}* (O'Keefe et al., 1998). The following transgenes were used: *P{isl-H-tau-myc}II* (Thor et al., 1997)*; P{lim3a-tau-myc}* (Thor et al., 1999); *P{GAL4-lim3b}* (Certel and Thor, 2004); *P{GAL4-elav}III; P{ UAS-Tau-MycGFP}III; P{hsFLP}12* (Bloomington stock # 1929); *P{hsFLP}122* (gift from A. Ghabrial); *[P{UAS(FRT.stop)mCD8-GFP.H}14, P{UAS(FRT.stop)mCD8-GFP.H}21B]* (Bloomington # 30032); *P{10UAS-HAFrazzled}86Fb* (Neuhaus-Follini and Bashaw, 2015a); *P{10UAS-Islet5xMyc}86Fb*. Transgenic *UAS-Islet5xMyc* flies were generated by BestGene Inc (Chino Hills, CA) using ΦC31-directed site-specific integration into landing sites at cytological position 86Fb. All crosses were carried out at 25°C. Embryos were genotyped using balancer chromosomes carrying *lacZ* markers or by the presence of epitope-tagged transgenes.

Molecular Biology

Islet-5Xmyc was cloned into a pUAST vector containing 10xUAS and an attB site for

PhiC31-mediated targeted insertion (p10UAST-attB). Full-length tailup isoform A cDNA

was amplified from *UAS-Islet* flies (Thor et al., 1997) and cloned in frame to a C-

terminal 5xMyc tag into p10UAST-attB. All constructs were fully sequenced.

Immunofluorescence and Imaging

Dechorionated, formaldehyde-fixed, methanol-devittellinized embryos were fluorescently

stained using standard methods. The following antibodies were used: Mouse anti-

Fasciclin-II/mAb 1D4 [Developmental Studies Hybridoma Bank, (DSHB), 1:100], mouse

anti-βgal (DSHB, 1:150), chick anti-ßgal (Abcam #9361; 1:1000), mouse anti-HA

(Covance, 1:500) rabbit anti-GFP (Invitrogen #A11122, 1:250), rabbit anti-c-Myc (Sigma

C3956, 1:500), Cyanine 3-conjugated goat anti-mouse (Jackson #115-165-003, 1:1000),

Cyanine-5-conjugated goat anti-mouse (Jackson #), Alexa-488-conjugated goat anti-

rabbit (Molecular Probes #A11008, 1:500), Cyanine-3 goat anti-chick (Abcam #97145;

1:500). Embryos were mounted in 70% glycerol/PBS. Fluorescent mRNA *in situ*

hybridization and quantification were performed as previously described (Santiago et al.,

2014). *fra* antisense probe was transcribed from linearized cDNA cloned into

pBluescript. Images were acquired using a spinning disk confocal system (Perkin Elmer)

built on a Nikon Ti-U inverted microscope using a Nikon OFN25 60× objective with a

Hamamatsu C10600-10B CCD camera and Yokogawa CSU-10 scanner head with

Volocity imaging software. Max projections were generated, cropped and processed

using ImageJ.

Single Cell Labeling

Embryos containing *hsFLP*, *UAS-FRTstopFRT-mCD8-GFP*, and *lim3b-Gal4* transgenes were collected overnight at 25°C in standard cages. Embryos were heat-shocked at 37°C the next morning for 3-5 minutes (FLP.122) or 45-60 minutes (FLP.12), and fixed 9 hours after heat shock using standard procedures. RP neurons were identified by the positions of their cell bodies; in mutant embryos, neurons with ambiguous cell body positions were excluded. Staining with *isl-H-tau-myc* and *lim3-tau-myc* transgenes confirmed that all RPs are found close to the midline and that the relative dorsal-ventral positions of RPs1/4, 3, and 5 are preserved in *isl* mutants (Landgraf et al., 1997).

Phenotypic quantification

Phenotypes were scored using Volocity and Imaris. For scoring *fra* and *robo2* expression, if the cell body of a neuron could be detected by the *in situ* signal, that neuron was scored as positive. RP3 neurons were identified by using *islet-tau-myc* or *lim3a-tau-myc* and their position; ventral apterous neurons were identified by using *ap-Gal4* and their position. All embryos were scored blind to genotype. For motor axon FasII phenotypes, Stage 17 embryos were filleted and imaged. Hemisegments in A2-A6 in which a FasII+ axon could not be detected between muscles 6 and 7 were scored as lacking the 6/7 innervation. In the *elavGal4>UAS-Fra* rescue experiment, hemisegments in which a FasII+ axon could be detected near muscles 6 and 7 but failed to innervate the cleft were scored as stalled. All embryos were scored blind to genotype. For RP3 dendrite scoring, Stage 17 embryos were filleted and imaged. Dendritic arbors were traced using the filament tool on Imaris software (Bitplane). Filaments were created using the GFP

channel, and then overlaid onto the FasII channel to score the presence of dendrites in the intermediate region of the neuropil (defined as the area in between the medial and the intermediate FasII+ paths). For filament length quantification, dendrites of the contralateral arbor found in the intermediate zone were selected on the Imaris program, and the measurements of their lengths were exported and summed. Then, all dendrite segments were selected; their lengths were exported and summed. The primary neurite and axon were excluded from length measurements. For RP1,4, and 5 dendrite scoring, Stage 17 embryos were filleted and imaged. Z stacks were examined on Volocity software, and the presence of a dendritic projection in the intermediate zone was scored.

Statistics

For statistical analysis, comparisons were made between genotypes using the Student's t-test or Fisher's exact test, as appropriate. For multiple comparisons, a post-hoc Bonferroni correction was applied. For statistical analysis, comparisons were made between genotypes using the Student's t-test or Fisher's exact test, as appropriate. For multiple comparisons, a post-hoc Bonferroni correction was applied. Outliers were not excluded from statistical analyses. Sample sizes are indicated in the figures or in figure legends, and were selected based on values in previous studies in the field that allow for reproducible detection of statistically significant differences between genotypes.

Figure 3.1. *Islet* is required for *fra* expression in the RP3 motor neurons.
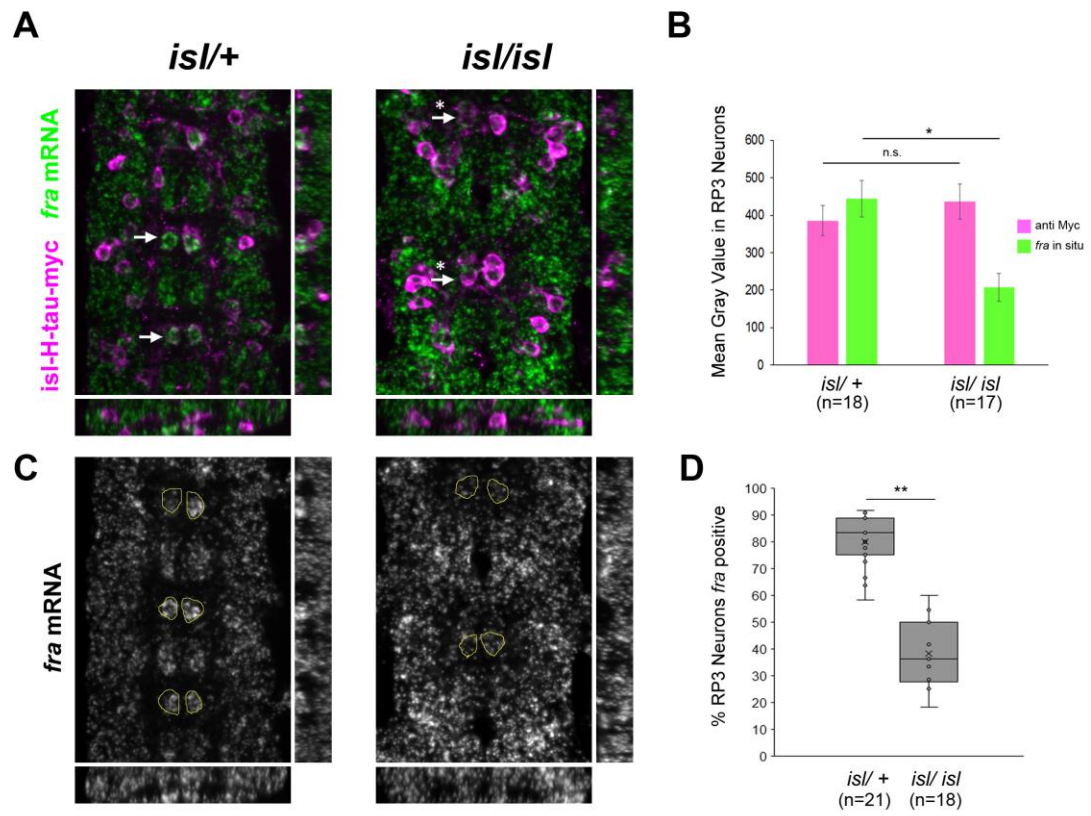
Figure 3.1. *Islet* **is required for** *fra* **expression in the RP3 motor neurons.**

A, C: Fluorescent *in situ* hybridization for *fra* in stage 15 embryos. Anterior is up. In *isl/+* embryos, *fra* mRNA (green) is enriched in the cell bodies of the RP3 motor neurons (arrows in A, circles in C), which are labeled by the *isl-H-tau-myc* transgene (magenta). *isl* mutants display reduced *fra* signal in RP3 motor neurons (arrows with asterisks in A).

B: Quantification of the *fra* in situ and *isl-tau-myc* signal in RP3 neurons by measuring pixel intensity. *isl* mutants have decreased *fra* expression but no difference in *isl-tau-myc* signal (*p<0.001, Student's t-test). N=number of images analyzed. Error bars indicate the standard error of the mean. **D**: Box and whisker plot of the % of RP3 neurons positive for *fra* (see Methods for details on scoring). The mean is indicated by the x. Inner points and outlier points are displayed. An exclusive median method was used to calculate quartiles. *Isl/isl* mutants have a significant decrease in the percentage of *fra+* RP3 motor neurons compared to *isl/+* embryos (**p<1x10^{-5}, Student's t-test). N=number of embryos. *isl/+* denotes *tup^{isl}/CyO,Wgβg* or *Df(2L)Exel7072/ CyO,Wgβg. isl/isl* denotes *tup^{isl}/ Df(2L)Exel7072*. Similar results were observed with a different *isl* allelic combination (data not shown).

Figure 3.2. Islet, Hb9 and Lim3 bind to the *fra* locus in embryos (Wolfram et al., 2014).
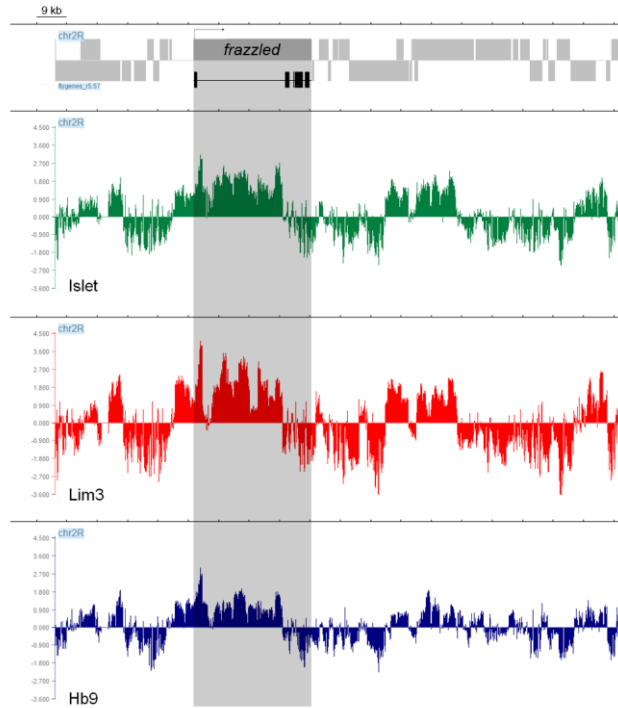
Figure 3.2. Islet, Hb9 and Lim3 bind to the *fra* locus in embryos (Wolfram et al., 2014).

DAM-ID data indicates that Islet, Hb9, and Lim3 bind to regions immediately upstream of *fra*, and within *fra*'s first intron, in *Drosophila* embryos (Wolfram et al., 2014, GEO accession # GSE53446). *fra* was identified as a putative target for these factors using a False Discovery Rate (FDR) value <0.1% (Wolfram et al., 2014). The transcription unit of *fra* is highlighted; the arrow indicates the direction of transcription. Exons are represented below as black boxes. The average of normalized log2-transformed ratios from multiple biological replicates of Islet-DAM binding relative to the DAM-only control are plotted in green; the analogous values are shown below for Lim3 (red) and Hb9 (blue).

Figure 3.3. *Islet* and *hb9* act in parallel to regulate RP3 guidance to its target muscles; *islet* acts through *fra.*
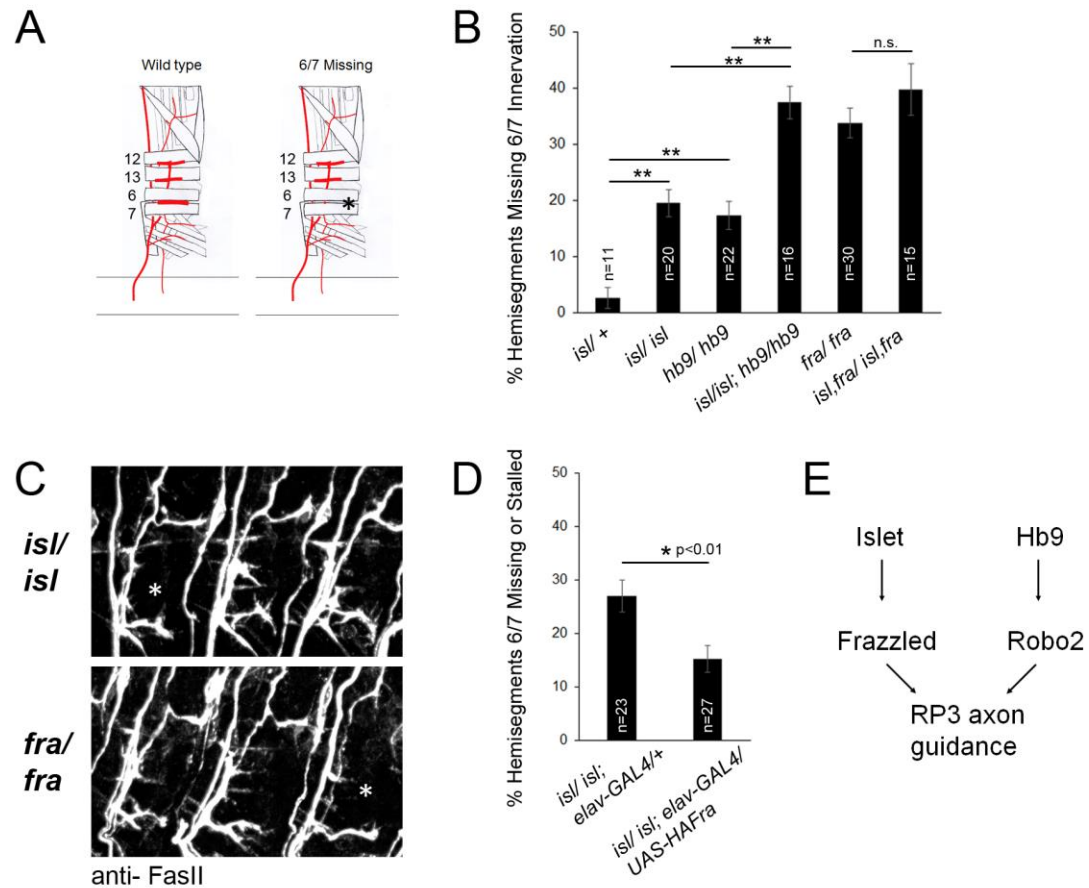
Figure 3.3. *Islet* and *hb9* act in parallel to regulate RP3 guidance to its target muscles; *islet* acts through *fra.*

A: Schematic of two hemisegments; dorsal is up and anterior is left. The asterisk indicates the absence of muscle 6/7 innervation by RP3. **B**: Quantification of muscle 6/7 innervation defects. *isl; hb9* double mutants have an additive phenotype compared to the single mutants, whereas *isl, fra* double mutant embryos are not enhanced relative to *fra* mutants (**p<0.001). **C**: *fra* or *isl* mutant embryos stained for FasII, which labels all motor axons. Asterisks indicate an absence of muscle 6/7 innervation. **D**: Quantification of 6/7 defects in *isl* mutants over-expressing *HA-Frazzled* in all neurons, compared to sibling mutants. **E**: Model for how Islet and Hb9 act through distinct downstream effectors to regulate RP3 axon guidance (see also Santiago et al 2014). In **B**, *isl/+* denotes *Df(2L)Exel7072/CyO,Wgβg*. *isl/isl* denotes *Df(2L)Exel7072/ Df(2L)Exel7072*. *hb9/hb9* denotes *hb9^{kk30}/hb9^{ad121}*. *isl/isl; hb9/hb9* denotes *Df(2L)Exel7072/Df(2L)Exel7072; hb9^{kk30}/hb9^{ad121}*. *fra/fra* denotes *fra^3/fra^3*. *isl,fra/isl,fra* denotes *Df(2L)Exel7072,fra^3/ Df(2L)Exel7072,fra^3*. In **D**, *isl/isl* denotes *tup^{isl}/Df(2L)Exel7072*. N=number of embryos. Error bars indicate the standard error of the mean.

Figure 3.4. Hb9 and Lim3 are not required for *fra* expression in RP3 neurons; Islet is not required for *robo2* expression; *robo2* and *fra* act in parallel to regulate RP3 axon guidance.
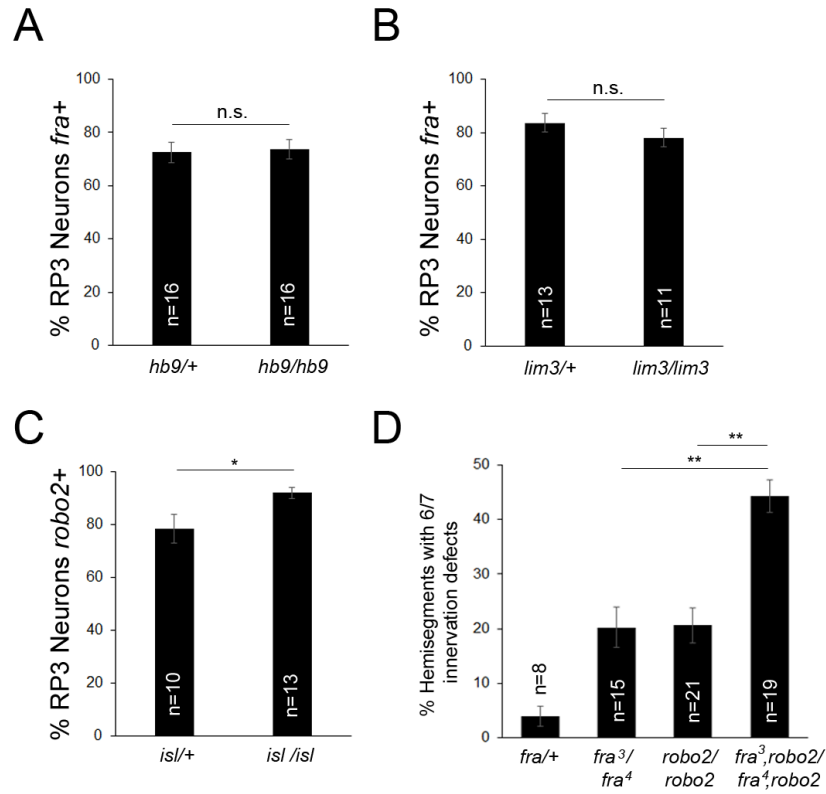
Figure 3.4. Hb9 and Lim3 are not required for *fra* expression in RP3 neurons; Islet is not required for *robo2* expression; *robo2* and *fra* act in parallel to regulate RP3 axon guidance.

A: Quantification of *fra in situ* in A2-A7 of stage 15-16 *hb9/+* and *hb9/hb9* embryos. RP3 neurons were labeled by *hb9^{Gal4}* and scored as positive or negative for *fra* mRNA, blind to genotype. There is no significant difference in the number of RP3 neurons positive for *fra* in *hb9/hb9* embryos (p=0.8). **B**: Quantification of *fra in situ* in A2-A7 of stage 15 *lim3/+* and *lim3/lim3* embryos. RP3 neurons were labeled by *lim3a-tau-myc* and scored as positive or negative for *fra*, blind to genotype. There is no significant difference in the number of RP3 neurons positive for *fra* in *lim3/lim3* embryos (p=0.27). **C**: Quantification of *robo2 in situ* in stage 15 *isl/+* and *isl/isl* mutant embryos. RP3 neurons were labeled by *lim3a-tau-myc* and scored as positive or negative for *robo2*, blind to genotype. *isl/isl* embryos displayed a slight increase in the % of *robo2+* RP3 neurons (*p<0.05). **D**: Quantification of muscle 6/7 innervation defects in A2-A6 of late stage 17 embryos. *robo2; fra* double mutants have an additive phenotype compared to the single mutants (**p<0.001). *hb9/+* denotes *hb9^{Gal4}/+*. *hb9/hb9* denotes *hb9^{Gal4}/hb9^{ad121}*. *lim3/+* denotes *lim3^{bd6}/CyO,Wgβg* or *lim3^{bd7}/ CyO,Wgβg*. *lim3/lim3* denotes *lim3^{bd6}/ lim3^{bd7}* . *isl/+* denotes *tup^{1}/CyO,Wgβg* or *Df(2L) Exel7072/CyO,Wgβg*. *isl/isl* denotes *tup^{1}/Df(2L)Exel7072*. *fra/+* denotes *fra^{3}/CyO,Wgβg* or *fra^{4}/CyO,Wgβg*. *robo2/robo2* denotes *robo2^{123}/ robo2^{33}* . *fra^{3},robo2/fra^{4},robo2* denotes *fra^{3},robo2^{123}/ fra^{4},robo2^{135}*. N=number of embryos. Error bars indicate the standard error of the mean.

Figure 3.5 *Islet* **gain of function in a subset of interneurons induces** *fra* **expression**

and a *fra***-dependent midline crossing phenotype.**
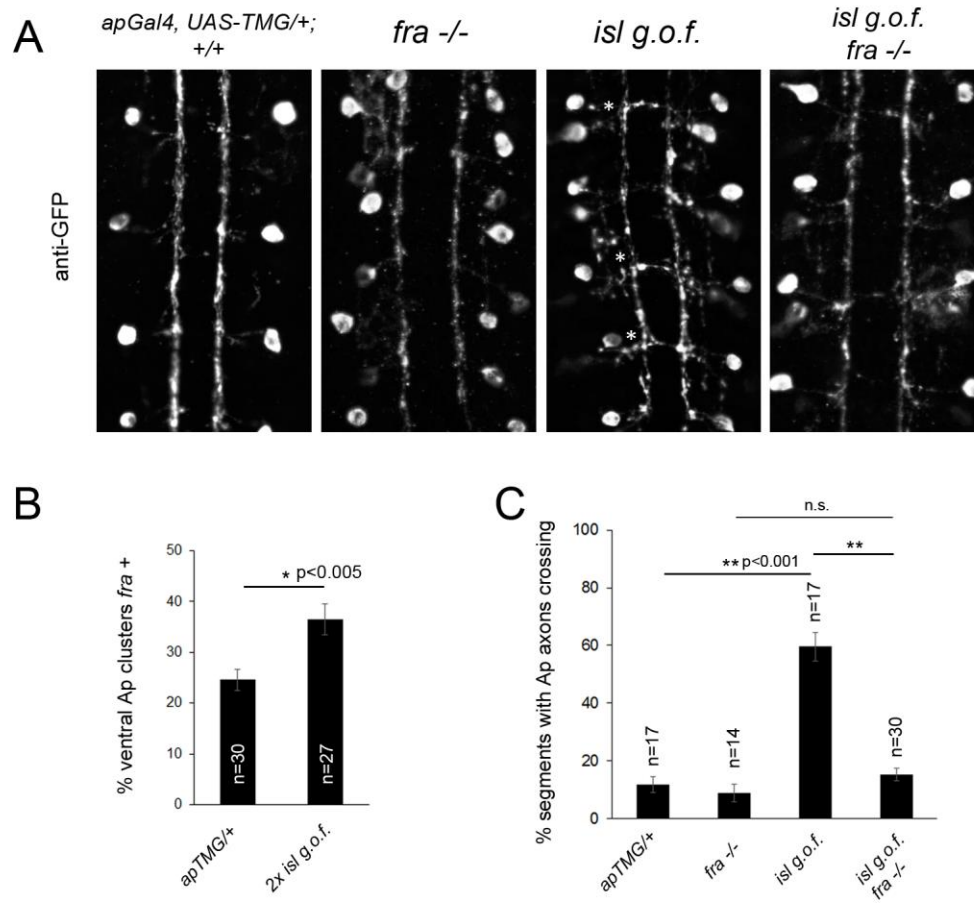
Figure 3.5. *Islet* **gain of function in a subset of interneurons induces** *fra* **expression and a** *fra***-dependent midline crossing phenotype.**

A: Stage 17 embryos in which the apterous (ap) neurons are labeled with ap^{Gal4}>*UAS-TauMycGFP*. Islet over-expression causes a strong ectopic crossing phenotype (asterisk), which is fully suppressed when Islet is over-expressed in *fra* mutants. **B**: Quantification of *fra+* ventral ap neurons in wild type embryos, and embryos over-expressing Islet, following fluorescent *in situ* for *fra* mRNA. Over-expression from two copies of *UAS-Islet* causes significant upregulation of *fra* in ventral apterous neurons (*p<0.005, Student's t-test). **C**: Quantification of ap axon crossing. Islet gain of function causes a strong ectopic crossing phenotype (**p<0.001, Student's t-test) which is fully suppressed when Islet is over-expressed in *fra* mutants. *fra/fra* denotes *fra³,ap^{Gal4}/fra³,UAS-TMG. isl g.o.f.* denotes *ap^{Gal4},UAS-TMG/+; UAS-Islet5xMyc/+. isl g.o.f. in fra -/-* denotes *fra³,ap^{Gal4}/fra³,UAS-TMG; UAS-Islet5xMyc/+. 2x isl g.o.f.* denotes *ap^{Gal4}, UAS-TMG/+; UAS-Islet5xMyc/UAS-Islet5xMyc*. N=number of embryos. Error bars indicate the standard error of the mean.

Figure 3.6. *Islet* is not required for *fra* expression in ventrally-projecting RP neurons during the stage when RP axons cross the midline, but by stage 14 is required for *fra* expression in RP1 and RP3 neurons.
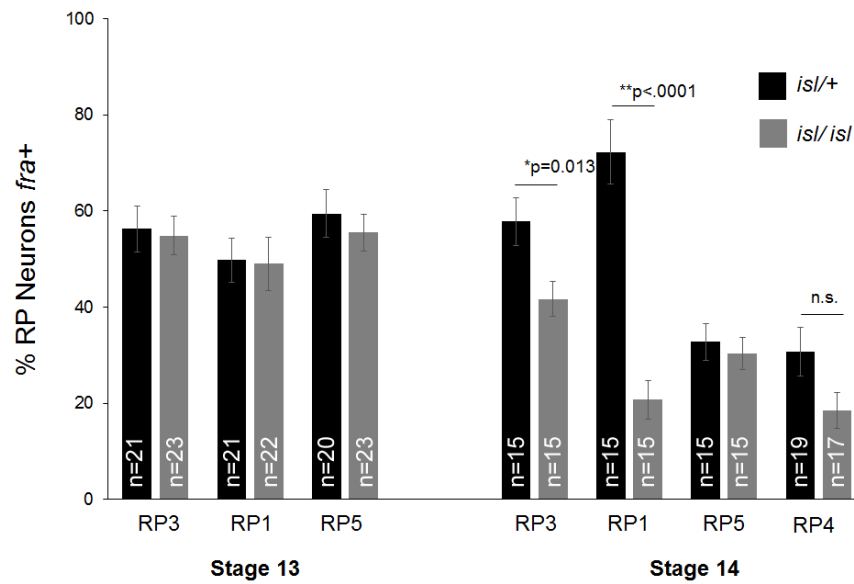
Figure 3.6. *Islet* is not required for *fra* expression in ventrally-projecting RP neurons during the stage when RP axons cross the midline, but by stage 14 is required for *fra* expression in RP1 and RP3 neurons.

Quantification of *fra* in situ in stage 13 and 14 *isl +/-* and *isl -/-* mutant embryos. RP neurons were labeled by *isl-H-tau-myc* and scored as positive or negative for *fra* mRNA in A2-A7, blind to genotype. *isl* mutants do not display reduced *fra* expression in RP1, RP3, or RP5 neurons compared to heterozygote controls at stage 13, which corresponds to a stage when RP axons are navigating the midline. By stage 14, which corresponds to a stage when RP axons have exited the nerve cord, *isl* mutants display reduced *fra* expression in RP3 and RP1 neurons, but not in RP4 or RP5. Too few RP4 neurons were labeled by *isl-H-tau-myc* at stage 13 to score *fra* expression. *isl/+* denotes *tup^{isl}/CyO,Wgβg* or *Df(2L) Exel7072/CyO,Wgβg*. *isl/isl* denotes *tup^{isl}/Df(2L)Exel7072*. N=number of embryos. Error bars indicate the standard error of the mean.

Figure 3.7. A difference in the dendritic positions of two classes of motor neurons correlates with a difference in *fra* expression; Netrin protein is detected in the intermediate zone of the neuropile.
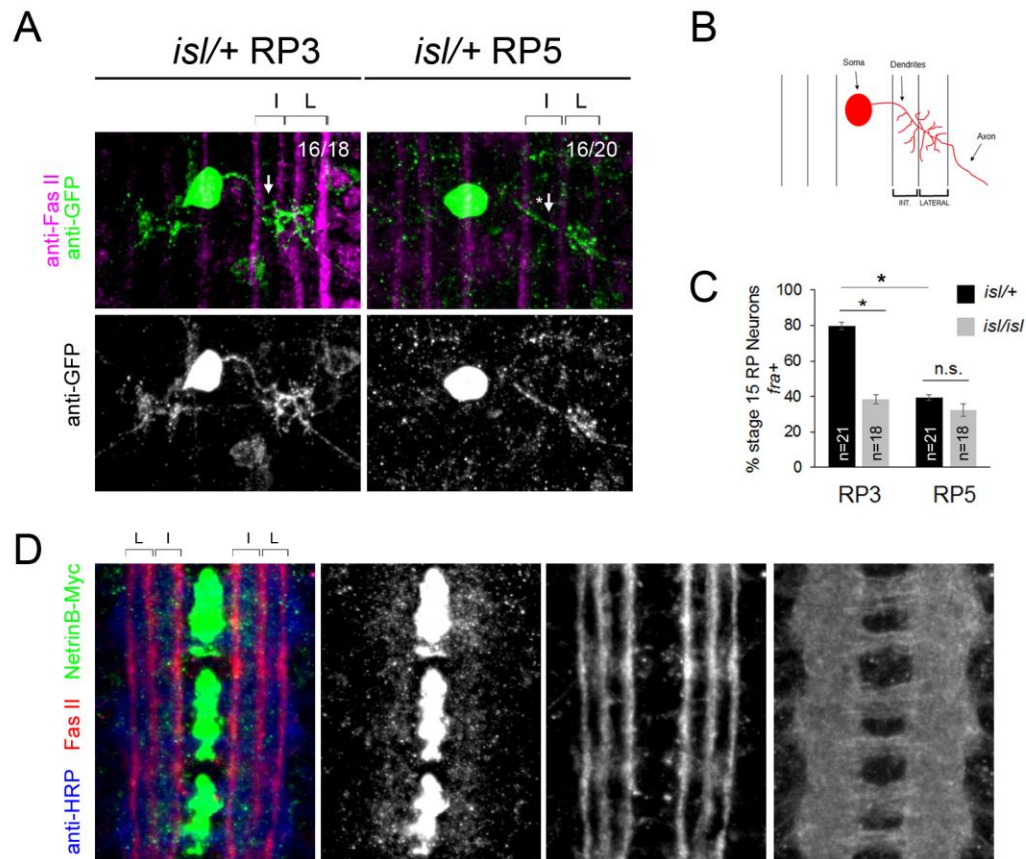
Figure 3.7. A difference in the dendritic positions of two classes of motor neurons correlates with a difference in *fra* expression; Netrin protein is detected in the intermediate zone of the neuropile.

A: Single-labeled neurons from Stage 17 *isl/+* embryos. RP3 and RP5 neurons are labeled with anti-GFP (green), and FasII+ axons (magenta) are stained to distinguish medio-lateral zones. The intermediate zone (arrow) is innervated by RP3 dendrites, but not by RP5 dendrites (arrow with asterisk). **B**: Cartoon of an RP motor neuron (red), with the soma, contralateral dendrites, and axon labeled. FasII+ axon pathways are drawn in black. The intermediate zone refers to the space in between the medial and FasII+ axon tracts. **C**: Quantification of the percentage of RP3 or RP5 neurons scored as positive for *fra* in *isl/+* and *isl/isl* embryos at stage 15. Significantly more RP3 neurons than RP5 neurons express *fra* in *isl/+* embryos (*p<0.001). *isl* is not required for *fra* expression in RP5 (p=0.26). N=number of embryos. Error bars indicate the standard error of the mean. *isl/+* denotes *tup^{isl}/CyO,Wgβg* or *Df(2L)Exel7072/ CyO,Wgβg*. *isl/isl* denotes *tup^{isl}/ Df(2L)Exel7072*. **D**: Stage 17 embryo expressing myc-tagged NetrinB (green) from its endogenous locus and stained with anti-Fas II (red), to delineate medio-lateral zones, and anti-HRP (blue) to label all axons. NetrinB is highly expressed in midline glia, and is also detected on axons in the neuropile, including in the zone in between the medial and intermediate FasII+ pathways.

Figure 3.8. *Islet* **regulates the medial-lateral targeting of RP3 dendrites in the**
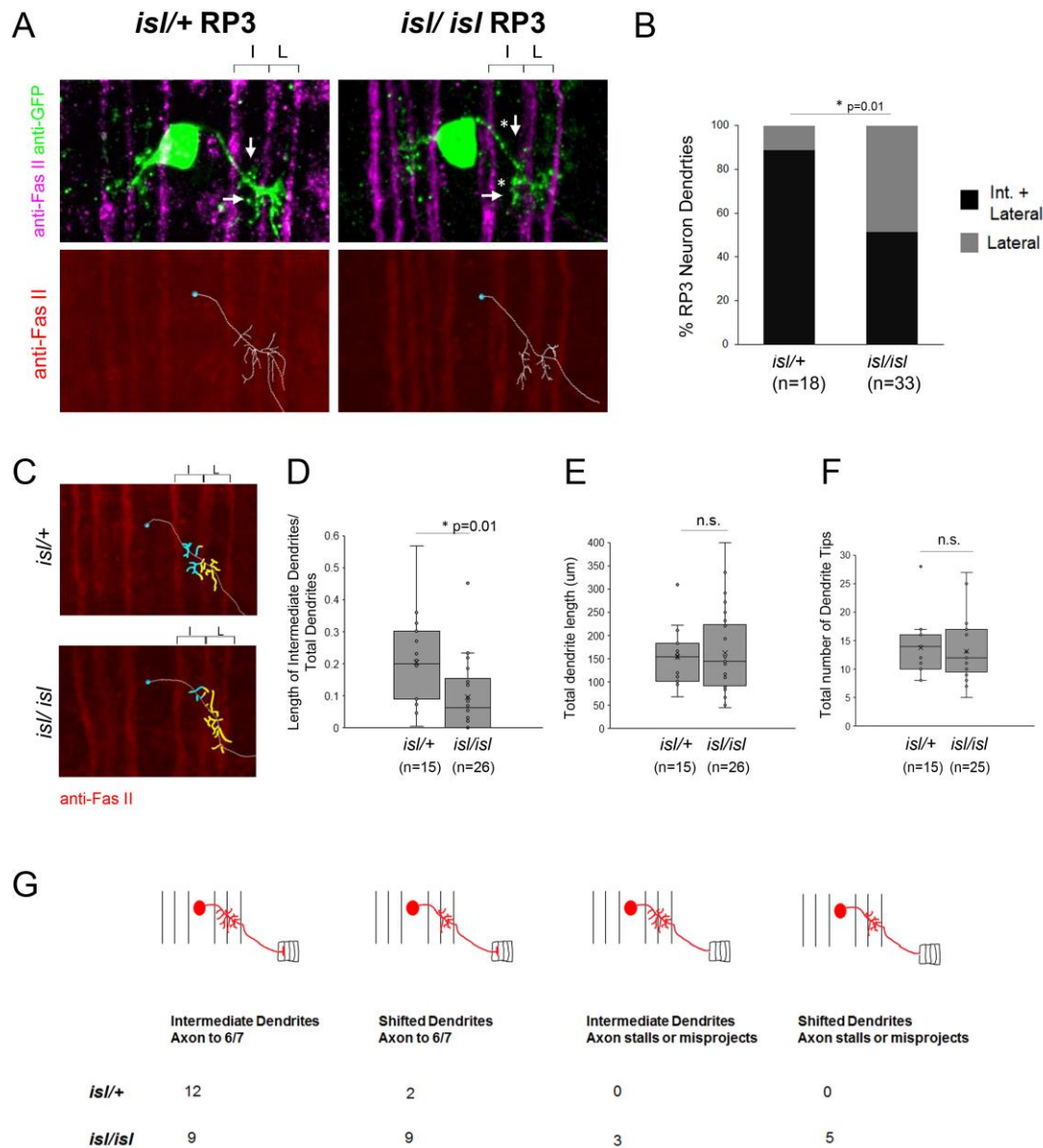
central nervous system.

Figure 3.8. *Islet* **regulates the medio-lateral targeting of RP3 dendrites in the central nervous system.**

A: Single-labeled RP3 neurons from Stage 17 embryos of the indicated genotypes. Top row: RP3 neurons are labeled with anti-GFP (green), and FasII axons (magenta) are stained. Arrows point to dendrites in the intermediate zone; arrows with asterisks point to dendrites that do not detach away from the intermediate FasII+ axons. Bottom row: Contralateral dendrites were traced on Imaris using the Filament plugin; traces are shown as skeletons (white) against the FasII+ axons (red). **B**: Percentage of RP3 neurons that target their contralateral dendrites to intermediate and lateral regions of the nerve cord. Fewer RP3 dendrites are present in the intermediate zone in *isl/isl* embryos (*$p<0.05$, Fisher's exact test). **C**: Representative examples of dendrite skeletons in *isl/+* and *isl/isl* embryos in which intermediate and lateral dendrites are artificially color-coded in cyan and yellow, respectively. FasII+ axons are in red. **D**: Box and whisker plots of the total length of RP3 contralateral dendrites in the intermediate zone divided by the total length of RP3 contralateral dendrites. *isl/isl* neurons display a reduction in the fraction of dendrites found in the intermediate zone ($p=0.014$, Student's t-test). **E**: Box and whisker plots of the total length of contralateral RP3 dendrites. There is no significant difference between *isl/+* and *isl/isl* neurons ($p=0.75$). **F**: Box and whisker plots of the total number of contralateral dendrite tip endings. There is no significant difference between *isl/+* and *isl/isl* embryos ($p=0.67$). **G:** Summary of axon and dendrite defects detected in *isl/+* and *isl/isl* RP3 neurons. N=number of neurons. *isl/+* denotes *tup^{isl}, lim3b-Gal4/CyO,elavβg*. *isl/isl* denotes *tup^{isl}, lim3b-Gal4/Df(2L)Exel7072*.

Figure 3.9. *Fra* regulates the medio-lateral targeting of RP3 dendrites.
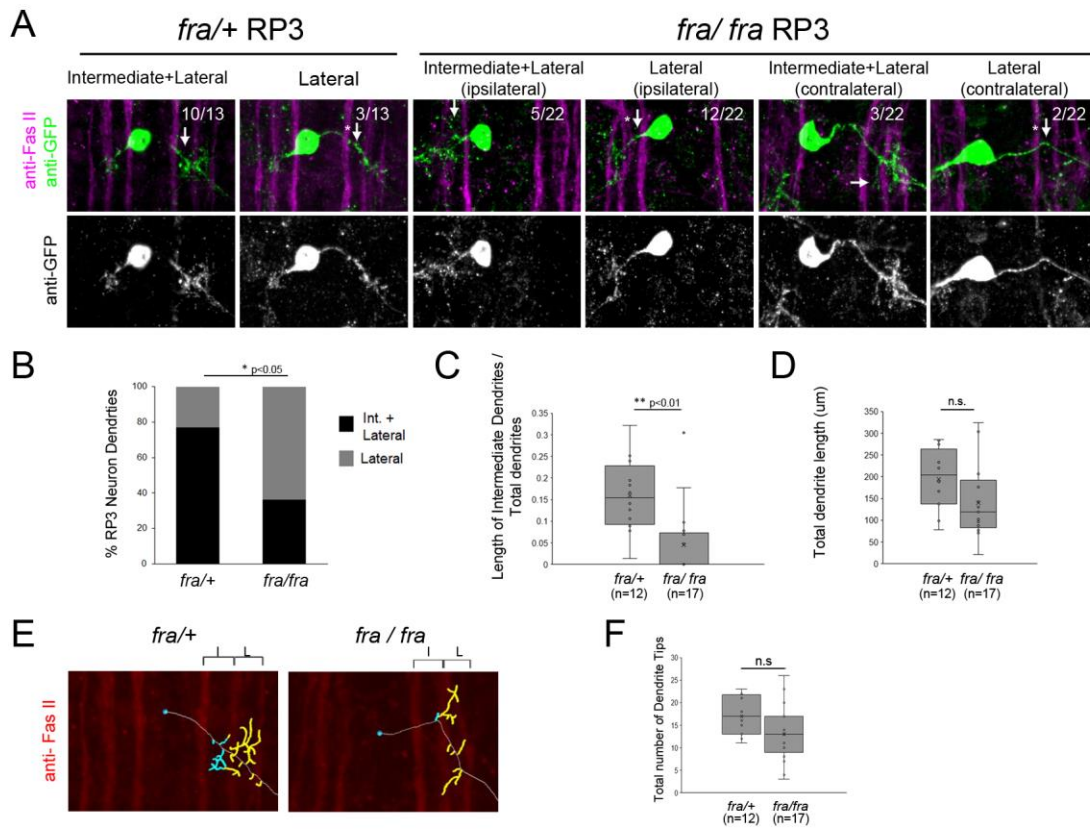
Figure 3.9. *Fra* regulates the medio-lateral targeting of RP3 dendrites.

A: RP3 neurons from Stage 17 *fra/+* or *fra/fra* embryos. RP3 neurons are labeled with anti-GFP (green), and FasII+ axons are stained (magenta). Many dendritic arbors fail to target the intermediate zone in *fra/fra* mutants (arrows with asterisks); this phenotype does not correlate with defects in midline crossing. Arrows point to dendrites in the intermediate zone. Images in which the labeled RP3 neuron was on the right side of the nerve cord were flipped horizontally for ease of visualization. **B**: Quantification of the percentage of RP3 neurons that target their dendrites to intermediate and lateral regions of the nerve cord; significantly fewer RP3 dendrites are present in the intermediate zone in *fra/fra* embryos (*$p<0.05$, Fisher's exact test). **C:** Box and whisker plots showing the length of RP3 dendrites in the intermediate zone divided by the total length of RP3 dendrites in *fra/+* and *fra/fra* neurons. There is a significant reduction in the fraction of intermediate dendrites in *fra* mutants (**$p<0.001$, Student's t-test). **D:** Box and whisker plot of total dendrite lengths; there is no significant change between *fra/+* embryos and *fra/fra* mutants, although the mutants displayed a trend toward a decrease ($p=0.07$). **E:** Representative examples of RP3 dendrite skeletons in which intermediate and lateral dendrites are color-coded in cyan and yellow, respectively. **F:** Box and whisker plot of total dendrite tip numbers; there is no significant change between *fra/+* embryos and *fra* mutants, although the mutants displayed a trend toward a decrease ($p=0.06$). In C, D, and F, the mean is indicated by the x. Inner points and outlier points are displayed. An exclusive median method was used to calculate quartiles. N=number of neurons. *fra/+* denotes *fra³, lim3b-Gal4/CyO,elavßg*. *fra/fra* denotes *fra³, lim3b-Gal4/fra³*.

Figure 3.10. Additional examples of RP3 neuron traces in *isl/+*, *isl/isl*, *fra/+*, and *fra/fra* embryos.

isl/+

isl/isl

fra/+

fra/fra

anti- FasII
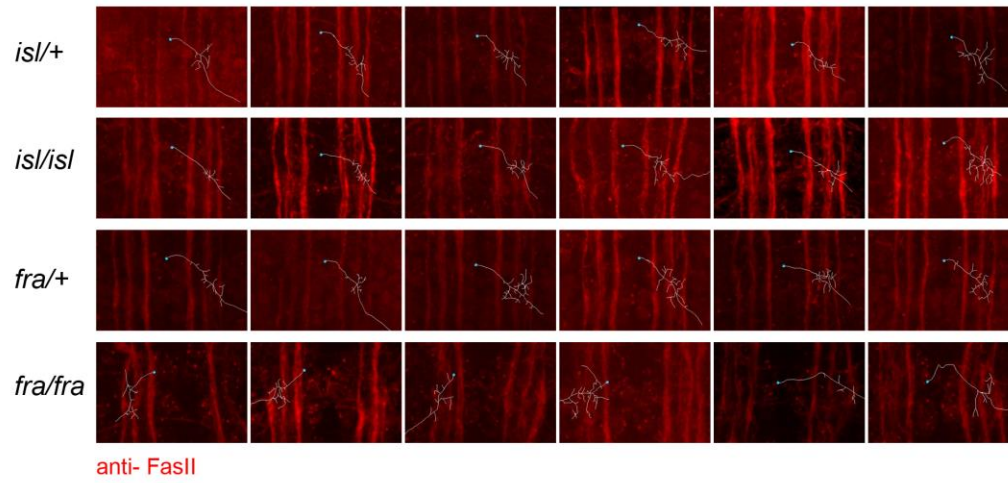
Figure 3.10. Additional examples of RP3 neuron traces in *isl/+*, *isl/isl*, *fra/+*, and *fra/fra* embryos.

Cropped images of RP3 neuron skeletons (white) that were generated by the Filament tool on Imaris software (Bitplane) were selected as representative examples of each genotype (see Methods). The blue dot indicates the position of the cell body. To facilitate visualization, images were flipped so that the contralateral dendritic arbor is always on the right side of the image, and the ipsilateral arbor on the left. FasII antibody staining (red) labels three sets of axons on each side of the midline. *isl/+* denotes *tup^{isl}, lim3b-Gal4/CyO,elavβg*. *isl/isl* denotes *tup^{isl}, lim3b-Gal4/Df(2L)Exel7072*.

Figure 3.11. RP1 and 4 dendrites are shifted laterally in *isl/isl* embryos; RP1

neurons require *isl* for *fra* expression at stage 15.
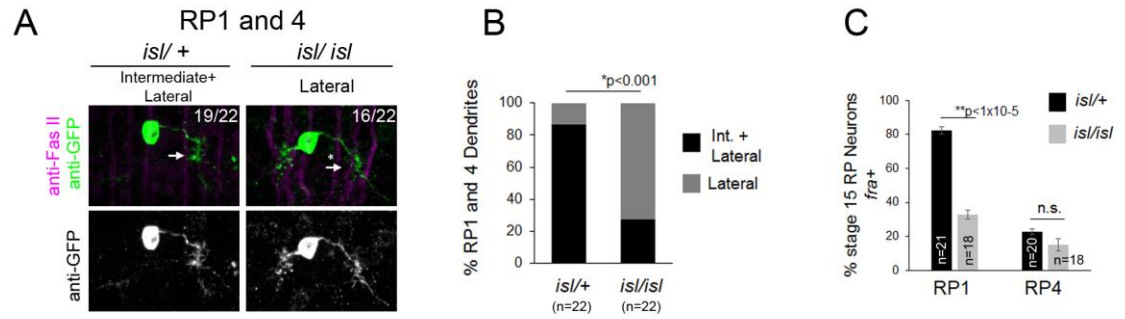
Figure 3.11. RP1 and 4 dendrites are shifted laterally in *isl/isl* embryos; RP1 neurons require *isl* for *fra* expression at stage 15.

A: RP1 and 4 neurons from Stage 17 *isl/+* or *isl/isl* embryos (green). Anti-FasII staining is in magenta. As their cell bodies are found at similar dorsal and medial positions, we could not distinguish between RP1 and 4 in our single cell labeling experiments, and scored them together. The majority of RP1/RP4 neurons target their dendrites to the intermediate and lateral region of the nerve cord in *isl/+* embryos (arrow), whereas many avoid the intermediate zone in *isl* mutants (arrow with asterisk). **B**: Quantification of the percentage of RP1 and RP4 neurons that target their dendrites to intermediate or lateral regions of the nerve cord. *isl* mutants display a significant reduction in the percentage of RP1 and RP4 dendritic arbors found in the intermediate zone (*p<0.001, Fisher's exact test). **C**: Quantification of percentage of RP neurons positive for *fra* mRNA at stage 15 in *isl/+* and *isl/isl* embryos. In control embryos, fewer RP4 neurons than RP1 neurons express *fra*. *isl* is not required for *fra* expression in RP4 neurons (p=0.2), but is required for *fra* expression in RP1 neurons (**p<1×10^{-5}, Student's t-test). Error bars indicate the standard error of the mean. N=number of embryos. *isl/+* denotes *tup^{isl}/CyO,Wgβg* or *Df(2L)Exel7072/ CyO,Wgβg. isl/isl* denotes *tup^{isl}/ Df(2L)Exel7072*.

Figure 3.12. Cell-type specific over-expression of Frazzled in *isl* RP3 motor neurons rescues the medio-lateral position of their dendrites.
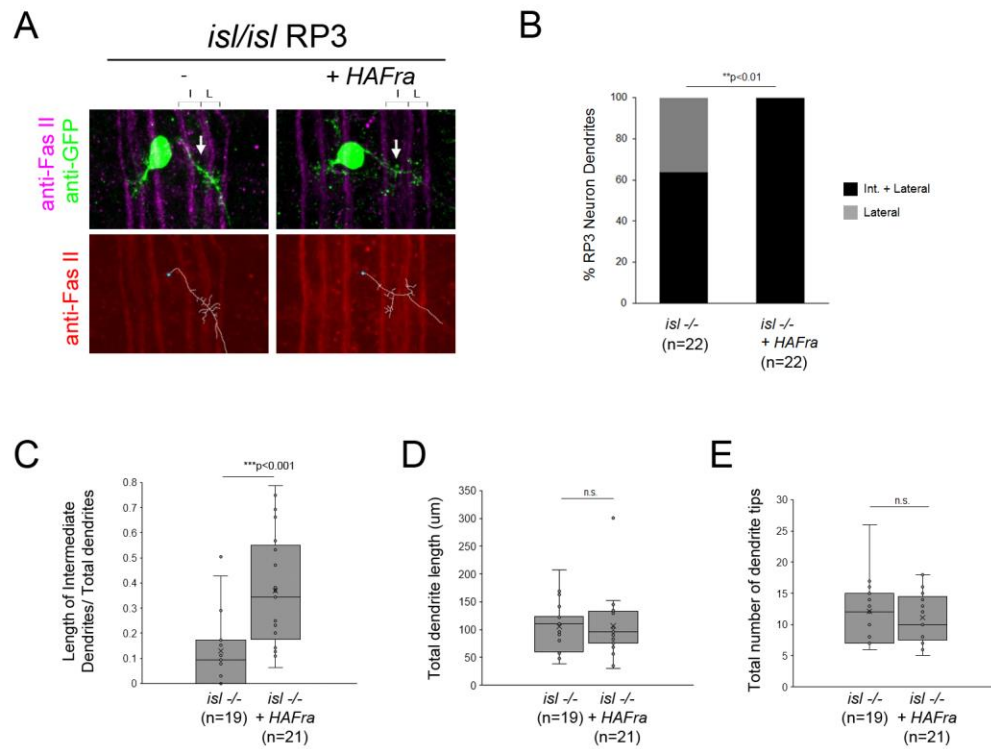
Figure 3.12. Cell-type specific over-expression of Frazzled in *isl* RP3 motor neurons rescues the medio-lateral position of their dendrites.

A: Single-cell labeled RP3 neurons from Stage 17 embryos of the indicated genotypes. Top row: RP3 neurons are labeled with anti-GFP (green), and FasII+ axons (magenta) are stained to distinguish medio-lateral zones. Arrows point to dendrites in the intermediate zone. Images in which the contralateral dendrites were oriented to the left were flipped to facilitate visualization and comparison of neurons. Bottom row: Contralateral dendrites were traced on Imaris; traces are shown as skeletons (white) against FasII+ axons (red).

B: Percentage of RP3 neurons that target their dendrites to intermediate and lateral regions of the nerve cord. All RP3 dendrites are present in the intermediate zone in *isl/isl* embryos over-expressing Frazzled, whereas many dendrites in sibling *isl/isl* embryos lacking the transgene fail to target the intermediate zone (**p<0.01, Fisher's exact test).

C: Box and whisker plots of the lengths of RP3 contralateral dendrites in the intermediate zone divided by the total length of RP3 contralateral dendrites. *isl/isl* neurons over-expressing Frazzled display an increase in the fraction of intermediate dendrites compared to *isl/isl* neurons (***p<0.001, Student's t-test). **D**: Box and whisker plots of total lengths of contralateral RP3 dendrites. There is no significant difference between *isl/isl* neurons and *isl/isl* neurons over-expressing Fra (p=0.95). **E**: Box and whisker plots of the total number of contralateral dendrite tip endings. There is no significant difference between *isl/isl* embryos and *isl/isl* embryos over-expressing Fra (p=0.5). N=number of neurons. *isl/isl* denotes *tup^{isl}, lim3b-Gal4/Df(2L)Exel7072*. *isl/isl+ HAFra* denotes *tup^{isl}, lim3b-Gal4/Df(2L)Exel7072; UAS-HAFrazzled 86fb/+*.

Acknowledgements

I would like to thank members of the Bashaw lab for their comments during the

development of this manuscript. We thank Richard Baines and Tony Southall with help

processing and visualizing the genome-wide DAM ID data.

CHAPTER 4

ROBO2 ACTS IN TRANS TO INHIBIT SLIT-ROBO1 REPULSION IN PRE-CROSSING COMMISSURAL AXONS

During nervous system development, commissural axons cross the midline despite the presence of repellant ligands. In *Drosophila*, commissural axons avoid premature responsiveness to the midline repellant Slit by expressing the endosomal sorting receptor Commissureless, which reduces surface expression of the Slit receptor Roundabout1 (Robo1). Here, we describe a distinct mechanism to inhibit Robo1 repulsion and promote midline crossing, in which Roundabout2 (Robo2) binds to and prevents Robo1 signaling. Unexpectedly, we find that Robo2 is expressed in midline cells during the early stages of commissural axon guidance, and that over-expression of Robo2 can rescue *robo2*-dependent midline crossing defects non-cell autonomously. We show that the extracellular domains required for binding to Robo1 are also required for Robo2's ability to promote midline crossing, in both gain-of-function and rescue assays. These findings indicate that at least two independent mechanisms to overcome Slit-Robo1 repulsion in pre-crossing commissural axons have evolved in *Drosophila.*

137

Introduction

      The secreted Slit repellents and their Roundabout (Robo) receptors constitute a repulsive axon guidance system whose function is conserved across a wide range of animal taxa including vertebrates, planarians, nematodes, and insects (Brose and Tessier-Lavigne, 2000; Evans and Bashaw, 2012). Slits are normally expressed at the midline of the central nervous system (CNS), and axons expressing Robo receptors are thus repelled from the midline (Battye et al., 1999, Brose et al., 1999, Kidd et al., 1999). Prior to crossing the midline, commissural neurons in vertebrates and insects prevent premature responsiveness to Slit by regulating the expression and activity of Roundabout (Robo) receptors through a variety of mechanisms (Evans and Bashaw, 2010a; Neuhaus-Follini and Bashaw, 2015b). For example, the divergent Robo receptor Robo3/Rig-1 in vertebrates negatively regulates the activity of the Robo1 and Robo2 receptors in pre-crossing commissural axons in the spinal cord, thereby allowing midline crossing (Sabatier et al., 2004). In *Drosophila*, Commissureless (Comm) antagonizes Slit-Robo1 repulsion by preventing the trafficking of the Robo1 receptor to the growth cone, instead diverting newly synthesized Robo1 into the endocytic pathway (Keleman et al., 2002; Keleman et al., 2005; Kidd et al., 1998a). As commissural axons approach the midline, Comm expression is high, allowing axons to cross the midline (Keleman et al., 2002). Once the midline is reached, Comm is down regulated, restoring Robo1-dependent Slit sensitivity and ensuring that commissural axons do not re-cross the midline. Accordingly, loss of Robos or Slits can cause axons to ectopically cross the midline, while loss of Comm or Robo3/Rig1 prevents commissural axons from crossing (Kidd et al., 1998b; Kidd et al., 1999; Long et al., 2004; Sabatier et al., 2004; Tear et al., 1996).

In *Drosophila*, the three members of the Roundabout (Robo) receptor family (Robo1, Robo2, and Robo3) cooperate to control multiple aspects of axon guidance during embryonic development, including midline repulsion of axons and the formation of longitudinal axon pathways at specific mediolateral positions within the nerve cord. Although Robo2 contributes to promoting midline repulsion, gain-of-function genetic experiments suggest that in some contexts Robo2 can also promote midline crossing (Rajagopalan et al., 2000a; Simpson et al., 2000a). More recently endogenous roles for *robo2* in promoting midline crossing were identified during the guidance of foreleg gustatory neurons in the adult, as well as during the guidance of interneurons in the embryonic CNS (Mellert et al., 2010; Spitzweck et al., 2010). Robo2's pro-crossing role in the embryo is highlighted in *frazzled* and *Netrin* mutant backgrounds, in which midline attraction is partially compromised (Spitzweck et al., 2010). In the absence of Netrin-dependent midline axon attraction, loss of *robo2* (but not *robo1* or *robo3)* leads to a dramatic disruption in midline crossing that is far more severe than the complete loss of Netrins, indicating that *robo2* likely acts in parallel to Netrin-Fra to promote midline crossing (Spitzweck et al., 2010).

In a complementary series of gain-of-function experiments using a panel of chimeric receptors comprising different regions of Robo1 and Robo2 fused together, we have previously shown that Robo2's ability to promote ectopic midline crossing correlates with the presence of the first and second immunoglobulin-like domains (Ig1 and Ig2) within its extracellular domain (Evans and Bashaw, 2010b). Consistent with these observations, replacing endogenous Robo2 by homologous recombination with chimeric receptors, in which the cytoplasmic domains of the Robo1 and Robo2 receptors

139

were exchanged, reveals that the Robo2-1 chimeric receptor (containing the extracellular region of the Robo2 receptor) can rescue the commissural guidance defect observed in *Netrin, robo2* mutants more effectively than the reciprocal chimeric receptor (Spitzweck et al., 2010). However, the mechanism by which Robo2 promotes midline crossing remains unclear. Two alternative models could account for Robo2's role in promoting midline crossing of commissural axons. First, Robo2 may act as an attractive receptor to signal midline attraction in response to a ligand produced by midline glia, analogous to Frazzled/DCC's role in Netrin-dependent midline attraction. Indeed, a role for Robo2 in mediating attractive responses to Slit has been described in the context of muscle cell migration (Kramer et al., 2001). Alternatively, Robo2 may antagonize Slit-Robo1 repulsion by preventing Robo1 from signaling in response to midline-derived Slit, similar to the proposed role of Robo3/Rig-1 in pre-crossing commissural axons in the vertebrate spinal cord (Figure 4.1). Although Comm is an essential regulator of Robo1 activity in *Drosophila*, low levels of Robo1 escape Comm-dependent sorting and can be detected on commissural axons, raising the question of whether and how the activity of these Robo1 receptors is regulated (Kidd et al., 1998b).

Here we show that in addition to its cell-autonomous role in midline repulsion, Robo2 acts non-autonomously to promote midline crossing by inhibiting canonical Slit-Robo1 repulsion, and offer insights into the molecular and cellular mechanisms underlying this activity of Robo2. We find that the cytoplasmic domain of Robo2 is dispensable for its pro-crossing role, suggesting that Robo2 does not transduce a midline attractive signal, and that Robo2 over-expression can suppress *comm* mutants, supporting a model in which Robo2 antagonizes Slit-Robo1 repulsion. Moreover, Robo2 can bind to

Robo1 in *Drosophila* embryonic neurons, and this biochemical interaction, like Robo2's pro-crossing role, correlates with the presence of Ig1 and Ig2. Surprisingly, we observe that Robo2 is able to promote midline crossing of axons non-cell autonomously when mis-expressed in midline cells, and we further show that Robo2 is expressed in midline glia and neurons during the early stages of commissure formation. Finally, we find that restoring Robo2 expression in midline cells can rescue midline crossing of axons in *robo2, fra* double mutants and that this rescue activity is dependent on Ig1 and Ig2. Together, our results indicate that Robo2 acts non-autonomously to bind to Robo1 and prevent Slit-Robo1 repulsion in pre-crossing commissural axons. This model accounts for Robo2's seemingly paradoxical roles in both promoting and inhibiting midline crossing, and explains how the small amount of Robo1 present on pre-crossing commissural axons might be prevented from responding to Slit.

Results

The midline attractive ligand Netrin and its receptor Frazzled (Fra) are the only known attractive ligand-receptor pair in *Drosophila*, yet many commissural axons still cross the midline in the absence of attractive Netrin-Frazzled signaling (Kolodziej et al., 1996, Mitchell et al., 1996). It has recently been demonstrated that the Robo family receptor Robo2 acts independently of Netrin and Fra to promote midline crossing, through an as yet unknown mechanism (Spitzweck et al., 2010). In *robo2, fra* double mutants, midline crossing of commissural axons is severely compromised, leading to thin or absent commissures, a phenotype that is qualitatively and quantitatively more severe than loss of *fra* alone (Figure 4.1). This phenotype can be observed by staining the entire

axon scaffold with anti-HRP antibodies (Figure 4.1 A-D) or by labeling a subset of

commissural axons using *eg-GAL4* in *robo2, fra* double mutants (Figure 4.1 F-I). To

quantify the midline crossing defects, we scored the number of segments in which the

EW axons, which normally cross the midline in the posterior commissure, fail to cross

(Figure 4.1). We find that in *robo2, fra* double mutants approximately 70% of EW axons

fail to cross the midline, compared to around 30% in *fra* mutants. Analysis of cell fate

markers including Eg, even-skipped and zfh1 revealed no gross differences in

segmentation and neuronal differentiation in *robo2, fra* double mutants, and although the

cell bodies of the EW neurons were sometimes displaced, they were easily identifiable

(data not shown). Importantly, restoring Robo2 expression by introducing one copy of an

83.9 kb *robo2* BAC transgene that includes the entire 40 kb *robo2* transcription unit in

this background significantly rescues the EW axon crossing defects (Figure 4.1 E, J),

confirming that this is a *robo2*-dependent phenotype.

Robo2's pro-crossing activity does not require its cytoplasmic domain

If Robo2 were to act as a midline attractive receptor (Figure 4.1, model 1), its

cytoplasmic domain would likely be required for midline attraction. To test whether the

Robo2 cytoplasmic domain contributes to its pro-crossing activity, we tested whether a

truncated Robo2 receptor lacking its cytoplasmic domain (Robo2ΔC) could promote

midline crossing when mis-expressed in embryonic neurons. We found that, as with full-

length Robo2, pan-neural mis-expression of Robo2ΔC (with *elav-GAL4*) produced strong

ectopic crossing of FasII-positive axons in the embryonic CNS (Figure 4.2). Indeed, the

Robo2ΔC mis-expression phenotype was stronger than full-length Robo2. In contrast,

pan-neural over-expression of Robo1 did not generate ectopic crossing (Figure 4.2). In these experiments, all UAS-Robo transgenes are expressed from the same genomic insertion site in order to ensure that they are expressed at similar levels. Importantly, the pro-crossing activity of Robo2ΔC is unlikely to be caused solely by a dominant-negative effect of the truncated receptor, as a similarly truncated form of Robo1 (Robo1ΔC) has a qualitatively weaker ectopic crossing phenotype when combined with *elav-GAL4* (Figure 4.2). Robo2ΔC expression, unlike Robo1ΔC, leads to ectopic crossing of all of the ipsilateral FasII axon bundles and also results in many segments exhibiting a Slit-like phenotype (Figure 4.2). Due to the strong phenotypic effects of the targeted insertion lines of Robo1ΔC and Robo2ΔC, we also compared the phenotypes generated by lower levels of expression of the two truncated receptors using standard UAS inserts and observed that Robo2ΔC is significantly more potent at driving ectopic midline crossing than comparable levels of the Robo1ΔC receptor (Figure 4.3). Together, these observations indicate that the pro-crossing activity of Robo2 is independent of the cytoplasmic domain and argue against the idea that Robo2 promotes midline crossing by signaling attraction.

Robo2's pro-crossing activity does not strictly depend on Slit binding

Slit is the canonical ligand for Robo family receptors, and all three *Drosophila* Robos can bind to the single *Drosophila* Slit (Howitt et al., 2004). To test whether Robo2's pro-crossing activity depends on its ability to bind Slit, we deleted the canonical Slit-binding domain (the first immunoglobulin-like domain: Ig1) from Robo2. As predicted by previous *in vitro* binding studies using *Drosophila* Robo1 (Brose et al.,

1999; Fukuhara et al., 2008) we found that deleting Ig1 from Robo2 prevented Slit

binding in cultured *Drosophila* cells (Figure 4.4). Pan-neural over-expression of Robo2

produces a phenotype in which some axons are repelled from the midline, and some

axons ectopically cross the midline, reflecting Robo2's two opposing activities in

regulating midline crossing. As expected, deleting the Ig1 domain prevents Robo2 from

signaling midline repulsion *in vivo*, both broadly in all neurons (Figure 4.5) and in a

subset of commissural neurons (the EW neurons, labeled by *eg-GAL4*) (Figure 4.4),

confirming that Slit binding is required for Robo2-mediated repulsion. In contrast, we

found that the Robo2 receptor lacking Ig1 retained a partial ability to promote ectopic

midline crossing of FasII-positive axons, indicating that the pro-crossing activity of

Robo2 does not strictly depend on its ability to bind Slit (Figure 4.5). Notably, the ectopic

crossing phenotype produced by Robo2ΔIg1 mis-expression was significantly weaker

than that caused by mis-expression of full-length Robo2 (Figure 4.5). This result suggests

that the Ig1 domain contributes to, but is not strictly required for, promotion of midline

crossing by Robo2.

Robo2's Ig2 domain is required for its pro-crossing activity

We have previously shown that Robo2's pro-crossing activity is conferred at least

in part by its Ig2 domain: replacing the Ig1-Ig2 region of Robo1 with the equivalent

region from Robo2 (Robo1$^{R2Ig1+2}$) confers Robo2-like pro-crossing activity to Robo1

(Evans and Bashaw, 2010b). Further, replacing Ig1-Ig2 of Robo2 with Robo1 Ig1-Ig2

(Robo2$^{R1Ig1+2}$) abolishes its pro-crossing activity (Evans and Bashaw, 2010b). To

directly test whether Ig2 is necessary for Robo2 to promote midline crossing, we

generated a Robo2 receptor lacking Ig2 but with all other Ig domains intact (Robo2ΔIg2). We found that deleting Robo2's Ig2 domain did not interfere with Slit binding (Figure 4.4), nor did it affect Robo2's ability to signal repulsion in commissural neurons (Figure 4.4). However, deletion of Robo2's Ig2 domain strongly disrupted its ability to promote ectopic midline crossing (Figure 4.5). These results contrast with those observed with Robo2ΔIg1, which lacks Slit-dependent midline repulsive activity but retains some pro-midline crossing activity (Figures 4.4 and 4.5). These data indicate that Robo2's Ig2 domain is essential for promoting midline crossing when Robo2 is mis-expressed in all neurons. In these experiments, all UAS-Robo transgenes are expressed from the same genomic insertion site in order to ensure that they are expressed at similar levels. In addition, we assayed the protein localization and expression levels of Robo2 and its deletion variants and observed comparable surface expression in cultured S2R+ cells *in vitro*, as well as comparable expression levels and localization in CNS axons *in vivo* (Figure 4.6).

Robo2 can promote crossing non-autonomously

Midline crossing is strongly reduced in *robo2, fra* double mutants, and pan-neural mis-expression of Robo2 can promote ectopic midline crossing. However, it is unclear whether Robo2 acts autonomously or non-autonomously to promote midline crossing. The ectodomain-dependent nature of Robo2's pro-crossing activity and our pan-neural mis-expression assays do not distinguish between these possibilities. Notably, we have never observed a clearly cell-autonomous pro-crossing phenotype caused by Robo2. In contrast to the very different phenotypes caused by pan-neural mis-expression of these

two truncated receptors (where Robo2ΔC is much more potent at inducing midline crossing than Robo1ΔC), Robo1ΔC and Robo2ΔC induce similar low levels of ectopic crossing when expressed in a subset of ipsilateral neurons, the apterous neurons (Figure 4.7A). We interpret this as a cell-autonomous dominant-negative effect of these truncated receptors. In contrast, full-length Robo2 is unable to autonomously promote midline crossing of the apterous axons (Evans and Bashaw, 2010b). Instead, Robo2 mis-expression redirects apterous axons to lateral regions of the neuropile. In the course of examining this lateral positioning activity of Robo2, we mis-expressed Robo2 in a second class of longitudinal interneurons: those labeled by *hb9-GAL4*. Intriguingly, we observed two distinct phenotypes in embryos where *hb9-GAL4* drives Robo2 expression. First, *hb9*-positive axons were shifted to more lateral positions within the neuropile. Second, *hb9*-negative FasII-positive axons ectopically crossed the midline (Figure 4.7B). These results suggest that Robo2 can autonomously specify the lateral position of *hb9*-positive axons, while non-autonomously instructing FasII axons to cross the midline. We note that *hb9-GAL4* expression initiates earlier than *ap-GAL4* and includes a larger number of neurons, including some located near the CNS midline (such as the RP motor neurons), suggesting the possibility that early midline-proximal expression of Robo2 accounts for the non-autonomous effect observed with *hb9-GAL4*.

To more explicitly test whether Robo2 can promote midline crossing non-autonomously, we used *slit-GAL4* to drive Robo2 expression in midline glia and neurons. We found that mis-expression of Robo2 or Robo2ΔC in midline cells caused many FasII-positive axons which do not express *slit-GAL4* to ectopically cross the midline, confirming that Robo2 can act non-autonomously to promote midline crossing of axons,

and that this effect does not depend on the cytoplasmic domain (Figure 4.8). We observed

a significantly milder effect with mis-expression of Robo1, suggesting that Robo2's non-

cell autonomous activity is not solely a consequence of Slit titration (Figure 4.8).

Moreover, the non-cell autonomous activity of Robo2 appears to be Ig1/Ig2-dependent,

as Robo1$^{R2Ig1+2}$ but not Robo2$^{R1Ig1+2}$ promoted strong ectopic midline crossing when

expressed using *slit-GAL4* (Figure 4.8). In addition, expression of Robo2 variants missing

either Ig1 or Ig2 with *slit-Gal4* did not result in any ectopic midline crossing (Figure 4.8).

The requirement for both Ig1 and Ig2 in this context contrasts with our findings with pan-

neural mis-expression, in which Robo2 ΔIg1 retained some pro-crossing activity.

However, it is worth noting that the phenotype generated by *elav-GAL4* mis-expression

of Robo2 is stronger than that generated by *slit-GAL4*, perhaps because *slit-GAL4* is

expressed in a much smaller number of cells.

Robo2 is expressed in midline glia and neurons during commissure formation

Robo2 can promote midline crossing when expressed in a subset of embryonic

neurons and glia, and endogenous *robo2* contributes to midline crossing of commissural

axons. During embryogenesis, *robo2* expression is dynamically regulated: it is broadly

expressed in neurons during early stages of CNS development, including transient

expression in a number of ipsilateral pioneer neurons, and later becomes restricted to

neurons whose axons form longitudinal pathways in the lateral regions of the neuropile

(Simpson et al., 2000a). To gain additional insight into Robo2's role in promoting

midline crossing of commissural neurons, we examined *robo2* mRNA and protein

expression in embryos during the early stages of axon pathfinding, when the first

147

commissural axons are crossing the midline (stages 12-13). Using fluorescent mRNA *in situ* hybridization, we were able to detect *robo2* mRNA expression in cells labeled by *slit-GAL4* in late stage 12 embryos, when pioneer commissural axons are crossing the midline (Figures 4.9 and 4.10). *Robo2* mRNA expression persists through the end of stage 13, but is no longer detectable by stage 14; thus, midline expression of *robo2* coincides with the time when most commissural axons are crossing the midline (Figure 4.10). Moreover, a *robo2-GAL4* enhancer-trap insertion is expressed in midline glia at this time, as detected by anti-GFP staining in *robo2-GAL4, UAS-TauMycGFP* embryos (Figure 4.9A). Expression of UAS-HARobo2 with *robo2-Gal4* and detection of transgenic Robo2 with anti-HA reveals an expression pattern that closely resembles the endogenous pattern of Robo2 protein (data not shown). In addition, we could detect weak expression of Robo2 protein produced by an HA-tagged knock-in allele of *robo2* (Spitzweck et al., 2010) in a subset of *slit-GAL4* expressing cells at stage 12, confirming that Robo2 protein is produced in midline cells during the stages of commissural axon pathfinding, and raising the possibility that Robo2 endogenously acts in these cells to promote midline crossing of commissural axons (Figure 4.9B).

Midline expression of Robo2 rescues the commissural defects in fra, robo2 mutants

Robo2 can promote midline crossing non-autonomously, and endogenous *robo2* expression can be detected in *slit-GAL4*-expressing cells as well as in contralateral and ipsilateral neurons during the initial stages of commissure formation (Figure 4.9 and data not shown). Our ability to partially rescue midline crossing in *robo2, fra* double mutants with the *robo2* BAC confirms that this is a *robo2*-specific phenotype, but does not

address in which cells *robo2* acts to instruct commissural axons to cross the midline. To address this question, we attempted to rescue *robo2*'s endogenous pro-crossing activity by restoring *robo2* expression in restricted subsets of cells in *robo2, fra* double mutants. We first expressed Robo2 in the commissural EW neurons (using *eg-GAL4*). We found that neither full-length Robo2 nor Robo2ΔC can rescue midline crossing when expressed autonomously in the EW neurons, suggesting that Robo2 does not act cell autonomously to promote midline crossing (Figure 4.11). We next attempted to rescue midline crossing in *robo2, fra* double mutants by expressing Robo2 using *slit-GAL4*. Strikingly, we found that driving Robo2 expression in these cells significantly restores posterior commissure formation (Figure 4.9C-G). Furthermore, this effect is dependent on Ig1 and Ig2 (Figure 4.9C-G). Cell-type specific loss of function experiments will be necessary to confirm the site of Robo2's endogenous activity, and our attempts to recapitulate the *robo2, fra* phenotype by over-expression of RNAi transgenes have so far been unsuccessful, likely because of the difficulty of achieving sufficient knockdown in embryonic stages. Nevertheless, our results suggest that Robo2 promotes midline crossing non-cell autonomously, and may act in midline glia and neurons, where it is expressed during the stages of commissural axon pathfinding.

Robo2 can antagonize Slit-Robo1 repulsion

Robo2 can promote midline crossing of axons independently of its cytoplasmic domain, suggesting that Robo2 does not promote crossing by acting as an attractive signaling receptor. Does Robo2 antagonize Slit-Robo1 repulsion? In order to test this hypothesis, we took advantage of *comm* mutants, which provide a genetic background in

which hyperactive Slit-Robo1 signaling prevents midline crossing. In *comm* mutants, endogenous Robo1 is inappropriately trafficked to the growth cone plasma membrane in pre-crossing commissural axons, triggering premature Slit repulsion and preventing commissure formation. We reasoned that if Robo2 antagonizes Slit-Robo1 repulsion, then Robo2 mis-expression might restore midline crossing in *comm* mutant embryos. Indeed, pan-neural mis-expression of Robo2 with *elav-GAL4* significantly restored commissure formation in *comm* mutant embryos (Figure 4.12). To specifically test the Ig1/Ig2-dependence of Robo2's pro-crossing activity in this assay, we mis-expressed the Ig1+2 chimeric receptors (Robo1$^{R2Ig1+2}$ and Robo2$^{R1Ig1+2}$) with *elav-GAL4* in *comm* mutant embryos. We found that pan-neural mis-expression of Robo1$^{R2Ig1+2}$ in *comm* mutant embryos strongly suppressed the commissureless phenotype and restored midline crossing of many axons, as assayed by anti-HRP antibody staining, while mis-expression of Robo2$^{R1Ig1+2}$ had a much milder effect (Figure 4.12). These results suggest that Robo2 promotes midline crossing in an Ig1/Ig2-dependent manner by antagonizing canonical Slit-Robo1 repulsion.

We were also able to suppress the *comm* mutant phenotype by over-expressing Robo2 using *slit-GAL4,* and this effect was fully dependent on both Ig1 and Ig2 of Robo2 (Figure 4.12). This is consistent with our observations that Robo2 can act non-cell autonomously to promote ectopic midline crossing (Figure 4.8) and rescue midline crossing defects (Figure 4.9) in an Ig1/2-dependent manner. Of note, the suppressive effect of Robo2 expression in *comm* mutants is much greater when expressed in midline cells than when expressed pan-neurally (Figure 4.12). This is likely because when expressed pan-neurally, in addition to its pro-crossing activity, full-length Robo2 also has

repulsive activity. In contrast, when expressed in midline cells, Robo2 would be unable to act as a repulsive receptor.

Robo2 binds to Robo1 in vivo and the interaction depends on Ig1 and Ig2

As shown above, Robo2 is able to antagonize Slit-Robo1 repulsion in an Ig1/Ig2-dependent manner. One possibility is that Robo2 may form an inhibitory receptor-receptor complex with Robo1 to prevent it from signaling midline repulsion. If this is the case, we reasoned that we might be able to detect a physical interaction between Robo2 and Robo1 in embryonic protein extracts. To test this idea, we mis-expressed epitope-tagged forms of Robo1 and Robo2 in *Drosophila* embryonic neurons with *elav-GAL4* and looked for physical interactions by co-immunoprecipitation (Figure 4.13). We found that Robo1-myc and HA-Robo2 co-immunoprecipitated from embryonic lysates when both were expressed in embryonic neurons (Figure 4.13A). Interactions were also observed between Robo1 and the closely related Robo3 receptor, but not with a similarly tagged and structurally related Fra receptor (Figure 4.13A). As we would predict from our gain of function experiments, Robo2's ability to bind to Robo1 is independent of its cytoplasmic domain (Figure 4.14). Strikingly, however, Robo2's ability to bind Robo1 depends on the Ig1-Ig2 region of Robo2, as Robo1$^{R2Ig1+2}$ was readily co-immunoprecipitated with Robo1, while binding between Robo1 and the reciprocal receptor Robo2$^{R1Ig1+2}$ was only weakly detected (Figure 4.13B). Consistently, deleting both of the Ig1 and Ig2 domains from Robo2 results in a diminished interaction with Robo1 *in vivo* and *in vitro* (Figures 4.13 and 4.14). Thus, we see a correlation between the presence of the Ig1 and Ig2 domains, a biochemical interaction with Robo1, and pro-

151

crossing activity in the Robo2 receptor. These observations suggest that Robo2 may promote midline crossing through inhibitory interactions with Robo1, likely mediated at least in part by the Robo2 Ig1 and Ig2 domain. Of note, the Ig2 domain is essential for Robo2's pro-crossing activity, but is not required for the interactions with Robo1 or with Slit, suggesting the existence of an Ig2-specific activity that is distinct from the ability to bind Robo1 or Slit. One possible mechanism that could explain how receptor-receptor interactions could prevent Robo1 signaling is through blocking the access of Slit to the Ig1 region of Robo1. Deleting Robo1's Ig1 domain does not significantly attenuate the interaction with Robo2, but further experiments will be necessary to determine if Robo2 interferes with Robo1's interaction with Slit (Figure 4.14).

Our biochemical experiments examining receptor-receptor interactions when the Robo receptors are expressed in all neurons do not distinguish between cis and trans interactions. As we observed that Robo2 is able to non-cell autonomously inhibit Robo1 repulsion and promote midline crossing, we reasoned that we might be able to detect physical interactions between Robo1 and Robo2 receptors when they are presented in trans. We tested this prediction by transfecting *Drosophila* cultured S2R+ cells with either Robo1-myc or HA-tagged Robo2 and assaying for physical interactions by co-immunoprecipitation. Although we detected strong interactions between Robo1 and Robo2 in co-transfected cells, we could not detect interactions in cells that were transfected separately and mixed together (Figure 4.14 and data not shown). However, when we mixed the membrane lysates of cells that were transfected separately, we observed that Robo1 readily co-immunoprecipitated Robo2, in an Ig1/2 dependent manner (Figure 4.13). These data suggest that physical interactions can occur between

152

Robo1 and Robo2 receptors that are expressed in different cells, and are consistent with the possibility of a physical interaction occurring across cell membranes *in vivo*. It is important to recognize, however, that binding detected with mixed cell lysates could occur in either cis or trans, and that future work should more rigorously evaluate the potential for trans interactions.

Robo2's Ig2 domain is required for its endogenous activity in promoting midline crossing

Our data are consistent with a non-autonomous requirement for Ig1 and Ig2 of Robo2 in antagonizing Robo1 to promote midline crossing. However, the genetic data supporting this model arise from gain of function and rescue experiments using GAL4/UAS over-expression. In order to more rigorously address the endogenous requirement for Robo2 in promoting midline crossing, we generated modified BACs and evaluated the ability of either wild-type Robo2 or Robo2ΔIg2 to restore midline crossing in *robo2, fra* double mutants, when expressed under *robo2*'s endogenous control elements. As Ig1 is required for both Robo2's pro-crossing activity and for its repulsive signaling output, the Robo2ΔIg2 variant provides a more specific reagent for testing our model. Therefore, we modified the original Robo2 BAC by recombineering to insert wild-type Robo2 cDNA or Robo2ΔIg2 cDNA, and introduced these BAC transgenes into *robo2, fra* double mutants. We determined the rescuing activity of each BAC through two assays: first, by scoring midline crossing of EW axons labeled by *eg-GAL4*, and second, by analyzing commissure formation in embryos stained with anti-HRP to label all axons (Figure 4.15).

153

We found that the ability of the Robo2 BAC to rescue midline crossing defects in *robo2*, *fra* double mutants was strongly impaired by deleting the Ig2 domain. In the EW crossing assay, one copy of the Robo2 FL cDNA BAC provides a significant rescue of *robo2, fra* double mutants at stage 16, whereas one copy of the Robo2 ΔIg2 BAC has no effect (Figure 4.15A-D). Of note, removing one allele of *robo2* enhances midline crossing defects in *fra* mutants, explaining in part the incomplete rescue (Figure 4.15). In addition, it is likely that the Robo2 BAC does not contain all of the regulatory elements required for *robo2*'s pro-crossing function, as one copy of the BAC does not restore EW crossing back to the levels of *fra* mutants heterozygous for *robo2* (Figure 4.15).

We also assessed the ability of the BAC transgenes to rescue midline crossing defects when analyzing all axons using anti-HRP. By this method, we see a robust rescue in posterior commissure (PC) formation in *robo2, fra* double mutant embryos with one copy of the Robo2 cDNA BAC compared to controls (Figure 4.15E-H). In contrast, the Robo2 ΔIg2 BAC provides a much weaker rescue (Figure 4.15G). The partial rescue by the Robo2ΔIg2 BAC in this assay suggests that the severe *fra, robo2* phenotype is due to the combined requirement for multiple activities of Robo2, including one that is Ig2-independent. Nevertheless, these data unambiguously reveal an endogenous requirement for Robo2's Ig2 domain during commissural axon guidance. Importantly, the Robo2ΔIg2 BAC fully rescues Robo2's repulsive activity at the midline (data not shown), further demonstrating that the Ig2 domain is specifically required for Robo2 to successfully promote midline crossing, but not for other known activities of the Robo2 receptor. Taken together, these results demonstrate a requirement for Robo2's Ig2 domain in

154

promoting midline crossing when expressed under its endogenous control elements, and strongly support the model that Robo2 promotes midline crossing of commissural axons by antagonizing repulsion through an Ig1/Ig2-mediated inhibitory interaction with Robo1.

Discussion

In this manuscript we have described a role for Robo2 in promoting midline crossing through inhibition of Slit-Robo1 repulsion. Loss of function experiments point to an endogenous requirement for Robo2 in promoting midline crossing. Additional genetic analyses indicate that Robo2 can antagonize Robo1 in the absence of its cytoplasmic domain and that this inhibitory effect can be generated by non-cell autonomous expression of Robo2. These observations, together with the demonstration that Robo2 variants that promote midline crossing are potent suppressors of *comm* mutants, supports the model that Robo2 inhibits Slit-Robo1 repulsion, rather than acting as a receptor that promotes midline axon attraction. Biochemical and gain of function genetic analyses show that Robo2 can bind to Robo1 *in vivo* through its Ig1 and Ig2 domains and that this binding interaction correlates with Robo2's pro-crossing activity. Furthermore, cell type specific rescue experiments and analysis of Robo2 mRNA and protein expression are consistent with a requirement for Robo2 in midline cells, and support an endogenous requirement for Robo2's Ig2 domain in promoting midline crossing. Taken together, the data in this manuscript support the model that Robo2 expressed in cells other than commissural neurons acts to inhibit Robo1 receptor activity through extracellular domain binding interactions, and that this activity ensures the

precise execution of midline guidance (Figure 4.16). Our model reconciles two previously confounding observations: one, that a small amount of Robo1 protein is detectable on commissural axons as they cross the midline, yet this pool of Robo1 is unable to signal midline repulsion; and two, that the single known isoform of Robo2 can act to both promote and inhibit midline crossing.

Multiple mechanisms ensure precise and robust regulation of Robo1 repulsion

Given the prominent role that Comm plays in regulating Robo1 receptor expression to prevent premature responses to Slit, it is fair to ask why it is necessary to invoke a second mechanism to down-regulate Robo1 receptor signaling. Indeed, in wild-type animals, there is no obvious requirement for Robo2's pro-crossing activity, at least not at the embryonic midline in the populations of neurons that we have assayed. A requirement for Robo2 in promoting midline crossing in otherwise wild type animals has been described for the guidance of foreleg gustatory neurons in the adult nervous system, although it is not clear in this context if the same mechanism that we have described is at work (Mellert et al., 2010). Nevertheless, a clear endogenous contribution for Robo2 at the embryonic midline can be demonstrated in conditions where attractive guidance cues, such as Netrin, are compromised. One probable explanation for the existence of this second regulatory mechanism is that it confers robustness on the essential process of midline circuit formation, and that this is important to the animal when developmental conditions are not optimal.

While Comm is an efficient and potent negative regulator of Robo1 trafficking to the growth cone surface, it is clear that not all Robo1 is prevented from reaching the surface in the presence of Comm. Low levels of Robo1 can be detected on commissural axons by immunostaining and immunoelectron microscopy (Kidd et al., 1998a). Data from surface labeling experiments indicate that Comm acts on newly synthesized Robo1, and the question of how Robo1 receptors already present on the plasma membrane prior to the initiation of *comm* expression might be regulated remains unresolved (Keleman et al., 2002). The role of Robo2 may thus be to negatively regulate the low levels of Robo1 that escape Comm-dependent sorting.

In addition to the complementary actions of Comm, a cell autonomous regulator of Robo1 trafficking (Keleman et al., 2002, Keleman et al., 2005), and Robo2, a cell non-autonomous inhibitor of Robo1 signaling (this study), it is likely that there are additional levels of regulation that contribute to preventing premature response to midline Slit. In particular, a recent study shows quite convincingly that Comm's role in sorting Robo1 is insufficient to explain how Robo1 activity is limited in pre-crossing commissural axons. Specifically, embryos in which the endogenous Robo1 receptor is replaced with a variant of Robo1 that is insensitive to the sorting activity of Comm by homologous recombination show no defects in midline crossing (Gilestro, 2008). This observation is in marked contrast to the prediction of the sorting model, in which embryos carrying a Comm-resistant Robo1 receptor would be expected to resemble *comm* mutants. It will be of great interest to obtain an explanation for this paradoxical finding and to determine what additional functions or targets of Comm could also ensure the regulation of Slit-dependent repulsion.

157

Inhibitory receptor-receptor interactions in trans: a new mechanism to regulate axon guidance

Our results suggest that Robo2 can inhibit Robo1 activity and that this effect is mediated by receptor-receptor interactions between the Robo2 and Robo1 extracellular domains. Cis-inhibitory interactions, such as those that occur between the transmembrane protein Kekkon 1 and the epidermal growth factor receptor (EGFr) (Ghiglione et al., 2003), and between ligand and receptor pairs, as in the cases of Ephs/ephrins and Notch/Delta, have been well documented (Del Álamo et al., 2011; Kao and Kania, 2011; Yaron and Sprinzak, 2012). While we were not able to detect trans interactions by co-immunoprecipitation or by an S2 cell aggregation assay (data not shown), our genetic data strongly suggest that Robo2 acts in trans to inhibit Robo1 signaling. A recent *in vitro* screen for trans interactions among *Drosophila* cell surface receptors did not report a direct interaction between Robo1 and Robo2, suggesting that if trans interactions do occur, they might be mediated by a cofactor (Ozkan et al., 2013). Indeed, Slit-dependent trans interactions between Robo1 and Robo2 have been proposed to play a role in the migration of sensory neurons in the *Drosophila* peripheral nervous system, although in this case Robo2 is thought to promote Slit-Robo repulsive signaling by presenting Slit to Robo receptors expressed in trans (Kraut and Zinn, 2004).

Previous studies have defined growth factor and morphogen receptor regulatory mechanisms that bear some resemblance to the mechanism that we have described here. For example, epidermal growth factor receptor (EGFr) signaling and Bone Morphogenetic Protein receptor (BMPr) signaling can be attenuated cell non-

autonomously by various inhibitory factors, such as Argos for EGFrs and Noggin for BMPrs (Klein et al., 2004; Walsh et al., 2010). In the case of EGFr, receptor signaling is blocked because the soluble inhibitory factor Argos binds to and sequesters the EGF ligand, thereby preventing receptor activation (Klein et al., 2008). The mechanism through which Robo2 regulates Robo1 is similar in that it acts cell non-autonomously and that it depends on extracellular interactions, but distinct, since Robo2 does not appear to act solely by binding and sequestering Slit, as the Robo2ΔIg2 receptor can still bind Slit, but is completely unable to inhibit Robo1 activity.

It remains to be determined, but a closer analogy may exist with the way Dickkopf (DKK) family proteins antagonize Wnt receptor signaling (Niehrs, 2006). In this case, secreted DKK binds to the lipoprotein related proteins (LRP5 and 6), which are co-receptors for Wnt, and prevents LRP interaction with the Frizzled/Wnt ligand receptor complex (Ahn et al., 2011; Chen et al., 2011). While Robo2 is not secreted, there is evidence that Robo1 receptor extracellular domains can be cleaved and shed into the extracellular space (Coleman et al., 2010), and we have observed that the Robo2 ectodomain can also be shed *in vitro* and *in vivo* (Evans and Bashaw, unpublished). In the future, it will be interesting to investigate whether Robo2 binding prevents Robo1 from interacting with Slit *in vivo,* and whether Robo2 receptor cleavage is important for its ability to promote midline crossing. Alternatively, Robo2 could prevent the recruitment of Robo1's downstream signaling molecules such as Enabled, Nck/Dock and Son of Sevenless (Bashaw et al., 2000; Fan et al., 2003; Yang et al., 2006).

How are the diverse axon guidance activities of the Robo2 receptor coordinated?

In addition to its Ig1/Ig2 dependent role in inhibiting Slit-Robo1 repulsion that we have described here, Robo2 has at least three other distinct axon guidance activities that can be attributed to different structural elements of the receptor. In the context of midline axon repulsion, Robo2 binds Slit through its extracellular Ig1 domain and cooperates with Robo1 to prevent abnormal midline crossing. It is not known how Robo2 signals repulsion, but based on receptor swap experiments that demonstrate that Robo1 can substitute for Robo2's midline repulsive activity, it seems likely that a common cytoplasmic signaling output shared by Robo1 and Robo2 (perhaps mediated by the shared CC0 or CC1 motifs) is important for repulsion (Spitzweck et al., 2010). Robo2 also directs the mediolateral position of axons in the CNS, an activity conferred by a combination of its extracellular Ig1 and Ig3 domains (Evans and Bashaw, 2010b)In this context, distinct biochemical properties conferred by Ig3 appear to direct Robo2 receptor multimerization, and this property correlates with the ability to regulate lateral position *in vivo* (Evans and Bashaw, 2010b). Finally, in addition to these activities, we have recently discovered a new function for Robo2 in regulating the guidance of specific populations of motor axons to their appropriate muscle targets. In this case, Robo2's guidance activity depends on unique features of its cytoplasmic domain (Santiago et al., 2014).

A major challenge for the future will be to understand how these diverse guidance activities are deployed at the right time and place to allow for appropriate guidance responses. One important factor that is likely to contribute to the coordination of these activities is the regulation of the spatial and temporal expression of Robo2. For example,

in late stage embryos, Robo2 protein expression is restricted to the lateral most regions of the longitudinal connectives where it is presumably acting to control lateral positioning, while in younger embryos *robo2* mRNA can be detected in ipsilateral pioneer neurons where it is likely contributing to midline repulsion. Robo2 is also detected in midline glia and neurons, where we propose it may act to prevent premature responses to Slit. At present, little is known about how these patterns of expression are established and temporally regulated, although we have recently shown that the homeodomain transcription factors *dHb9* and *nkx6* are required for *robo2* expression in a subset of motor neurons (Santiago et al., 2014).

While controlling the time and place of Robo2 expression is no doubt part of the explanation for how Robo2's diverse and sometimes opposing activities are coordinated, we expect that the distinct biochemical features of Robo2's different activities, as well as the potential interaction with context-specific cofactors will also play an important role. Here, we note that Robo2 does not appear to be able to promote midline crossing cell-autonomously, either in subsets of commissural neurons in rescue experiments, or in the apterous ipsilateral interneurons in gain-of-function experiments. This could be because Robo2 is unable to bind to Robo1 in cis *in vivo*, or alternatively because Robo1-Robo2 cis interactions confer a distinct outcome from the inhibitory effect of Robo2 presented from other cells. This is reminiscent of the different responses produced by cis and trans interactions between receptors and their ligands (Yaron and Sprinzak, 2012). How distinct signaling responses are triggered by the different structural conformations resulting from cis versus trans interactions remains poorly understood. Future experiments to define the mechanisms that control the specific expression domains and

161

biochemical activities of Robo2 promise to continue to offer new insights into the
molecular biology of axon guidance.

Experimental Procedures

Genetics

The following Drosophila mutant alleles were used: fra^3, fra^4, $robo2^{x33}$, $robo2^{x123}$,
$robo2^{x135}$, $comm^{E39}$, P{GawB}NP6273 ($robo2^{GAL4}$), eg^{MZ360} (eg-GAL4), ap-GAL4,
$dHb9^{GAL4}$, $robo2^{HArobo2}$. The following transgenes were used: P{10UAS-HARobo1}86Fb,
P{10UAS-HARobo2}86Fb, P{10UAS-HARobo2$^{\Delta Ig1}$}86Fb, P{10UAS-HARobo2$^{\Delta Ig2}$}86Fb,
P{10UAS-HARobo2$^{\Delta Ig1+2}$}86Fb, P{10UAS-HARobo1$^{\Delta C}$}86Fb, P{10UAS-
HARobo2$^{\Delta C}$}86Fb, P{UAS-HARobo1^{R2I1+2}}86Fb, P{UAS-HARobo2^{R1I1+2}}86Fb, P{UAS-
Robo1$^{\Delta C}$myc}2, P{UAS-Robo2$^{\Delta C}$myc}1, P{UAS-HARobo1^{R2I1+2}}, P{UAS-
HARobo2^{R1I1+2}}, P{UAS-Robo1myc}, P{UAS-HARobo2}T1, P{GAL4-elav.L}3 (elav-
GAL4), slit-GAL4, P{UAS-TauMycGFP}II, P{UAS-TauMycGFP}III. Transgenic flies
were generated by BestGene Inc. (Chino Hills, CA) or Rainbow Transgenic Flies Inc.
(Camarillo, CA) using ΦC31-directed site-specific integration into landing sites at
cytological position 86F (for UAS-Robo constructs) or 51C (for *robo2* BAC CH321-
22K18 and modified BACs). All crosses were carried out at 25°C. Embryos were
genotyped using balancer chromosomes carrying *lacZ* markers or by the presence of
epitope-tagged transgenes.

Molecular Biology

pUAST cloning: Robo coding sequences were cloned into a pUAST vector
(p10UASTattB) including 10xUAS and an attB site for ΦC31-directed site-specific
integration. All p10UASTattB constructs include identical heterologous 5′ UTR and
signal sequences (derived from the Drosophila wingless gene) and an N-terminal 3×HA
tag. Robo domain deletion variants created for this study were generated by PCR and
include the following amino acids (numbers refer to Genbank reference sequences
AAF46887 [Robo1] and AAF51375 [Robo2]): Robo2$^{\Delta Ig1}$ (187-1463), Robo2$^{\Delta Ig2}$ (84-186,
281-1463), Robo2$^{\Delta Ig1+2}$ (281-1463), Robo1$^{\Delta C}$ (56-950), Robo2$^{\Delta C}$ (84-1022).

robo2 BAC and recombineering: The *robo2* BAC CH321-22K18 was generated by the
P[acman] consortium (Venken et al., 2009) and obtained from BACPAC Resources
(bacpac.chori.org). Modified BACs were generated by replacing *robo2* exons 2-14 and
intervening introns with untagged or HA-tagged cDNAs via recombineering. Briefly,
partial *robo2* cDNAs plus a kanamycin-resistance selective marker were cloned into a
plasmid vector flanked by 50bp homology arms matching the 3' end of the *robo2* first
intron and the beginning of the *robo2* 3' UTR. This cassette was excised by PmeI
digestion and electroporated into DY380 cells containing the original CH321-22K18
BAC in which expression of lambda recombination genes had been induced by heat
shock. Potential recombinant BACs were selected on LB plates containing
chloramphenicol (12.5 µg/ml) and kanamycin (25 µg/ml), and verified by PCR
amplification and sequencing of the entire recombineered region.

Immunofluorescence and Imaging

Dechorionated, formaldehyde-fixed, methanol-devittellinized embryos were fluorescently stained using standard methods. The following antibodies were used in this study: Rabbit anti-HA (Covance PRB-101C, 1:2000), Mouse anti beta-tubulin (E7, DSHB, 1:100), Mouse anti-HA (Covance 16B12, 1:250), FITC-conjugated goat anti-HRP (Jackson # 123-095-021, 1:250), Alexa-647 conjugated goat-anti-HRP (Jackson #123-605-021 1:500), mouse anti-Fasciclin-II/mAb 1D4 [Developmental Studies Hybridoma Bank, (DSHB), 1:100], mouse anti-βgal (DSHB, 1:150), rabbit anti-GFP (Invitrogen #A11122, 1:500), rabbit anti-c-Myc (Sigma C3956, 1:500), Cyanine 3-conjugated goat anti-mouse (Jackson #115-165-003, 1:1000), Alexa-488-conjugated goat anti-rabbit (Molecular Probes #A11008, 1:500). Embryos were mounted in 70% glycerol/PBS. Fluorescent mRNA in situ hybridization was performed as described, with digoxigenin labeled probe (Yang et al., 2009). Phenotypes were analyzed and images were acquired using a spinning disk confocal system (Perkin Elmer) built on a Nikon Ti-U inverted microscope using a Nikon OFN25 60x objective with a Hamamatsu C10600-10B CCD camera and Yokogawa CSU-10 scanner head with Volocity imaging software. Images were processed using ImageJ.

Biochemistry

Slit binding assay: *Drosophila* S2R+ cells were cultured at 25ºC in Schneider's media plus 10% fetal calf serum. To assay Slit binding, cells were plated on poly-L-lysine coated coverslips in six-well plates (Robo-expressing cells) or untreated six-well plates (Slit-expressing cells) at a density of $1\text{-}2\times10^6$ cells/ml, and transfected with pRmHA3-

GAL4 and HA-tagged pUAST-Robo or untagged pUAST-Slit plasmids using Effectene transfection reagent (Qiagen). GAL4 expression was induced with 0.5 mM $CuSO_4$ for 24 hours, then Slit-conditioned media was harvested by adding heparin (2.5 ug/ml) to Slit-transfected cells and incubating at room temperature for 20 minutes with gentle agitation. Robo-transfected cells were incubated with Slit-conditioned media at room temperature for 20 minutes, then washed with PBS and fixed for 20 minutes at 4ºC in 4% formaldehyde. Cells were permeabilized with PBS+0.1% Triton X-100, then stained with antibodies diluted in PBS+2mg/ml BSA. Antibodies used were: mouse anti-SlitC (c555.6D, DSHB, 1:50), rabbit anti-HA (Covance, 1:2000), Cy3 goat anti-mouse (Jackson Immunoresearch, 1:500), and Alexa488 goat anti-rabbit (Molecular Probes, 1:500). After antibody staining, coverslips with cells attached were mounted in Aquamount. Confocal stacks were collected using a Leica SP5 confocal microscope and processed by NIH ImageJ and Adobe Photoshop software.

Surface labeling: For surface labeling in S2R+ cells, cells were plated on poly-L-lysine coated coverslips and transfected with pRmHA3-GAL4 and HA-tagged pUAST-Robo2 plasmids using Effectene, as described above. GAL4 expression was induced with 0.5 mM $CuSO_4$ for 24 hours, then cells were washed in cold PBS and blocked in PBS+5% normal goat serum (NGS) for 20 minutes at 4°C. Cells were incubated in primary antibodies diluted in PBS+5% NGS for 30 minutes at 4°C, then washed three times in cold PBS. Cells were fixed for 15 minutes at 4°C in 4% paraformaldehyde (PFA) in PBS, followed by three washes in PBS and incubation with secondary antibodies diluted in PBS+5% NGS for 30 minutes at room temperature. For staining with detergent, cells

were fixed 24 hours after GAL4 induction in 4% PFA for 15 minutes at room temperature, permeabilized in 0.1% Triton/PBS (PBT) for 5 minutes, blocked in PBT+5% NGS for 20 minutes, and incubated overnight in primary antibodies diluted in PBT+5% NGS. After three washes in PBT, secondary antibodies were added as described above. After secondary antibodies, cells were washed three times in PBS and coverslips were mounted in Aquamount.

Co-immunoprecipitation: Approximately 100 µl of embryos co-expressing Myc-tagged and HA-tagged UAS Robo transgenes in all neurons with *elav-GAL4* were lysed in 0.5 ml of TBS-V (150mM NaCl, 10mM Tris ph8, 1mM ortho-vanadate) supplemented with 1% Surfact-AMPS NP40 (Thermo), protease inhibitors (Roche Complete), and 1mM PMSF by manual homogenization using a plastic pestle. After homogenization, embryos were incubated with gentle rocking at 4°C for 10 minutes and centrifuged in a pre-chilled rotor for 10 minutes at 14000rpm. The soluble phase was removed and incubated with 1-2 µg of anti-Myc antibody (Millipore) for 45 minutes with gentle rocking at 4°C. 50 µl of a 50% slurry of proteinA and proteinG agarose (Invitrogen) were added to the tubes and samples were incubated for an additional 30 minutes with gentle rocking at 4°C. Samples were washed three times in lysis buffer and then boiled for 10 minutes in 50 µl of 2X Laemmli SDS Sample Buffer. Proteins were resolved by SDS Page and transferred to nitrocellulose for subsequent incubation with anti-myc (9E10, DHRSB) 1:1000 or anti-HA (16B12 Covance) 1:1000 overnight at 4°C in PBS supplemented with 5% dry milk and 0.1% Tween 20. After three washes in PBS/0.1% Tween 20, HRP-conjugated secondary antibodies were applied for 1 hour at room temperature. Signals

were detected using either ECL 2 or ECL Prime (Amersham) according to manufacturer's instructions.

For co-immunoprecipitation in *Drosophila* S2R+ cells, 10^6 cells were transfected with pRmHA3-GAL4, HA or Myc-tagged pUAST-Robo or untagged pUAST-Slit plasmids and induced 24 hours after transfection, as described above. 48 hours after transfection, cells were lysed in TBS-V (150mM NaCl, 10mM Tris ph8, 1mM ortho-vanadate) supplemented with 0.5% Surfact-AMPS NP40 (Thermo), protease inhibitors (Roche Complete) and 1 mM phenylmethanesulfonylfluoride (PMSF). Lysates were precleared with Protein A/G agarose for 30 min at 4°C, followed by addition of 1-2 ug of Rabbit anti-Myc (Millipore 06-549) or Rabbit anti-HA (Covance) for 1 hour at 4°C. 50 μl of a 50% slurry of proteinA and proteinG agarose (Invitrogen) were added, and samples were incubated for an additional 30 minutes with gentle rocking at 4°C. Samples were washed 3x in lysis buffer and boiled for 10 min in 50 μl of 2X Laemmli SDS Sample Buffer. For lysate mixing experiments, Slit-conditioned media was harvested 48 hours after transfection, as described above. pUAST-Robo1 and pUAST-Robo2 cell lysates were mixed for 1 hour at 4°C with gentle agitation before immunoprecipitation. In some conditions, Slit-conditioned media was added at 2X concentration to pUAST-Robo1 and pUAST-Robo2 cell lysates. SDS electrophoresis and Western blotting were performed as described above, and developed using WesternSure PREMIUM Chemiluminescent Substrate (Li-cor) according to manufacturer's instructions.

Statistics

For statistical analysis, comparisons were made between genotypes using the Student's t-test. For multiple comparisons, significance was assessed by using a Bonferroni correction.

Figure 4.1. Robo2 commissural guidance defects are rescued by a Robo2 BAC transgene.

169
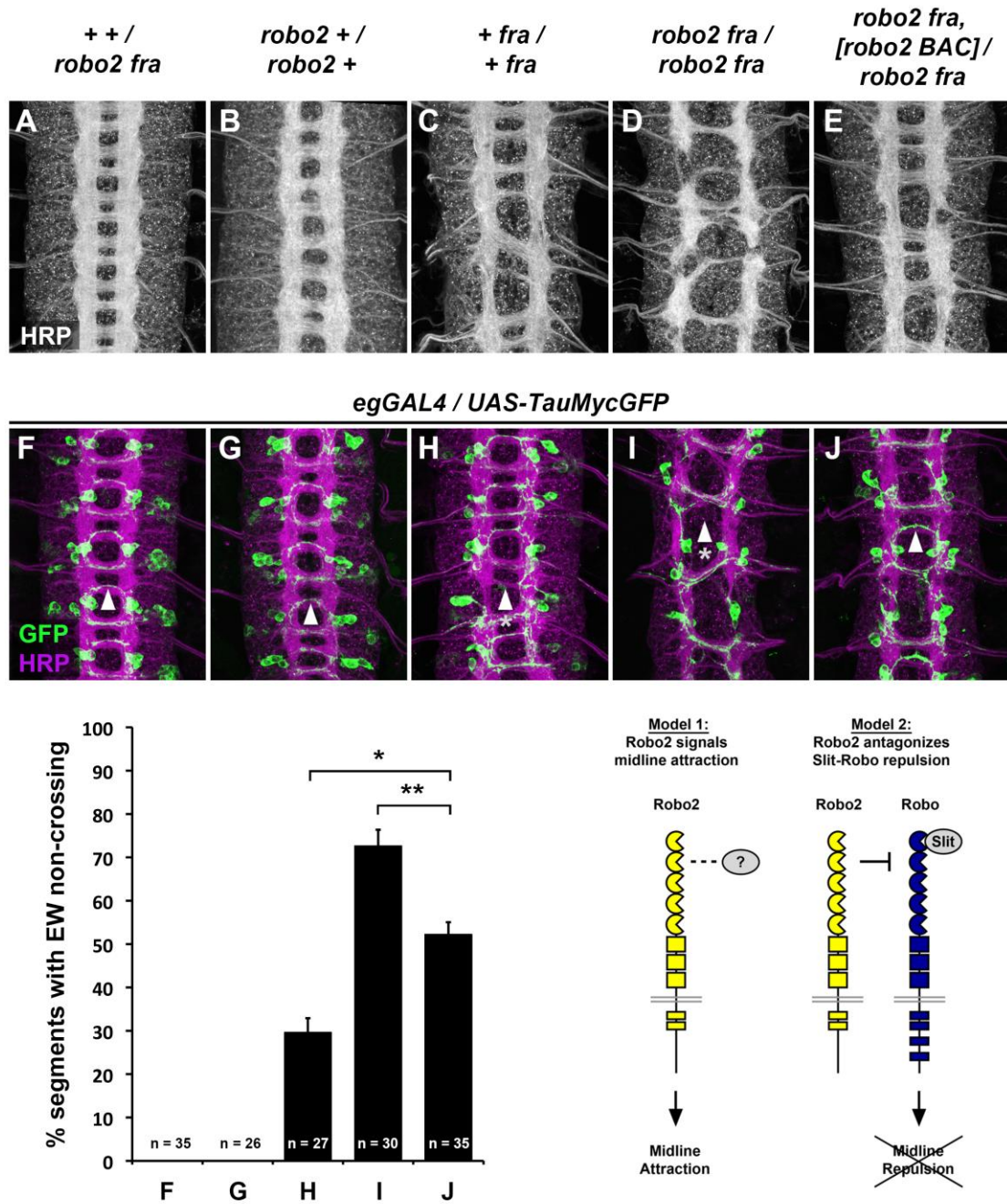
Figure 4.1. Robo2 commissural guidance defects are rescued by a Robo2 BAC transgene.

A-E: Stage 17 embryos stained with anti-HRP antibodies to label all CNS axons. **F-J**: Stage 15-16 embryos carrying *eg-GAL4* and *UAS-TauMycGFP* transgenes, stained with anti-HRP and anti-GFP antibodies. Anti-GFP labels cell bodies and axons of the eagle neurons (EG and EW). **A, F**: Embryos heterozygous for both *frazzled (fra)* and *robo2* display a wild-type arrangement of longitudinal and commissural axon pathways, and axons of the EW neurons cross the midline in the posterior commissure in 100% of segments (arrowhead). **B, G**: *robo2* mutants ($robo2^{123}/robo2^{33}$) display a mildly disorganized axon scaffold, but no defects in EW crossing. C, H: *fra* mutants (fra^3/fra^4) display thin commissures indicative of decreased midline crossing, and the EW axons fail to cross the midline in 30% of abdominal segments (arrowhead with asterisk). **D, I**: Simultaneous removal of *robo2* and *fra ($robo2^{123},fra^3/robo2^{135},fra^4$)* strongly enhances the midline crossing defects seen in *fra* single mutants. **E, J**: Midline crossing is partially restored in *robo2,fra* double mutants carrying one copy of an 83.9-kb *robo2* BAC transgene. Histogram quantifies EW midline crossing defects in the genotypes shown in **F-J**. Error bars represent s.e.m. *n*, number of embryos scored for each genotype. **Bottom right**: Two models for how Robo2 might promote midline crossing of commissural axons. Left, Robo2 may act as a midline attractive receptor to promote midline crossing in response to an unidentified ligand. Right, Robo2 may antagonize canonical Slit-Robo1 repulsive signaling to down-regulate midline repulsion and thus allow Robo1-expressing axons to cross the midline. (Experiments were performed by T.A.E.)

170

Figure 4.2. Robo2 can promote midline crossing independent of its cytoplasmic domain.
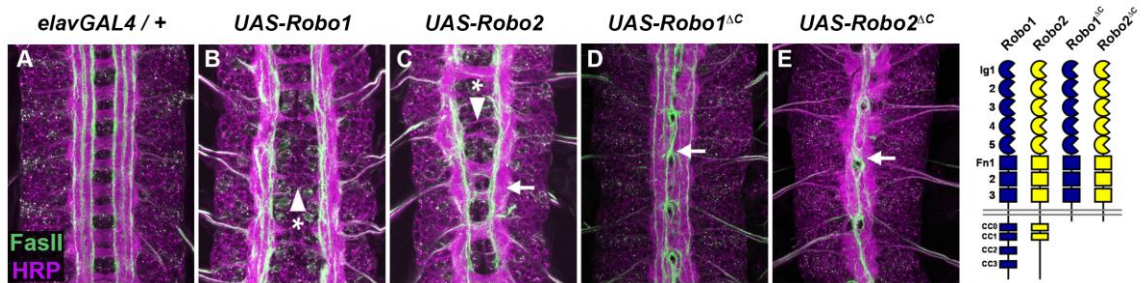
Figure 4.2. Robo2 can promote midline crossing independent of its cytoplasmic domain.

A-E: Stage 17 embryos carrying *elav-GAL4* and the indicated *UAS-Robo* transgenes, stained with anti-HRP (magenta) and the longitudinal pathway marker anti-FasciclinII (FasII; green). **A**: Embryos carrying *elav-GAL4* alone exhibit a wild-type arrangement of axon pathways, including distinct anterior and posterior commissures and three FasII-positive longitudinal pathways that do not cross the midline. **B**: In *elav-GAL4/UAS-Robo1* embryos, commissure formation is strongly impaired, and no ectopic midline crossing of FasII-positive axons is observed. **C**: Mis-expression of Robo2 with *elav-GAL4* produces a biphasic phenotype, where some segments appear nearly commissureless (arrowhead with asterisk) while others exhibit ectopic crossing reminiscent of *robo1* mutants (arrow). See Figure 5 for quantification of ectopic crossing in *elav-GAL4/UAS-Robo2* embryos. **D, E**: Mis-expression of truncated forms of Robo1 (Robo1ΔC) or Robo2 (Robo2ΔC) with *elav-GAL4* induces ectopic crossing in 100% of segments, although the Robo2ΔC mis-expression phenotype is qualitatively more severe than Robo1ΔC. In *elav-GAL4/UAS-Robo1ΔC* embryos (**D**) only the medial FasII pathway crosses the midline and the axon scaffold overall exhibits a *robo1*-like appearance, while in *elav-GAL4/UAS-Robo2ΔC* embryos (**E**) all three FasII-positive pathways collapse at the midline in nearly every segment and the axon scaffold appears *slit*-like. All UAS-Robo transgenes shown here were inserted into the same genomic location (86FB) to ensure equivalent expression levels. (Experiments were performed by T.A.E.)

172

Figure 4.3. Comparison of Robo1ΔC and Robo2ΔC gain of function activities.
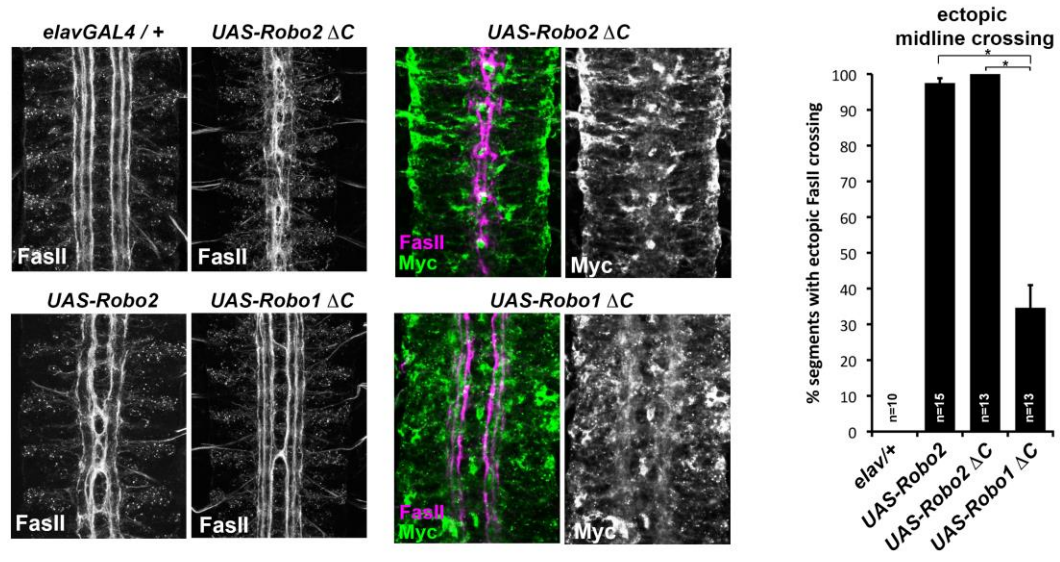
Figure 4.3. Comparison of Robo1ΔC and Robo2ΔC gain of function activities.

Since the effects of expressing ΔC transgenes in the 86Fb insertion site are too potent to allow quantitative comparison, we used traditional UAS insertion lines that are expressed at lower and comparable levels (right panels, anti-Myc is shown in green and anti-FasII in magenta) to compare activities of Robo1ΔC and Robo2ΔC. In embryos expressing only an *elav-GAL4* transgene (top left) FasII axons appear wild-type and remain ipsilateral. Mis-expression of Robo2 leads to a high level of ectopic crossing. Robo2ΔC expression results in a much greater degree of ectopic midline crossing than does Robo1ΔC. Segments with ectopic midline crossing of FasII axons are quantified on the right. Significance was assessed by multiple comparisons using the Student's t-test and a Bonferroni correction (*p<0.001). Error bars represent s.e.m. *n*, number of embryos scored for each genotype. (Experiments were performed by T.A.E. and C.S.)

Figure 4.4. Slit binding and Robo gain of function.
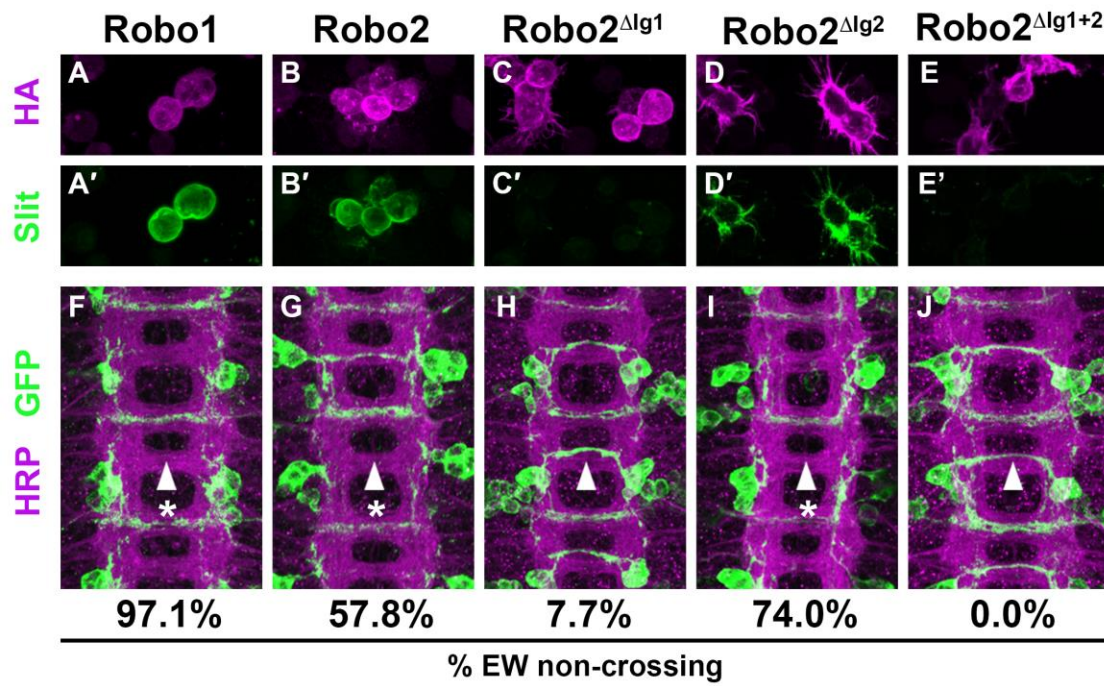
Figure 4.4. Slit binding and Robo gain of function.

A-E: Slit conditioned media was collected and used to treat cells expressing the indicated HA-tagged receptors. Receptor expression is shown with anti-HA in the top panels (magenta) and anti-Slit staining is shown in the bottom panels (green). Robo1 (**A**), Robo2 (**B**), and Robo2ΔIg2 (**D**) bind efficiently to Slit, while little to no binding is detected in cells expressing Robo2ΔIg1 (**C**) or Robo2ΔIg1+2 (**E**). **F-J**: Stage 16 embryos expressing the indicated transgene in the Eg commissural interneurons. HRP labels the axon scaffold (magenta) and anti-GFP labels the Eg neurons. The percentages under each panel indicate the percentage of EW axons that fail to cross the midline in each condition. Expression of Robo1 (**F**), Robo2 (**G**) and Robo2ΔIg2 (**I**) all lead to strong disruption of midline crossing, while expression of Robo2ΔIg1 (**H**), and Robo2ΔIg1+2 (**J**) result in little to no crossing defects. (Experiments were performed by T.A.E.)

Figure 4.5. Robo2's pro-crossing activity depends on its Ig2 domain.

177
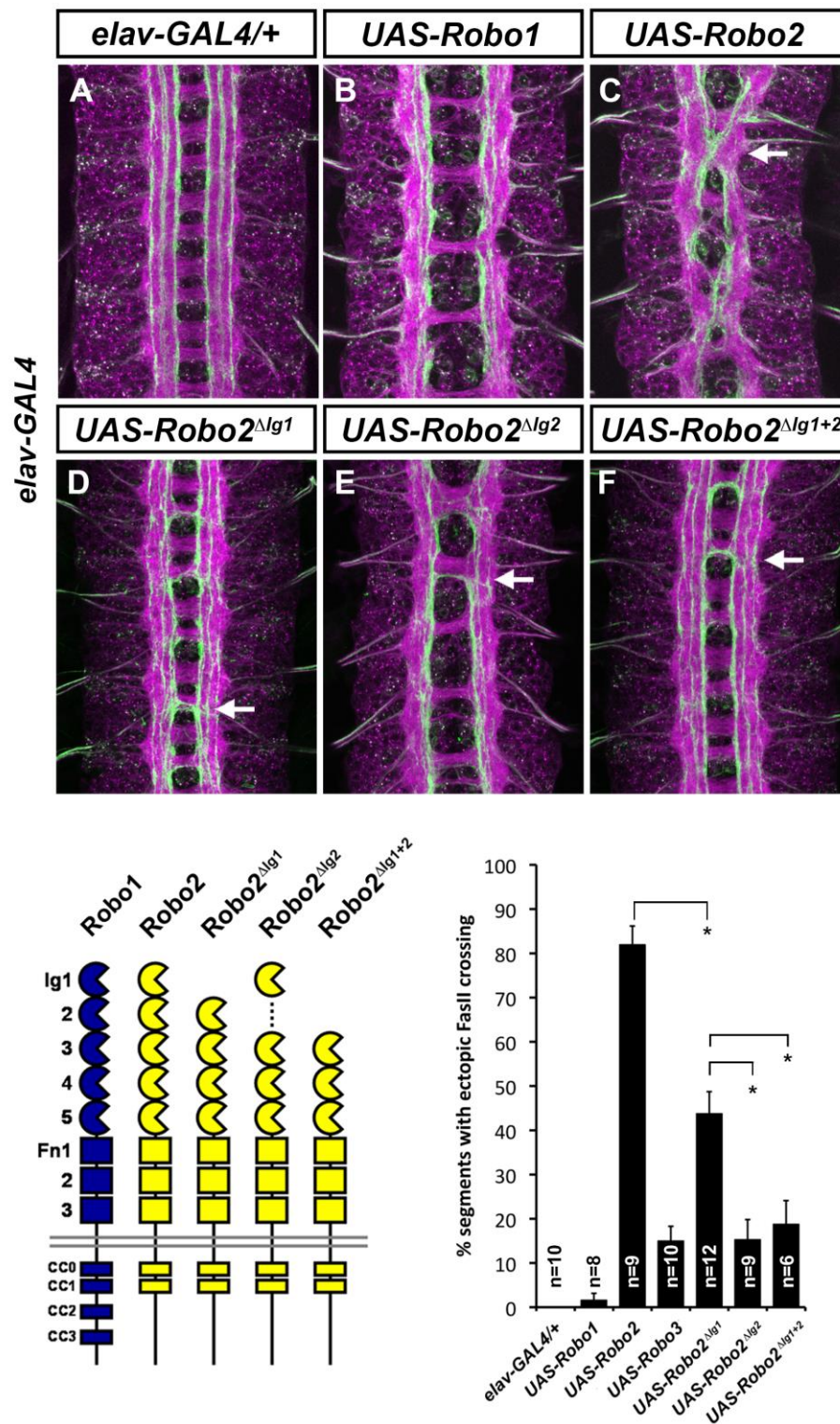
Figure 4.5. Robo2's pro-crossing activity depends on its Ig2 domain.

A-F: Stage 17 embryos carrying *elav-GAL4* and the indicated *UAS-Robo* transgenes, stained with anti-HRP and anti-FasII. **A**: Embryos carrying *elav-GAL4* alone exhibit a wild-type arrangement of axon pathways, including three FasII-positive longitudinal pathways that do not cross the midline. **B**: Robo1 does not promote midline crossing of FasII-positive axons when misexpressed in all neurons with *elav-GAL4*. **C**: Misexpression of full-length Robo2 induces ectopic midline crossing in over 80% of segments (arrow). **D**: Deleting the Ig1 domain (Robo2$^{\Delta Ig1}$) disrupts Slit binding but does not completely prevent Robo2 from promoting midline crossing. **E, F**: Robo2 receptors lacking the Ig2 domain (Robo2$^{\Delta Ig2}$) or both the Ig1 and Ig2 domains (Robo2$^{\Delta Ig1+2}$) are unable to promote ectopic midline crossing above background levels (both are comparable to Robo3; see histogram). Schematics show domain composition of receptors shown in A-F. All UAS-Robo transgenes shown here were inserted into the same genomic location (86FB) to ensure equivalent expression levels. Histogram quantifies ectopic midline crossing in the indicated genotypes. Significance was assessed by multiple comparisons using the Student's t-test and a Bonferroni correction (*$p<0.01$). Error bars represent s.e.m. *n*, number of embryos scored for each genotype. (Experiments were performed by T.A.E.)

Figure 4.6. Robo2 transgenes are localized to axons and expressed at equivalent levels *in vivo*, and are present at the surface of S2R+ cells *in vitro*.
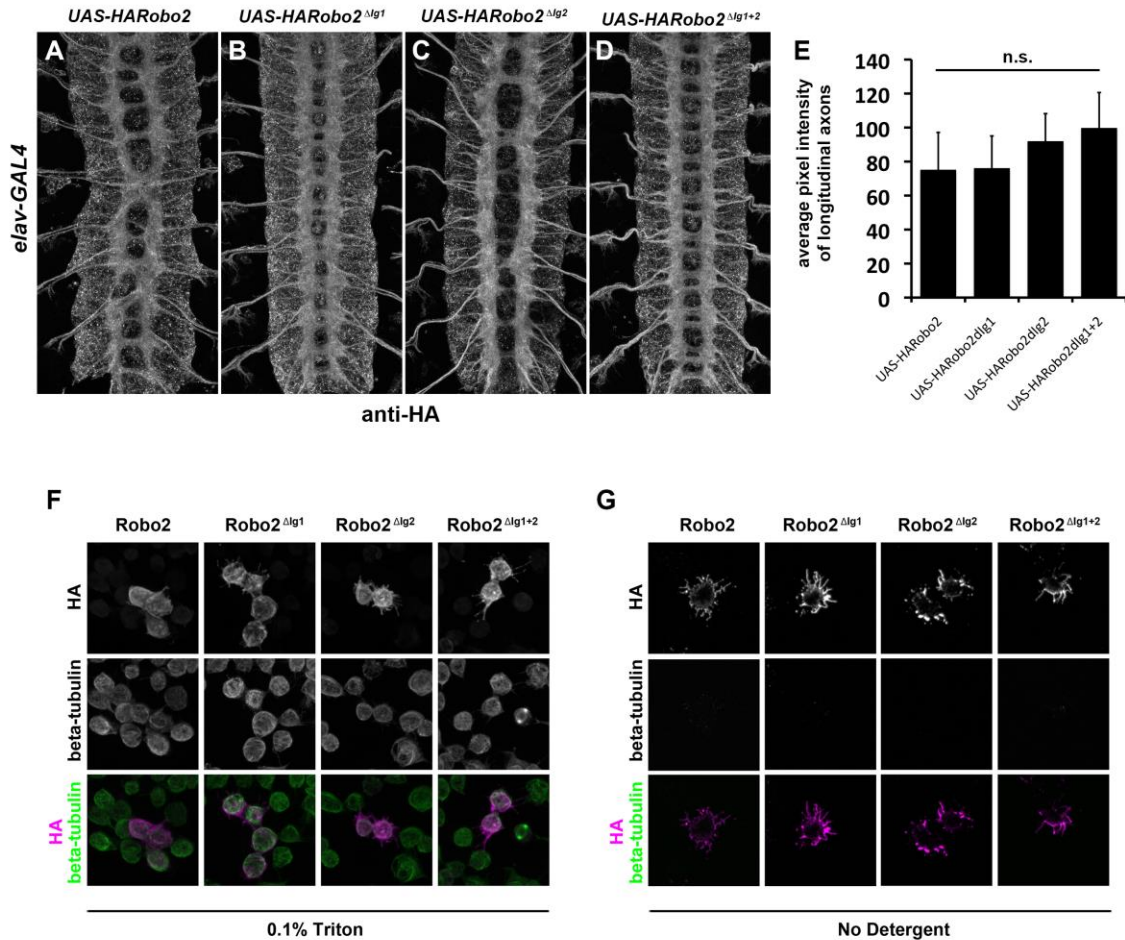
Figure 4.6. Robo2 transgenes are localized to axons and expressed at equivalent levels *in vivo*, and are present at the surface of S2R+ cells *in vitro*.

A-E: Embryos carrying *elav-GAL4* and the indicated *UAS-Robo2* transgenes were stained with anti-HA antibodies and imaged via confocal microscopy. Staining and imaging conditions were identical for all samples. **A-D**: Representative images of embryos expressing each transgene and stained with anti-HA. All Robo2 variants are localized to axons when expressed pan-neurally. **E**: Quantification of pixel intensity for each transgenic line. Confocal max projections through the entire neuropile were collected for three stage 16 embryos for each line, and average pixel intensity was measured across five 25-pixel regions within the longitudinal axon pathways for each embryo. Bar graph shows average pixel intensity across the three embryos for each line. Error bars indicate standard deviation. Average pixel intensity values were not significantly different for any of the four transgenic lines by Student's t-test. **F**: S2R+ cells transfected with the indicated Robo2 constructs were permeabilized and stained with anti-HA and anti-tubulin antibodies. No differences were observed in the localization or expression of the different HA-Robo2 variants. Staining and imaging conditions were identical for all samples. **G**: S2R+ cells transfected with the indicated Robo2 constructs were incubated with anti-HA and anti-tubulin antibodies at 4°C for 30 minutes, in the absence of detergent. All Robo2 proteins were robustly detected at the cell surface by this method, with no noticeable differences in localization or staining intensity; no tubulin signal was detected, confirming that cells were not permeabilized. Staining and imaging conditions were identical for all samples. (Experiments in A-E were performed by T.A.E. Experiments in F-G were performed by C.S.)

Figure 4.7 Robo2 acts cell non-autonomously to promote midline crossing in ipsilateral neurons.
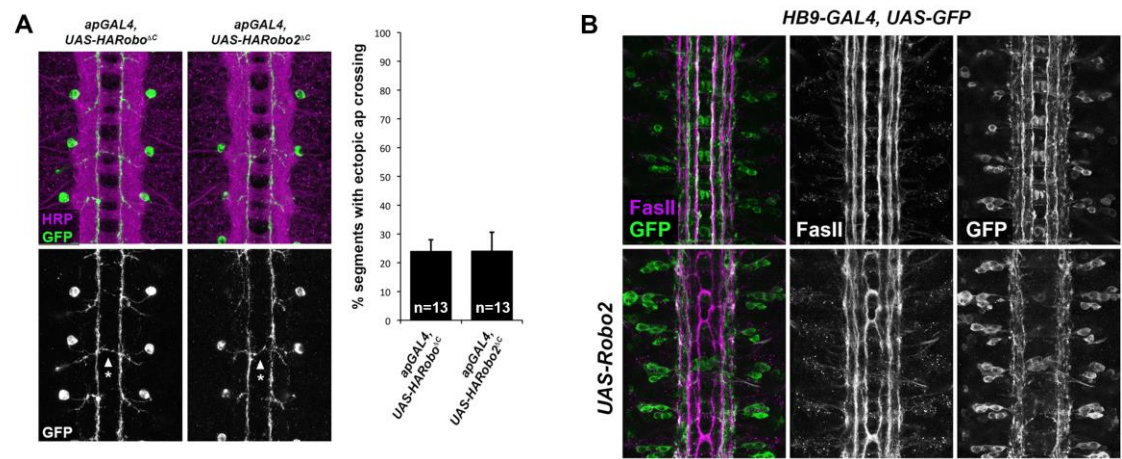
Figure 4.7. Robo2 acts cell non-autonomously to promote midline crossing in ipsilateral neurons.

A: Stage 17 embryos stained with anti-HRP (magenta) and anti-GFP (green) antibodies. Anti-GFP labels the apterous (ap) cell bodies and axons, which normally project ipsilaterally. Mis-expression of Robo2ΔC in ap neurons results in a mild ectopic crossing phenotype, which is similar to the effect of Robo1ΔC (arrowheads with asterisks). Segments with ectopic crossing of ap axons are quantified in the histogram. **B**: Stage 17 embryos stained with anti-FasII (magenta) and anti-GFP (green) antibodies. Anti-GFP labels the axons of *hb9-GAL4* expressing cells. Mis-expression of Robo2 with *hb9-GAL4* results in a lateral shift of *hb9-Gal4+* axons, and causes FasII+ axons that do not express *hb9-GAL4* to ectopically cross the midline. (Experiments were performed by T.A.E.)

Figure 4.8. Robo2 can promote crossing non cell-autonomously.
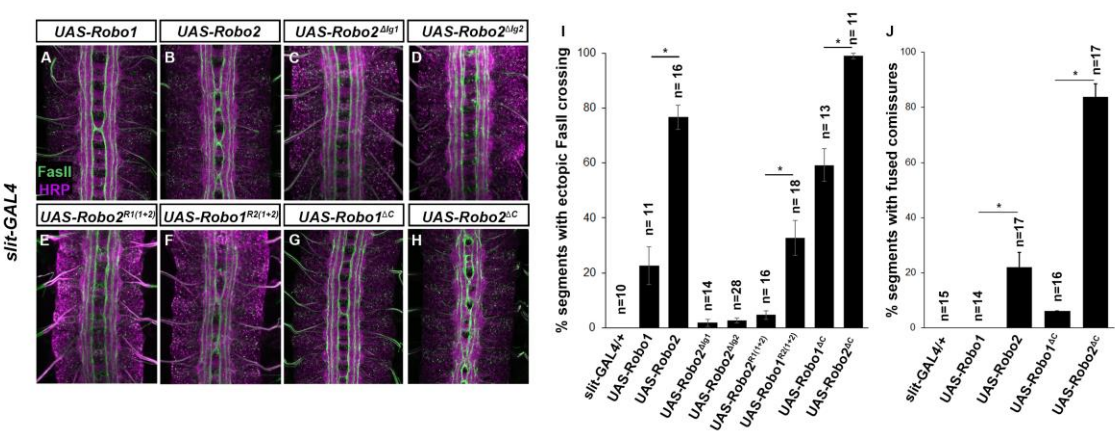
Figure 4.8. Robo2 can promote crossing non cell-autonomously.

A-D: Stage 17 embryos stained with anti-HRP (magenta) and anti-FasII (green). **A, B**: Mis-expression of Robo1 (**A**) in midline cells using *slit-GAL4* results in a mild ectopic crossing phenotype. In contrast, mis-expression of Robo2 (**B**) produces a much stronger effect, as indicated by quantification of ectopic FasII crossing in the histogram (**I**). **C, D**: Mis-expression of either Robo2ΔIg1 (**C**) or Robo2ΔIg2 (**D**) with *slit-GAL4* does not produce ectopic crossing of FasII axons. **E, F**: Consistent with requirement of Robo2's first two IG domains, the chimeric protein Robo1$^{R2IG(1+2)}$ produces an ectopic crossing phenotype (**E**), whereas Robo2$^{R1(IG1+2)}$ has no effect (**F**). G, H: Mis-expression of Robo2ΔC with *slit-GAL4* also results in severe ectopic crossing defects (**H**) that are much stronger than those observed with Robo1ΔC (**G**), as indicated by quantification of ectopic FasII crossing (**I**) and fused commissures observed in anti-HRP stained embryos (**J**). All UAS-Robo transgenes were inserted into the same genomic location (86FB). Significance was assessed by multiple comparisons using the Student's t-test and a Bonferroni correction (*p<0.001). Error bars represent s.e.m. *n*, number of embryos scored for each genotype. (Experiments were performed by T.A.E. and C.S.)

Figure 4.9. *Robo2* **is expressed in midline cells during commissural axon path-finding, and over-expressing** *robo2* **with** *slit-GAL4* **restores midline crossing in** *robo2, fra* **double mutants.**
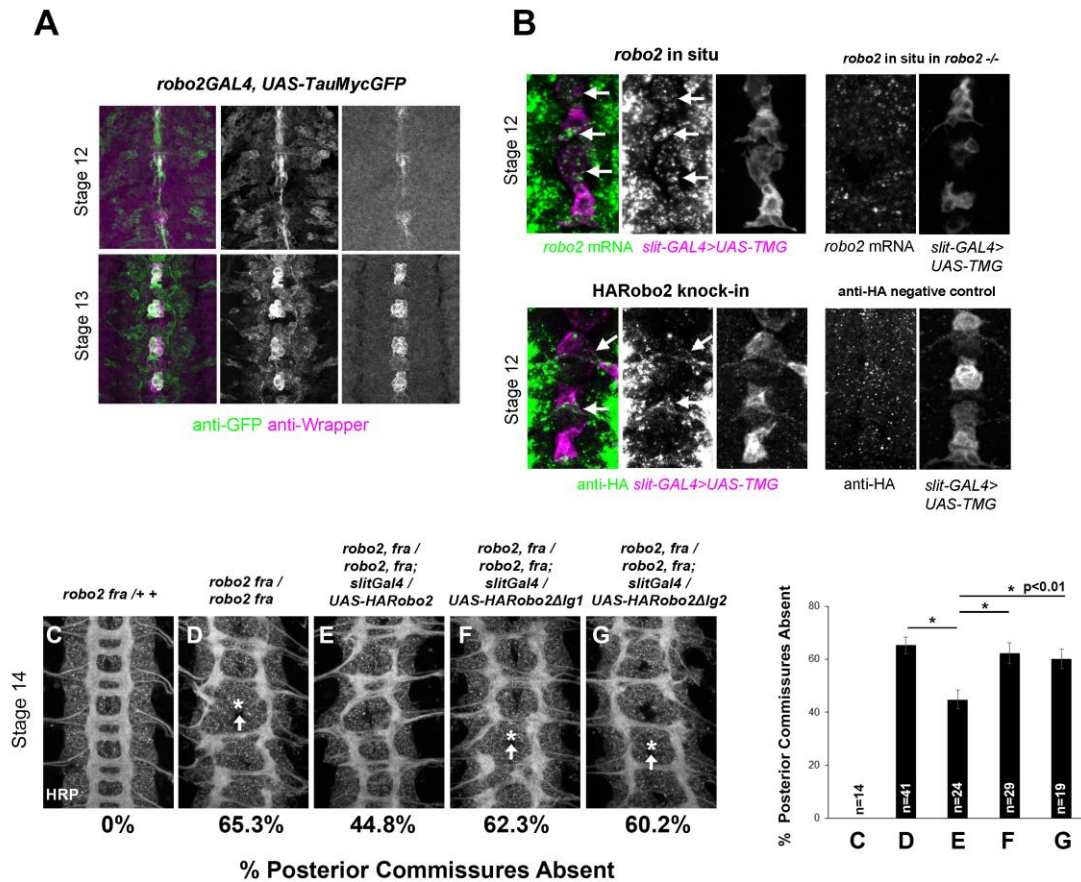
Figure 4.9. *Robo2* **is expressed in midline cells during commissural axon path-finding, and over-expressing** *robo2* **with** *slit-GAL4* **restores midline crossing in** *robo2, fra* **double mutants.**

A: A *robo2-GAL4* enhancer trap that recapitulates *robo2*'s endogenous expression pattern drives *UAS-TauMycGFP* expression (green) in midline cells at stages 12-13, when many commissural axons cross the midline. Midline glia are labeled by an anti-wrapper antibody (magenta). **B**, Top: Fluorescent *in situ* for *robo2* mRNA (green). *robo2* is transiently expressed in midline glia and neurons (magenta) during stage 12 (arrows). The *in situ* signal is not observed in *robo2* mutant embryos (right). **B**, bottom: Robo2 protein is expressed in midline cells during the stages of commissural axon path finding, as shown by the expression pattern of a HA-tagged *robo2* cDNA knock-in allele (*robo2^{HArobo2}*). Stage 12 embryos carrying *robo2^{HArobo2}*, *slit-GAL4* and *UAS-TauMycGFP* show HARobo2 expression in *slitGAL4*-expressing cells (arrows), whereas this signal is not detected in control embryos (right). **C-G**: Stage 14 embryos stained with anti-HRP antibodies to label all CNS axons. The absence of posterior commissures (PC) was scored in A1-A8 (arrows indicate examples of missing commissures). The PC defects of *robo2, fra* double mutants (**D**) are significantly rescued by over-expressing *UAS-Robo2* with *slit-GAL4* (**E**), whereas over-expression of *UAS-Robo2ΔIg1* (**F**) or *UAS-Robo2ΔIg2* (**G**) has no effect. Embryos were scored blind to genotype. Significance was assessed by one-way ANOVA followed by multiple comparisons using the Student's t-test and a Bonferroni correction (*p<0.01). Error bars represent s.e.m. *n*, number of embryos scored for each genotype. (Experiments in A performed by T.A.E. All others performed by C.S.)

Figure 4.10. *Robo2* **mRNA is transiently expressed in midline cells.**
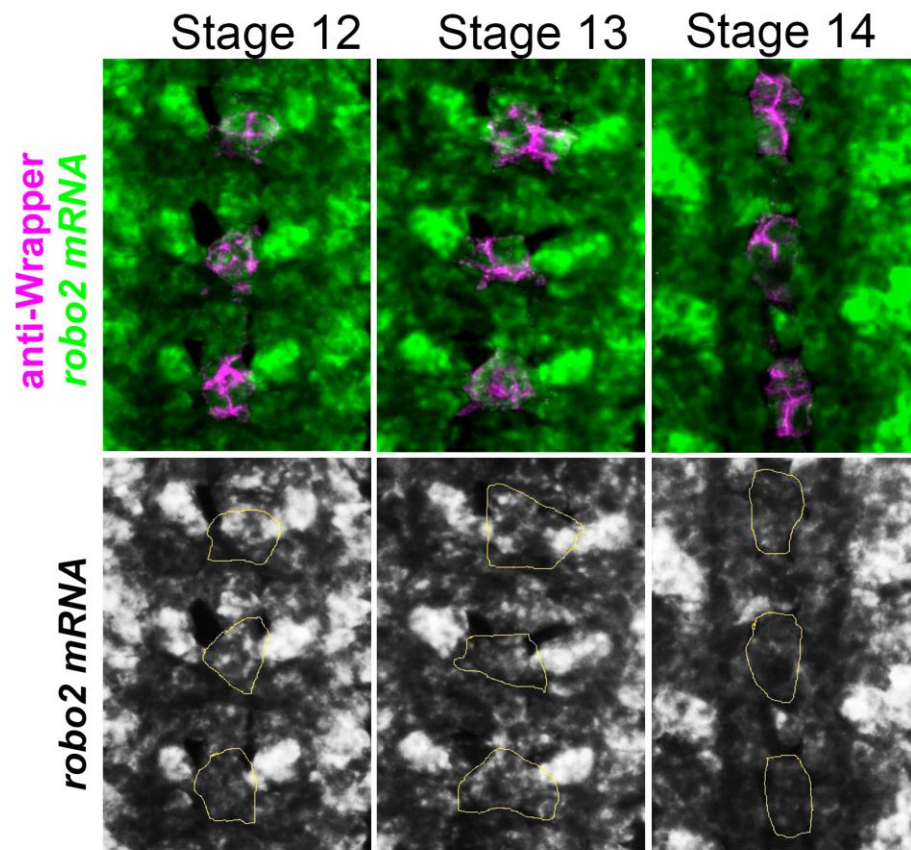
Figure 4.10. *robo2* **mRNA is transiently expressed in midline cells.**

Fluorescent *in situ* for *robo2* mRNA (green). Midline glia are labeled by anti-Wrapper (magenta) and circled in yellow in the single channel images (bottom). *robo2* is transiently expressed in midline glia during stages 12 and 13, but is no longer detected there by stage 14. (Experiments were performed by C.S.)

Figure 4.11. Robo2 cannot rescue midline crossing cell autonomously.
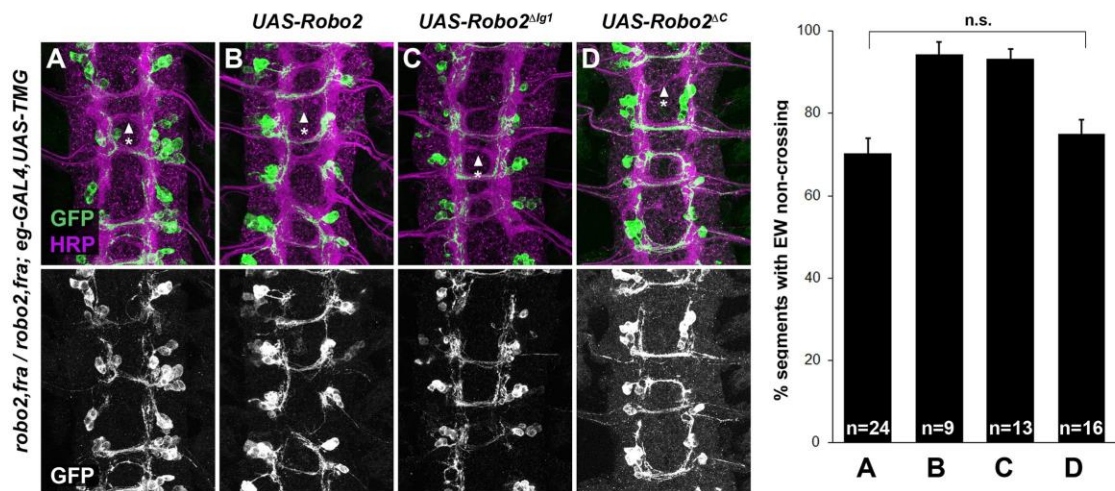
Figure 4.11. Robo2 cannot rescue midline crossing cell autonomously.

A-D: Stage 16 embryos of the indicated genotypes stained with anti-HRP (magenta) and anti-GFP (green) antibodies. Anti-GFP labels the EG and EW cell bodies and axons. EW crossing defects in *robo2, fra* double mutants (**A**) are not rescued by *eg-GAL4* mediated over-expression of *UAS-Robo2* (**B**), *UAS-Robo2 ΔIG1* (**C**), or *UAS-Robo2ΔC* (**D**), suggesting that Robo2 cannot act cell autonomously to promote midline crossing. Segments with non-crossing EW axons are indicated by arrowheads with asterisks. Significance was assessed by multiple comparisons using the Student's t-test and a Bonferroni correction. No significant differences between any of the genotypes were observed ($p > 0.3$). Error bars represent s.e.m. *n*, number of embryos scored for each genotype. (Experiments performed by T.A.E.).

Figure 4.12. Robo2 receptors that promote midline crossing suppress *comm* mutants.
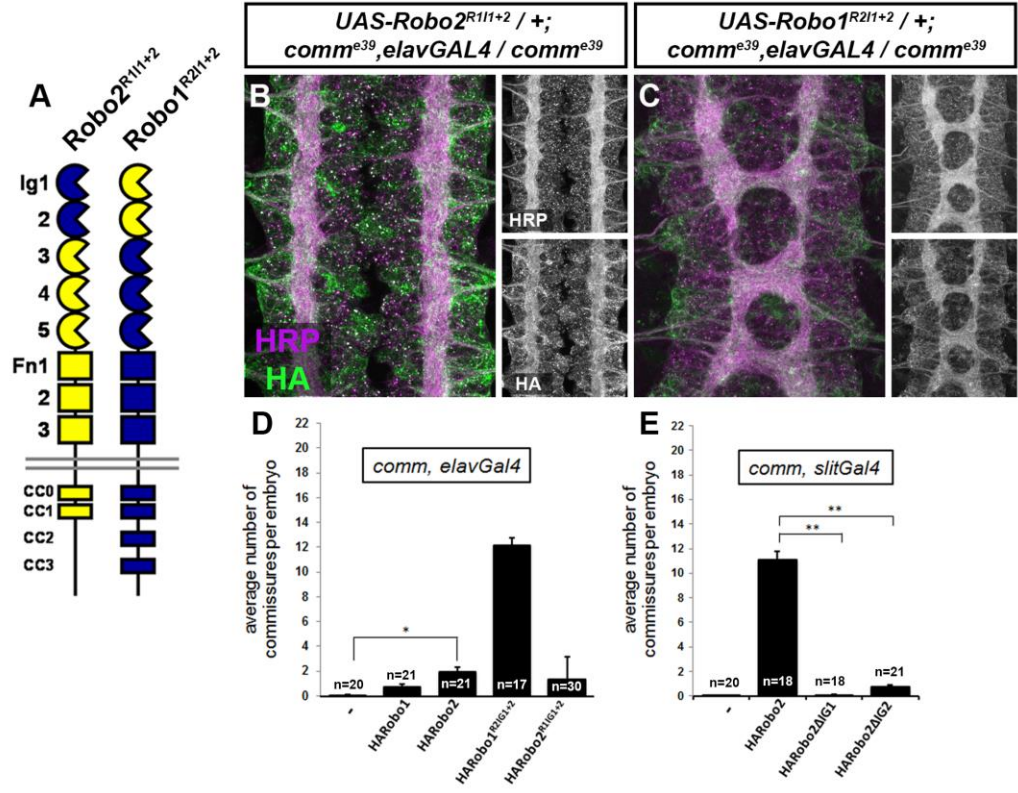
Figure 4.12. Robo2 receptors that promote midline crossing suppress *comm* mutants.

A: Schematic diagram of the two chimeric receptors shown in (**B**) and (**C**). Robo1 sequences are depicted in blue and Robo2 sequences are depicted in yellow. **B, C**: Stage 16 embryos of the indicated genotype stained with anti-HRP to visualize CNS axons and anti-HA to visualize the epitope tagged chimeric receptor. Single channel images of HRP and HA are presented to the right of the color panels. Expression of the HA-Robo2$^{R1Ig1-2}$ chimeric receptor in a *comm* mutant background (**B**) does not restore commissure formation, while expression of the reciprocal HA-Robo1$^{R2Ig1+2}$ chimeric receptor (**C**) strongly suppresses the *comm* mutant phenotype. D, E: Quantification of the average number of commissures per embryo in *comm* mutants expressing the indicated HA-tagged receptor transgenes in either all neurons using *elav-GAL4* (**D**) or in midline cells using *slit-GAL4* (**E**). Significance was assessed by one-way ANOVA followed by multiple comparisons using the Student's t-test and a Bonferroni correction (*p<0.0001) (**p<1.0 e-10). Error bars represent s.e.m. *n*, number of embryos scored for each genotype. (Experiments performed by G.J.B.)

Figure 4.13. Robo2 binds to the Robo1 receptor *in vitro* and *in vivo*.
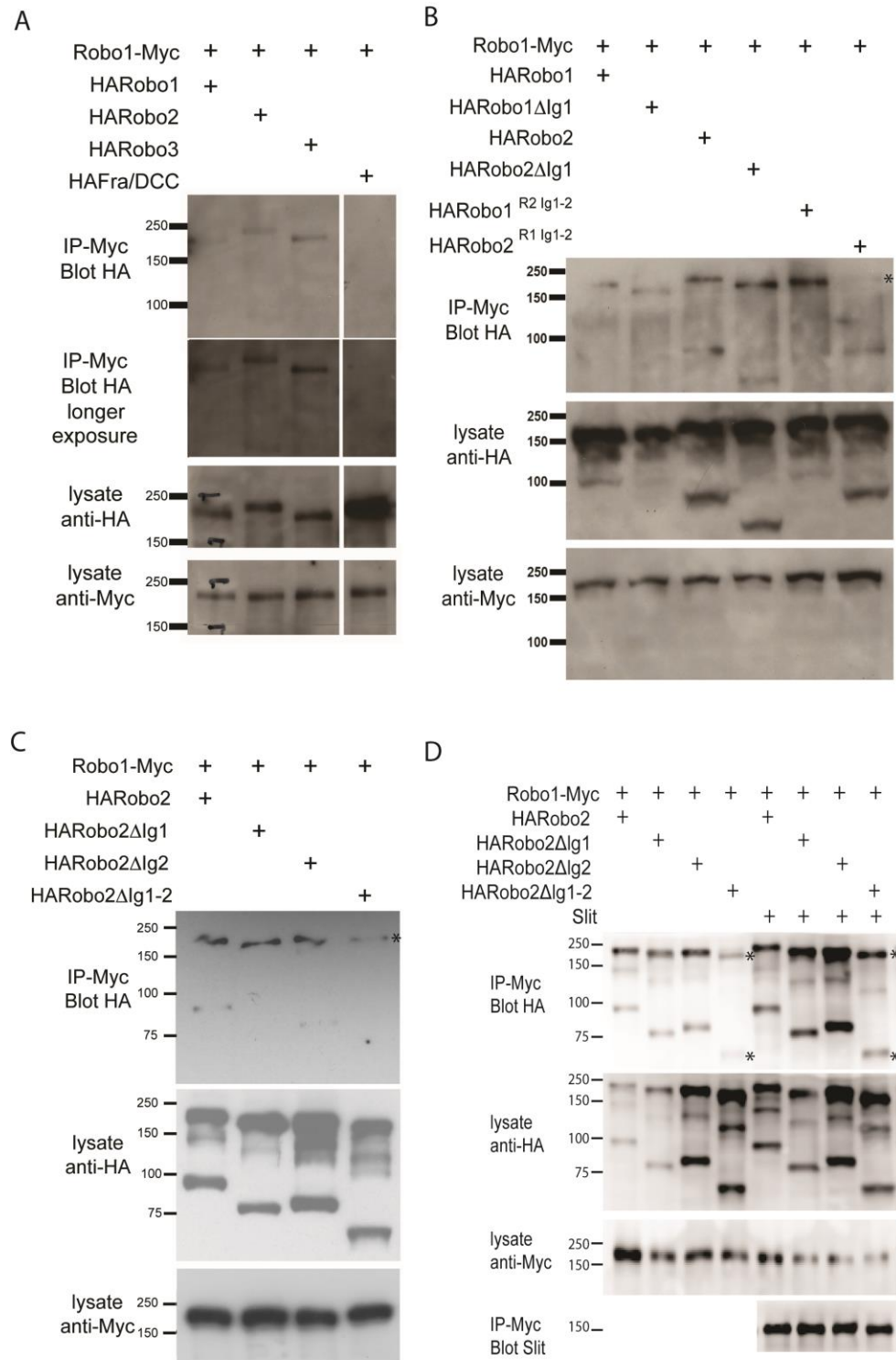
Figure 4.13. Robo2 binds to the Robo1 receptor *in vitro* and *in vivo*.

A-C: Protein extracts from embryos expressing Robo1-Myc and various HA-tagged receptors in all neurons were immunoprecipitated with anti-Myc antibodies and analyzed by western blot. Immunoprecipitates were probed with anti-HA (top blots) and total lysates were compared for HA expression and Myc expression to ensure that equal inputs were analyzed. Representative western blots from multiple experiments are shown. **A**: Robo1-Myc binds to HARobo1, HARobo2 and HARobo3, but not to a HA-tagged Fra receptor (two exposures are shown). Total lysate blots reveal comparable loading with the exception of the Fra negative control in which there is substantially more HA-tagged receptor. **B**: Robo1-Myc binds efficiently to HARobo2, HARobo2ΔIg1 and the HARobo1Robo2 (IG1-2) chimera, but not to the reciprocal chimera that has Ig1 and Ig2 domains from Robo1 (asterisk). **C**: Deletion of either Robo2 Ig1 or Ig2 alone does not affect Robo1 binding, while deleting both domains results in reduced binding (asterisk). **D**: Cell lysates of S2R+ cells separately transfected for Robo1-Myc or HA-tagged Robo2 variants were mixed, immunoprecipitated with anti-Myc, and analyzed by western blot. Robo1-Myc binds efficiently to HARobo2, HARobo2ΔIg1, and HARobo2ΔIg2, and less well to HARobo2ΔIg1+2 (asterisks). In lanes 1-4, cells were untreated; in lanes 5-8, cells were treated with Slit-conditioned media before lysing. We note that in addition to detection of the predicted full-length Robo2 receptor with anti-HA, we also routinely detect a smaller ~80kD fragment that corresponds to an extracellular domain cleavage product. The size of this fragment is shifted to predictably smaller sizes when Ig1, Ig2 or both Ig1 and Ig2 are deleted. (Experiments performed by G.J.B. and E.A.)

Figure 4.14. Robo2 binding to Robo1 does not depend on its cytoplasmic domain or on Robo1's Ig1 domain.
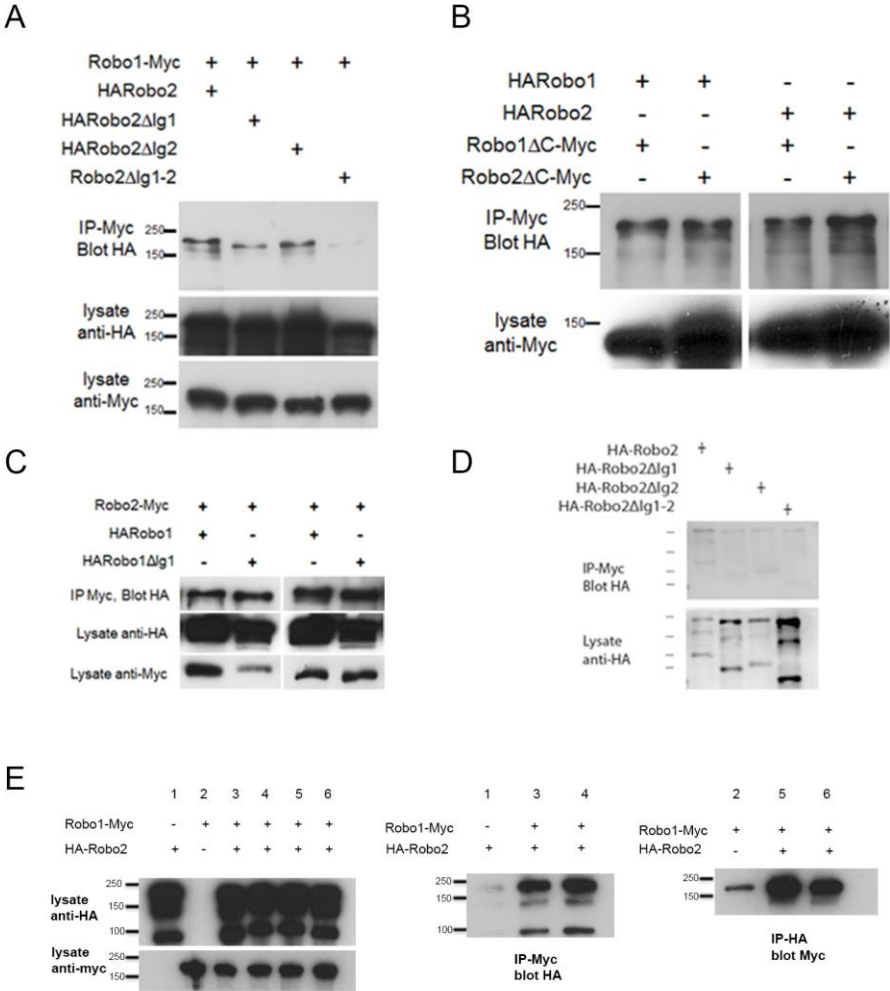
Figure 4.14. Robo2 binding to Robo1 does not depend on its cytoplasmic domain or on Robo1's Ig1 domain. **A-C:** Protein extracts from embryos expressing Robo1-Myc and various HA-tagged receptors in all neurons were immunoprecipitated with anti-Myc antibodies and analyzed by western blot. Immunoprecipitates were probed with anti-HA (top blot) and total lysates were compared for HA expression and Myc expression to ensure that equal inputs were analyzed. Representative western blots from multiple experiments are shown. **A:** Deletion of either Robo2 Ig1 or Ig2 alone does not substantially affect Robo1 binding, while deleting both domains results in reduced binding. **B:** Extracts from embryos co-expressing either HARobo1 or HARobo2, and either Robo1ΔC-Myc or Robo2ΔC-Myc were analyzed for interactions. Both of the C-terminal truncation receptor variants can efficiently pull down both HARobo1 and HARobo2 indicating that binding is independent of the cytoplasmic domain. **C:** Similar experiments to those described above and in the legend to the main Figure 11 indicate that Robo2 does not bind to the Slit-binding Ig1 region of Robo1. **D:** Lysates of S2R+ cells expressing HA-tagged Robo2 variants were mixed with lysates of untransfected cells, and immunoprecipitated with anti-Myc. Very little Robo2 protein was detected in the immunoprecipitates. **E**: S2R+ cells were co-transfected with Robo1-Myc and HA-Robo2 and immunoprecipitated with anti-Myc (middle panel) or anti-HA (right panel). A strong interaction was detected between Robo1 and Robo2 when the pull-down was performed in either direction. (Experiments in A-D were performed by G.J.B. and E.A. Experiments in E were performed by C.S.)

196

Figure 4.15. Robo2's endogenous activity in promoting midline crossing depends on Ig2.
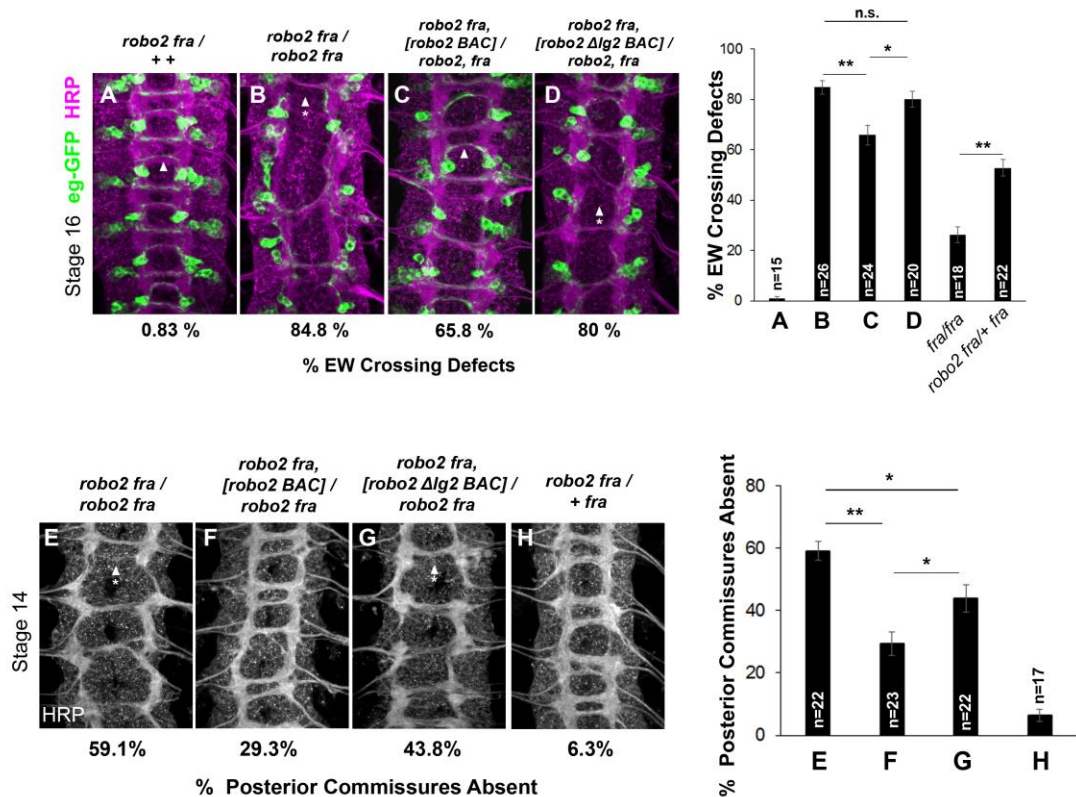
Figure 4.15. Robo2's endogenous activity in promoting midline crossing depends on Ig2.

A-D: Stage 16 embryos stained with anti-HRP (magenta) and anti-GFP (green) antibodies. Anti-GFP labels the EG and EW cell bodies and axons. Arrowheads indicate EW axons that have crossed the midline and arrowheads with asterisks indicate non-crossing EW axons. **A**: Almost all EW axons cross the midline in *robo2, fra/+, +* double heterozygotes. **B**: EW crossing defects are observed in 85% of segments in *robo2, fra* double mutants. **C-D**: The FL Robo2 cDNA BAC transgene (**C**) significantly rescues EW crossing, to 66% of segments with defects (Student's t-test, **p<0.001) whereas the Robo2ΔIG2 transgene (**D**) does not significantly rescue. Right: Removing one copy of *robo2* significantly enhances midline crossing defects in *fra* mutants. **E-H**: Stage 14 embryos of the indicated genotypes stained with anti-HRP. Posterior commissures were scored in abdominal segments A1-A8. Missing posterior commissures are indicated by arrowheads with asterisks. **E-G**: The posterior commissure defects of *robo2, fra* double mutants are significantly rescued by a full-length (FL) Robo2 cDNA BAC transgene (Student's t-test, **p<0.001) (**F**), as well as by a Robo2ΔIG2 BAC (*p<0.05) (**G**). The Robo2ΔIG2 BAC does not rescue as well as FL Robo2 (p*<0.05). All embryos were scored blind to genotype. Significance was assessed by one-way ANOVA followed by multiple comparisons using the Student's t-test and a Bonferroni correction. Error bars represent s.e.m. *n*, number of embryos scored for each genotype. (Experiments were performed by C.S.)

Figure 4.16. Model for Robo2 inhibition of Slit-Robo repulsion.

Model for Robo2 inhibition of Slit-Robo repulsion
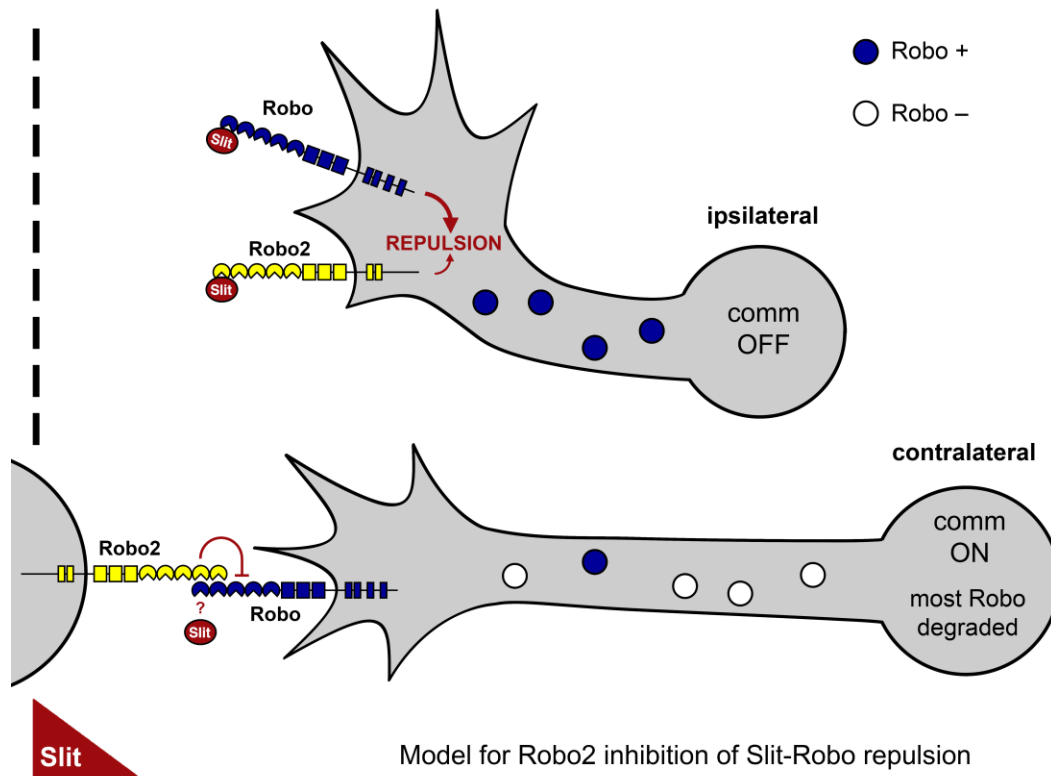
Figure 4.16. Model for Robo2 inhibition of Slit-Robo repulsion.

In contralateral neurons, the endosomal sorting receptor Comm is expressed, and it prevents the majority of Robo1 from reaching the growth cone surface. We propose that Robo2 acts non-autonomously in midline cells to bind to and inhibit the low level of Robo1 that escapes Comm-dependent sorting. This mechanism is revealed in contexts where axon attraction to the midline is limited. In ipsilateral neurons, Comm is not expressed, and Robo2 works together with Robo1 to mediate repulsion from the midline in response to Slit.

Acknowledgments

I would like to thank members of the Bashaw lab for their thoughtful comments and ideas during the development of this manuscript. We thank Dr. Barry Dickson for providing the Robo knock-in alleles. This chapter was published in the following article:

Evans, T. A., Santiago, C., Arbeille, E. and Bashaw, G. J. (2015). Robo2 acts in trans to inhibit Slit-Robo1 repulsion in pre-crossing commissural axons. *Elife* **4**, e08407.

CHAPTER 5

CONCLUSIONS AND FUTURE DIRECTIONS

My thesis research identified regulatory relationships between transcription factors and axon guidance receptors in multiple contexts in the *Drosophila* embryonic nervous system, and described a new mechanism by which the Robo2 receptor regulates midline crossing. In this chapter, I explore several directions of future research that stem from these findings.

Mechanisms by which Hb9 and Nkx6 regulate their targets in motor neurons

The mechanisms by which Hb9, Nkx6, and Islet regulate their targets remain to be determined. Our finding that Hb9's Engrailed homology domain is essential for motor axon guidance and *robo2* regulation suggests that Hb9 acts as a repressor. Similar structure-function experiments assessing the *in vivo* requirement for the identified repressor and activator domains of Nkx6 would shed insight into its mechanism in RP3 neurons (Syu et al., 2009). In addition, fusion proteins consisting of the Hb9 or Nkx6 homeodomains attached to strong repressor or activator domains can be used in rescue assays to directly test whether Hb9 and Nkx6 act as repressors or activators.

The vertebrate orthologs of Hb9 and Nkx6 act as repressors to regulate transcription factor expression in the spinal cord, and *Drosophila* Hb9 and Nkx6 act in parallel to repress the transcription factors *eve* and *vnd* in the embryo (Broihier et al., 2004; Lee et al., 2008a; Muhr et al., 2001). If Hb9 or Nkx6 are acting as repressors in motor neurons, candidate downstream transcription factors that impinge on *robo2* or

robo3 can be screened. Our preliminary data does not indicate that *eve*, *vnd*, or the

Drosophila orthologs of the vertebrate Hb9 and Nkx6 targets are the factors that regulate

robo2 or *robo3* (data not shown; see Discussion in Chapter 2). A recent microarray by

Skeath and colleagues identified dozens of additional transcription factors that are down-

regulated upon pan-neural co-expression of Hb9 and Nkx6 (Lacin et al., 2014). As a first

approach to test these candidates, *in situs* can be performed to examine their expression.

We would expect that a factor normally repressed by Hb9 and Nkx6 in the RP3 or MP1

motor neurons would be expressed at low levels in these cells in wild type embryos, and

would be de-repressed upon loss of *hb9* or *nkx6*. In addition, if Hb9 induces *robo2* in

apterous neurons by repressing an intermediate factor, this factor should be expressed at

high levels in wild type apterous neurons, and at low levels upon *hb9* gain of function.

Second, candidate transcription factors can be screened for their ability to repress *robo2*

or *robo3* when over-expressed pan-neurally. An alternative strategy would be to co-

express the candidates with Hb9 in apterous neurons, and to determine whether or not

artificial expression of the candidate suppresses the lateral shift phenotype. This approach

would have the advantage of being more high throughput than experiments assessing

gene expression, but the disadvantage of not reflecting the endogenous expression

patterns of *robo2* or *robo3*. Further genetic experiments, such as making double mutants

between *hb9* and promising candidates, would help us identify factors that act in the Hb9

pathway.

      An open-ended approach to identify downstream targets of Hb9 or Nkx6 could be

pursued by performing RNA sequencing of subsets of motor neurons isolated by

fluorescent activated cell sorting (FACS) in *hb9* or *nkx6* mutant embryos. Our lab used a

similar strategy to identify targets of Eve in dorsally-projecting motor neurons in a recently published microarray analysis (Zarin et al., 2014). Restricted labeling of MP1 neurons can be achieved by using *C544-Gal4*. dMP2, a gut-innervating *hb9+* motor neuron that requires *hb9* for expression of the insulin-like neuropeptide Ilp-7, can be specifically labeled using *dMP2-Gal4* (Miguel-Aliaga et al., 2004; Miguel-Aliaga et al., 2008). There are no identified Gal4 drivers that would selectively label the RP3 motor neurons; instead, an intersectional strategy could be used. Combining a Gal4 line and a LexA line whose expression patterns exclusively overlap in the ventrally-projecting RP motor neurons, and expressing different fluorescent proteins with each driver, would allow for double-positive cells to be sorted. I have obtained several *islet-LexA* lines for this purpose, and the analysis of their expression patterns is in progress. It would also be informative to analyze changes in gene expression shared by all cells that endogenously express Hb9, using *hb9-Gal4*. Although labor intensive, an RNA sequencing approach would allow us to identify novel downstream targets of Hb9 and Nkx6, including genes that may be important for other aspects of motor neuron identity, as discussed below.

Could Hb9 and Nkx6 be acting as activators in *Drosophila* motor neurons? A result that demonstrates this would be surprising, as Hb9 and Nkx6 proteins have only been shown to act as repressors in the nervous system (Lee et al., 2008a; Muhr et al., 2001; Nishi et al., 2015; William et al., 2003). Interestingly, *Drosophila* Nkx6 contains both activator and repressor activities that map to different residues, though these activities were not tested for function *in vivo* (Syu et al., 2009). Its mammalian ortholog Nkx6.1 binds to genes that are upregulated as well as to genes that are downregulated upon *Nkx6.1* loss of function in pancreatic beta cells (Schaffer et al., 2013; Taylor et al.,

2013). Intriguingly, neither of Hb9's putative repressor domains are required for *robo3*

expression in MP1 neurons, or for the lateral position of intermediate *hb9-Gal4+* axons.

Perhaps Hb9 and/or Nkx6 have opposing transcriptional activities that are used for

different aspects of nervous system development, as has been shown for Hox factors in

the spinal cord (Dasen et al., 2003). Demonstrating that Hb9 acts an activator *in vivo*

would have far-reaching implications, as it is a key regulator of nervous system and

pancreatic development. Homozygous mutations in MNX1, the human ortholog of Hb9,

are associated with neonatal diabetes and severe neurological defects, while heterozygous

mutations are associated with Currarino syndrome, a poorly understood disease

characterized by anorectal malformation (Bonnefond et al., 2013; Flanagan et al., 2014).

Mechanism by which Islet regulates *fra* in motor neurons

      Islet and its vertebrate orthologs act as transcriptional activators, and DAM-ID

data from *Drosophila* embryos suggest it binds directly to the *fra* locus (Tao et al., 2007,

Lee et al., 2008, Cho et al., 2014, Wolfram et al. 2014). To identify cis-regulatory regions

within *fra* that drive expression in motor neurons, transgenic lines can be made in which

putative *fra* enhancers are placed upstream of a reporter gene. I have generated several

GFP reporter lines using enhancers found within *fra*'s first intron, and while they all

drive expression in subsets of embryonic neurons, I have not identified enhancers that

drive expression in the RPs (data not shown). Once a cis-regulatory element is found to

drive expression in cells of interest, a requirement for *isl* can be tested by monitoring

reporter expression in *isl* mutants, and by mutating the predicted Islet binding sites in the

transgene. In addition, a modified version of chromatin immunoprecipitation (ChIP) can

be tried in order to enhance the signal to noise ratio of Islet binding (Agelopoulos et al., 2014). In this approach, *lacO*, the DNA binding sequence for the bacterial repressor LacI, is inserted next to the cis-regulatory region in the reporter transgene. Cell-type specific expression of an epitope-tagged lacI protein allows for efficient immunoprecipitation of chromatin from a restricted group of cells. A second round of ChIP can then be performed against the transcription factor of interest. The most rigorous demonstration that Islet directly regulates *fra* would require mutating identified Islet binding sites within *fra*'s endogenous locus using genome engineering techniques, in order to determine whether *fra* expression in RP motor neurons persists. The Crispr/Cas9 method could be used for this purpose (Xu et al., 2015).

Exploring the requirements for *Drosophila* motor neuron transcription factors in regulating neuronal identity throughout life

Hobert and colleagues coined the term 'terminal selector' to describe transcription factors that are expressed in restricted classes of post-mitotic neurons and that coordinately regulate multiple late-arising features of their differentiation, including electrophysiological properties, neurotransmitter identity, target selection, and synaptogenesis (Hobert 2016). While several examples of such transcription factors have been described in *C. elegans*, and a few in vertebrates, it remains unclear how general this regulatory strategy is (Hobert and Flames, 2009; Kratsios et al., 2012; Lodato et al., 2014). In *Drosophila* embryos, Baines et al. have shown that the intrinsic physiological properties of ventrally-projecting motor neurons are distinct from those of dorsally-projecting motor neurons, and that these properties are regulated in part by Islet and Eve

(Pym et al., 2006, Wolfram et al., 2012). Eve represses the Slowpoke ion channel and the acetylcholine receptor nAcRalpha-96Aa when over-expressed, whereas Islet endogenously regulates the intrinsic properties of ventrally-projecting motor neurons through repression of the Shaker ion channel (Pym et al., 2006; Wolfram et al., 2012). Whether these transcription factors regulate additional genes that determine functional properties of motor neurons remains unknown. RNA-sequencing approaches like those described above would allow us to identify novel targets of Hb9, Nkx6, and Islet in ventrally-projecting motor neurons, and would determine if they act as general regulators of multiple aspects of RP identity.

We have found that in addition to its previously known roles in regulating the electrical properties and the axon trajectory of ventrally-projecting motor neurons, Islet controls the targeting of their dendrites. Single cell-labeling experiments like those performed in Chapter 3 would determine whether Hb9, Nkx6, or Eve also regulate dendrite development in motor neurons, and whether the larval myotopic map is established by a group of core factors that regulate both axon and dendrite targeting. Subsets of interneurons that are pre-synaptic to the RP motor neurons are beginning to be identified, including some which can be genetically labeled, and it will be of high interest to determine whether disruptions in the molecular programs that regulate motor neuron differentiation and dendrite morphology result in defects in circuit connectivity, at both the anatomical and functional levels (Couton et al., 2015; Heckscher et al., 2015).

We do not know if the *Drosophila* motor neuron transcription factors continue to be expressed throughout larval stages, but this could readily be monitored by antibody staining. If these factors persist, knockdown experiments could be performed to

determine if they are required for the maintenance of motor neuron morphology or function. Interestingly, Landgraf and colleagues found that the dendrites of dorsally-projecting motor neurons grow throughout larval stages (Zwart et al., 2013), and an analysis of third instar larvae demonstrated that the dendrites of different classes of motor neurons are found within stereotyped medio-lateral zones that largely match those for embryonic motor neurons (Kim et al., 2009; Mauss et al., 2009). Whether motor neuron dendrites continuously require Netrin/Frazzled and Slit/Robo signaling for the selection of the appropriate medio-lateral trajectories as they grow is not known. This question could be answered by using the same single cell labeling strategy I developed to label embryonic motor neurons, combined with well-established techniques to stain larvae. Temporal control of gene knockdown could be achieved using the Gene Switch system, in which the DNA binding domain of GAL4 is fused to the activation domain of a steroid hormone receptor that requires ligand binding for activation (Osterwalder et al., 2001). *Drosophila* larvae can be fed or soaked in the ligand to allow for efficient induction of UAS target genes. Keshishian and colleagues identified approximately 50 Gene Switch Gal4 lines that are expressed in larval motor neurons; screening for lines expressed in ventrally-projecting motor neurons would allow for cell-type specific knockdown of genes using *UAS-RNAi* transgenes (Nicholson et al., 2008). If Robo or Fra receptors are required post-embryonically for dendrite position during larval stages, we could ask whether their expression in larvae requires Hb9, Nkx6 or Islet, or has become dependent on other factors. Indeed, if Hb9, Nkx6, Islet or Eve are expressed throughout larval stages, the Gene Switch system could be used to asked if they play post-embryonic roles in motor neuron maturation, function, or the maintenance of cell identity.

208

Transcriptional regulation of Robo2's pro-crossing function

Our data indicates that Robo2 acts non cell-autonomously to regulate commissural axon guidance, and that Robo2 over-expression in midline cells restores midline crossing in *robo2, fra* double mutants. Cell-type-specific over-expression of a *UAS-Robo2 RNAi* transgene in *fra* mutants would confirm that Robo2 endogenously acts in midline cells to promote midline crossing. Gal4 lines that vary in the localization and timing of their expression patterns should be tried, together with multiple *UAS-Robo2 RNAi* inserts and *Dicer2* over-expression. We do not have a Robo2 antibody, but can monitor endogenous Robo2 protein levels by using the *HA-robo2* knock-in allele.

Identifying additional upstream factors that regulate *robo2* expression in different populations of cells would help us understand how its distinct activities are regulated. The Crews lab identified dozens of transcription factors that are expressed in subsets of midline neurons and glia (Wheeler et al., 2006). Analyses of embryos mutant for these genes would allow us to determine if they regulate *robo2*. The intriguing possibility that Robo2 acts in *hb9+* or *nkx6+* cells to promote midline crossing remains unexplored. Although *robo2* expression in the RP3 neurons peaks at late stages of embryogenesis, low levels of *robo2* could be acting earlier to inhibit Robo1. An enhancement of the *fra* phenotype upon removal of *hb9* or *nkx6* might indicate that *robo2* acts in the RP neurons, or in other *hb9+* or *nkx6+* cells, to promote midline crossing, though future experiments would be necessary to rule out alternative explanations for such a result.

The identification of regulatory elements within the *robo2* locus that drive its expression in different cell types would further help us understand where *robo2* acts to promote midline crossing, and might allow for the identification of novel factors that

regulate its expression. For instance, if cis-regulatory elements that drive expression in midline cells are identified, a bioinformatic analysis using Phylocon can be carried out to identify predicted conserved transcription factor binding sites, as in (Lacin et al., 2014). These candidates could then be tested for their roles in *robo2* regulation and midline crossing. Finally, genome editing can be performed to mutate or delete different cis-regulatory elements in order to disrupt endogenous *robo2* expression in a cell-type specific manner. This would allow us to conclusively determine where *robo2* is required to exert its different activities.

Investigating the mechanism by which Robo2 promotes midline crossing

We have found that Robo2 promotes midline crossing by inhibiting Robo1-mediated repulsion in a non-cell autonomous manner, but the mechanism by which Robo2 interferes with Robo1 signaling remains to be defined. Experiments in cultured cells would determine if the presence of Robo2, either in cis or in trans, interferes with any of the known events involved in Robo1 signaling. These include Robo1 cleavage by the metalloprotease Kuzbanian/ADAM10 (Kuz); Robo1 internalization and association with early endosomal markers; Robo1's interaction with the adaptor protein Dock; re-localization of the downstream effector Sos to the membrane; and activation of the small GTPase Rac (Chance and Bashaw, 2015; Coleman et al., 2010; Fan et al., 2003; Yang and Bashaw, 2006). Preliminary data do not indicate that Robo2 interferes with Robo1's ability to bind Slit, as determined by the S2R+ cell overlay assay (Tim Evans, personal communication). In addition, surface plasmon resonance experiments using purified Robo Ig domains demonstrate that Robo1 binds to its recognition site on Slit with higher

affinity than Robo2 does (Evans and Bashaw, 2010b). Similar biochemical experiments would allow us to more quantitatively assess whether Robo2 interferes with the Robo1-Slit interaction in an Ig2-dependent manner, and to further characterize the interaction between Robo1 and Robo2, by determining if it is direct and by identifying the regions of Robo1 that mediate it.

We observe cleavage of the Robo2 receptor to produce stable ectodomain fragments both *in vitro* and *in vivo*, but it remains unknown whether Robo2 cleavage is necessary for its pro-crossing function. Interestingly, both of the ectodomain cleavage products that are detected in lysates are pulled down by Robo1, and preliminary data indicate that a secreted form of Robo2 that lacks a transmembrane domain can also interact with Robo1 in S2R+ cells (data not shown). It will be informative to make *UAS-Robo2 ecto* transgenic flies in order to test for this variant's ability to bind and inhibit Robo1 *in vivo*. If the secreted Robo2 ectodomain does not have pro-crossing activity, this could indicate that Robo2 must interact with a necessary co-factor that is only present at the surface of the cell from which it is expressed. Alternatively, we may find that Robo2 shedding enhances its ability to bind and inhibit Robo1. Preliminary data indicates that Robo2 is cleaved by the Kuz metalloprotease *in vitro* (Rebecca Chance, personal communication). It will be important to confirm that Kuz also cleaves Robo2 *in vivo*, and to try to make an uncleavable version of Robo2, for instance by using a similar strategy as was used to make uncleavable Robo1, another substrate of Kuz (Coleman et al., 2010). A better understanding of the form of Robo2 that promotes midline crossing would further explain how Robo2's opposing activities are so tightly controlled in space and time.

Concluding Remarks

It is well-established that individual axon guidance receptors have evolved to perform many different functions in the developing animal. Indeed, *Drosophila* Robo2 might be an extreme example of such a multi-purpose receptor, as it has at least four distinct functions in the embryonic nervous system in addition to its roles in muscle and heart development (Evans, 2016; Kramer et al., 2001; Santiago-Martínez et al., 2006; Santiago-Martínez et al., 2008). It is less clear whether conserved regulatory factors act across cell types and biological processes to regulate the same target genes in different contexts.

Islet's function in regulating *fra* during both axon and dendrite development demonstrates that an individual transcription factor can control multiple aspects of morphogenesis through the same downstream effector. It remains to be seen if this strategy is conserved in other systems. In the vertebrate spinal cord, many of the cues present at the midline (Netrins, Semaphorins, Ephrins) are also found in the periphery, suggesting that their respective receptors may play multiple roles during the different stages of motor neuron differentiation (Huber et al., 2005; Kania and Jessell, 2003; Poliak et al., 2015). As the cues and receptors that regulate motor neuron dendrite positioning in the spinal cord are unknown, it remains to be determined whether vertebrate motor neuron transcription factors coordinately regulate axon and dendrite guidance through common effectors.

Hb9's ability to regulate Robo receptors is harnessed by the developing embryo in at least two distinct types of neurons, with very different effects, demonstrating how regulatory relationships can be redeployed across cell types. Could the relationships we

have described be conserved in tissues outside the nervous system? Islet and Fra are expressed in cardioblasts in the *Drosophila* embryo, and play key roles in the formation of the developing heart, though it remains to be determined whether *islet* regulates *fra* there (Boukhatmi et al., 2012; Macabenta et al., 2013; Mann et al., 2009; Tao et al., 2007; Zmojdzian and Jagla, 2013). The vertebrate orthologs of Hb9, Nkx6 and Islet are highly and specifically expressed in pancreatic cells, and are essential regulators of pancreatic development and beta cell maturation (Ahlgren et al., 1997; Harrison et al., 1999; Murtaugh and Melton, 2003; Pan et al., 2015; Schaffer et al., 2013). Intriguingly, pancreatic endocrine cells also express many cell adhesion molecules and axon guidance receptors, including Robos (Yang et al., 2013). It is exciting to speculate that the regulatory relationships we have identified in the *Drosophila* embryonic nervous system might be conserved across species and tissue types.

In summary, my thesis work identified roles for Hb9 and Islet in specifying axon and dendrite morphology through the regulation of Robo and Frazzled receptors in the *Drosophila* embryo, and described a new activity for Robo2 in promoting midline crossing. Future work investigating the mechanisms by which these transcription factors and their effectors act promise to continue to shed insight into the principles that govern nervous system development. As activity-dependent transcriptional mechanisms will continuously remodel the structure and function of a neuron during late stages of development and adulthood, it will be of high interest to determine whether regulatory relationships that are used during the hard-wired stages of embryonic development, such as those described here, are re-deployed to allow for plasticity throughout life.

213

REFERENCES

Agelopoulos, M., McKay, D. J. and Mann, R. S. (2014). cgChIP: A cell type-and gene-specific method for chromatin analysis. In *Hox Genes: Methods and Protocols*, pp. 291–306.

Ahlgren, U., Pfaff, S. L., Jessell, T. M., Edlund, T. and Edlund, H. (1997). Independent requirement for ISL1 in formation of pancreatic mesenchyme and islet cells. *Nature* **385**, 257–260.

Ahn, V. E., Chu, M. L. H., Choi, H. J., Tran, D., Abo, A. and Weis, W. I. (2011). Structural basis of Wnt signaling inhibition by Dickkopf binding to LRP5/6. *Dev. Cell* **21**, 862–873.

Allan, D. W., Park, D., St Pierre, S. E., Taghert, P. H. and Thor, S. (2005). Regulators acting in combinatorial codes also act independently in single differentiating neurons. *Neuron* **45**, 689–700.

Allen, J. and Chilton, J. K. (2009). The specific targeting of guidance receptors within neurons: Who directs the directors? *Dev. Biol.* **327**, 4–11.

Appel, B., Korzh, V., Glasgow, E., Thor, S., Edlund, T., Dawid, I. B. and Eisen, J. S. (1995). Motoneuron fate specification revealed by patterned LIM homeobox gene expression in embryonic zebrafish. *Development* **121**, 4117–25.

Arber, S., Han, B., Mendelsohn, M., Smith, M., Jessell, T. M. and Sockanathan, S. (1999). Requirement for the homeobox gene Hb9 in the consolidation of motor neuron identity. *Neuron* **23**, 659–74.

Baek, M., Enriquez, J. and Mann, R. S. (2013). Dual role for Hox genes and Hox co-factors in conferring leg motoneuron survival and identity in Drosophila. *Development* **140**, 2027–38.

Bai, G. and Pfaff, S. L. (2011). Protease Regulation: The Yin and Yang of Neural Development and Disease. *Neuron* **72**, 9–21.

Bashaw, G. J., Kidd, T., Murray, D., Pawson, T. and Goodman, C. S. (2000). Repulsive axon guidance: Abelson and Enabled play opposing roles downstream of the roundabout receptor. *Cell* **101**, 703–15.

Baumgardt, M., Miguel-Aliaga, I., Karlsson, D., Ekman, H. and Thor, S. (2007). Specification of neuronal identities by feedforward combinatorial coding. *PLoS Biol.* **5**, e37.

Bonanomi, D., Chivatakarn, O., Bai, G., Abdesselem, H., Lettieri, K., Marquardt, T., Pierchala, B. A. and Pfaff, S. L. (2012). Ret is a multifunctional coreceptor that integrates diffusible- and contact-axon guidance signals. *Cell* **148**, 568–82.

Bonnefond, A., Vaillant, E., Philippe, J., Skrobek, B., Lobbens, S., Yengo, L., Huyvaert, M., Cavé, H., Busiah, K., Scharfmann, R., et al. (2013). Transcription factor gene MNX1 is a novel cause of permanent neonatal diabetes in a consanguineous family. *Diabetes Metab.* **39**, 276–280.

Boukhatmi, H., Frendo, J. L., Enriquez, J., Crozatier, M., Dubois, L. and Vincent, a. (2012). Tup/Islet1 integrates time and position to specify muscle identity in Drosophila. *Development* **139**, 3572–3582.

Brankatschk, M. and Dickson, B. J. (2006). Netrins guide Drosophila commissural axons at short range. *Nat. Neurosci.* **9**, 188–194.

Bravo-Ambrosio, A., Mastick, G. and Kaprielian, Z. (2012). Motor axon exit from the mammalian spinal cord is controlled by the homeodomain protein Nkx2.9 via Robo-Slit signaling. *Development* **139**, 1435–46.

Brierley, D. J., Blanc, E., Reddy, O. V., VijayRaghavan, K. and Williams, D. W. (2009). Dendritic targeting in the leg neuropil of Drosophila: The role of midline signalling molecules in generating a myotopic map. *PLoS Biol.* **7**, e1000199.

Broihier, H. T. and Skeath, J. B. (2002). Drosophila homeodomain protein dHb9 directs neuronal fate via crossrepressive and cell-nonautonomous mechanisms. *Neuron* **35**, 39–50.

Broihier, H. T., Kuzin, A., Zhu, Y., Odenwald, W. and Skeath, J. B. (2004). Drosophila homeodomain protein Nkx6 coordinates motoneuron subtype identity and axonogenesis. *Development* **131**, 5233–42.

Brose, K. and Tessier-Lavigne, M. (2000). Slit proteins: Key regulators of axon guidance, axonal branching, and cell migration. *Curr. Opin. Neurobiol.* **10**, 95–102.

Brose, K., Bland, K., Wang, K., Arnott, D., Henzel, W., Goodman, C. S., Tessier-Lavigne, M. and Kidd, T. (1999). Slit proteins bind Robo receptors and have an evolutionarily conserved role in repulsive axon guidance. *Cell* **96**, 795–806.

Catela, C., Shin, M. M. and Dasen, J. S. (2015). Assembly and Function of Spinal Circuits for Motor Control. *Annu. Rev. Cell Dev. Biol* **31**, 669–98.

Catela, C., Shin, M. M., Lee, D. H., Liu, J. P. and Dasen, J. S. (2016). Hox Proteins Coordinate Motor Neuron Differentiation and Connectivity Programs through Ret/Gfra Genes. *Cell Rep.* **14**, 1901–1915.

Certel, S. J. and Thor, S. (2004). Specification of Drosophila motoneuron identity by the combinatorial action of POU and LIM-HD factors. *Development* **131**, 5429–39.

Chance, R. K. and Bashaw, G. J. (2015). Slit-Dependent Endocytic Trafficking of the Robo Receptor Is Required for Son of Sevenless Recruitment and Midline Axon Repulsion. *PLoS Genet.* **11**, e1005402.

Chatzigeorgiou, M., Yoo, S., Watson, J. D., Lee, W.-H., Spencer, W. C., Kindt, K. S., Hwang, S. W., Miller, D. M., Treinin, M., Driscoll, M., et al. (2010). Specific roles for DEG/ENaC and TRP channels in touch and thermosensation in C. elegans nociceptors. *Nat. Neurosci.* **13**, 861–8.

Chédotal, A. and Rijli, F. M. (2009). Transcriptional regulation of tangential neuronal migration in the developing forebrain. *Curr. Opin. Neurobiol.* **19**, 139–45.

Chen, Z., Gore, B. B., Long, H., Ma, L. and Tessier-Lavigne, M. (2008). Alternative splicing of the Robo3 axon guidance receptor governs the midline switch from attraction to repulsion. *Neuron* **58**, 325–32.

Chen, S., Bubeck, D., MacDonald, B. T., Liang, W. X., Mao, J. H., Malinauskas, T., Llorca, O., Aricescu, A. R., Siebold, C., He, X., et al. (2011). Structural and functional studies of LRP6 ectodomain reveal a platform for Wnt signaling. *Dev. Cell* **21**, 848–861.

Cho, H.-H., Cargnin, F., Kim, Y., Lee, B., Kwon, R.-J., Nam, H., Shen, R., Barnes, A. P., Lee, J. W., Lee, S., et al. (2014). Isl1 directly controls a cholinergic neuronal identity in the developing forebrain and spinal cord by forming cell type-specific complexes. *PLoS Genet.* **10**, e1004280.

Coleman, H. a, Labrador, J.-P., Chance, R. K. and Bashaw, G. J. (2010). The Adam family metalloprotease Kuzbanian regulates the cleavage of the roundabout receptor to control axon repulsion at the midline. *Development* **137**, 2417–2426.

Coonan, J. R., Bartlett, P. F. and Galea, M. P. (2003). Role of EphA4 in defining the position of a motoneuron pool within the spinal cord. *J. Comp. Neurol.* **458**, 98–111.

Corty, M. M., Matthews, B. J. and Grueber, W. B. (2009). Molecules and mechanisms of dendrite development in Drosophila. *Development* **136**, 1049–61.

Couton, L., Mauss, A. S., Yunusov, T., Diegelmann, S., Evers, J. F. and Landgraf, M. (2015). Development of connectivity in a motoneuronal network in Drosophila larvae. *Curr. Biol.* **25**, 568–576.

Crowner, D., Madden, K., Goeke, S. and Giniger, E. (2002). Lola regulates midline crossing of CNS axons in Drosophila. *Development* **129**, 1317–25.

Crozatier, M. and Vincent, A. (2008). Control of multidendritic neuron differentiation in Drosophila: the role of Collier. *Dev. Biol.* **315**, 232–42.

Dalla Torre di Sanguinetto, S. A., Dasen, J. S. and Arber, S. (2008). Transcriptional mechanisms controlling motor neuron diversity and connectivity. *Curr. Opin. Neurobiol.* **18**, 36–43.

Dasen, J. S. (2009). *Transcriptional networks in the early development of sensory-motor circuits.* 1st ed. Elsevier Inc.

Dasen, J. S., Liu, J.-P. and Jessell, T. M. (2003). Motor neuron columnar fate imposed by sequential phases of Hox-c activity. *Nature* **425**, 926–933.

De Marco Garcia, N. V and Jessell, T. M. (2008). Early motor neuron pool identity and muscle nerve trajectory defined by postmitotic restrictions in Nkx6.1 activity. *Neuron* **57**, 217–31.

Del Álamo, D., Rouault, H. and Schweisguth, F. (2011). Mechanism and significance of cis-inhibition in notch signalling. *Curr. Biol.* **21**, 40–47.

Dickson, B. J. and Zou, Y. (2010). Navigating intermediate targets: the nervous system midline. *Cold Spring Harb. Perspect. Biol.* **2**, 1–16.

Dillon, A. K., Fujita, S. C., Matise, M. P., Jarjour, A. A., Kennedy, T. E., Kollmus, H., Arnold, H.-H., Weiner, J. A., Sanes, J. R. and Kaprielian, Z. (2005). Molecular control of spinal accessory motor neuron/axon development in the mouse spinal cord. *J. Neurosci.* **25**, 10119–30.

Ding, Q., Joshi, P. S., Xie, Z., Xiang, M. and Gan, L. (2011). BARHL2 transcription factor regulates the ipsilateral / contralateral subtype divergence in postmitotic dI1 neurons of the developing spinal cord. *Proc. Natl. Acad. Sci. U. S. A.* **109**, 1566–1571.

Dong, X., Liu, O. W., Howell, A. S. and Shen, K. (2013). An extracellular adhesion molecule complex patterns dendritic branching and morphogenesis. *Cell* **155**, 296–307.

Dottori, M., Hartley, L., Galea, M., Paxinos, G., Polizzotto, M., Kilpatrick, T., Bartlett, P. F., Murphy, M., Köntgen, F. and Boyd, A. W. (1998). EphA4 (Sek1) receptor tyrosine kinase is required for the development of the corticospinal tract. *Proc. Natl. Acad. Sci. U. S. A.* **95**, 13248–53.

Dudanova, I., Kao, T.-J., Herrmann, J. E., Zheng, B., Kania, A. and Klein, R. (2012). Genetic evidence for a contribution of EphA:ephrinA reverse signaling to motor axon guidance. *J. Neurosci.* **32**, 5209–15.

Eade, K. T., Fancher, H. A., Ridyard, M. S. and Allan, D. W. (2012). Developmental transcriptional networks are required to maintain neuronal subtype identity in the mature nervous system. *PLoS Genet.* **8**, e1002501.

Eastman, C., Horvitz, H. R. and Jin, Y. (1999). Coordinated transcriptional regulation of the unc-25 glutamic acid decarboxylase and the unc-47 GABA vesicular transporter by the Caenorhabditis elegans UNC-30 homeodomain protein. *J. Neurosci.* **19**, 6225–6234.

Eberhart, J., Swartz, M. E., Koblar, S. A., Pasquale, E. B. and Krull, C. E. (2002). EphA4 constitutes a population-specific guidance cue for motor neurons. *Dev. Biol.* **247**, 89–101.

Enriquez, J., Venkatasubramanian, L., Baek, M., Peterson, M., Aghayeva, U. and Mann, R. S. (2015). Specification of Individual Adult Motor Neuron Morphologies by Combinatorial Transcription Factor Codes. *Neuron* **86**, 955–970.

Escalante, A., Murillo, B., Morenilla-Palao, C., Klar, A. and Herrera, E. (2013). Zic2-Dependent Axon Midline Avoidance Controls the Formation of Major Ipsilateral Tracts in the CNS. *Neuron* **80**, 1392–1406.

Evans, T. A. (2016). Embryonic axon guidance : insights from Drosophila and other insects. *Curr. Opin. Insect Sci.* **18**, 11–16.

Evans, T. A. and Bashaw, G. J. (2010a). Axon guidance at the midline: of mice and flies. *Curr. Opin. Neurobiol.* **20**, 79–85.

Evans, T. A. and Bashaw, G. J. (2010b). Functional diversity of Robo receptor immunoglobulin domains promotes distinct axon guidance decisions. *Curr. Biol.* **20**, 567–72.

Evans, T. A. and Bashaw, G. J. (2012). Slit/Robo-mediated axon guidance in Tribolium and Drosophila: Divergent genetic programs build insect nervous systems. *Dev. Biol.* **363**, 266–278.

Evans, T. A., Santiago, C., Arbeille, E. and Bashaw, G. J. (2015). Robo2 acts in trans to inhibit Slit-Robo1 repulsion in pre-crossing commissural axons. *Elife* **4**, e08407.

Fambrough, D. and Goodman, C. S. (1996). The Drosophila beaten path gene encodes a novel secreted protein that regulates defasciculation at motor axon choice points. *Cell* **87**, 1049–58.

Fan, X., Labrador, J. P., Hing, H. and Bashaw, G. J. (2003). Slit stimulation recruits Dock and Pak to the roundabout receptor and increases Rac activity to regulate axon repulsion at the CNS midline. *Neuron* **40**, 113–27.

Ferreira, T., Ou, Y., Li, S., Giniger, E. and van Meyel, D. J. (2014). Dendrite architecture organized by transcriptional control of the F-actin nucleator Spire. *Development* **141**, 650–660.

Flanagan, S. E., De Franco, E., Lango Allen, H., Zerah, M., Abdul-Rasoul, M. M., Edge, J. A., Stewart, H., Alamiri, E., Hussain, K., Wallis, S., et al. (2014). Analysis of transcription factors key for mouse pancreatic development establishes NKX2-2 and MNX1 mutations as causes of neonatal diabetes in man. *Cell Metab.* **19**, 146–154.

Fujioka, M., Lear, B. C., Landgraf, M., Yusibova, G. L., Zhou, J., Riley, K. M., Patel, N. H. and Jaynes, J. B. (2003). Even-skipped, acting as a repressor, regulates axonal projections in Drosophila. *Development* **130**, 5385–400.

Fukuhara, N., Howitt, J. A., Hussain, S. A. and Hohenester, E. (2008). Structural and

functional analysis of slit and heparin binding to immunoglobulin-like domains 1 and 2 of Drosophila robo. *J. Biol. Chem.* **283**, 16226–16234.

Furrer, M.-P., Kim, S., Wolf, B. and Chiba, A. (2003). Robo and Frazzled/DCC mediate dendritic guidance at the CNS midline. *Nature* **6**, 223–230.

Furrer, M.-P., Vasenkova, I., Kamiyama, D., Rosado, Y. and Chiba, A. (2007). Slit and Robo control the development of dendrites in Drosophila CNS. *Development* **134**, 3795–3804.

Garces, A. and Thor, S. (2006). Specification of Drosophila aCC motoneuron identity by a genetic cascade involving even-skipped, grain and zfh1. *Development* **133**, 1445–55.

García-Frigola, C. and Herrera, E. (2010). Zic2 regulates the expression of Sert to modulate eye-specific refinement at the visual targets. *EMBO J.* **29**, 3170–83.

García-Frigola, C., Carreres, M. I., Vegar, C., Mason, C. and Herrera, E. (2008). Zic2 promotes axonal divergence at the optic chiasm midline by EphB1-dependent and -independent mechanisms. *Development* **135**, 1833–41.

Ghiglione, C., Amundadottir, L., Andresdottir, M., Bilder, D., Diamonti, J. a, Noselli, S., Perrimon, N. and Carraway III, K. L. (2003). Mechanism of inhibition of the Drosophila and mammalian EGF receptors by the transmembrane protein Kekkon 1. *Development* **130**, 4483–4493.

Gilestro, G. F. (2008). Redundant mechanisms for regulation of midline crossing in Drosophila. *PLoS One* **3**, e3798.

Grueber, W. B., Jan, L. Y. and Jan, Y. N. (2002). Tiling of the Drosophila epidermis by multidendritic sensory neurons. *Development* **129**, 2867–78.

Grueber, W. B., Jan, L. Y. and Jan, Y. N. (2003a). Different Levels of the Homeodomain Protein Cut Regulate Distinct Dendrite Branching Patterns of Drosophila Multidendritic Neurons. *Cell* **112**, 805–818.

Grueber, W. B., Ye, B., Moore, A. W., Jan, L. Y. and Jan, Y. N. (2003b). Dendrites of distinct classes of Drosophila sensory neurons show different capacities for homotypic repulsion. *Curr. Biol.* **13**, 618–626.

Harrison, K. A., Thaler, J., Pfaff, S. L., Gu, H. and Kehrl, J. H. (1999). Pancreas dorsal lobe agenesis and abnormal islets of Langerhans in Hlxb9-deficient mice. *Nat. Genet.* **23**, 71–75.

Hattori, Y., Sugimura, K. and Uemura, T. (2007). Selective expression of Knot/Collier, a transcriptional regulator of the EBF/Olf-1 family, endows the Drosophila sensory system with neuronal class-specific elaborated dendritic patterns. *Genes Cells* **12**, 1011–22.

Hattori, Y., Usui, T., Satoh, D., Moriyama, S., Shimono, K., Itoh, T., Shirahige, K. and Uemura, T. (2013). Sensory-neuron subtype-specific transcriptional programs controlling dendrite morphogenesis: genome-wide analysis of Abrupt and Knot/Collier. *Dev. Cell* **27**, 530–44.

He, S., Philbrook, A., McWhirter, R., Gabel, C. V., Taub, D. G., Carter, M. H., Hanna, I. M., Francis, M. M. and Miller, D. M. (2015). Transcriptional control of synaptic remodeling through regulated expression of an immunoglobulin superfamily protein. *Curr. Biol.* **25**, 2541–2548.

Heckscher, E. S., Zarin, A. A., Faumont, S., Clark, M. Q., Manning, L., Fushiki, A., Schneider-Mizell, C. M., Fetter, R. D., Truman, J. W., Zwart, M. F., et al. (2015). Even-Skipped+ Interneurons Are Core Components of a Sensorimotor Circuit that Maintains Left-Right Symmetric Muscle Contraction Amplitude. *Neuron* **88**, 314–329.

Helmbacher, F., Schneider-Maunoury, S., Topilko, P., Tiret, L. and Charnay, P. (2000). Targeting of the EphA4 tyrosine kinase receptor affects dorsal/ventral pathfinding of limb motor axons. *Development* **127**, 3313–24.

Herrera, E., Brown, L., Aruga, J., Rachel, R. A., Dolen, G., Mikoshiba, K., Brown, S. and Mason, C. a (2003). Zic2 patterns binocular vision by specifying the uncrossed retinal projection. *Cell* **114**, 545–57.

Hidalgo, A. and Brand, A. H. (1997). Targeted neuronal ablation : the role of pioneer neurons in guidance and fasciculation in the CNS of Drosophila. *Development* **124**, 3253–3262.

Hobert, O. (2011). Regulation of terminal differentiation programs in the nervous system. *Annu. Rev. Cell Dev. Biol.* **27**, 681–96.

Hobert, O. (2015). *Terminal Selectors of Neuronal Identity*. 1st ed. Elsevier Inc.

Hobert, O. and Flames, N. (2009). Gene regulatory logic of dopaminergic neuron differentiation. *Nature* **458**, 885–889.

Hong, W., Mosca, T. J. and Luo, L. (2012). Teneurins instruct synaptic partner matching in an olfactory map. *Nature* **484**, 201–7.

Hörnberg, H. and Holt, C. (2013). RNA-binding proteins and translational regulation in axons and growth cones. *Front. Neurosci.* **7**, 1–9.

Howell, K., White, J. G. and Hobert, O. (2015). Spatiotemporal control of a novel synaptic organizer molecule. *Nature* **523**, 83–87.

Howitt, J. A., Clout, N. J. and Hohenester, E. (2004). Binding site for Robo receptors revealed by dissection of the leucine-rich repeat region of Slit. *EMBO J.* **23**, 4406–4412.

Huang, Z., Yazdani, U., Thompson-peer, K. L., Kolodkin, A. L. and Terman, J. R. (2007). Crk-associated substrate (Cas) signaling protein functions with integrins to specify axon guidance during development. *Development* **134**, 2337–2347.

Huber, A. B., Kania, A., Tran, T. S., Gu, C., De Marco Garcia, N., Lieberam, I., Johnson, D., Jessell, T. M., Ginty, D. D. and Kolodkin, A. L. (2005). Distinct roles for secreted semaphorin signaling in spinal motor axon guidance. *Neuron* **48**, 949–64.

Huberman, A. D., Clandinin, T. R. and Baier, H. (2010). Molecular and cellular mechanisms of lamina-specific axon targeting. *Cold Spring Harb. Perspect. Biol.* **2**, a001743.

Hughes, C. L. and Thomas, J. B. (2007). A sensory feedback circuit coordinates muscle activity in Drosophila. *Mol. Cell. Neurosci.* **35**, 383–96.

Hwang, R. Y., Zhong, L., Xu, Y., Johnson, T., Zhang, F., Deisseroth, K. and Tracey, W. D. (2007). Nociceptive neurons protect Drosophila larvae from parasitoid wasps. *Curr. Biol.* **17**, 2105–16.

Inamata, Y. and Shirasaki, R. (2014). Dbx1 triggers crucial molecular programs required for midline crossing by midbrain commissural axons. *Development* **141**, 1260–71.

Iyer, S. C., Wang, D., Iyer, E. P. R., Trunnell, S. A., Meduri, R., Shinwari, R., Sulkowski, M. J. and Cox, D. N. (2012). The RhoGEF trio functions in sculpting class specific dendrite morphogenesis in Drosophila sensory neurons. *PLoS One* **7**, e33634.

Jan, Y.-N. and Jan, L. Y. (2010). Branching out: mechanisms of dendritic arborization. *Nat. Rev. Neurosci.* **11**, 316–28.

Jaworski, A. and Tessier-Lavigne, M. (2012). Autocrine/juxtaparacrine regulation of axon fasciculation by Slit-Robo signaling. *Nat. Neurosci.* **15**, 367–9.

Jaworski, A., Long, H. and Tessier-Lavigne, M. (2010). Collaborative and specialized functions of Robo1 and Robo2 in spinal commissural axon guidance. *J. Neurosci.* **30**, 9445–53.

Jinushi-Nakao, S., Arvind, R., Amikura, R., Kinameri, E., Liu, A. W. and Moore, A. W. (2007). Knot/Collier and Cut control different aspects of dendrite cytoskeleton and synergize to define final arbor shape. *Neuron* **56**, 963–78.

Kania, A. and Jessell, T. M. (2003). Topographic motor projections in the limb imposed by LIM homeodomain protein regulation of ephrin-A:EphA interactions. *Neuron* **38**, 581–96.

Kania, A., Johnson, R. L. and Jessell, T. M. (2000). Coordinate roles for LIM

homeobox genes in directing the dorsoventral trajectory of motor axons in the vertebrate limb. *Cell* **102**, 161–73.

Kao, T.-J. and Kania, A. (2011). Ephrin-mediated cis-attenuation of Eph receptor signaling is essential for spinal motor axon guidance. *Neuron* **71**, 76–91.

Kastenhuber, E., Kern, U., Bonkowsky, J. L., Chien, C.-B., Driever, W. and Schweitzer, J. (2009). Netrin-DCC, Robo-Slit, and heparan sulfate proteoglycans coordinate lateral positioning of longitudinal dopaminergic diencephalospinal axons. *J. Neurosci.* **29**, 8914–26.

Keleman, K., Rajagopalan, S., Cleppien, D., Teis, D., Paiha, K., Huber, L. A., Technau, G. M. and Dickson, B. J. (2002). Comm sorts robo to control axon guidance at the Drosophila midline. *Cell* **110**, 415–27.

Keleman, K., Ribeiro, C. and Dickson, B. J. (2005). Comm function in commissural axon guidance: cell-autonomous sorting of Robo in vivo. *Nat. Neurosci.* **8**, 156–163.

Kidd, T., Brose, K., Mitchell, K. J., Fetter, R. D., Tessier-lavigne, M., Goodman, C. S. and Tear, G. (1998a). Roundabout controls axon crossing of the CNS midline and defines a novel subfamily of evolutionarily conserved guidance receptors. *Cell* **92**, 205–215.

Kidd, T., Russell, C., Goodman, C. S. and Tear, G. (1998b). Dosage-sensitive and complementary functions of roundabout and commissureless control axon crossing of the CNS midline. *Neuron* **20**, 25–33.

Kidd, T., Bland, K. S. and Goodman, C. S. (1999). Slit is the midline repellent for the robo receptor in Drosophila. *Cell* **96**, 785–94.

Kim, S. and Chiba, A. (2004). Dendritic guidance. *Trends Neurosci.* **27**, 194–202.

Kim, M. D., Wen, Y. and Jan, Y. N. (2009). Patterning and organization of motor neuron dendrites in the Drosophila larva. *Dev. Biol.* **336**, 213–221.

Klein, R. (2012). Eph/ephrin signalling during development. *Development* **139**, 4105–9.

Klein, D. E., Nappi, V. M., Reeves, G. T., Shvartsman, S. Y. and Lemmon, M. A. (2004). Argos inhibits epidermal growth factor receptor signalling by ligand sequestration. *Nature* **430**, 1040–1044.

Klein, D. E., Stayrook, S. E., Shi, F., Narayan, K. and Lemmon, M. A. (2008). Structural basis for EGFR ligand sequestration by Argos. *Nature* **453**, 1271–5.

Kolodkin, A. L. and Tessier-Lavigne, M. (2011). Mechanisms and molecules of neuronal wiring: a primer. *Cold Spring Harb. Perspect. Biol.* **3**,.

Kolodziej, P. A., Timpe, L. C., Mitchell, K. J., Fried, S. R., Goodman, C. S., Jan, L.

Y. and Jan, Y. N. (1996). frazzled Encodes a Drosophila member of the DCC immunoglobulin subfamily and is required for CNS and motor axon guidance. *Cell* **87**, 197–204.

Komiyama, T. and Luo, L. (2007). Intrinsic Control of Precise Dendritic Targeting by an Ensemble of Transcription Factors. *Curr. Biol.* **17**, 278–285.

Komiyama, T., Johnson, W. a, Luo, L. and Jefferis, G. S. X. E. (2003). From lineage to wiring specificity. POU domain transcription factors control precise connections of Drosophila olfactory projection neurons. *Cell* **112**, 157–67.

Kostadinov, D. and Sanes, J. R. (2015). Protocadherin-dependent dendritic selfavoidance regulates neural connectivity and circuit function. *Elife* **4**, 1–23.

Kramer, S. G., Kidd, T., Simpson, J. H. and Goodman, C. S. (2001). Switching repulsion to attraction: changing responses to slit during transition in mesoderm migration. *Science* **292**, 737–40.

Kramer, E. R., Knott, L., Su, F., Dessaud, E., Krull, C. E., Helmbacher, F. and Klein, R. (2006). Cooperation between GDNF/Ret and ephrinA/EphA4 signals for motor-axon pathway selection in the limb. *Neuron* **50**, 35–47.

Kratsios, P., Stolfi, A., Levine, M. and Hobert, O. (2012). Coordinated regulation of cholinergic motor neuron traits through a conserved terminal selector gene. *Nat. Neurosci.* **15**, 205–14.

Kratsios, P., Pinan-Lucarré, B., Kerk, S. Y., Weinreb, A., Bessereau, J. L. and Hobert, O. (2015). Transcriptional coordination of synaptogenesis and neurotransmitter signaling. *Curr. Biol.* **25**, 1282–1295.

Kraut, R. and Zinn, K. (2004). Roundabout 2 regulates migration of sensory neurons by signaling in trans. *Curr. Biol.* **14**, 1319–1329.

Krawchuk, D. and Kania, A. (2008). Identification of genes controlled by LMX1B in the developing mouse limb bud. *Dev. Dyn.* **237**, 1183–92.

Kullander, K., Croll, S. D., Zimmer, M., Pan, L., McClain, J., Hughes, V., Zabski, S., DeChiara, T. M., Klein, R., Yancopoulos, G. D., et al. (2001). Ephrin-B3 is the midline barrier that prevents corticospinal tract axons from recrossing, allowing for unilateral motor control. *Genes Dev.* **15**, 877–88.

Kullander, K., Butt, S. J. B., Lebret, J. M., Lundfald, L., Restrepo, C. E., Rydström, A., Klein, R. and Kiehn, O. (2003). Role of EphA4 and EphrinB3 in local neuronal circuits that control walking. *Science* **299**, 1889–92.

Labrador, J. P., O'keefe, D., Yoshikawa, S., McKinnon, R. D., Thomas, J. B. and Bashaw, G. J. (2005). The homeobox transcription factor even-skipped regulates netrin-receptor expression to control dorsal motor-axon projections in Drosophila.

Curr. Biol. **15**, 1413–9.

Lacin, H., Rusch, J., Yeh, R. T., Fujioka, M., Wilson, B. a, Zhu, Y., Robie, A. a, Mistry, H., Wang, T., Jaynes, J. B., et al. (2014). Genome-wide identification of Drosophila Hb9 targets reveals a pivotal role in directing the transcriptome within eight neuronal lineages, including activation of nitric oxide synthase and Fd59a/Fox-D. *Dev. Biol.* **388**, 117–33.

Landgraf, M. and Thor, S. (2006). Development and structure of motoneurons. *Int. Rev. Neurobiol.* **75**, 33–53.

Landgraf, M., Bossing, T., Technau, G. M. and Bate, M. (1997). The origin, location, and projections of the embryonic abdominal motorneurons of Drosophila. *J. Neurosci.* **17**, 9642–55.

Landgraf, M., Roy, S., Prokop, A., VijayRaghavan, K. and Bate, M. (1999). even-skipped determines the dorsal growth of motor axons in Drosophila. *Neuron* **22**, 43–52.

Landgraf, M., Jeffrey, V., Fujioka, M., Jaynes, J. B. and Bate, M. (2003). Embryonic origins of a motor system: Motor dendrites form a myotopic map in Drosophila. *PLoS Biol.* **1**, 221–230.

Layden, M. J., Odden, J. P., Schmid, A., Garces, A., Thor, S. and Doe, C. Q. (2006). Zfh1, a somatic motor neuron transcription factor, regulates axon exit from the CNS. *Dev. Biol.* **291**, 253–63.

Lee, S., Lee, B., Joshi, K., Pfaff, S. L., Lee, J. W. and Lee, S.-K. (2008a). A regulatory network to segregate the identity of neuronal subtypes. *Dev. Cell* **14**, 877–89.

Lee, R., Petros, T. J. and Mason, C. A. (2008b). Zic2 regulates retinal ganglion cell axon avoidance of ephrinB2 through inducing expression of the guidance receptor EphB1. *J. Neurosci.* **28**, 5910–9.

Lee, B., Lee, S., Agulnick, A. D., Lee, J. W. and Lee, S.-K. (2016). Ssdps are required for LIM-complexes to induce transcriptionally active chromatin and specify spinal neuronal identities. *Development* 1721–1731.

Lefebvre, J. L., Sanes, J. R. and Kay, J. N. (2015). Development of Dendritic Form and Function. *Annu. Rev. Cell Dev. Biol.* **31**, 741–77.

Li, W., Wang, F., Menut, L. and Gao, F.-B. (2004). BTB/POZ-zinc finger protein abrupt suppresses dendritic branching in a neuronal subtype-specific and dosage-dependent manner. *Neuron* **43**, 823–34.

Liu, O. W. and Shen, K. (2012). The transmembrane LRR protein DMA-1 promotes dendrite branching and growth in C. elegans. *Nat. Neurosci.* **15**, 57–63.

Liu, Q.-X., Hiramoto, M., Ueda, H., Gojobori, T., Hiromi, Y. and Hirose, S. (2009). Midline governs axon pathfinding by coordinating expression of two major guidance systems. *Genes Dev.* **23**, 1165–70.

Livet, J., Sigrist, M., Stroebel, S., De Paola, V., Price, S. R., Henderson, C. E., Jessell, T. M. and Arber, S. (2002). ETS gene Pea3 controls the central position and terminal arborization of specific motor neuron pools. *Neuron* **35**, 877–92.

Lodato, S., Molyneaux, B. J., Zuccaro, E., Goff, L. A., Chen, H.-H., Yuan, W., Meleski, A., Takahashi, E., Mahony, S., Rinn, J. L., et al. (2014). Gene co-regulation by Fezf2 selects neurotransmitter identity and connectivity of corticospinal neurons. *Nat. Neurosci.*

Long, H., Sabatier, C., Ma, L., Plump, A., Yuan, W., Ornitz, D. M., Tamada, A., Murakami, F., Goodman, C. S. and Tessier-Lavigne, M. (2004). Conserved roles for Slit and Robo proteins in midline commissural axon guidance. *Neuron* **42**, 213–23.

Luria, V., Krawchuk, D., Jessell, T. M., Laufer, E. and Kania, A. (2008). Specification of Motor Axon Trajectory by Ephrin-B : EphB Signaling : Symmetrical Control of Axonal Patterning in the Developing Limb. *Neuron* **60**, 1039–1053.

Macabenta, F. D., Jensen, A. G., Cheng, Y. S., Kramer, J. J. and Kramer, S. G. (2013). Frazzled/DCC facilitates cardiac cell outgrowth and attachment during Drosophila dorsal vessel formation. *Dev. Biol.* **380**, 233–242.

Mann, T., Bodmer, R. and Pandur, P. (2009). The Drosophila homolog of vertebrate Islet1 is a key component in early cardiogenesis. *Development* **136**, 317–326.

Marcos-Mondéjar, P., Peregrín, S., Li, J. Y., Carlsson, L., Tole, S. and López-Bendito, G. (2012). The Lhx2 transcription factor controls thalamocortical axonal guidance by specific regulation of Robo1 and Robo2 receptors. *J. Neurosci.* **32**, 4372–85.

Maro, G. S., Gao, S., Olechwier, A. M., Hung, W. L., Liu, M., Ozkan, E., Zhen, M. and Shen, K. (2015). MADD-4/Punctin and Neurexin Organize C. elegans GABAergic Postsynapses through Neuroligin. *Neuron* **86**, 1420–1432.

Mauss, A., Tripodi, M., Evers, J. F. and Landgraf, M. (2009). Midline signalling systems direct the formation of a neural map by dendritic targeting in the Drosophila motor system. *PLoS Biol.* **7**, e1000200.

Mazzoni, E. O., Mahony, S., Closser, M., Morrison, C. A., Nedelec, S., Williams, D. J., An, D., Gifford, D. K. and Wichterle, H. (2013). Synergistic binding of transcription factors to cell-specific enhancers programs motor neuron identity. *Nat. Neurosci.* **16**, 1219–27.

Mellert, D. J., Knapp, J.-M., Manoli, D. S., Meissner, G. W. and Baker, B. S. (2010). Midline crossing by gustatory receptor neuron axons is regulated by fruitless, doublesex and the Roundabout receptors. *Development* **137**, 323–332.

Miguel-Aliaga, I., Allan, D. W. and Thor, S. (2004). Independent roles of the dachshund and eyes absent genes in BMP signaling, axon pathfinding and neuronal specification. *Development* **131**, 5837–48.

Miguel-Aliaga, I., Thor, S. and Gould, A. P. (2008). Postmitotic specification of Drosophila insulinergic neurons from pioneer neurons. *PLoS Biol.* **6**, 0538–0551.

Mitchell, K. J., Doyle L., J. L., Serafini, T., Kennedy, T. E., Tessier-Lavigne, M., Goodman, C. S. and Dickson, B. J. (1996). Genetic analysis of Netrin genes in Drosophila: Netrins guide CNS commissural axons and peripheral motor axons. *Neuron* **17**, 203–215.

Mosca, T. J., Hong, W., Dani, V. S., Favaloro, V. and Luo, L. (2012). Trans-synaptic Teneurin signalling in neuromuscular synapse organization and target choice. *Nature* **484**, 237–41.

Muhr, J., Andersson, E., Persson, M., Jessell, T. M. and Ericson, J. (2001). Groucho-mediated transcriptional repression establishes progenitor cell pattern and neuronal fate in the ventral neural tube. *Cell* **104**, 861–873.

Murtaugh, L. C. and Melton, D. A. (2003). Genes, signals, and lineages in pancreas development. *Annu. Rev. Cell Dev. Biol.* **19**, 71–89.

Nagel, J., Delandre, C., Zhang, Y., Förstner, F., Moore, A. W. and Tavosanis, G. (2012). Fascin controls neuronal class-specific dendrite arbor morphology. *Development* **139**, 2999–3009.

Neuhaus-Follini, A. and Bashaw, G. J. (2015a). The Intracellular Domain of the Frazzled/DCC Receptor Is a Transcription Factor Required for Commissural Axon Guidance. *Neuron* **87**, 751–763.

Neuhaus-Follini, A. and Bashaw, G. J. (2015b). Crossing the embryonic midline: molecular mechanisms regulating axon responsiveness at an intermediate target. *Wiley Interdiscip Rev Dev Biol* **4**, 377–389.

Nicholson, L., Singh, G. K., Osterwalder, T., Roman, G. W., Davis, R. L. and Keshishian, H. (2008). Spatial and temporal control of gene expression in drosophila using the inducible geneSwitch GAL4 system. I. Screen for larval nervous system drivers. *Genetics* **178**, 215–234.

Niehrs, C. (2006). Function and biological roles of the Dickkopf family of Wnt modulators. *Oncogene* **25**, 7469–7481.

Nishi, Y., Zhang, X., Jeong, J., Peterson, K. A., Vedenko, A., Bulyk, M. L., Hide, W.

A. and McMahon, A. P. (2015). A direct fate exclusion mechanism by Sonic hedgehog-regulated transcriptional repressors. *Development* **142**, 3286–93.

Nóbrega-Pereira, S., Kessaris, N., Du, T., Kimura, S., Anderson, S. and Marín, O. (2008). Postmitotic Nkx2-1 controls the migration of telencephalic interneurons by direct repression of guidance receptors. *Neuron* **59**, 733–45.

O 'Donnell, M. P. and Bashaw, G. J. (2013). Src Inhibits Midline Axon Crossing Independent of Frazzled/ Deleted in Colorectal Carcinoma (DCC) Receptor Tyrosine Phosphorylation. *J. Neurosci.* **33**, 305–314.

O'Donnell, M., Chance, R. K. and Bashaw, G. J. (2009). Axon growth and guidance: receptor regulation and signal transduction. *Annu. Rev. Neurosci.* **32**, 383–412.

O'Keefe, D., Thor, S. and Thomas, J. (1998). Function and specificity of LIM domains in Drosophila nervous system and wing development. *Development* **125**, 3915–3923.

Odden, J. P., Holbrook, S. and Doe, C. Q. (2002). Drosophila HB9 is expressed in a subset of motoneurons and interneurons, where it regulates gene expression and axon pathfinding. *J. Neurosci.* **22**, 9143–9.

Osterwalder, T., Yoon, K. S., White, B. H. and Keshishian, H. (2001). A conditional tissue-specific transgene expression system using inducible GAL4. *PNAS* **2001**, 12596–12601.

Ozkan, E., Carrillo, R. A., Eastman, C. L., Weiszmann, R., Waghray, D., Johnson, K. G., Zinn, K., Celniker, S. E. and Garcia, K. C. (2013). An extracellular interactome of immunoglobulin and LRR proteins reveals receptor-ligand networks. *Cell* **154**,.

Pabst, O., Rummelies, J., Winter, B. and Hans-Henning, A. (2003). Targeted disruption of the homeobox gene Nkx2.9 reveals a role in development of the spinal accessory nerve. *Development* **130**, 1193–1202.

Paixão, S., Balijepalli, A., Serradj, N., Niu, J., Luo, W., Martin, J. H. and Klein, R. (2013). EphrinB3/EphA4-mediated guidance of ascending and descending spinal tracts. *Neuron* **80**, 1407–20.

Pak, W., Hindges, R., Lim, Y.-S., Pfaff, S. L. and O'Leary, D. D. M. (2004). Magnitude of binocular vision controlled by islet-2 repression of a genetic program that specifies laterality of retinal axon pathfinding. *Cell* **119**, 567–78.

Palmesino, E., Rousso, D. L., Kao, T.-J., Klar, A., Laufer, E., Uemura, O., Okamoto, H., Novitch, B. G. and Kania, A. (2010). Foxp1 and Lhx1 coordinate motor neuron migration with axon trajectory choice by gating reelin signaling. *PLoS Biol.* **8**, e1000446.

Pan, F. C., Brissova, M., Powers, A. C., Pfaff, S. and Wright, C. V. E. (2015). Inactivating the permanent neonatal diabetes gene Mnx1 switches insulin-producing β-cells to a δ-like fate and reveals a facultative proliferative capacity in aged β-cells. *Development* **142**, 3637–48.

Pinan-Lucarré, B., Tu, H., Pierron, M., Cruceyra, P. I., Zhan, H., Stigloher, C., Richmond, J. E. and Bessereau, J.-L. (2014). C. elegans Punctin specifies cholinergic versus GABAergic identity of postsynaptic domains. *Nature* **511**, 466–70.

Poliak, S., Morales, D., Croteau, L.-P., Krawchuk, D., Palmesino, E., Morton, S., Jean-François, C., Charron, F., Dalva, M. B., Ackerman, S. L., et al. (2015). Synergistic integration of Netrin and ephrin axon guidance signals by spinal motor neurons Sebastian. *Elife* 1–26.

Polleux, F., Ince-Dunn, G. and Ghosh, A. (2007). Transcriptional regulation of vertebrate axon guidance and synapse formation. *Nat. Rev. Neurosci.* **8**, 331–40.

Prasad, B. C., Ye, B., Zackhary, R., Schrader, K., Seydoux, G. and Reed, R. R. (1998). unc-3, a gene required for axonal guidance in Caenorhabditis elegans, encodes a member of the O/E family of transcription factors. *Development* **125**, 1561–8.

Puram, S. V and Bonni, A. (2013). Cell-intrinsic drivers of dendrite morphogenesis. *Development* **140**, 4657–71.

Pym, E. C. G., Southall, T. D., Mee, C. J., Brand, A. H. and Baines, R. A. (2006). The homeobox transcription factor Even-skipped regulates acquisition of electrical properties in Drosophila neurons. *Neural Dev.* **1**, 3.

Rajagopalan, S., Nicolas, E., Vivancos, V., Berger, J. and Dickson, B. J. (2000a). Crossing the midline: roles and regulation of Robo receptors. *Neuron* **28**, 767–77.

Rajagopalan, S., Vivancos, V., Nicolas, E. and Dickson, B. J. (2000b). Selecting a longitudinal pathway: Robo receptors specify the lateral position of axons in the Drosophila CNS. *Cell* **103**, 1033–45.

Sabatier, C., Plump, A. S., Le, M., Brose, K., Tamada, A., Murakami, F., Lee, E. Y.-H. P. and Tessier-Lavigne, M. (2004). The divergent Robo family protein Rig-1/Robo3 is a negative regulator of slit responsiveness required for midline crossing by commissural axons. *Cell* **117**, 157–69.

Sakai, N., Insolera, R., Sillitoe, R. V, Shi, S.-H. and Kaprielian, Z. (2012). Axon sorting within the spinal cord marginal zone via Robo-mediated inhibition of N-cadherin controls spinocerebellar tract formation. *J. Neurosci.* **32**, 15377–87.

Salzberg, Y., Díaz-Balzac, C. A., Ramirez-Suarez, N. J., Attreed, M., Tecle, E., Desbois, M., Kaprielian, Z. and Bülow, H. E. (2013). Skin-derived cues control

arborization of sensory dendrites in Caenorhabditis elegans. *Cell* **155**, 308–20.

Sander, M., Paydar, S., Ericson, J., Briscoe, J., Berber, E., German, M., Jessell, T. M. and Rubenstein, J. L. R. (2000). Ventral neural patterning by Nkx homeobox genes: Nkx6.1 controls somatic motor neuron and ventral interneuron fates. *Genes Dev.* **14**, 2134–2139.

Santiago, C. and Bashaw, G. J. (2014). Transcription factors and effectors that regulate neuronal morphology. *Development* **141**, 4667–4680.

Santiago, C., Labrador, J.-P. and Bashaw, G. J. (2014). The homeodomain transcription factor Hb9 controls axon guidance in Drosophila through the regulation of Robo receptors. *Cell Rep.* **7**, 153–65.

Santiago-Martínez, E., Soplop, N. H. and Kramer, S. G. (2006). Lateral positioning at the dorsal midline: Slit and Roundabout receptors guide Drosophila heart cell migration. *Proc. Natl. Acad. Sci. U. S. A.* **103**, 12441–6.

Santiago-Martínez, E., Soplop, N. H., Patel, R. and Kramer, S. G. (2008). Repulsion by Slit and Roundabout prevents Shotgun/E-cadherin-mediated cell adhesion during Drosophila heart tube lumen formation. *J. Cell Biol.* **182**, 241–248.

Schaffer, A. E., Taylor, B. L., Benthuysen, J. R., Liu, J., Thorel, F., Yuan, W., Jiao, Y., Kaestner, K. H., Herrera, P. L., Magnuson, M. A., et al. (2013). Nkx6.1 Controls a Gene Regulatory Network Required for Establishing and Maintaining Pancreatic Beta Cell Identity. *PLoS Genet.* **9**,.

Shen, K. and Scheiffele, P. (2010). Genetics and Cell Biology of Building Specific Synaptic Connectivity. *Annu. Rev. Neurosci.* **33**, 473–507.

Shirasaki, R. and Pfaff, S. L. (2002). Transcriptional codes and the control of neuronal identity. *Annu. Rev. Neurosci.* **25**, 251–81.

Shirasaki, R., Lewcock, J. W., Lettieri, K. and Pfaff, S. L. (2006). FGF as a target-derived chemoattractant for developing motor axons genetically programmed by the LIM code. *Neuron* **50**, 841–53.

Simpson, J. H., Kidd, T., Bland, K. S. and Goodman, C. S. (2000a). Short-range and long-range guidance by slit and its Robo receptors. Robo and Robo2 play distinct roles in midline guidance. *Neuron* **28**, 753–66.

Simpson, J. H., Bland, K. S., Fetter, R. D. and Goodman, C. S. (2000b). Short-range and long-range guidance by Slit and its Robo receptors: a combinatorial code of Robo receptors controls lateral position. *Cell* **103**, 1019–32.

Smith, S. T. and Jaynes, J. B. (1996). A conserved region of engrailed, shared among all en-, gsc-, Nk1-, Nk2- and msh-class homeoproteins, mediates active transcriptional repression in vivo. *Development* **122**, 3141–50.

Smith, C. J., Watson, J. D., Spencer, W. C., O'Brien, T., Cha, B., Albeg, A., Treinin, M. and Miller, D. M. (2010). Time-lapse imaging and cell-specific expression profiling reveal dynamic branching and molecular determinants of a multi-dendritic nociceptor in C. elegans. *Dev. Biol.* **345**, 18–33.

Smith, C. J., O'Brien, T., Chatzigeorgiou, M., Spencer, W. C., Feingold-Link, E., Husson, S. J., Hori, S., Mitani, S., Gottschalk, A., Schafer, W. R., et al. (2013). Sensory neuron fates are distinguished by a transcriptional switch that regulates dendrite branch stabilization. *Neuron* **79**, 266–80.

Spitzweck, B., Brankatschk, M. and Dickson, B. J. (2010). Distinct protein domains and expression patterns confer divergent axon guidance functions for Drosophila Robo receptors. *Cell* **140**, 409–20.

Sugimura, K., Satoh, D., Estes, P., Crews, S. T. and Uemura, T. (2004). Development of morphological diversity of dendrites in Drosophila by the BTB-zinc finger protein Abrupt. *Neuron* **43**, 809–822.

Sulkowski, M., Iyer, S., Kurosawa, M., Iyer, E. and Cox, D. N. (2011). Turtle functions downstream of Cut in differentially regulating class specific dendrite morphogenesis in Drosophila. *PLoS One* **6**, e22611.

Sun, L. O., Jiang, Z., Rivlin-Etzion, M., Hand, R., Brady, C. M., Matsuoka, R. L., Yau, K.-W., Feller, M. B. and Kolodkin, A. L. (2013). On and off retinal circuit assembly by divergent molecular mechanisms. *Science* **342**, 1241974.

Syed, D. S., Gowda, S. B. M., Reddy, O. V., Reichert, H. and VijayRaghavan, K. (2016). Glial and neuronal Semaphorin signaling instruct the development of a functional myotopic map for Drosophila walking. *Elife* **5**, 1–18.

Syu, L.-J., Uhler, J., Zhang, H. and Mellerick, D. M. (2009). The Drosophila Nkx6 homeodomain protein has both activation and repression domains and can activate target gene expression. *Brain Res.* **1266**, 8–17.

Tao, Y., Wang, J., Tokusumi, T., Gajewski, K. and Schulz, R. A. (2007). Requirement of the LIM Homeodomain Transcription Factor Tailup for Normal Heart and Hematopoietic Organ Formation in Drosophila melanogaster. *Mol. Cell. Biol.* **27**, 3962–3969.

Taylor, B., Liu, F. F. and Sander, M. (2013). Nkx6.1 Is Essential for Maintaining the Functional State of Pancreatic Beta Cells. *Cell Rep.* **4**, 1262–1275.

Tear, G., Harris, R., Sutaria, S., Kilomanski, K., Goodman, C. S. and Seeger, M. a (1996). commissureless controls growth cone guidance across the CNS midline in Drosphila and encodes a novel membrane protein. *Neuron* **16**, 501–514.

Thaler, J., Harrison, K., Sharma, K., Lettieri, K., Kehrl, J. and Pfaff, S. L. (1999). Active suppression of interneuron programs within developing motor neurons

revealed by analysis of homeodomain factor HB9. *Neuron* **23**, 675–87.

Thaler, J. P., Lee, S.-K., Jurata, L. W., Gill, G. N. and Pfaff, S. L. (2002). LIM Factor Lhx3 Contributes to the Specification of Motor Neuron and Interneuron Identity through Cell-Type-Specific Protein-Protein Interactions. *Cell* **110**, 237–249.

Thor, S. and Thomas, J. B. (1997). The Drosophila islet gene governs axon pathfinding and neurotransmitter identity. *Neuron* **18**, 397–409.

Thor, S. and Thomas, J. B. (2002). Motor neuron specification in worms, flies and mice: conserved and "lost" mechanisms. *Curr. Opin. Genet. Dev.* **12**, 558–64.

Thor, S., Andersson, S. G. E., Tomlinson, A. and Thomas, J. B. (1999). A LIM-homeodomain combinatorial code for motor- neuron pathway selection. *Nature* **397**, 76–80.

Tsalik, E. L., Niacaris, T., Wenick, A. S., Pau, K., Avery, L. and Hobert, O. (2003). LIM homeobox gene-dependent expression of biogenic amine receptors in restricted regions of the C. elegans nervous system. *Dev. Biol.* **263**, 81–102.

Tsubouchi, A., Caldwell, J. C. and Tracey, W. D. (2012). Dendritic filopodia, Ripped Pocket, NOMPC, and NMDARs contribute to the sense of touch in Drosophila larvae. *Curr. Biol.* **22**, 2124–34.

Tsuchida, T., Ensini, M., Morton, S. B., Baldassare, M., Edlund, T. and Jessell, T. M. (1994). Topographic Organization of Embryonic Motor Neurons Defined by Expression of LIM Homeobox Genes. *Cell* **79**, 957–970.

Tu, H., Pinan-Lucarré, B., Ji, T., Jospin, M. and Bessereau, J. L. (2015). C. elegans Punctin Clusters GABA-A Receptors via Neuroligin Binding and UNC-40/DCC Recruitment. *Neuron* **86**, 1407–1419.

Vallstedt, A., Muhr, J., Pattyn, A., Pierani, A., Mendelsohn, M., Sander, M., Jessell, T. M. and Ericson, J. (2001). Different levels of repressor activity assign redundant and specific roles to Nkx6 genes in motor neuron and interneuron specification. *Neuron* **31**, 743–55.

van den Berghe, V., Stappers, E., Vandesande, B., Dimidschstein, J., Kroes, R., Francis, A., Conidi, A., Lesage, F., Dries, R., Cazzola, S., et al. (2013). Directed migration of cortical interneurons depends on the cell-autonomous action of Sip1. *Neuron* **77**, 70–82.

Vrieseling, E. and Arber, S. (2006). Target-induced transcriptional control of dendritic patterning and connectivity in motor neurons by the ETS gene Pea3. *Cell* **127**, 1439–52.

Walsh, D. W., Godson, C., Brazil, D. P. and Martin, F. (2010). Extracellular BMP-antagonist regulation in development and disease: Tied up in knots. *Trends Cell*

Biol. **20**, 244–256.

Way, J. C. and Chalfie, M. (1989). The mec-3 gene of Caenorhabditis elegans requires its own product for maintained expression and is expressed in three neuronal cell types. *Genes Dev.* **3**, 1823–1833.

Wheeler, S. R., Kearney, J. B., Guardiola, A. R. and Crews, S. T. (2006). Single-cell mapping of neural and glial gene expression in the developing Drosophila CNS midline cells. *Dev. Biol.* **294**, 509–24.

William, C. M., Tanabe, Y. and Jessell, T. M. (2003). Regulation of motor neuron subtype identity by repressor activity of Mnx class homeodomain proteins. *Development* **130**, 1523–1536.

Williams, S. E., Mann, F., Erskine, L., Sakurai, T., Wei, S., Rossi, D. J., Gale, N. W., Holt, C. E., Mason, C. A. and Henkemeyer, M. (2003). Ephrin-B2 and EphB1 mediate retinal axon divergence at the optic chiasm. *Neuron* **39**, 919–35.

Wilson, J. M., Hartley, R., Maxwell, D. J., Todd, A. J., Lieberam, I., Kaltschmidt, J. a, Yoshida, Y., Jessell, T. M. and Brownstone, R. M. (2005). Conditional rhythmicity of ventral spinal interneurons defined by expression of the Hb9 homeodomain protein. *J. Neurosci.* **25**, 5710–9.

Wilson, S. I., Shafer, B., Lee, K. J. and Dodd, J. (2008). A molecular program for contralateral trajectory: Rig-1 control by LIM homeodomain transcription factors. *Neuron* **59**, 413–24.

Winberg, M. L., Noordermeer, J. N., Tamagnone, L., Comoglio, P. M., Spriggs, M. K., Tessier-Lavigne, M. and Goodman, C. S. (1998). Plexin A is a neuronal semaphorin receptor that controls axon guidance. *Cell* **95**, 903–16.

Wolfram, V., Southall, T. D., Brand, A. H. and Baines, R. A. (2012). The LIM-homeodomain protein islet dictates motor neuron electrical properties by regulating K(+) channel expression. *Neuron* **75**, 663–74.

Wolfram, V., Southall, T. D., Günay, C., Prinz, A. A., Brand, A. H. and Baines, R. A. (2014). The transcription factors Islet and Lim3 combinatorially regulate ion channel gene expression. *J. Neurosci.* **34**, 2538–43.

Xu, J., Ren, X., Sun, J., Wang, X., Qiao, H. H., Xu, B. W., Liu, L. P. and Ni, J. Q. (2015). A Toolkit of CRISPR-Based Genome Editing Systems in Drosophila. *J. Genet. Genomics* **42**, 141–149.

Yan, Z., Zhang, W., He, Y., Gorczyca, D., Xiang, Y., Cheng, L. E., Meltzer, S., Jan, L. Y. and Jan, Y. N. (2013). Drosophila NOMPC is a mechanotransduction channel subunit for gentle-touch sensation. *Nature* **493**, 221–5.

Yang, L. and Bashaw, G. J. (2006). Son of sevenless directly links the Robo receptor to

rac activation to control axon repulsion at the midline. *Neuron* **52**, 595–607.

Yang, L., Cai, C.-L., Lin, L., Qyang, Y., Chung, C., Monteiro, R. M., Mummery, C. L., Fishman, G. I., Cogen, A. and Evans, S. (2006). Isl1Cre reveals a common Bmp pathway in heart and limb development. *Development* **133**, 1575–85.

Yang, L., Garbe, D. S. and Bashaw, G. J. (2009). A frazzled/DCC-dependent transcriptional switch regulates midline axon guidance. *Science* **324**, 944–7.

Yang, Y. H. C., Manning Fox, J. E., Zhang, K. L., MacDonald, P. E. and Johnson, J. D. (2013). Intraislet SLIT-ROBO signaling is required for beta-cell survival and potentiates insulin secretion. *Proc. Natl. Acad. Sci. U. S. A.* **110**, 16480–5.

Yap, C. C. and Winckler, B. (2012). Harnessing the Power of the Endosome to Regulate Neural Development. *Neuron* **74**, 440–451.

Yaron, A. and Sprinzak, D. (2012). The cis side of juxtacrine signaling: A new role in the development of the nervous system. *Trends Neurosci.* **35**, 230–239.

Zarin, A. A., Daly, A. C., Hülsmeier, J., Asadzadeh, J. and Labrador, J.-P. (2012). A GATA/homeodomain transcriptional code regulates axon guidance through the Unc-5 receptor. *Development* **139**, 1798–805.

Zarin, A. A., Asadzadeh, J. and Labrador, J.-P. (2013). Transcriptional regulation of guidance at the midline and in motor circuits. *Cell. Mol. Life Sci.* 71(3). 419-32.

Zarin, A. A., Asadzadeh, J., Hokamp, K., McCartney, D., Yang, L., Bashaw, G. J. and Labrador, J.-P. (2014). A transcription factor network coordinates attraction, repulsion, and adhesion combinatorially to control motor axon pathway selection. *Neuron* **81**, 1297–311.

Zelina, P., Blockus, H., Zagar, Y., P??res, A., Friocourt, F., Wu, Z., Rama, N., Fouquet, C., Hohenester, E., Tessier-Lavigne, M., et al. (2014). Signaling switch of the axon guidance receptor Robo3 during vertebrate evolution. *Neuron* **84**, 1258–1272.

Zhang, Y., Ma, C., Delohery, T., Nasipak, B., Foat, B. C., Bounoutas, A., Bussemaker, H. J., Kim, S. K. and Chalfie, M. (2002). Identification of genes expressed in C. elegans touch receptor neurons. *Nature* **418**, 331–335.

Zhong, L. and Hwang, R. Y. (2010). Pickpocket Is a DEG / ENaC Protein Required for Mechanical Nociception in Drosophila Larvae. *Curr. Biol.* **20**, 429–434.

Zlatic, M., Landgraf, M. and Bate, M. (2003). Genetic specification of axonal arbors: atonal regulates robo3 to position terminal branches in the Drosophila nervous system. *Neuron* **37**, 41–51.

Zmojdzian, M. and Jagla, K. (2013). Tailup plays multiple roles during cardiac outflow

assembly in Drosophila. *Cell Tissue Res.* **354**, 639–645.

Zwart, M. F., Randlett, O., Evers, J. F. and Landgraf, M. (2013). Dendritic growth gated by a steroid hormone receptor underlies increases in activity in the developing Drosophila locomotor system. *Proc. Natl. Acad. Sci.* **110**, E3878–E3887.